Studies on the palladium catalysed methoxycarbonylation of ethene

Graham Ronald Eastham

Studies on the Palladium Catalysed Methoxycarbonylation of Ethene

Volume 1

Graham Ronald Eastham

Submitted for the degree of

Doctor of Philosophy

University of Durham

Department of Chemistry

1998

Acknowledgements

I would like to thank all my colleagues at I.C.I. Wilton for their help in making this thesis possible. In particular, I would like to thank Dr. R. P. Tooze for his supervision, help and encouragement throughout.

I would also like to thank Dr. M. Kilner for his supervision and encouragement. I must also thank Prof. W. Clegg and Dr. M. Elsegood of the University of Newcastle upon Tyne, for all the structural determinations in this thesis. Thanks also to Dr. C. Jacob of the University of Liverpool for help with V. T. NMR studies.

Finally I would like to thank my family and, in particular, Andrea for whom these last few sentences cannot be written fast enough. May I never stop learning but may I learn to do it in work time. At least for a while anyway.

The material contained in this thesis has not been submitted for examination for any other degree or part thereof, at the University of Durham or any other institution. The material contained herein is the sole work of the author except where formally acknowledged by reference.

Abstract

A series of complexes of the type [(L-L)Pd(alkene)], where (L-L) is a diphosphine ligand and the alkene is dibenzylideneacetone (dba), benzoquinone or tetracyanoethene have been synthesised. These complexes have been evaluated as pre-catalysts in the methoxycarbonylation of ethene (80^0C, 10 bar CO/ethene, MeOH, 20 $MeSO_3H$). Where (L-L) is the diphosphine 1,2-bis(di-*tert*-butylphosphinomethyl)benzene and the alkene is dba, rates in excess of 40,000 moles methyl propionate/mole Pd/hr are obtained at 99.6% selectivity. The catalytic activity and selectivity is found to critically depend on the nature of the diphosphine ligand, with 1,2-bis(diphenylphosphinomethyl)benzene complexes giving rise to high molecular wieght, perfectly alternating CO/ethene co-polymer.

Several of the pre-catalyst complexes have been characterised by single crystal X-ray diffraction, and factors common to both methyl propionate selective catalysts and co-polymer selective catalysts have been identified. The phosphine ligands chosen in this study all readily form complexes with $Pd_2(dba)_3$. The complexes have the formula [(P-P)Pd(dba)] where the bidentate phosphine binds as a chelate ligand to a single palladium atom. The environment around the palladium is essentially trigonal planar, with only small dihedral angles between P_2Pd and PdC_2 planes observed.

Detailed studies of the reaction of the complexes [(L-L)Pd(alkene)] with methanesulphonic acid have been undertaken. The reaction product is shown to depend on the nature of the diphosphine ligand and the alkene. The catalytic activity is discussed with reference to the ability of the reaction products to enter the catalytic cycle.

The coordination chemistry of several diphosphines when mixed with Pd(II) salts has been studied. Several complexes have been characterised by X-ray crystallography and the features related to the observed catalytic activity. The reaction chemistry has also been explored and related to the observed catalysis. A mechanism which takes account of all the results reported in this thesis is presented

CONTENTS

Abbreviations

Å	Angstrom (10^{-10} metres)
br	broad
BQ/bq	benzoquinone
Bu^t	2-methyl-2-propyl
cm^{-1}	wavenumber
Cy	cyclohexyl
CO	carbon monoxide
d	doublet
dba	*trans-trans*-dibenzylideneacetone
dippe	1,2-bis(di-*iso*-propylphosphino)ethane
dippp	1,3-bis(di-*iso*-propylphosphino)propane
dippb	1,4-bis(di-*iso*-propylphosphino)butane
dppe	1,2-bis(diphenylphosphino)ethane
dppp	1,3-bis(diphenylphosphino)propane
dppf	1,1'-bis(diphenylphosphino)ferrocene
dbu^{t}pe	1,2-bis(di-*tert*-butylphosphino)ethane
dbu^{t}pp	1,3-bis(di-*tert*-butylphosphino)propane
DPEphos	bis[2-(diphenylphosphino)phenyl]ether
Et	ethyl
eV	electron volt
FAB	fast atom bombardment
FT	Fourier transform
FT-IR	Fourier transform infrared
GC	Gas Chromatography
g	gramme
hr	hour
Hz	hertz
I.R.	infrared
K	Kelvin
L	ligand
m	multiplet
M^+	molecular ion
Me	methyl
MeP	Methyl propionate
MeOH	methanol
$MeSO_3H$	methanesulphonic acid
MS	Mass Spectrometry
MW	molecular wieght
MALDI-TOF	matrix assisted laser desorption ionisation-time of flight
mg	milligramme
min	minutes
m/z	mass to charge ratio
mmol	millimole

NMR	Nuclear Magnetic Resonance
OAc	acetate
OTs	tosylate
Pe^t	2-methyl-2-butyl
Ph	phenyl
Pr^i	isopropyl
$P(^iPr)_3$	Tri-*iso*-propylphosphine
ppm	parts per million
s	singlet
tcne	tetracyanoethene
TPP	triphenylphosphine
VT	Variable Temperature
vs	very strong
xantphos	4,6-bis(diphenylphosphino)-10,10-dimethyl -10H-dibenzo[b,e][1,4]oxasiline
o-	ortho (the number 2 position on a phenyl ring)
η	hapticity
^0C	degrees Celsius
ν	stretching frequency
$^xJ_{AB}$	spin-spin coupling constant between atoms A and B via X bonds
$\{^1H\}$	proton decoupled

CHAPTER 1

Introduction to the Palladium Phosphine Catalysed Methoxycarbonylation of Ethene

1.1 Introduction

Recently, we have seen the results of much industrial and academic research in the area of homogeneous catalysis in the form of patents from several companies.[1] The driving force for this research is both environmental and economic, with processes based on cheap, readily available starting materials offering clean conversion at high turnover and selectivity being sought.

The rapid development of homogeneous catalysts has coincided with a period of rapid progress in experimental techniques, such as nuclear magnetic resonance spectroscopy to study these systems. Catalytic mechanisms are considerably easier to study in homogeneous systems than heterogeneous systems, where these powerful spectroscopic methods can be used to assign structures and follow reaction kinetics. Particularly impressive advances have been made by making use of the progress in X-ray crystallography combined with computer technology. Single crystal X-ray structural analysis of a complex catalyst enables us to investigate the arrangement of ligands around the metal and to model the possible interaction with substrates, thus allowing plausible arguments regarding the reaction mechanism to be advanced.

One must be cautious in making deductions about a reaction mechanism based only on information derived from a transition metal complex isolated as a solid from a catalyst system. Whilst a species may be close to that in a real catalytic cycle, it may also be a species in a blind alley, separate from the main catalytic cycle. The real situation may be somewhat different from that which one concludes on the basis of a study of an isolated model complex.

Palladium and its complexes have been widely studied as potential catalysts for the production of industrially important materials, as well as for synthetic transformations, where

enantioselectivity rather than turnover frequency is important[2]. In many transformations including the recently patented catalytic process of ethene/CO co-polymerisation[1] for example, phosphine ligands are required for the observed activity and selectivity. Recently, the phosphine 1,3-bis(di-*tert*-butylphosphino)propane has been shown to exhibit 99.6% selectivity to methylpropionate[16] with the above palladium(II) catalysts.[1] The simple substitution of phenyl groups by *tert*-butyl groups results in a complete change in catalyst selectivity (1,3-bis(diphenylphosphino)propane produces co-polymers in the above catalyst systems). I.C.I. have even more recently claimed the use of 1,2-bis(di-*tert*-butylphosphinomethyl)benzene with a palladium(II) salt in the presence of weakly-coordinating anions to give methylpropionate in 99.8% selectivity.[17] One aim of this thesis is to study the 1,2-bis(di-*tert*-butylphosphinomethyl)benzene catalytic system, to evaluate the requirements of the ligand for methylpropionate selectivity.

This thesis details the results of a study of the palladium-catalysed methoxycarbonylation of ethene and the influence of the phosphine ligand on the reaction rate and selectivity. The aim is to understand further the mechanism of the catalysis and the role of the phosphine ligand. With this in mind, this introduction seeks to review briefly the role of phosphine ligands in complexes of the transition metals, the palladium chemistry, relevant to methoxycarbonylation and features of the phosphine structure important to the progress of the reaction.

1.2 The Role of Phosphine Ligands

Tertiary phosphine ligands (PR_3) play an extremely important role in the coordination chemistry of the late transition elements. They are important because they constitute one of the few series of ligands in which electronic and steric properties can be altered in a systematic and predictable way over a wide range by varying R. They also stabilize an exceptionally wide variety of metal species of interest to the organometallic chemist as their phosphine complexes $(R_3P)_nM$--L.

1.2.1 Electronic Factors

The role of a phosphine ligand in a organometallic complex or catalytic cycle is normally described in terms of either electronic or steric factors. The electronic factors involved in the bonding of phosphine ligands to transition metals can be divided into two groups: 1) σ donation of electrons from the phosphorus to the metal and; 2) π back acceptance of electrons from the metal onto the ligand.[3]

1) Phosphines, like NH_3 have a lone pair of electrons, and donation of this lone pair to a metal results in the formation of a σ bond (P→M). The strength of this bond depends on both the ability of the metal to accept electron density and the capability of the phosphine to donate electron density. The latter is often illustrated in terms of the pK_a values which are a measure of the phosphine Bronsted acidity and not Lewis basicity, which is perhaps more appropriate. The pKa values for selected phosphines are illustrated in the table below; a high pKa indicates σ bonding will be dominant. The ability of a metal to accept electron density depends on a number of factors such as oxidation state, coordinative saturation, geometry and the 18 electron rule, all of which influence the electro-positivity of the metal centre. The more electropositive the metal centre, the stronger will be the σ bonds formed.

Phosphine	$P(^tBu)_3$	PEt_3	Me_2PPh	PPh_3	$P(4\text{-}F\text{-}C_6H_4)_3$
pK_a	11.4	8.69	6.49	2.73	1.97

Table 1.0 pKa Values for Selected Phosphines

2) Unlike NH_3, phosphine ligands also act as π acids to an extent that also depends on the nature of the R groups of the PR_3 ligand. For alkyl phosphines, the π acidity is weak; aryl, aryloxy, and dialkylamino groups are successively more effective in promoting π acidity. In the extreme case of PF_3 , the π acidity becomes as great as that found for CO.

In the case of CO, it has long been recognised that it is the π^* orbital which accepts electrons from the metal.[3] In phosphines, it is only relatively recently that the σ^* orbitals of the P-R bonds have been recognised as having a role in the acceptance of electron density.

The energy of the acceptor orbitals is dependent on R, with electronegative groups lowering the energy of the P-R σ^* orbitals, thus facilitating back bonding. Occupation of the P-R σ^* suggests that the P-R bond should lengthen slightly on binding to transition metals. This is often masked by a simultaneous shortening of the P-R bond due to the σ component of the bond (lone pair donation) which results in a decrease in P (lone pair) -R (bonding pair) repulsions.

One measure of the changing electronic effects in PR_3 complexes of transition metals as one changes the nature of R has been developed by Tolman.[4] The CO stretching frequencies of a range of complexes of the type $LNi(CO)_3$, where L is a range of phosphine ligands of the type PR_3, have been compared. The strong donor phosphines have been shown to increase the electron density on nickel, which passes some of this increase along to the CO by back donation. This back donation lowers the CO stretching frequency observed, and this can be plotted to show the following trend of increasing CO stretching frequency: $P(alkyl)_3 < P(aryl)_3 < P(aryloxy)_3$.

1.2.2 Steric Factors

The second factor that is important in the discussion of phosphine ligands and their role in organometallic chemistry and catalysis is the steric bulk. The size or steric bulk of a phosphine PR_3 can be varied by changing R, and the steric environments created as a result of changing R groups in metal complexes are considered to be more important than electronic factors in determining stereochemistry, structure and reactivity of complexes. The number of phosphine ligands which can fit around the metal changes as the R groups increase in size. For bulky phosphines such as PCy_3, the coordinatively unsaturated complex $[Pt(PCy_3)_3]$ forms which has a vacant coordination site at the metal centre for interaction of smaller ligands, but not for a fourth bulky phosphine. The availability of vacant coordination sites at coordinatively unsaturated metal centres is central to homogeneous catalytic processes.

The steric bulk of phosphines can be quantified using the concept of cone angle developed by Tolman.[4] This is defined as the angle of the cone which encompasses all of the ligand in a space filling model of PR_3, in which all of the phosphorus substituents are folded as far as possible from the metal. The centre of the metal is at the apex of the cone.

The effect of steric bulkiness of phosphine ligands on the stability and reactivity of complexes is illustrated by the rate of decarbonylation of the acetylmolybdenum complex $CpMo(CO)_2L(COCH_3)$[5], where L= phosphine ligand. The first order rate constant for the decarbonylation increases with an increase in phosphine cone angle, reflecting the increased ease of dissociation of the phosphine from the intermediate, coordinatively saturated complex to generate the coordinatively unsaturated complex $CpMo(CO)_2(COCH_3)$ which has a vacant site which then allows decarbonylation to proceed.

1.3 Coordination Chemistry of Palladium

Palladium is well known to occur in the 0, +2 and +4 formal oxidation states of which the +2 oxidation state is the most common. Complexes of palladium in the zero oxidation state have a filled d-shell, i.e. d^{10} electron configuration. The ligands, mostly phosphines, alkenes or alkynes, donate into empty sp-hybridised metal orbitals and complexes are probably only stable when extensive back donation can take place. The number of ligands, two or four, depends predominantly on their steric bulk.

The +2 oxidation state is more complicated. Virtually all d^8 palladium complexes have square planar coordination geometries. In these complexes the empty $d_{x^2-y^2}$ orbital is shifted to higher energy as a result of the ligand field splitting. Ligand bonding involves sp^2d-hybridised orbitals that include this empty $d_{x^2-y^2}$ orbital. These square planar complexes have two open coordination sites that have nucleophillic as well as electrophillic character. The reason for this latter feature is that these complexes have a filled d_{z^2} orbital and an empty p_z orbital.

In the +4 formal oxidation state, palladium has a d^6 configuration and is normally octahedrally coordinated. This oxidation state for palladium is relatively unstable with only a few examples reported.[6] The ligands bind to sp^3d^2 metal orbitals, giving rise to 18-electron species.

1.4 Palladium Catalysed Carbonylation of Alkenes

Most of the reported data in this area is directed towards the formation of so-called polyketones, i.e. the perfectly alternating co-polymer of ethene and carbon monoxide. These co-polymers are of great interest for several reasons. Firstly, as a monomer, carbon monoxide is plentiful and inexpensive. Secondly, the presence of the carbonyl chromophore makes the polymers photodegradable. Thirdly, the carbonyl functionality can potentially be easily modified chemically, meaning that the polymers can serve as intermediates for other classes of functional polymers. The perfectly alternating nature of these polymers allows for a high concentration of reactive carbonyl groups in these polymers. Fourthly, the perfectly alternating alkene-carbon monoxide co-polymers have a very high mechanical strength which is thought to result from their high crystallinity.

Nickel-based catalysts for the co-polymerisation of ethene-carbon monoxide were developed by Reppe and Magin[7] in the late 1940s. These catalysts were based on $K_2Ni(CN)_4$ and produced oligomers of ethene and carbon monoxide in addition to diethyl ketone and propionic acid. These nickel-based systems have been improved upon and modified,[8] and systems similar to those developed for the oligomerisation of ethene (SHOP) have been shown to be active catalysts for the CO/ethene co-polymerisation.

Palladium-based systems for the CO/ethene co-polymerisation, first disclosed in the late 1960s,[9] were based on bis(tertiaryphosphine)palladium dichloride complexes. The main disadvantages of these catalysts were the severe conditions (250°C, 2000bar) required for operation and the low yields of polymer. The significant developments in this area came in the early 1980s with the publication by Sen and co-workers[10] of details of tertiary phosphine modified palladium complexes containing the weakly coordinating tetrafluoroborate anion. These were reported to co-polymerise CO/ethene under very mild conditions. Following on from this work, Drent and co-workers at Shell research in Amsterdam showed that the use of chelating bis-(phosphines), in particular 1,3-bis(phosphino)propanes, resulted in significantly enhanced co-polymerisation rates and catalyst lifetimes. This work is described in a series of patents[1] and has subsequently been developed to a commercial scale by Shell. Interestingly, the initial research was targeted at the synthesis of methyl propionate and the initial catalysts tested were palladium systems formed from the combination of palladium acetate with an

excess of triphenylphosphine (TPP) and a Bronsted acid. In methanol solution with hydrogen chloride as the acid component, the reaction proceeded under mild conditions at a moderate rate to give methyl propionate with high selectivity (>98%). Replacement of hydrogen chloride with p-toluenesulphonic acid resulted in a considerable rate enhancement without loss of selectivity.

The ability to switch selectivity by changing from a monodentate to a bidentate phosphine is a key theme of this thesis, and therefore the proposed mechanism of this selectivity change will be reviewed in detail along with the mechanism of catalysis and the proposed role of the anion.

1.4.1 Mechanism of Co-Polymerisation of Ethene and Carbon Monoxide

The proposed catalytic cycles for the co-polymerisation of CO/ethene are illustrated in scheme 1.0 below. The evidence for the presence of two interlinked catalytic cycles comes from an analysis of the end groups of the co-polymers formed.[11] The lower molecular weight oligomer fractions were analysed by GC-MS and shown to contain $CH_3CH_2(COCH_2CH_2)nCOOMe$ (**1**) ketone and ester end groups, $MeO(COCH_2CH_2)nCOOMe$ (**2**) ester end groups only and $CH_3CH_2(COCH_2CH_2)nCOCH_2CH_3$ (**3**) ketone end groups only, where n >0. The production of these different end groups is rationalised by reference to the different initiation and termination pathways for the two cycles discussed below.

Two initiation mechanisms have been proposed. The first producing ester end groups by starting with a palladium carbomethoxy species. The so-called "methoxycarbonyl mechanism" creates this carbomethoxy species by either CO insertion into a palladium methoxide or by direct attack of methanol on coordinated CO. The second initiation pathway produces ketone end groups by insertion of ethene into a palladium hydride followed by CO insertion into the resulting alkyl and is referred to as the "hydride mechanism".

Two termination mechanisms have been proposed for the termination of the polymer chain. Firstly, in the methoxycarbonyl mechanism, the protonolysis of the palladium alkyl bond to produce a saturated ketone end group. If, as shown in the scheme, the proton comes from methanol, then a palladium methoxide is proposed to reform to initiate the next polymer

chain. The second termination mechanism proposed is alcoholysis of the palladium acyl bond to give an ester end group.

An interesting observation of this catalysis is that the end-group analysis changes as the temperature of the co-polymerisation is changed. At low temperature (85°C), the majority of the products are the keto esters which can arise from either mechanism. There are only small quantities of the diesters and diketones formed. The absence of the so-called crossover products is suggested to indicate that one initiation and one termination mechanism dominate. At high temperature (125°C), the selectivity for the latter products is approximately 50% and this is suggested to be evidence that the transfer between the two cycles is rapid and that both cycles contribute to the catalysis with comparable rates.

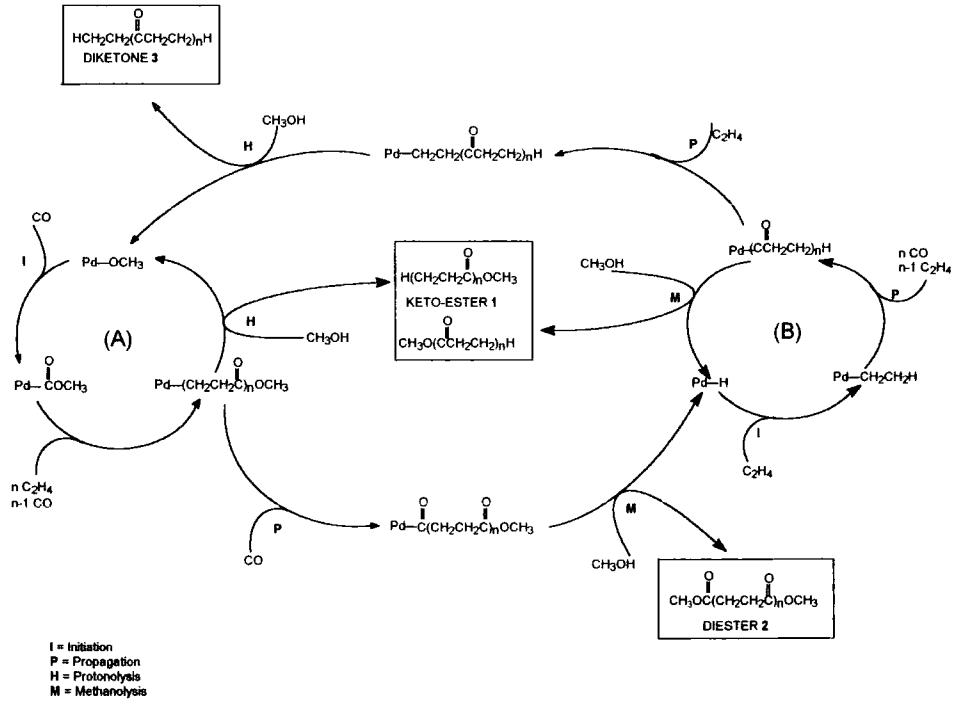

Scheme 1.0 Proposed Mechanism of Ethene/CO Co-polymerisation

1.4.2 The Role of Non-Coordinating Anion in the Methoxycarbonylation of Ethene

The catalytically active species in polyketone formation is thought to be a d^8 square planar cationic palladium complex L_2PdP^+, where L_2 represents the bidentate ligand and **P** is

the growing polymer chain.[11] The fourth coordination site at palladium may be filled by an anion, a solvent molecule, a carbonyl group of the chain, or a monomer molecule. Model studies indicate that having a strongly coordinating group at this position strongly reduces the rates of the insertion steps. Thus competition for the vacant site seems to be an important factor affecting catalysis, and therefore the presence of weakly coordinating anions will serve to increase the rate of catalysis by making the vacant site more readily available to substrate molecules. Organometallic compounds having weakly coordinating anions e.g. BF_4^-, PF_6^-, have been shown to be highly reactive,[12] the anions being leaving groups are easily displaced by other ligands under very mild conditions. For this reason BF_4^- and PF_6^- complexes have proven to be useful starting materials in preparative organometallic synthesis. Also known are complexes where, despite the electronic unsaturation of the metal, the anion remains uncoordinated.[12] In these cases the vacant coordination site is even more accessible by reactant molecules and the metal centre in the case of the above palladium complex **(L_2PdP^+)** would always be part of a cationic species. The mechanism of alkene insertion has been studied[20] and $[Pd(PPh_3)_2Me)solv)]^+$and $[Pd(PPh_3)_2(COMe)solv)]^+$ have both been shown to be active catalysts, whilst the neutral species $[Pd(PPh_3)_2Me(I)]$, $[Pd(PPh_3)_2(COMe)(I)]$, $[Pd(PPh_3)_2(Cl)_2]$ and $[Pd(PPh_3)_4]$ were all inactive. The active co-polymerisation catalytic species has also been shown to involve monocationic species by Sen[10] when monocationic palladium alkyl and acetyl complexes are used to initiate co-polymerisation. The formation of an electrophilic metal centre is an important feature in the catalysis. The formation of a more electrophilic palladium centre with the weakly coordinating anions was indicated by ^{31}P NMR spectroscopic monitoring of the stages in the preparation of the acid-promoted catalyst systems.[13] For example, addition of two mole equivalents of p-toluenesulphonic acid to an equimolar mixture of diacetopalladium(II) and dppp in acetone was reported to result in a high frequency shift from 11.1 to 17.5 ppm (relative to H_3PO_4). This deshielding of the phosphorus atoms can be attributed to the donation of electron density from the dppp phosphorus atoms to a more electrophilic palladium centre which is produced upon replacement of acetate anions by p-toluenesulphonate anions. This is thought to contribute to the increased reactivity because the lower electron density on the palladium centre may result in lower binding energies between the palladium and the co-monomers, due to less back donation from metal to ligand. The intermediate palladium species which are involved in the catalytic cycle would therefore be less stable, with the result that transformations between them would require relatively lower activation energies and so proceed at a higher rate.

1.4.3 The Influence of Phosphine Ligands in the Methoxycarbonylation of Ethene

1) Monodentate vs Bidentate

As mentioned earlier, the study of TPP as a ligand with palladium catalysts similar to the co-polymerisation catalysts leads to the formation of methyl propionate. Low boiling methyl propionate is related to the high melting co-polymer through the general formula $H(CH_2CH_2CO)_nOMe$ where, for MeP, n=1. Methyl propionate can be viewed, then, as the first of the series of linear-alternating polyketo-ester molecules and the target molecule of the reactions studied in this thesis.

Drent and others[11,13] report the following generalization. Under conditions of polyketone catalysis, cationic palladium(II) catalysts modified with excess monodentate phosphine and Bronsted acids of weakly coordinating anions selectively give methyl propionate with high rates. Whilst it is not claimed that all bidentate phosphine modified palladium catalysts give co-polymer, it is suggested that monodentate phosphines do not give rise to co-polymer, and bidentate phosphine does not give rise to MeP under the above conditions. The following is suggested as a mechanism for the dramatic switch in selectivity observed, described with reference to the hydride mechanism, although the explanation applies equally to the methoxycarbonyl mechanism.

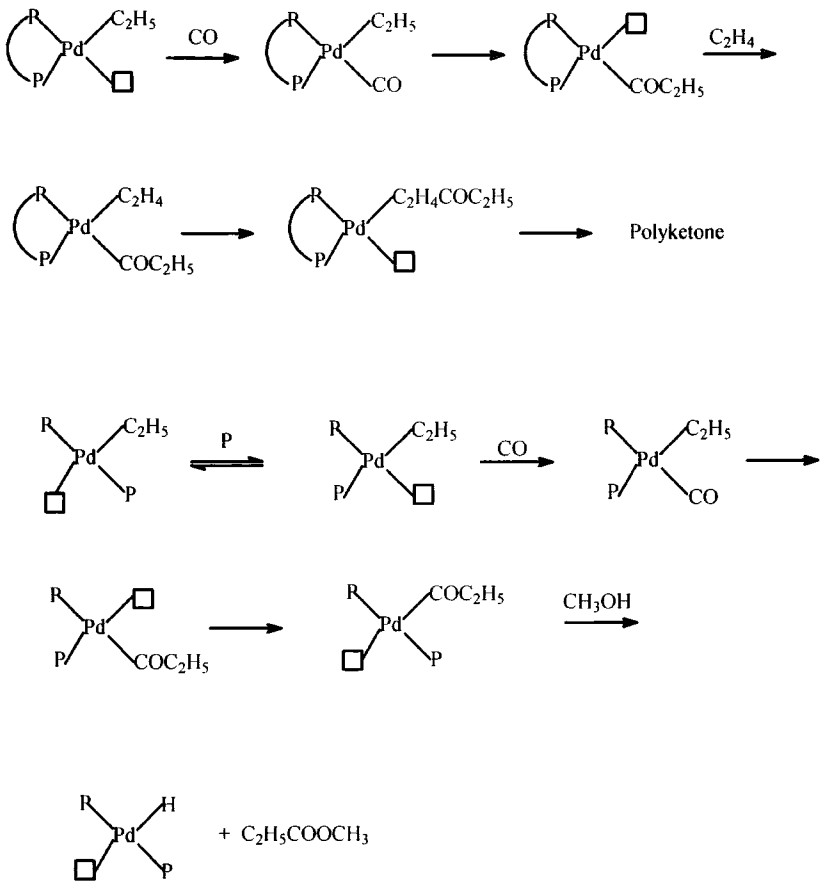

Scheme 1.1 Influence of Phosphine on Selectivity

The key point in the catalytic cycle is the formation and reaction of the palladium acyl intermediate, which can either insert further ethene and CO and go on to become high molecular weight co-polymer, or it can chain terminate via methanolysis to give MeP. The most obvious difference between bidentate phosphine and monodentate phosphine is that, in the former, the phosphorous atoms always occupy adjacent *cis* positions in a metal complex. Specifically, in a square planar palladium(II) complex, this means the available coordination sites available for reaction (without phosphine dissociation) are also in adjacent *cis* positions. With monodentate phosphine, the phosphines can coordinate *trans* to each other and, for the relief of steric hindrance, very often do.

If bidentate phosphines are used, the initial palladium hydride or the growing polymer chain and the empty fourth coordination site are always *cis* to each other, which is the most favourable position for insertion reactions. The insertion of, for example, ethene into the

palladium acyl is straightforward under these conditions and occurs preferentially to chain termination. If monodentate phosphines are used, it is suggested that both the palladium alkyl and the palladium acyl intermediates prefer a *trans* orientation of the phosphine ligands for steric and electronic reasons. Clearly, if we require *cis* coordination positions for polymer chain growth, the formation of *trans* phosphine complexes will be problematic. It is suggested that the *trans* isomers allow chain termination to predominate, especially at the high phosphine:palladium ratios required to sustain high rates with monodentate phosphine. These differences are summarized in the equations illustrated in scheme 1.1.

2) Influence of Phosphine Bridge Length on Selectivity

A study of the change in bridge length versus activity gave the results shown in the table below.

Formula	**Abbreviation**	**$H(CH_2CH_2CO)_nOCH$ (n=)**	**Reaction Rate g/g Pd/hr**
$Ph_2P(CH_2)PPh_2$	(dppm)	2	1
$Ph_2P(CH_2)_2PPh_2$	(dppe)	100	1,000
$Ph_2P(CH_2)_3PPh_2$	(dppp)	180	6,000
$Ph_2P(CH_2)_4PPh_2$	(dppb)	45	2,300
$Ph_2P(CH_2)_5PPh_2$	(dpppee)	6	1,800
$Ph_2P(CH_2)_6PPh_2$	(dpphe)	2	5

Table 1.1 Palladium Catalysed Co-polymerisation of Ethene/CO The Effect of Bridge Length on Activity[13]

Quite clearly, the chelate phosphine 1,3-bis(diphenylphosphino)propane is the preferred choice, giving both the highest activity and highest molecular weights. Both reducing and increasing the carbon bridge length from the n=3 optimum severely affect the activity and degree of polymerization.

The work of Milstein[14] also describes clear effects of the structure of the phosphine ligand on the activity and selectivity of reactions of palladium complexes. It also

attempts to investigate the nature of these differences by a study of the solution and solid state nature of the complexes formed between structurally different phosphines and palladium.

This work involves the study of the synthetically useful carbonylation of aryl halides catalysed by palladium, which can be used in the production of a range of products such as aldehydes, acids, amides and lactones. The industrial utilization of this reaction has been limited by the fact that only bromides or iodides can be used rather than the more attractive chlorides which are more readily available and cheaper. The lower reactivity of the chlorides has been ascribed to the lower tendency of the chlorides to undergo oxidative addition to zerovalent palladium. In an effort to offset this, a range of electron-rich chelate bidentate phosphine-stabilized complexes of palladium of the type PdL_2, where L= $R_2P(CH_2)_nPR_2$ (R= *iso*-propyl), was studied. The results showed a clear dependence of reactivity on ligand structure. The results shown in the table below were obtained in the carbonylation of chlorobenzene and are discussed below.[14]

Ligand	Conversion(%)
dippp (n = 3)	80
dippb (n = 4)	40
dippe (n = 2)	30
dppp (n = 3)	15
$P(^iPr)_3$	0

Table 1.2 Influence of Phosphine Ligand on Reactivity in the Palladium Catalysed Carbonylation of Aryl Halides[14]

A similar trend to that observed by Drent is found with maximum activity being found where n = 3 in the chelate phosphine and increase or decrease in the bridge length from this results in decreased activity. Also worthy of note is the inactivity when a monodentate phosphine is employed and the poor activity when dppp is used. The poor activity associated with dppp is ascribed to the requirement for an electron-rich metal centre. The authors postulate that the oxidative addition of alkyl halide is the rate-determining step and that this is much more rapid for the more electron-rich palladium complex of dippp. An attempt was made to understand further the origin of the above effect of bridge length on activity by

studying the solution and solid state structures of a range of zerovalent complexes of palladium with the relevant bidentate phosphines. It was found that the structures of the complexes formed critically depended on the phosphine carbon bridge length. The structures shown below were identified:

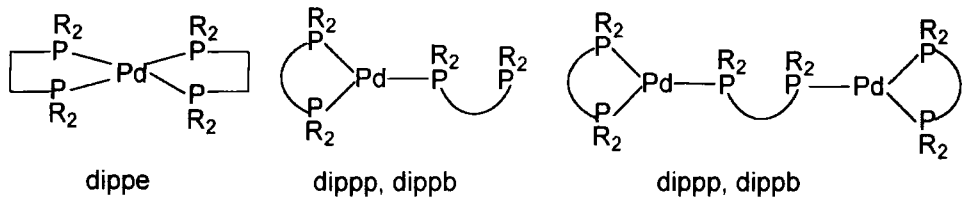

Figure 1.0

Having identified the above structural types, Milstein went on to study the reaction of these compounds with aryl chlorides and again found differences in the product depending on the nature of the phosphine. Whereas the dippe complex did not react possibly due to the stability of the bis chelate complex formed, the dippp complex gave the *cis* product and the dippb complex gave the *trans* isomer (see Figure 1.1 below).

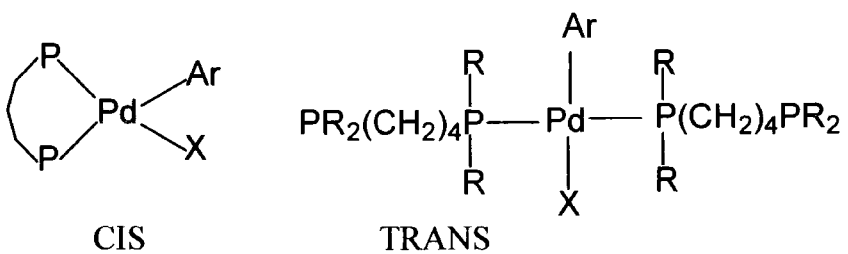

Figure 1.1

Mechanistic studies[14] showed that the above products were the kinetic products, i.e. not the products of equilibrium isomerisation. The carbonylation of aryl halides is widely believed to proceed via dissociation of phosphine to give an electronically and cooordinatively unsaturated 14 electron intermediate, to which the aryl halide oxidatively adds. The structure of the product is then believed to reflect the structure of the intermediate. Since both exist as T-shaped trigonal complexes, two alternative pathways exist, chelate opening to give a *trans* η^{1}-bis-phosphine, or ligand dissociation to give the *cis*-chelate.

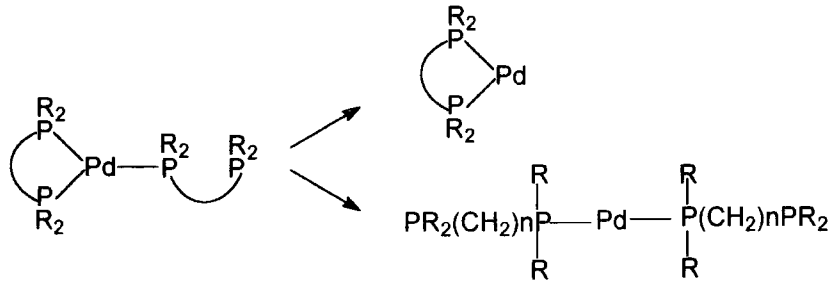

Scheme 1.2

The evidence presented indicated that the former is predominant for dippb and the latter for dippp. This reflects the competition between chelate strength and the *trans* effect of the phosphine ligands.

The above conclusions from the work of Milstein on the influence of phosphine bridge length on the carbonylation of aryl halides can be used to gain some insight into the methoxycarbonylation reactions studied by Drent. The results obtained by Drent using bidentate aryl phosphines $Ph_2P(CH_2)_nPPh_2$ where n=2-6, seem consistent with the simplistic argument concerning chelate strength. Thus, dppe n=2 gives a very stable bis chelate and hence a low rate but high molecular weight co-polymer, dppp n=3 is the perfect choice as above combining high rate with high molecular weight, and dppb n=4, by virtue of its ability to give *trans* complexes, produces lower molecular weight material at a lower rate. This is even more marked on going to dpppe. This assumes that Drent's basic mechanistic hypothesis is correct, simply that *trans* complexes favour termination reactions relative to propagation and hence give lower molecular weights while *cis* complexes favour propagation.

1.4.4 Why is Perfectly Alternating Co-Polymer Formed?

The explanation for the perfectly alternating nature of the co-polymer formed by the Shell patented palladium catalysts invokes the internal coordination of the growing polymer chain to the palladium centre. It is suggested that, after each ethene insertion, the polymer chain end acts as a chelating ligand in which the oxygen atom of the β-carbonyl group coordinates to the electrophilic palladium atom to form a five-membered chelate ring. The electrostatic interaction between the positive palladium centre and the negative oxygen atom

is probably the main driving force for this chelate forming reaction. The result of this internal coordination is to introduce a barrier to further coordination and insertion of a reactant molecule. It is suggested that carbon monoxide, which binds more strongly to palladium and probably requires less space than alkenes to coordinate, can more readily displace the carbonyl group and then insert. Alkene coordination to Pd(II) in this chelate is too weak to displace the carbonyl group in this stable five-membered ring structure. The same is not felt to be true in the six-membered chelate which would result from internal coordination of the polymer chain after carbon monoxide insertion. Ethene will be able to displace readily the carbonyl group and then insert to regenerate the next five-membered ring species.

The above hypothesis seeks to rationalize the absence of double ethene insertions. Double carbon monoxide insertions do not take place because they are thermodynamically disfavoured.[15] Also apparent from the above hypothesis is an explanation for the lack of products which result from chain termination by β-elimination. For β-elimination to occur, the β-H has to approach the palladium atom, but this is inhibited by coordination of the carbonyl group to palladium. The inhibition of β-elimination in metallocycles is well known.[3]

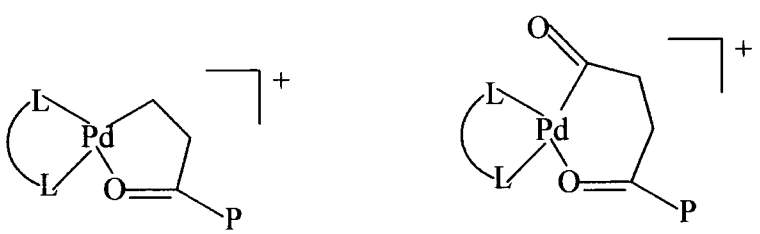

Five membered ring Six membered ring

Figure 1.2 Structures Resulting from Internal Coordination of Polymer Chains in Ethene/CO Co-polymerisation

1.5 The Use of Di-*tert*-butyl Substituted Phosphines

Recently, the phosphine 1,3-bis(di-*tert*-butylphosphino)propane has been shown to exhibit 99.6% selectivity to methylpropionate[16] with palladium(II) catalysts. The simple substitution of phenyl groups by *tert*-butyl groups results in a complete change in catalyst

selectivity. This result directly contradicts Drent's published claim that bidentate phosphine leads to the formation of perfectly alternating co-polymer.[11,13] I.C.I. have even more recently claimed the use of 1,2-bis(di-*tert*-butylphosphinomethyl)benzene with a palladium(II) salt in the presence of weakly-coordinating anions to give methylpropionate in 99.8% selectivity.[17] This thesis reports the study of the 1,2-bis(di-*tert*-butylphosphinomethyl)benzene catalytic system, to evaluate the requirements of the ligand for methylpropionate selectivity.

Work by Spencer *et al*, suggests the bulky 1,3-bis(di-*tert*-butylphosphino)propane and 1,2-bis(di-*tert*-butylphosphinomethyl)benzene stabilises previously unobserved complexes of palladium, which may give an insight into the unusual activities and selectivites observed for these *tert*-butyl substituted phosphine-modified catalysts.[18] The work is primarily concerned with 1,2-bis(di-*tert*-butylphosphine)ethane, 1,3-bis(di-*tert*-butylphosphino)propane and 1,2-bis(di-*tert*-butylphosphinomethyl)benzene and deals with the preparation of platinum alkene complexes (and palladium in some cases) of these phosphines and protonation with HBF_4 and sulphonic acids. The reaction of palladium(0) alkene complexes with these acids is used in this work reported here as the method of activation of the palladium. A review of this literature may provide insight on the types of species formed and the properties imparted to the palladium complexes by the *tert*-butyl substituted phosphine ligands.

The platinum(II) complex $[(L\text{-}L)PtCl_2]$, (L-L) = 1,2-bis(di-*tert*-butylphosphinomethyl)benzene is synthesised from *cis*-$[(Bu^tCN)_2\ PtCl_2]$ by displacement of the nitrile groups by phosphine. The complex produced is then reduced to give the corresponding *cis*-dihydride in almost quantitative yield. The formation of a *cis*-dihydride stable to reductive elimination of hydrogen is unusual even for platinum. The formation of the *cis*-platinum(II) dihydride is reported as only possible when 1,2-bis(di-*tert*-butylphosphinomethyl)benzene is used as the stabilizing phosphine ligand.

Of most interest is the observation that the *cis*-platinum(II) dihydride, when treated with hydrochloric acid in diethyl ether, is converted into the monohydride, and even prolonged treatment with dry hydrochloric acid in ether failed to yield the dichloride. The stability of the mono-hydride is surprising. As outlined above, in the methoxycarbonylation of ethylene, palladium hydrides are postulated in one possible mechanism as key intermediates. It is not known whether the palladium analogue of the above platinum

dihydride can be made or not or, more importantly, whether the monohydride is stable or not. In palladium systems of the ligand 1,2-bis(di-*tert*-butylphosphinomethyl)benzene, one might expect activation energies to be lower than in platinum systems for similar processes, suggesting the materials will be inherently less stable.

Further work by Spencer's group probed the structures of protonated platinum and palladium complexes, particularly where the agent of protonation (acid) contains a non-coordinating anion, found to be important in certain catalytic reactions. In this thesis, the synthesis and characterization of a number of similar complexes is reported. Thus, the complexes [(L-L)Pt(η^2-C_7H_{10})] and [(L-L)Pd(η^2-C_7H_{10})], where

i) C_7H_{10} =norbornene

ii) (L-L)= *o*– $C_6H_4(CH_2PBu^t_2)_2$, M= Pt and Pd

= $Bu^t_2P(CH_2)_2PBu^t_2$, M= Pt and Pd

= $Bu^t_2P(CH_2)_3PBu^t_2$, M= Pt only

were reacted with $HBF_4.OEt_2$ to yield cationic complexes, reported to be stabilized by agostic interaction of the β CH with the metal centre. The reaction proceeds according to scheme 1.3.

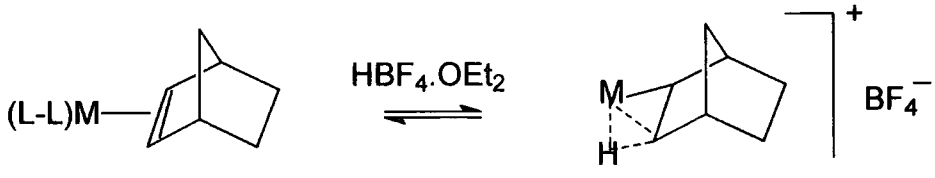

Scheme 1.3

A number of interesting points are raised in this work.

i) The synthesis of the starting material for platinum involves treatment of [Pt(η^2–C_7H_{10})$_3$] (tris-alkene complex) with the phosphine (L-L), but this route does not work for the equivalent palladium complexes. An alternative route using [Pd(η^3–C_3H_5)(η-C_5H_5)] with the appropriate diphosphine is reported. This serves to emphasize that care is required in drawing conclusions about palladium chemistry by extrapolation from platinum chemistry.

ii) Protonation of [Pt (η^2–C_7H_{10})(L-L)] with either HBF_4.OEt or CF_3SO_3H in ether at 0^0C affords micro-crystalline complexes of formula [Pt (C_7H_{11})(L-L)(Y)] where Y= the anion of the respective acid. The palladium complexes [Pd (C_7H_{11})(L-L)(Y)] are obtained similarly, but in lower yield using HBF_4.OEt as the acid. Use of CF_3SO_3H was not reported to lead to the isolation of $CF_3SO_3^-$ salts, but rather resulted in the formation of uncharacterized species. This suggests potential differences in the reactivity of different acids and the stability of the derivatives of respective non-coordinating anions. In the work of Drent[11] *et al*, sulphonic non-coordinating anions are reported to result in the highest activities of the palladium co-polymerisation catalysts, whereas Milani[20] shows those based on PF_6^- and BF_4^- are more active with nitrogen ligands such as bipyridine and phenanthroline.

iii) No bands attributable to metal-hydride are observable in the I.R. spectra of these complexes. However, low temperature NMR of all the compounds studied in the temperature range 300-194K show a low frequency signal typical of discrete hydride ligands on Pt/Pd. One explanation for this absence of evidence of protonation at room temperature is that the complex is reacting to form a protonated species in which the agostic form is favoured. Low temperature NMR is necessary to freeze out the rotation around the metal-alkyl bond, such that the agostic interaction can be observed on the NMR time scale.

The activity of the agostic complexes in, for example, methoxycarbonylation of ethylene can be readily rationalised with reference to the following equilibrium.

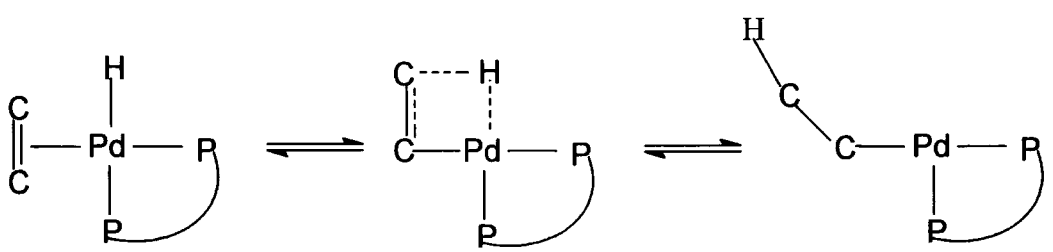

Scheme 1.4

This equilibrium is thought to lie over to the right-hand side and catalysis is initiated by a) coordination of carbon monoxide, b) migratory insertion to give a palladium acyl species and c) methanolysis to give a methyl ester and regenerate a palladium hydride.

This work goes on further to discuss the relationship between the phosphine ligand and the extent of the β hydrogen agostic interaction in the platinum norbornyl complexes. Spencer[18] *et al* suggest that the chelate ring size and the bulk of the substituents at phosphorus influence the structure of the complex adopted. They base their argument on the observed values of Pt-H and Pt-P couplings in respective complexes of different phosphines. The implication is that the smaller diphosphines L-L = ($Bu^t_2P(CH_2)_2PBu^t_2$; P-Pt-P 89^{0}C) favour an alkene-hydride type structure (highest values of J_{Pt-H}, lowest values of $J_{Pt-Ptrans}$), while the larger diphosphines o–$C_6H_4(CH_2PBu^t_2)_2$ and $Bu^t_2P(CH_2)_3PBu^t_2$ favour alkyl-like structures. The P-Pt-P angles reported are 105^0 and 98-101^0 respectively (J_{Pt-H} 79 and 85Hz) as compared to a value of J_{Pt-H} of 136Hz for $Bu^t_2P(CH_2)_2PBu^t_2$.

A further literature report[18] suggests that, for the protonation of palladium ethyl complexes of the above phosphines, the agostic structures are thermodynamically more favoured in all cases. This is a clear distinction between palladium and platinum where there is reported to be a fine balance between ethene hydride and agostic ethyl which is controlled by the diphosphine ligand.

Later work by Spencer's group[18] continued to probe the protonation reactions, specifically the protonation of platinum complexes of the type [(L-L)Pt(η^2-C_4H_4)] and [(L-L)Pt$(Et)_2$] where (L-L)= o–$C_6H_4(CH_2PBu^t_2)_2$ (I), $Bu^t_2P(CH_2)_3PBu^t_2$ (II) and $Bu^t_2P(CH_2)_2PBu^t_2$ (III). Interestingly, protonation of both types of complex is reported to lead to the same product for a given phosphine ligand (see scheme 1.5). The preferred geometry of the resultant complex is stated to be under the control of the diphosphine ligand, in line with earlier results.

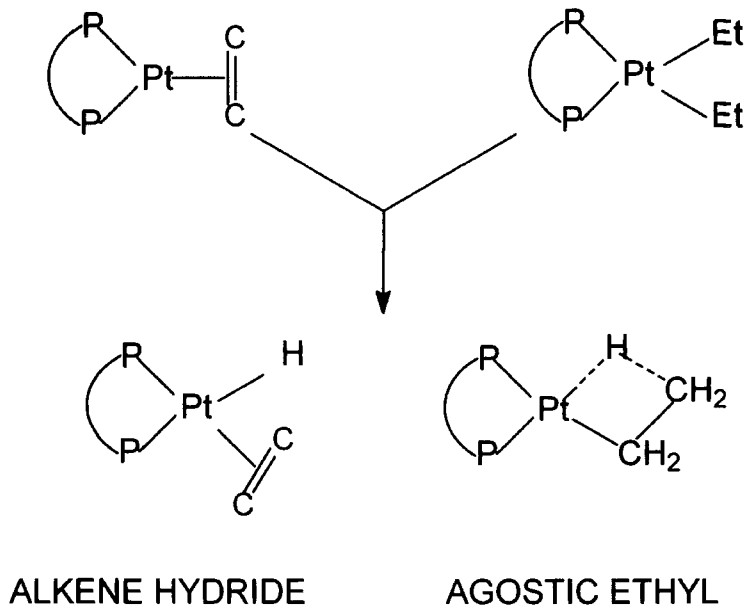

ALKENE HYDRIDE AGOSTIC ETHYL

Scheme 1.5

An exception to the above scheme is the complex $[(L\text{-}L)Pt(Et)_2]$ where (L-L) = $o\text{–}C_6H_4(CH_2PBu^t_2)_2$. This complex could not be made directly from $Pt(COD)(Et)_2$ and phosphine, the reaction resulting in the isolation of $[(L\text{-}L)Pt(\eta^2\text{-}C_2H_4)]$, presumably by β-hydrogen elimination from one ethyl group followed by reductive elimination of ethane. The reaction between $Pt(COD)(Et)_2$ and $o\text{–}C_6H_4(CH_2PBu^t_2)_2$ is reported to be much slower than for the comparative reaction with $Bu^t_2P(CH_2)_3PBu^t_2$ and $Bu^t_2P(CH_2)_2PBu^t_2$. Reaction was achieved by heating to 100° and this is probably what drives the elimination of ethane. It would appear that, at lower temperatures, reaction to give the desired product is not occurring. The exact reason for this is not known, but it is interesting to note that it only occurs with the $o\text{–}C_6H_4(CH_2PBu^t_2)_2$ ligand, which has the largest P-Pt-P angle and the most rigidity in the chelate backbone for the phosphines studied.

Protonation of both platinum complexes $[(L\text{-}L)Pt(\eta^2\text{-}C_4H_4)]$ and $[(L\text{-}L)Pt(Et)_2]$ by a range of non-coordinating acids results in either alkene hydride type structures or metal alkyl type structures. As with the norbornyl complexes, an alkene-hydride type structure is reported to be favoured when (L-L) = $Bu^t_2P(CH_2)_2PBu^t_2$ and the more metal-alkyl type structures are reported when (L-L) = $o\text{-}C_6H_4(CH_2PBu^t_2)_2$ and $Bu^t_2P(CH_2)_3PBu^t_2$.

A further documented difference between (L-L) = *o*-$C_6H_4(CH_2PBu^t_2)_2$ and the propane and ethane bridged *tert*-butyl phosphines is also worthy of note. The platinum(II) cations resulting from the protonation reactions having the structure $[(L\text{-}L)Pt(Et)]^+$ are reported to be unstable in dichloromethane with respect to loss of ethene, to form the dinuclear cations having the structure $[(L\text{-}L)_2Pt_2(\eta\text{-}H)_2]^{2+}$. The one exception is the complex $[(L\text{-}L)Pt(Et)]^+$ where (L-L) = *o*-$C_6H_4(CH_2PBu^t_2)_2$. It is suggested that the steric bulk of the phosphine may render the corresponding dinuclear complex too sterically hindered to be stable.

1.6 The Nature of the Catalyst-Active Centre

The selectivity switch observed between catalysts employing the phosphine ligands dppp and *o*-$C_6H_4(CH_2PBu^t_2)_2$ suggests a role for the steric bulk of the *tert*-butyl groups in modifying the active catalyst centre. The idea of a ligand modified steric environment being responsible for the changes in selectivity in a catalytic reaction is not a new one.[19] Barron et al have recently described the active catalytic centre in a series of ethene/CO co-polymerisation catalysts of palladium.

Table 1.3 details the results of a series of ethene/CO co-polymerisations carried out using catalyst precursor compounds $[\{R_2P(CH_2)_nPR_2\}Pd\{C(O)Bu^t\}Cl]$ (R = Ph, n = 2 (dppe), 3 = (dppp), 4 = (dppb); R = Me (dmpe), C_6H_{11} (dcpe), n = 2). An attempt is made to correlate the observed activity with a parameter calculated from solid state X-ray structural data of the precursor compounds. This parameter, referred to as the "pocket angle", has been calculated both in the PdP_2 plane and perpendicular to this plane (see Figure 1.3).

From the data in Table 1.3, it is suggested that there is an optimum size for the active site. Furthermore, catalysis is primarily dependent on the size of the "pocket angle" in the plane of the ligands around palladium. The rationale for this is that the most sterically crowded species formed during the catalytic cycle is the ethene complex $[\{R_2P(CH_2)_nPR_2\}Pd(H_2C{=}CH_2)C(O)R]^+$ which is formed as an intermediate prior to alkene insertion. In order for the alkene insertion/acyl migration to occur, the ethylene must be coplanar with the migrating acyl group. Thus, it is in the ligand plane that steric hindrance

becomes a controlling factor in ethene coordination/insertion.

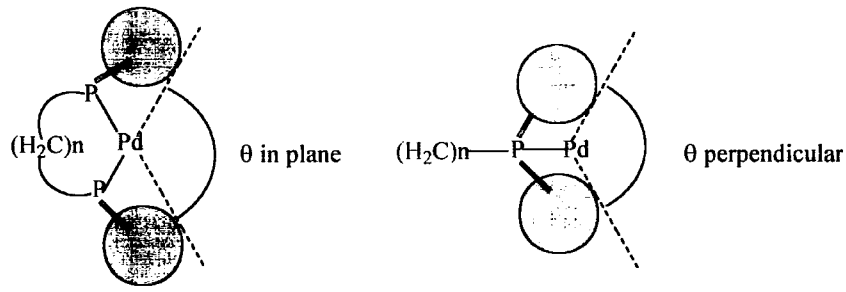

Figure 1.3 Calculation of Pocket Angles Used to Describe Dimensions of Catalyst

Phosphine	Bridge Length	Initial Rate dP/dt(psi.min^{-1})	Total Polymer Yield (g)	In-Plane Pocket Angle	Perpendicular Pocket Angle
dppe	2	0.19	0.22	132	129
dppp	3	0.75	1.42	108	146
dppb	4	0.12	0.03	93	102
dmpe	2		none	141	174
dcpe	2	0.83	1.25	106	115

Table 1.3 Catalytic Activity and Pocket Angles for a Series of Palladium Phosphine Complexes

The above pocket angles suggest an explanation for the comparable catalytic activity of catalysts which employ dppp and dcpe. These two phosphine ligands create a similar steric environment around palladium which is optimal for the coordination and insertion reactions necessary for catalysis to occur.

It has been proposed that, if the pocket angle of the $\{R_2P(CH_2)_nPR_2\}Pd$ moiety is sufficiently small (i.e. n=4), then ethene is precluded from complexation, the equilibrium shown in Figure 1.4 is shifted predominantly to the left.

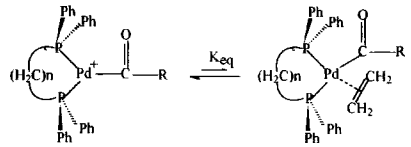

Figure 1.4

Thus, poor activity in the dppb catalyst is ascribed to a sterically crowded catalytic centre. This is in contrast to the work of Drent, Milstein and others, where the chelate stability and backbone flexibility are identified as key to the activity/selectivity in these catalysts.

The low activity of the dppe catalyst and the lack of activity in the dmpe catalyst have been suggested to be due to the formation of stable metallocycles, similar to those proposed by Drent et al to play a role in defining the perfectly alternating nature of the co-polymers. Such chelate formation will oppose the insertion of the next monomer unit (carbon monoxide) by blocking the required coordination site on palladium and thus inhibiting polymerization. The complexes of dppp and dcpe, which have a small pocket angle inhibit or preclude chelation as a result of steric repulsion between the phosphorus substituents and the carbonyl on the growing chain (see Figure 1.2). In contrast, the complexes with a large pocket angle (dppe, dmpe) will have significantly less steric hindrance and chelation may become so strong that the insertion of the next monomer is inhibited completely; therefore chain propagation cannot occur.

1.7 Aim and Scope of this Thesis

The selectivity to methylpropionate obtained in the palladium catalysed methoxycarbonylation of ethene with the bidentate *tert*-butyl substituted phosphine ligands has not been explained. In an attempt to understand the requirements of the ligand for catalysis, a study of the catalytic activity of a range phosphines was planned. The focus was on the bidentate ligands based on the xylene backbone (e.g. 1,2-bis(di-*tert*-butylphosphinomethyl)benzene) recently patented by I.C.I. and for which there is very little available literature. Phosphine palladium complexes have been characterised by

X-ray crystallography and the solid state parameters related to the observed activity/selectivity.

1.8 References

1. E. Drent, EP 0, 271, 144, **1988**.
   E. Drent, P.H.M. Budzelaar and W.W. Taylor, EP 0, 386, 833, **1996**.
   E. Drent and P.H.M. Budzelaar, EP 0, 386, 348, **1990**.
   E. Drent, P.H.M. Budzelaar, W.W. Taylor and J Staperasma, EP 0, 441, 447, **1991**.
   E. Drent, EP 0, 495, 547, 121, 965, **1984**.
   E. Drent, EP 0, 274, 795, 181, 014, **1986**.
   E. Drent, US 5, 210, 280, 235, 865, **1987**.
2. Jiro Tsuji, Palladium "*Reagents & Catalysts, Innovation in Organic Synthesis*", Wiley
   G. Wilkinson, E. W. Abel and F. G. A. Stone, "*Comprehensive Organometallic Chemistry*", Vol I & II, Pregamon Press, New York, 1982.
3. J.P. Collman, L.S. Hegadus, R.G. Norton and R.G. Finke, "*Principles and Applications of Organotransition Metal Chemistry*", University Science Books, Mill Valley (CA) USA, 1987.
   R.H. Crabtree, "*The Organometallic Chemistry of Transition Metals*", J. Wiley & Sons, New York, 1987.
4. C.A. Tolman, *Chem. Rev.*, **1977**, 77, 313.
5. A. Yamamotto,"*Organotransition Metal Chemistry*", J. Wiley & Sons, New York, 1986
6. P. K. Byers, A. J. Canty, B. W. Skelton and A. H. White, *J. Chem. Soc. Chem. Comm.* **1986**, 1722.
7. W. Reppe and A. Magin, US Patent 2, 557, 208, **1951**.
8. T. M. Shryne and H. V. Haller, US Patent 3, 984, 388, **1976**.
9. A. Gough, British Patent 1, 081, 304, **1967**.
10. A. Sen and T. Weng Lai, *J. Am. Chem. Soc.*, **1982**, 104, 3520.
    A. Sen and T. Weng Lai, *Organometallics*, **1984**, 3, 866.
11. E. Drent and P. H. M. Budzelaar, *Chem. Rev.*, **1996**, 96, 663.
12. W. Beck and K. Sunkel, *Chem. Rev.*, **1988**, 88, 1405.

13. E. Drent, J. A. M. van Broekhowen and M.J. Doyle, *J. Organomet. Chem.*, **1991**, 417, 235.

14. Y. Ben-David, M. Portnoy and D. Milstein,*J. Chem. Soc. Chem. Comm.*, **1989**, 1816.
Y. Ben-David, M. Portnoy and D. Milstein, *J. Am. Chem. Soc* **1989**, 111, 8742.
Y. Ben-David, M. Portnoy and D. Milstein, *Organometallics* **1972**, 11, 1995.
Y. Ben-David, M. Portnoy and D. Milstein, *Organometallics* **1993**, 12, 4734.
M. Portnoy and D. Milstein, *Organometallics* **1993**, 12, 1655.
M. Portnoy, F. Frolov and D. Milstein, *Organometallics* **1991**, 10, 3960.

15. P. Mergl and T. Ziegler, *Organometallics* **1996**, 15, 5519.
P. Mergl and T. Ziegler, *J. Am. Chem. Soc.* **1996**, 118, 7337.

16. E. Drent, EP 0, 495, 548.

17. R. P. Tooze, G. R. Eastham, K. Whiston and X. L. Wang, WO 96/19434.

18. N. Carr, B. L. Dunne, L. Mole, A. G. Orpen and J. L. Spencer, *J. Chem. Soc. Dalton Trans.* **1991**, 863.
N. Carr, L. Mole, A. G. Orpen and J. L. Spencer,*J. Chem. Soc. Dalton Trans.* **1992**, 2653.
F. M. Conroy-Lewis, L. Mole, A. D. Redhouse, S. A. Lister and J. L. Spencer, *J. Chem. Soc. Chem. Comm.* **1991**, 1601.
L. E. Crascall, J. L. Spencer, *J. Chem. Soc. Dalton Trans.* **1992**, 3445.

19. Y. Koide, S. G. Bott and A. R. Barron, *Organometallics*, **1996**, 15, 2213.

20. J. R. Norton and E. G. Samsel, *J. Am. Chem. Soc.*, **1984**, 106, 5505.

CHAPTER 2.0

The Evaluation of Palladium Phosphine Complexes as Pre-Catalysts in the Methoxycarbonylation of Ethene

2.1 Introduction

The aim of this chapter is to present the results of the catalyst testing carried out as part of this study. Explanations are not offered for the observed catalysis results; furthermore it is the objective in the remaining chapters of this thesis to present and discuss experimental results which do this. The catalyst testing has all been carried out with pre-formed palladium complexes in which the phosphine ligand is coordinated in a known manner to the palladium. The synthesis of these complexes is detailed elsewhere in this thesis and the characterization by crystallographic and spectroscopic means forms a part of the rationalization of the observed catalytic activity.

The background to the study as mentioned in the introduction is the surprising difference in activity of palladium catalysts based on the phosphine ligands 1,2-bis(di-*tert*-butylphosphinomethyl)benzene and 1,3-bis(di-*tert*-butylphosphino)propane patented by I.C.I. and Shell respectively. Concentrating primarily on the I.C.I. system in this section, we seek to understand how the catalyst selectivity and activity is sensitive to changes in the phosphorus substituent, the ligand backbone and the palladium source. Some alternate ligands of interest, are also evaluated for their activity in the methoxycarbonylation of ethene.

2.2 Experimental

The experiments fall into two catagories: i) those performed in the high pressure Semi Technical Scale (S.T.) facility at I.C.I. Wilton; and ii) those performed in a laboratory Bucchi glass autoclave. All units operate under the same conditions of temperature and pressure, but the Bucchi autoclave has a magnetic follower as its stirring mechanism to ensure gas/liquid mixing, whilst the S.T. autoclaves have a motor-driven stirrer capable of 1000 rpm stirring

speeds to ensure efficient gas/liquid mixing. This is important to ensure that the catalyst activities observed are not limited by mass transfer effects. The S.T. autoclaves also have continuous monitoring equipment enabling rate information to be obtained throughout the experiment.

S.T. Testing

General Experimental Procedure

Two different autoclaves were used in the S.T. testing program, which differ in the volume of catalyst solution used, and therefore the number of moles of catalyst complex added to maintain a standard concentration. The larger of the two is a two litre Hastelloy zipperclave, and to this was added 5.03 x 10^{-5} moles of complex in 300 cm^3 of reaction solution. The smaller stainless steel unit is 300 cm^3 in volume, and to this was added 1.66 x 10^{-5} moles of catalyst complex in 100 cm^3 total volume. The autoclave used was not felt to have an effect on the catalyst activities determined. A typical catalyst solution was made up as follows: The catalyst Pd[L-L]dba (5.03 x 10^{-5} moles) was weighed into a 500 cm^3 round-bottomed flask in a nitrogen filled glove box. The flask was then removed and connected to a standard vacuum/nitrogen line where 300 cm^3 of methanol/MeP in a 7:3 ratio by weight was added. The methanol/MeP mixture was degassed prior to addition to eliminate oxygen. The acid (methanesulphonic acid, 68µl, 1.0 x 10^{-3} moles) was added and the catalyst solution immediately transferred to the nitrogen flushed autoclave. In each experiment, after addition of the reaction solution, the autoclave was heated to 80°C. When at temperature, the autoclave was opened up to a reservoir containing a 1:1 mixture of CO and ethene to a pressure of 10bar. The catalyst activity was calculated by analyzing the rate of consumption of gas from the reservoir. This is equal to the rate of reaction if the gases obey the ideal gas law, and it is assumed that the catalyst is 100% selective. Stirring speed in all experiments was maintained at 1000 rpm for the duration of the catalyst test. At the end of the reaction the solutions were removed from the autoclave and analysed by GC.

Laboratory Testing

General Experimental Procedure

The general procedure was the same as the S.T. program except for the following important differences: 1) The catalyst concentrations were not kept constant and were varied throughout the range of experiments; 2) All experiments were performed in 100% methanol to maximize activity; 3) In the case of the laboratory rig, the reservoir was a 1:1 CO:Ethene cylinder with a gas regulator set to 10 bar. The pressure in the autoclave was maintained at a constant pressure, but no rate of gas uptake information is available. Catalyst turnover numbers are obtained from solution weight gains cross-checked with GC composition data.

2.2.1 Key to Catalysts Tested

The following table lists the phosphine ligands tested as catalysts and the palladium pre-catalyst complex form in which they were added to the reaction mixture. These pre-catalysts were all synthesised for this study and the numbering scheme is that used in chapter 3.0 where the synthesis and characterization are detailed.

Complex Number	Phosphine Ligand	Palladium complex
12	**o-$C_6H_4(CH_2PBu^t_2)_2$**	**(L-L)Pd(dba)**
13	**o-$C_6H_4(CH_2PPr^i_2)_2$**	**(L-L)Pd(dba)**
14	**o-$C_6H_4(CH_2PCy_2)_2$**	**(L-L)Pd(dba)**
15	**o-$C_6H_4(CH_2P(Bu^t)(Cy))_2$**	**(L-L)Pd(dba)**
16	**o-$C_6H_4(CH_2PPe^t_2)_2$**	**(L-L)Pd(dba)**
17	**o-$C_6H_4(CH_2P(Bu^t)(Pe^t))_2$**	**(L-L)Pd(dba)**
18	**o-$C_6H_4(CH_2PPh_2)_2$**	**(L-L)Pd(dba)**
19	**1,2-$C_2H_4(PBu^t_2)_2$**	**(L-L)Pd(dba)**
20	**1,3-$C_3H_6(PBu^t_2)_2$**	**(L-L)Pd(dba)**
21	**1,3-$C_3H_6(PPh_2)_2$**	**(L-L)Pd(dba)**
22	**PPh_3**	**$(L)_2$Pd(dba)**
23	**$C_{10}H_6$(2,3-$CH_2PBu^t_2)_2$**	**(L-L)Pd(dba)**
24	**DPEphos**	**(L-L)Pd(dba)**
25	**o-$C_6H_4(CH_2PBu^t_2)_2$**	**(L-L)Pt(dba)**

26	o-$C_6H_4(CH_2PBu^t_2)_2$	(L-L)Pd(styrene)
27	o-$C_6H_4(CH_2PBu^t_2)_2$	(L-L)Pd(BQ)
28	$C_{10}H_6(1,8\text{-}CH_2PBu^t_2)_2$	(L-L)Pd(BQ)
29	$1,4\text{-}C_4H_8(PBu^t_2)_2$	(L-L)Pd(BQ)
30	o-$C_6H_4(CH_2PCy_2)_2$	(L-L)Pd(BQ)
31	o-$C_6H_4(CH_2PPh_2)_2$	(L-L)Pd(BQ)
32	$1,3\text{-}C_3H_6(PBu^t_2)_2$	(L-L)Pd(BQ)
33	$C_{10}H_6(2,3\text{-}CH_2PBu^t_2)_2$	(L-L)Pd(BQ)
34	DPEphos	(L-L)Pd(BQ)
35	xantphos	(L-L)Pd(BQ)
36	dppf	(L-L)Pd(BQ)
37	o-$C_6H_4(CH_2PBu^t_2)_2$	(L-L)Pd(tcne)
38	o-$C_6H_4(CH_2PPh_2)_2$	(L-L)Pd(tcne)
39	DPEphos	(L-L)Pd(tcne)
40	o-$C_6H_4(CH_2PBu^t_2)_2$	^{1}(L-L)Pd(OAc)$_2$
41 [2]	o-$C_6H_4(CH_2PPr^i_2)_2$	^{2}(L-L)Pd(OAc)$_2$
42 [2]	$1,3\text{-}C_3H_6(PBu^t_2)_2$	^{2}(L-L)Pd(OAc)$_2$

1. Generated in-situ **2.** See chapter 5 for complex numbers

Table 2.0 Key to Catalyst Testing

2.3 Results

The results are presented in sections, where groups of related complexes are compared and discussed. Within each group, a standard complex **(12)** is presented for comparative purposes which was tested as part of the same series of tests where possible. In some cases more than one set of data for the standard **(12)** is presented; this serves to illustrate the variability within the data.

2.3.1 Catalysts Based on 1,2-bis(di-*tert*-butylphosphinomethyl)benzene (1)

The data for this series of experiments is presented in Table 2.1, Table 2.2, Figure 2.0 and Figure 2.1. The two graphs illustrate the rate versus time profile and the catalyst total

turnover frequency (moles MeP/mole Pd) against time. The first point to notice from Figure 2.0 and the data in Table 2.1 is the very high initial rates observed for these complexes and the rapid decay indicated by the steep slope of the line in the rate versus time plot. Taking complex **(12)**, the initial rate of 33000 moles MeP/mole Pd/hr drops to 16500 after 15 minutes, suggesting 50% of the catalyst is deactivated in this period. The rate of decay slows throughout the course of the reaction or, put another way, the catalyst half-life increases with time. This is indicated in Table 2.1 below.

Time(mins)	0	15	43	108	240
Rate (moles MeP/mole Pd/hr)	33,000	16,000	8,000	4,000	2,000

Table 2.1 Rate Versus Time Data For (12)

Complex	Initial Rate[1]	TON[2]	Selectivity
12	32,000	24,000	MeP
26	52,000	30,000	MeP
27	23,000	20,000	MeP
40	13,000	18,000	MeP
37	0	n/a	n/a

1. maximum initial rate moles MeP/mole Pd/hr. **2.** after 4 hours.

Table 2.2 Catalyst Test Results for Complexes of 1,2-bis(di-*tert*-butylphosphinomethyl)benzene

Activation of the catalyst by the addition of methanesulphonic acid to the dba complex **12** results in an immediate colour change from orange to deep red/purple. It is this solution that is fed to the autoclave as the reaction solution. When we perform the catalysis in the laboratory glass autoclave, we observe that the red/purple colour persists as we heat the solution to reaction temperature. On pressurization with CO/ethene gas uptake begins immediately and the red/purple colour begins to disappear. After 15 minutes the catalyst solution is pale yellow in colour and no further colour change is evident over the reaction period. This indicates that the red/purple complex formed on addition of acid has an efficient route into the catalytic cycle but is not part of the catalytic cycle itself. The nature of this compound and its route into the catalytic cycle is discussed in chapter 4 of this thesis,

where the reactions of several phosphine palladium(0) dba complexes with sulphonic acids have been studied. The other complexes of this xylyl ligand which show activity **(26, 27)**, react immediately with methanesulphonic acid to give a pale yellow solution, and this colour remains constant throughout the catalysis.

Figure 2.0 Influence of Palladium Pre-catalyst on Rate of MeP Made Versus Time for Complexes of 1,2-bis(di-*tert*-butylphosphinomethyl)benzene

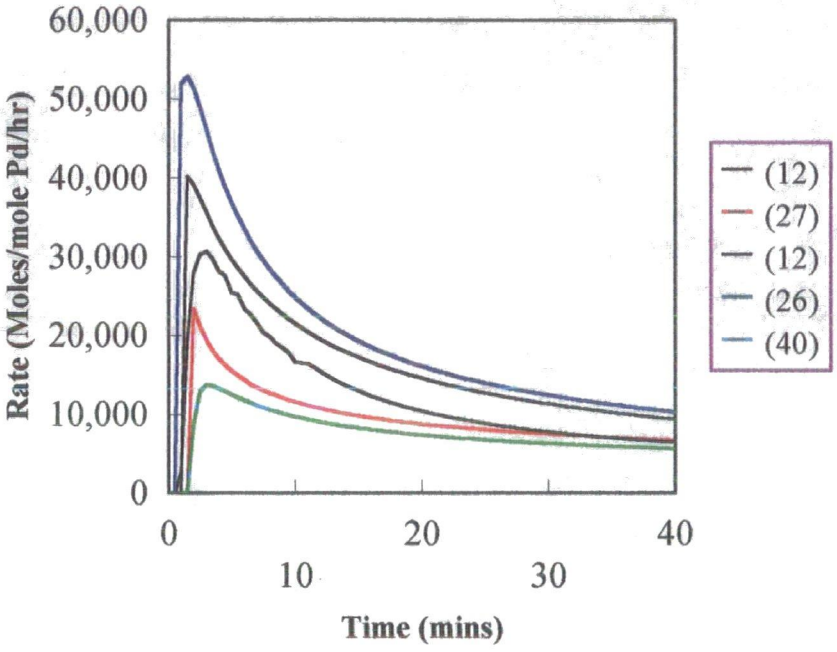

Figure 2.1 **Influence of Palladium Pre-catalyst on Turnover Number in MeP Synthesis for Complexes of 1,2-bis(di-*tert*-butylphosphinomethyl)benzene**

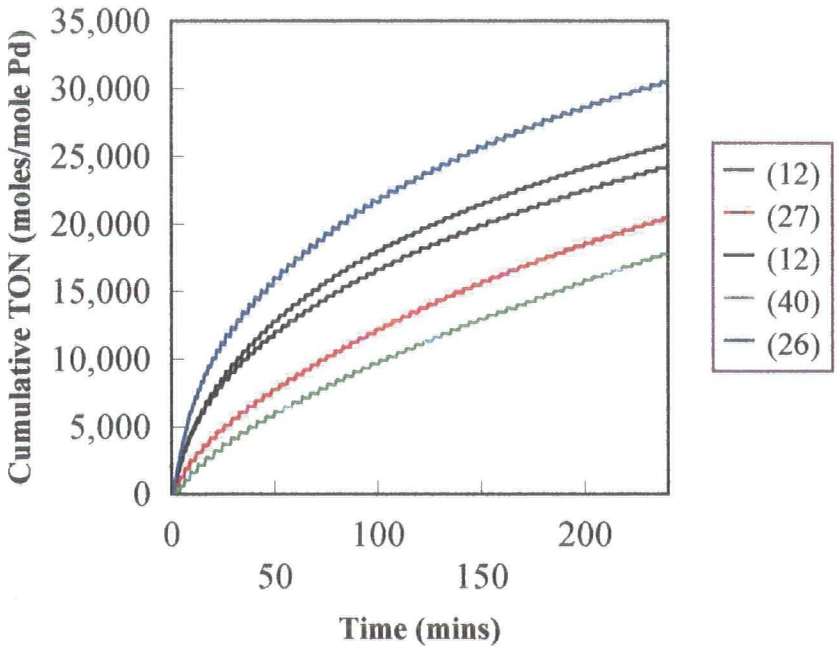

Looking at the data in Table 2.2, the first point to note is the significant difference in both initial rate and total turnover for palladium zero complexes of the xylyl ligand with different coordinated alkenes. The activity decreases in the following order styrene **(26)** >dba **(12)** >benzoquinone **(27)** >tcne **(37)**, with no induction periods apparent for any of these complexes under the standard conditions applied in this study. The styrene complex exhibited an exotherm on admission of CO/ethene, a feature not observed for the dba or benzoquinone complexes under standard conditions. This may suggest that there is a higher concentration of active catalyst resulting from activation of this pre-catalyst complex. The tcne complex **37** did not result in any observed catalytic activity. Where catalytic activity was observed, selectivity was in excess of 99% to MeP. The alternate alkenes present in the precursor complexes did not influence the reaction selectivity.

The reduced activity of the benzoquinone complex **27** is surprising given the common claim for the use of benzoquinone in patent literature, where it is added to increase catalyst lifetime.[1] We observe a reduction in initial rate of approximately 28% with no effect on catalyst stability i.e. the benzoquinone catalysts still exhibit rapid decay. This reduction in

activity for benzoquinone pre-catalysts is also observed for complexes of 1,3-bis(di-*tert*-butylphosphino)propane where the initial rate drops from 9000 moles MeP/mole catalyst/hr for the dba complex **(20)** to 3600 moles MeP/mole catalyst/hr for the benzoquinone complex **(32)**. This data is presented in Figure 2.4 and Table 2.5.

Palladium acetate, when used as a palladium source, also seems to give uniformly reduced activity for 1,3-bis(di-*tert*-butylphosphino)propane. Again, this seems surprising given the abundant patent literature claiming combinations of phosphine ligand and palladium acetate as the preferred combination for catalytic activity in systems for co-polymer formation using dppp.[2] This may, of course, be driven solely by economic concerns with palladium acetate being a readily available commercial source of palladium. The coordination chemistry of these ligands with palladium acetate is reported in chapter 5.0 and further addresses this effect.

The catalyst solutions from the reactions have been analysed by GC-MS and found to contain the same common minor components in all cases. The GC-MS results are summarised in Table 2.3 with the suggested likely source of each component indicated.

Several important points can be made from an analysis of this data:

1) The presence of palladium hydride and/or the hydride mechanism is implicated from the by-product analysis. Firstly, butene is detected. This could be an impurity in the ethene supply, but more likely results from the insertion of ethene into a palladium ethyl to form a palladium butyl fragment followed by β hydride elimination to give an alkene hydride and finally dissociation of the butene from the metal centre. The initial palladium ethyl fragment also derives from ethene insertion into a palladium hydride. Palladium catalysts of the type $[(L\text{-}L)Pd(X)_2]$, which produce co-polymers in the presence of carbon monoxide and ethene, will also oligomerise ethene if all of the carbon monoxide is consumed and only ethene remains. Furthermore, re-admission of CO leads to the continued formation of co-polymers.[3] Secondly, the formation of diethylketone most likely results from the insertion of a second ethene molecule into a palladium acyl fragment followed by protonolysis which can only have arisen from the hydride mechanism. The extremely high selectivities in the catalysis suggest that this does not occur very frequently. Thirdly, the formation of

formaldehyde via the oxidation of methanol is a known route to palladium hydride. This has been proposed by Drent and others as a likely route into the hydride mechanism in the absence of acid[4].

Species Identified	Likely Source
Formaldehyde	palladium catalysed methanol oxidation
dimethyl ether	methanol impurity/acid catalysed dehydration
butene	ethene dimerisation/ethene impurity
dimethoxymethane	methanol impurity/methanol + formaldehyde
diethyl ketone	2nd ethene insertion
$CH_3CH_2CO(CH_2)_2OCH_3$	co-polymerisation
propionic acid	water terminates catalytic cycle/ester hydrolysis
methyl ester of methane sulphonic acid	methanesulfonic acid + methanol
benzaldehyde	dba fragment
benzene acetic acid(α methoxy)methylester	dba fragment
methyl benzoate	dba fragment
$CH_3CH_2CO(CH_2)_2COOCH_3$	co-polymerisation
phenylpropenoic acid methylester	dba fragment

Table 2.3 GC-MS Characterization of Minor Species Present after Catalysis

2) There is evidence of further insertions of both ethene and carbon monoxide to give oligomeric species but, as with butene and diethyl ketone formation, this occurs extremely infrequently. It is not clear whether this high selectivity to MeP observed in this system is a thermodynamic or kinetic effect. A thermodynamic effect, whereby the further insertions are disfavoured on steric grounds due to the ligand bulk and termination of the catalytic cycle, is the favoured reaction, as opposed to a kinetic effect, whereby the termination of the catalytic cycle by methanolysis (hydride mechanism) or protonation (methoxycarbonyl mechanism) is very much faster than the rate of further insertion reactions.

3) The dba component of the catalyst may be degraded in the catalysis. This is not surprising given that dba contains two double bonds which can potentially coordinate to the metal centre.

4) The formation of methylmethanesulphonate demonstrates an unwanted acid-consuming reaction. This is important in any continuous process where ratios of acid:metal may need to be maintained. Acid needs to be fed continuously to the reaction to maintain a constant concentration.

In conclusion, the highest initial rates and turnover numbers for catalysts based on 1,2-bis(di-*tert*-butylphosphinomethyl)benzene are obtained using palladium(0) alkene complexes as the pre-catalyst. Most notably, the use of dba and styrene complexes in preference to benzoquinone complexes is found to give the best results. The use of the very strongly coordinating alkene, tcne, results in no catalytic activity whatsoever.

2.3.2 Variation of Xylene Phosphorus Substituent

The data for this series of experiments is presented in Table 2.4, Figure 2.2 and Figure 2.3. The two graphs illustrate the rate-versus-time profile and the catalyst total turnover against time. Surprisingly, the change from *tert*-butyl groups **(12)** to iso-propyl groups **(13)** on the phosphine results in the formation of some co-polymer. It is noteworthy that changing a methyl group for a proton results in a change in selectivity of the catalyst. According to literature precedent, both steric and electronic modifications are being made to the catalyst, and therefore it is difficult to assign the reactivity differences to one or the other. The synthesis of these complexes and their study by single crystal X-ray diffraction, reported in chapter 3.0 are attempts to deconvolute steric and electronic differences in the ground state and relate these to catalytic activity.

The phosphine ligands 1,3-bis(di-*iso*-propylphosphino)propane and 1,3-bis(di-*iso*-butylphosphino)propane have been claimed in patent literature to give polyketones in related palladium systems.[5] This, relative to the known selectivity to MeP of the closely related 1,3-bis(di-*tert*-butylphosphino)propane system, is similar to our findings

although, in the system studied in this thesis, only small amounts of polyketone are formed; the main catalytic product is MeP.

Also noteworthy for complex **13** is the much lower maximum initial rate and the time period taken to achieve maximum rate. This suggests that the activation of this catalyst is slower than for **12**. This induction period before maximum initial rate is attained is also a feature of the reactivity of complexes **15**, **16** and **17**. It would also appear that the longer the induction period, the lower the maximum initial rate. This may be relevant if one considers that there is a competition between activation of the precursor and its deactivation/decay, where the pre-catalyst may form a catalytically inactive species without ever having entered the catalytic cycle. Thus, efficient activation may give rise to very different results from those obtained in this study. The induction period effect also seems to be relevant only for the dba complexes, implying that dba is involved in the pre-catalytic intermediate complex.

It should be pointed out that the data presented in Figure 2.2 indicates that the catalysts have no activity throughout the induction period. In fact, this is not the case, but the data is unusable due to variations in the reservoir pressure resulting from temperature fluctuations on admitting gas to the autoclaves. These effects are only significant where low rates of gas uptake are analysed. The data presented is from the point where stable gas uptake could be monitored. Rate of gas uptake in the induction period is, in all cases, lower than the maximum initial rate illustrated in Figure 2.2 and Table 2.4.

Complex	Initial Rate[1]	TON[2]	Selectivity[3]	Lag Time[4]
12	35,000	24,000	MeP	0
13	5,800	6,000	MeP/Co-poly	18
14	0	0	trace co-poly[5]	n/a
15 frac 1	1,300	3,500	MeP	37
15 frac 2	2,300	5,000	MeP	33
16	1,000	2,400	MeP	45
17	5,800	6,400	MeP	9
18	0	0	n/a	n/a

1. Maximum initial rate moles product/mole catalyst/hr. **2.** After 4 hours. **3.** Where both MeP and co-polymer are formed the amounts of each have not been determined. **4.** Time taken before maximum initial rate is attained. **5.** Co-polymer forms as white precipitate in the catalyst solutions.

Table 2.4 **Influence of Phosphorus Substituent in the Ligand $C_6H_4(CH_2PR^1R^2)_2$ on the Methoxycarbonylation of Ethene**

Figure 2.2 **Influence of Phosphorus Substituent in Xylene-Based Catalysts on Rate of MeP Made Versus Time**

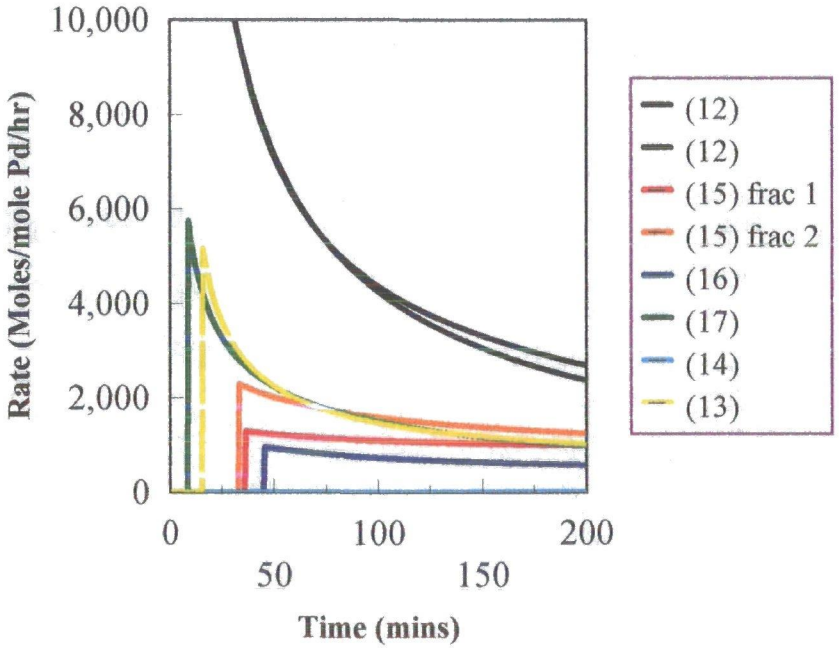

The cyclohexyl substituted phosphine ligand gives rise to catalysts which are almost completely inactive under the standard set of conditions applied in this study. A small amount of co-polymer is formed as a white insoluble precipitate, but the quantity is so small

that it does not register as a gas uptake on the monitoring equipment. This extreme sensitivity of the catalyst activity to small modifications in the steric and electronic properties of the phosphine ligand is surprising. The activity of this phosphine ligand has also been evaluated using alternative palladium(0) sources and more forcing conditions (see section 2.4.5).

The catalyst **15**, derived from the mixed substituent phosphine **3** (see chapter 3.0), has been evaluated as two separate fractions. This is due to the presence of stereo-isomers of this ligand which generate sterically different catalysts on coordination. Whilst it has not been possible to isolate pure fractions of a single stereo-isomer of the catalyst, it has been possible to generate two solid samples which contain significantly different amounts of specific isomers. This determination has been made by analysis of the ^{31}P NMR spectrum, where both samples give rise to different intensities of signals corresponding to different stereo-isomers (see chapter 3.0). The result of this study shows that the two isomeric materials do, in fact, have slightly different activities in the methoxycarbonylation of ethene. Surprisingly, though the presence of at least one *tert*-butyl group leads to MeP selectivity, no evidence for co-polymer formation was found. This result would seem to indicate the dominance of steric factors over electronic factors, with the electronic contribution from the isomers being constant.

Also of interest for these complexes is the long induction times. The maximum initial rate occurs after more than 30 minutes for both fractions. It seems surprising that changing one tert-butyl group for a cyclohexyl group on each phosphorus, (ie, changing from **12-15**) has such a profound effect on the activation mechanism. Studies in the laboratory autoclave with these stereochemical isomers indicate possible increased stability at elevated temperatures, with no evidence of palladium metal in catalyst tests carried out at 100^{0}C. The comparable experiment with complex **12** does generate palladium metal under these conditions.

Figure 2.3 Influence of Phosphorus Substituent In Xylene-Based Catalysts on MeP Made Versus Time

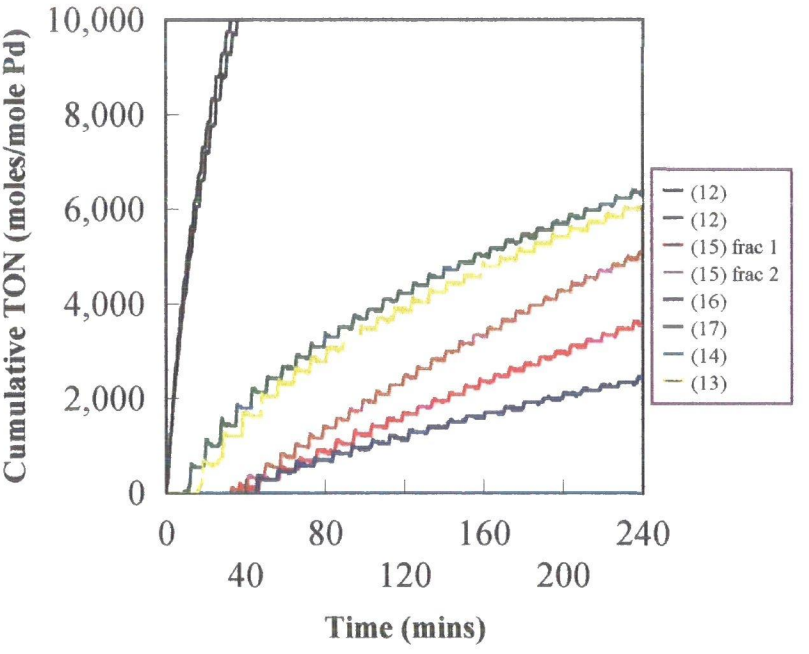

The *tert*-pentyl group in complexes **16** and **17** was introduced originally as a sterically less demanding but electronically similar group to *tert*-butyl. It was envisaged that the introduction of this group would give catalysts of comparable activity to **12** with enhanced stability. It was envisaged that the presence of an ethyl group in place of a methyl would allow release of steric congestion more easily. The results of this study show that comparable activity is clearly not the case. Again, the extreme sensitivity of the catalyst system to changes in the phosphorus substituent is apparent. The catalyst resulting from the mixed substituent phosphine **17** has been used as a mixture of isomers and shows low initial rates with long induction periods similar to those observed for the fractions of **15**. The complex **16**, on the other hand, shows much higher initial rates and much shorter induction periods, but still much lower than the standard (**12**).

The last complex tested was that derived from the phenyl substituted ligand **18**, where no activity was detected. Again this is surprising, given the known propensity of dppp and dppb complexes of palladium to give co-polymers under similar reaction conditions. Perhaps relevant is the observation from the laboratory autoclave that the red/purple colour, generated

on addition of methanesulphonic, persists throughout the catalysis, suggesting that formation of an active species is not occurring.

In conclusion, the catalysis is extremely sensitive to variations in the phosphorus subsistent on the xylene backbone. Only the dba complexes have been tested in this series and the long induction periods, before maximum initial rate is obtained, may be a function of activation of these species. The reaction of the dba complexes with acid results in the formation of deep red solutions, which persist for some time in the catalysis. Notably, though, solutions of the most active catalysts and solutions taken from the semi tech autoclave runs are all pale yellow in colour. This suggests that the complexes resulting from reaction of methanesulphonic acid with the dba complexes may have differing reactivity. As mentioned in the case of the dba pre-catalyst **(18)**, which incorporates the phenyl-substituted ligand **(8)**, a red colour persists throughout the test duration and no catalysis is observed. This ligand, tested as a benzoquinone pre-catalyst complex **(31)**, has been shown to result in polyketone formation. This again implicates the product of reaction of the dba complex with sulphonic acid. The reaction of all these complexes with sulphonic acids is investigated in chapter 4.0 of this thesis to further understand these effects.

2.3.3 Other *tert*-Butyl Substituted Bidentate Phosphines

2.3.3.1 Catalysts Based on Bidentate Alkyl Phosphines 1,2-bis(di-*tert*-butylphosphino)ethane, 1,3-bis(di-*tert*-butylphosphino)propane, 1,4-bis(di-*tert*-butylphosphino)butane

The data for this section is presented in Table 2.5 and Figures 2.4. and 2.5 to allow easy comparison within the series. Taking the simple alkyl bridged phosphines dbu^{t}pe, dbu^{t}pp, dbu^{t}pb, having a 2-, 3- and 4-carbon bridges respectively, only the 3-carbon bridged diphosphine results in any detectable catalytic activity. The dba complex **19** gives rise to an initial activity of 9000 moles MeP/mole Pd/hr and a total turnover number of 6000 moles MeP/Pd. The 2-carbon bridged diphosphine (dbu^{t}pe) is interesting in that there is no evidence for catalyst decomposition with perfectly clear solutions being recovered after catalyst testing. Interestingly, the ligand dcpe is reported when mixed with palladium acetate to result in catalysts which show good activity for co-polymer formation.[6] The total inactivity of the 4-carbon alkyl bridge phosphine complex **(29)** can be ascribed to its

instability under reaction conditions, with palladium metal being observed almost at once on introduction of CO/ethene to the system. Certainly one would have predicted a reduction in activity on going from dbu'pp to dbu'pb in line with the trend observed in going from dppp to dppb in the co-polymerisation catalysis.[3] The total lack of activity and rapid decomposition is, though, surprising; clearly the nature of the 4-carbon bridge complex is important in maintaining stability given the high activity achieved with the xylene bridged phosphine **(12)** complex.

Complex	Initial Rate[1]	TON[2]	Selectivity
(12)	27000	9000	MeP
19[3,4]	0	0	n/a
20	9,000	6,000	MeP
29	0	0	n/a
20	7,000	5,000	MeP
42	5500	3300	MeP
42	3800	1800	MeP
32	3600	1500	MeP
12[4]	n/a	5000	MeP
23[4]	n/a	4000	MeP
33	15000	6000	MeP
27	23000	20000	MeP
28	0	0	n/a

1. Maximum initial rate moles product/mole catalyst/hr. **2.** After 4 hours.

3. No evidence of decomposition. **4.** Carried out in lab autoclave.

Table 2.5 Influence of Phosphine Bridge Length on Activity in the Methoxycarbonylation of Ethene

The maximum activity of catalysts based on the propane-bridged diphosphine **(20)** is approximately one third that obtained with the analogous xylene phosphine based catalyst **(12)**. The reaction profiles are, however, similar with high initial activity and rapid decay observed. The catalysts derived from the dba pre-catalyst **(20)** give the highest initial rates and total turnovers, with those catalysts derived from the benzoquinone and acetate giving lower activity. This is in line with the observations for the catalysts based on 1,2-bis(di-*tert*-butylphosphinomethyl)benzene.

Figure 2.4 **Rate Versus Time Plot for Complexes of 1,3-bis(di-*tert*-butylphosphino)propane**

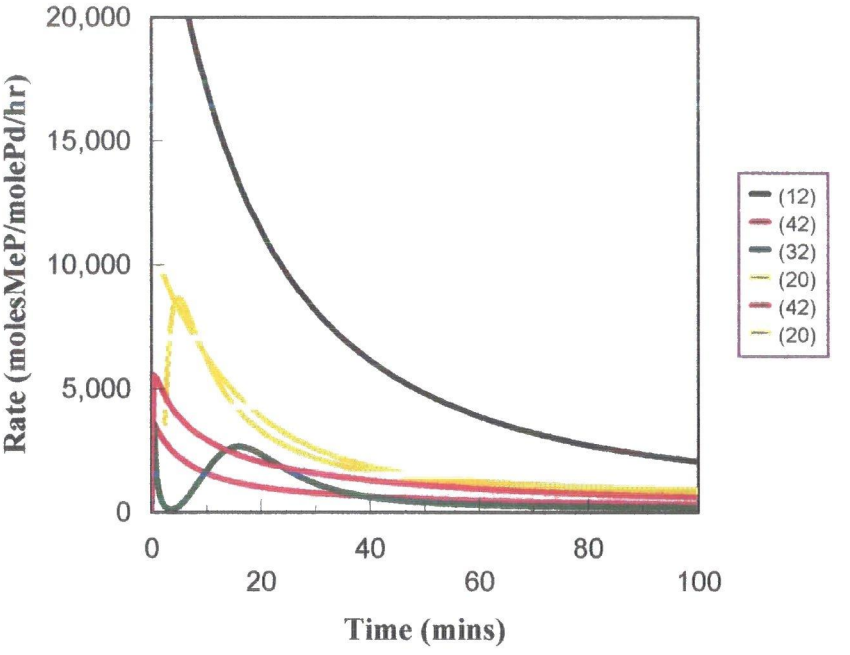

Figure 2.5 **Turnover Number Plot for Complexes of 1,3-bis(di-*tert*-butylphosphino)propane**

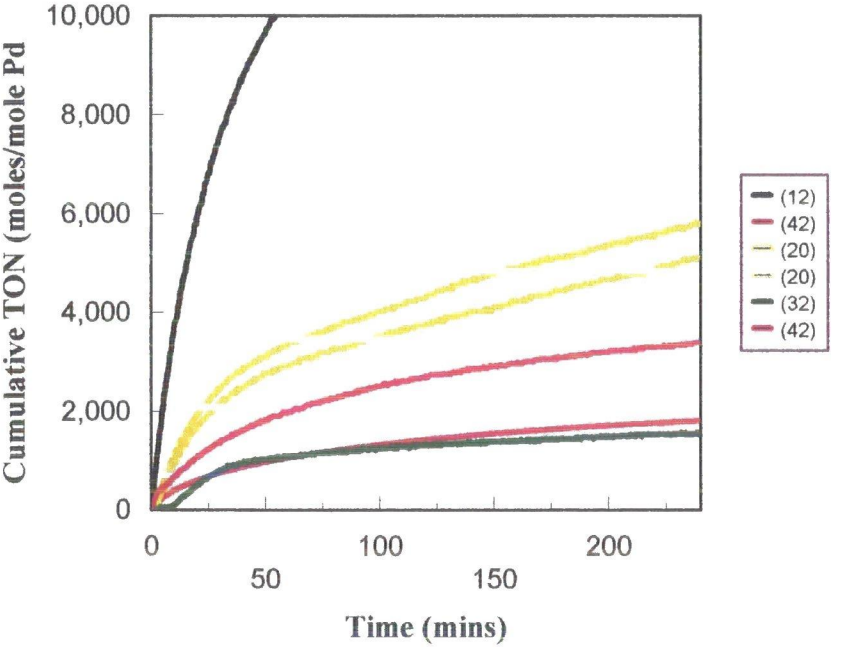

2.3.3.2 Catalysts Based on Naphthyl Backbones 2,3-bis(di-*tert*-butylphosphinomethyl)naphthalene and 1,8-bis(di-*tert*-butylphosphinomethyl)naphthalene

The data for this section is presented in Table 2.5 and has not been illustrated graphically. The ligand 2,3-bis(di-*tert*-butylphosphinomethyl)naphthalene gives activities which are lower than those obtained for complexes of the ligand 1,2-bis(di-*tert*-butylphosphinomethyl)benzene. The dba complexes have only been compared using data collected using the laboratory autoclave **(12, 23)**, but a significant difference of 1000 turnovers is observed. The benzoquinone complexes **(27, 33)** differ quite significantly with lower initial rates and total turnovers observed for **(33)**. Interestingly, the catalysts based on 1,8-bis(di-*tert*-butylphosphinomethyl)naphthalene **(28)** show a complete lack of activity. In a similar manner to the catalyst based on **(29)**, catalyst decomposition occurs rapidly with palladium metal observed immediately on addition of CO/ethene. The 1,8-bis(di-*tert*-butylphosphinomethyl)naphthalene ligand was synthesised to generate catalysts where the P-Pd-P bite angle is $>105^0$ and it seems likely that the P-Pd-P chelate ring formed is not stable. This is not unreasonable given the fact that the chelate ring would contain 8 atoms and large ring sizes would be anticipated to be less stable than smaller ring sizes.

2.3.4 Catalysts Based on 1,2-bis(di-*iso*-propylphosphinomethyl)benzene Influence of Pre-catalyst Form on Catalytic Activity

The data for these experiments is presented in Table 2.6 and Figure 2.6 and 2.7. In this example, the rate-versus-time plot is illustrated and this clearly shows the difference in rate over the course of the reaction for the two complexes. The dba complex **(13)**, also discussed in section 2.4.1, exhibits a high maximum initial rate which is achieved after a short induction period, whereas the acetate complex **(41)** exhibits a much lower initial rate but the rate of catalyst decay, as judged by visual inspection of the slope of the rate-versus-time plot, appears to be slower. The turnover number plot also shows a marked difference between the two complexes, with the catalyst based on the acetate complex giving a higher total turnover than the initial rate; a feature not observed for any of the other alkyl-substituted xylene-based ligand systems. Both of these catalyst solutions, when removed from the autoclave, showed evidence for the formation of co-polymers, evidenced

by a fine white precipitate which settled out on standing. The amount of co-polymer, though, is difficult to ascertain accurately as it coats the insides of the autoclave. In both of these examples, less than 200mg was isolated.

Complex	Initial Rate[1]	TON[2]	Selectivity
(13)	5,800	6,000	MeP/Co-poly
41	1,100	3,300	MeP/Co-poly

1. Maximum initial rate moles product/mole catalyst/hr. 2. After 4 hours.

Table 2.6 Comparison of Activity in Complexes of 1,2-bis(di-*iso*-propylphosphinomethyl)benzene

Figure 2.6 Rate Plot for Complexes of 1,2-bis(di-*iso*-propylphosphinomethyl)benzene

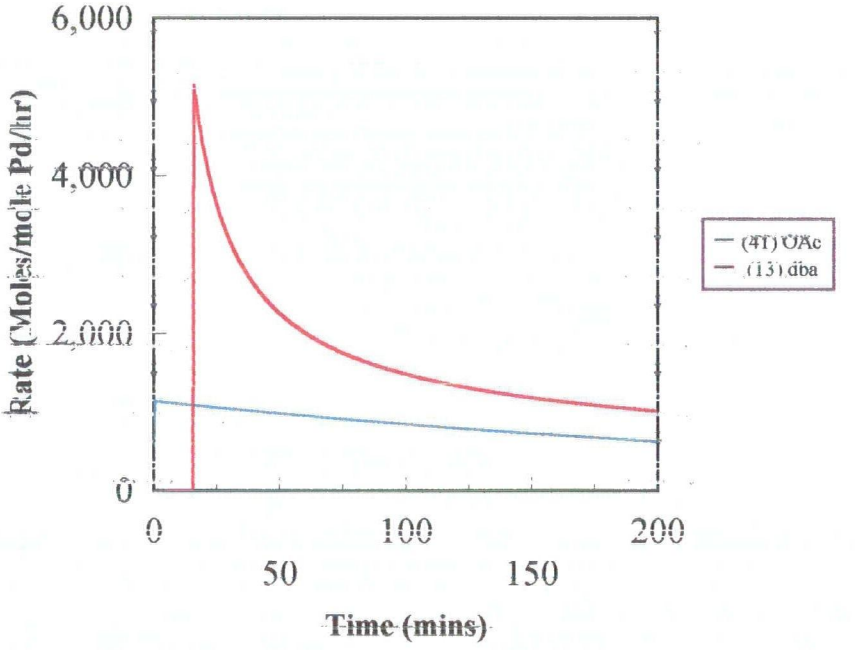

Figure 2.7 Turnover Plot for Complexes of 1,2-bis(di-*iso*-propylphosphinomethyl)benzene

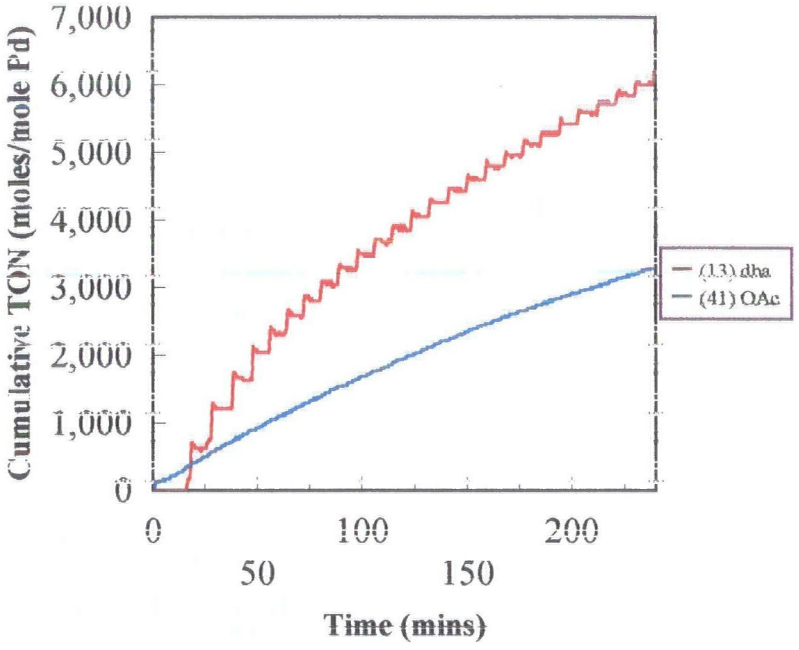

2.3.5 Catalysts Based on Phenyl-Substituted Phosphine Ligands

Comparison of the Activity of some Novel Phenyl-Substituted Bidentate Phosphines in the Methoxycarbonylation of Ethene

The results of catalytic testing studies for catalysts derived from several phenyl-substituted bidentate phosphine ligands are displayed in Table 2.7 and selected examples are illustrated in Figure 2.8 (rate-versus-time plot) and Figure 2.9 (turnover-versus-time plot). The catalysts derived from the phosphine ligand DPEphos **(24, 34)** and Xantphos **(35)** both give MeP with the DPEphos-derived catalyst giving small quantities of co-polymer. Final solutions of the DPEphos catalysts were slightly cloudy on removal from the autoclave, indicating co-polymer formation. This was not observed in the same system when tested in the laboratory glass unit. The glass autoclave, because of the inefficent stirring mechanism, is felt to be mass-transfer limited with respect to CO. Thus, in the efficiently stirred Semi Tech autoclaves, the further insertion of CO occurs more often, resulting in some co-polymer formation. The formation of co-polymer is confirmed by I.R. analysis of the solid which settles out on standing. These ligands represent the first examples of phenyl-substituted bidentate phosphines which give preferentially MeP and not

co-polymers. The initial rates are significantly less than the most active *tert*-butyl-substituted phosphine-based catalysts, but the stability seems very different. The initial rate for the DPEphos catalyst introduced as the dba complex is 1700 moles product/mole catalyst/hr which falls to 1000 moles product/mole catalyst/hr after 4 hours. The initial half life is of the order of hours rather than minutes observed for the most active catalysts **(12)** studied. The dba complex **(24)** is more active than the BQ complex **(34)**, in line with the trend observed for the other MeP selective catalysts tested in this study. It also exhibits an induction period before maximum initial rate is achieved, again in line with the observations for many of the catalysts introduced as dba complexes.

The two other ligands evaluated in this section 1,2-bis(diphenylphosphinomethyl)benzene and dppf both produce co-polymer . The former, when evaluated as the BQ complex **(31)**, gave co-polymer at a constant rate. Catalyst stability is very much less than observed for the highly MeP selective systems. Also of interest is the lack of activity of the dba complex **(18)** when evaluated in the laboratory autoclave. The activation of this complex is similar to that observed for the other dba complexes tested **(12-17)** with a dark red colour developing on addition of acid. In the catalyst test, this red colour persisted throughout the course of the run, suggesting that the conversion to a catalytically active species is not occurring extensively in this case.

The BQ complex **(31)** on addition of methanesulphonic acid rapidly forms a yellow solution and this, when added to the S T autoclaves, generates co-polymer. In one experiment under standard conditions, 8.0g of co-polymer was isolated. This observation of increased activity and stable rates (see Figure 2.8) with the BQ complexes for co-polymer selective catalysts contradicts the trend observed for MeP selective catalysts where the dba complexes are the more active and catalyst stability is poor. The reactions of these complexes with sulphonic acids is discussed in chapter 4.0 in an attempt to understand these results.

The catalyst activity of dppf complexes, on the other hand, is unremarkable with co-polymer being formed at low rates with moderate to poor stability observed for the catalyst complexes.

Figure 2.8 Rate Versus Time Plot for Phenyl Substituted Bidentate Ligands

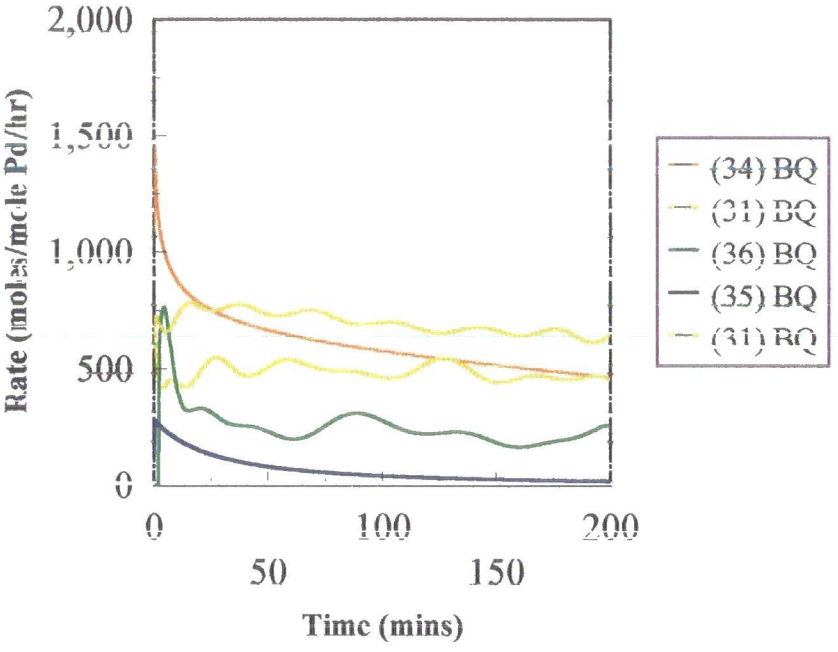

Figure 2.9 Turnover Plot for Phenyl Substituted Bidentate Ligands

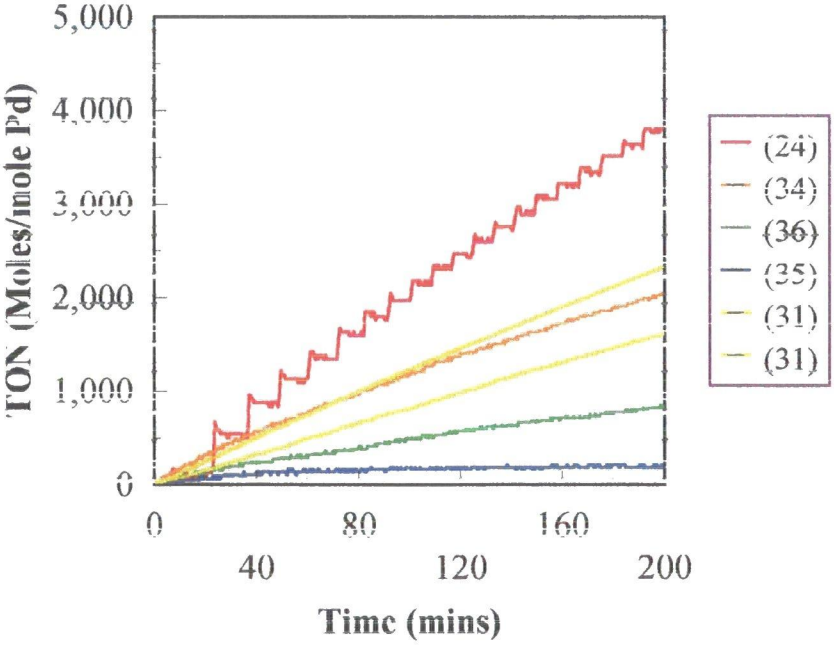

Complex	Initial Rate[1]	TON[2]	Selectivity[3]
24	1,700	4,500	MeP/co-poly
34	1,500	2,300	MeP/co-poly
35	270	650	MeP
36	750	1,400	co-poly
22	0	0	MeP
21	n/a	n/a	co-poly
31	600	2,000	co-poly
31	700	2,700	co-poly

1. Maximum initial rate moles product/mole catalyst/hr. 2. After 4 hours.
3. Where both MeP and co-polymer are formed the amounts of each have not been determined. 4. Time taken before maximum initial rate is attained.
5. Carried out in lab autoclave.

Table 2.7 Comparison of the Activity of Some Phenyl Substituted Bidentate Phosphines on Activity in the Methoxycarbonylation of Ethene

2.3.6 Characterization of Co-Polymer

The co-polymer formed from utilizing the complex **(31)** has been characterized by MALDI-TOF mass spectroscopy and the result illustrated in Figure 2.10 below. This shows the mass spectrum obtained, with expansions of the data at either end of the molecular weight range detected. Several points can be made from this data:

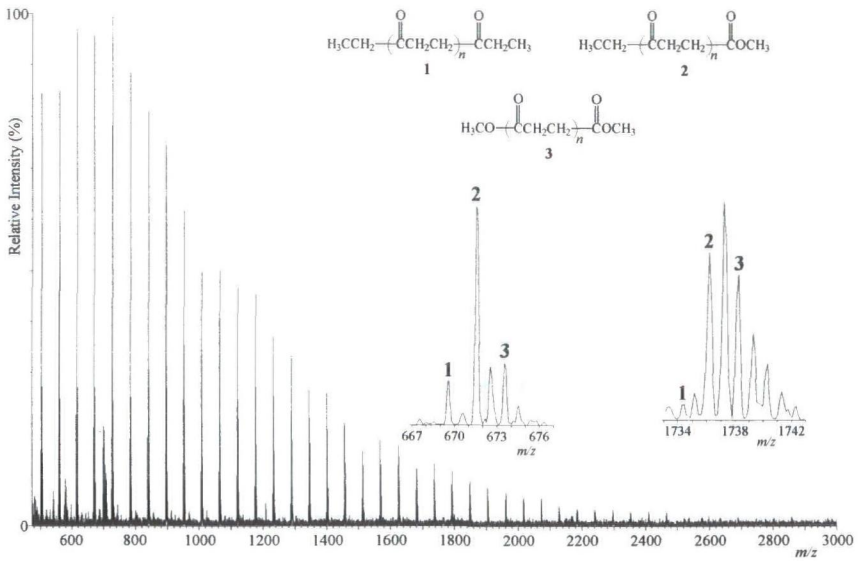

MALDI-TOF Spectrum of Ethene/CO Copolymer

Figure 2.10

1) The co-polymer repeat units of 56 mass units can be easily seen. Moreover, an expansion of the spectrum reveals the presence of different polymer end groups. The two possible mechanisms (hydride Vs methoxycarbonyl) give rise to different initiation and termination pathways. This leads to three possible combinations of polymer end groups. These are i) "diketone" having COC_2H_5 at each end resulting from hydride initiation and termination, ii) "ketoester" having COC_2H_5 at one end and $COOCH_3$ at the other; this arises from initiation by one mechanism and termination by the other, and iii) "diester" resulting from methoxycarbonyl initiation and termination. The presence of all three end groups is revealing as it demonstrates that, in the co-polymerisation selective catalysts, both mechanisms are in operation.

2) The relative proportions of the three polymer types described above appear to change with increasing molecular weight. The proportion of the "diester" product is much less in the low molecular weight end of the spectrum, where the "diketone" and "ketoester" polymer ends predominate. At the high molecular weight end, however, the proportion of the "diester" ended polymer is much higher. This implies a favouring of the methoxycarbonyl mechanism for the production of high MW polymer.

2.4 Conclusions

Several general conclusions can be made from the catalyst testing results. As mentioned previously, the remainder of this thesis presents the results of experiments designed to further understand and explain the observed experimental data.

1. Within the xylene-based family of phosphine ligands, catalyst activity shows an acute sensitivity to phosphorus substituent. The *tert*-butyl substituted ligand leads to highly active, if unstable, catalyst systems. Small variations in the phosphorus substituent lead to a substantial reduction in catalytic activity, although there is some indication that the catalysts are more stable. Also apparent is the decrease in selectivity on moving to less sterically demanding and more π acidic phosphine ligands. The extreme situation is for the phenyl-substituted xylene-based phosphine which is selective for co-polymer. It is not possible to deconvolute the steric and electronic influences of the phosphine ligand without more detailed study. In chapter 3 the palladium pre-catalysts are characterised in detail in order to understand the electronic and steric differences the phosphine ligands impart at the metal centres.

2. Of the *tert*-butyl substituted ligands studied, only the propane-bridged and the rigid xylene and naphthyl-bridged ligands give rise to MeP selectivity. It is clear that there is something special about the xylene/naphthyl backbone which is important for MeP selectivity. The simple 4-carbon butyl bridge, which also would result in a seven-membered chelate ring, decomposes rapidly under catalytic conditions giving no MeP.

3. The nature of the palladium pre-catalyst complex, used for catalyst testing, has a large influence on the observed catalytic activity, with an indication that the catalyst activation is sensitive to the nature of the other ligands present. The reactions of these pre-catalyst complexes with sulphonic acids are reported in chapter 4.0 and the data fully discussed in order to better understand this effect.

4. The use of phenyl substituted diphosphine complexes to synthesize MeP has been demonstrated for the first time. The synthesis and characterization by X-ray crystallography of these complexes are discussed in chapter 2.0. Common features in the ground state of the

pre-catalyst complexes are explored to develop a unifying theory which explains the observed selectivites.

5. Catalysts having good stability which make co-polymers have been identified. Stability is desirable in the synthesis of MeP and the stability/selectivity relationship is explored in later chapters.

2.5 References

1. E. Drent and J. A. Van Broekhoven; Eur. Pat. Appl. 235, 865. **1987**.
2. E. Drent; Eur. Pat. Appl. 121, 965 A2. **1984**.
3. E. Drent, J. A. M. van Broekhowen and M. J. Doyle, *J. Organomet. Chem.*, **1991**, 417, 235.
   E. Drent and P. H. M. Budzelaar, *Chem. Rev.*, **1996**, 96, 663.
4. E. Drent and P.H.M. Budzelaar, *Chem. Rev.*, **1996**, 96, 663.
   M. Portnoy, F. Frolov and D. Milstein, *Organometallics* **1991**, 10, 3960
5. Chapter 1 and references therein.
6. Y. Koide, S. G. Bott and A. R. Barron, *Organometallics*, **1996**, 15, 2213.

CHAPTER 3

The Synthesis of Novel Phosphine Ligands and their Zerovalent Palladium Complexes

3.1 Introduction

As discussed in the previous chapter, the formation of alternating ethene/CO co-polymers and esters, resulting from alternating insertion of ethene and CO, is reported to be governed by the nature of the phosphine coordinated to the metal centre.[1] Bidentate phosphines are reported to lead to co-polymer formation and monodentate phosphines lead to ester formation in the presence of alcohols. The reported exceptions to this are limited[1] and the most striking illustration is the use of 1,3-bis(di-*tert*-butylphosphino)propane which, when combined with palladium acetate and a sulphonic acid, leads to the rapid conversion of ethene/CO and methanol to methyl propionate.[2] Latterly I.C.I. have developed a catalyst for this conversion which incorporates the phosphine ligand 1,2-bis(di-*tert*-butylphosphinomethyl)benzene.[3] This is claimed to have superior performance to the propane-bridged phosphine system.

In this chapter, the synthesis of a range of bidentate phosphine ligands based on the o-xylene backbone is reported. These ligands, along with several other ligands whose synthesis is known,[4] are then utilized in the synthesis of palladium (0) alkene complexes. The aim is to make a range of complexes of the type [(P-P)Pd(alkene)] for use as potential pre-catalysts in the methoxycarbonylation of ethene.

The synthesis of such complexes has been developed for a number of reasons. 1) It standardizes the evaluation of the catalytic activity based on known coordination geometry of the phosphine ligands. 2) It fixes the initial oxidation state at palladium (0). This is desirable given the reported result that the triphenylphosphine based catalyst systems which use palladium acetate generate palladium (0) in situ[5] in the form of $[(PPh_3)_4Pd]$. Thus the most well studied system, is known to be able to enter the catalytic cycle via a palladium (0) species. 3) It was hoped that, by varying the ligand structure whilst fixing oxidation state and

coordinated alkene, structure activity relationships could be developed. The catalytic activity using the palladium (0) alkene complexes as pre-catalysts has been reported in chapter 2 . Here, we report the synthesis and characterization by spectroscopic and crystallographic techniques. The features of the complexes are discussed with reference to published data. Several of the compounds synthesised in this study have been the subjected to single crystal X-ray diffraction techniques to study structure/property relationships in these catalysts.

The phosphine ligands synthesised and used in this study, and the complexes formed as palladium(0) pre-catalysts, fall into 3 categories.

1) Those based on the o-xylene backbone having the formula $[C_6H_4(CH_2PR^1R^2)_2]$, where R^1, R^2 can be Bu^t, Pr^i, Cy, Pe^t, Ph. The overall aim is to more accurately define the requirements of the ligand for activity in the palladium catalysed methoxycarbonylation of ethene.

2) Bidentate phosphines not having the o-xylene backbone. These include phosphine ligands with known activity in the catalysis under study (dppp, d^{t}bupp, PPh_3) and also new ligands designed to further define the requirements of the phosphine ligand in the palladium catalysed methoxycarbonylation of ethene.

3) Complexes based on the ligand $[o\text{-}C_6H_4(CH_2PBu^t_2)_2]$, with different bound alkenes. These variations in the alkene coordinated to palladium in the zerovalent pre-catalyst are to study the influence of the alkene on the initiation of catalysis.

3.2 Experimental Aspects

All reactions were carried out under a dry, oxygen-free nitrogen atmosphere, using standard vacuum line techniques. The solvents used were purchased in anhydrous form packaged under nitrogen in *sure seal* bottles and were used as supplied. Tetrahydrofuran was dried over sodium benzophenone and freshly distilled before use. The phosphines, 1,2-bis(dicyclohexylphosphino)ethane, 1,2-bis(di-*tert*-butylphosphino)ethane, 1,3-bis(di-*tert*-butylphosphino)propane were supplied by Prof. Peter Edwards of Cardiff University and were used as supplied. The phosphines 1,4-bis(di-*tert*-butylphosphino)butane,

2,2'(diphenylphosphino)phenyl ether (DPEphos) and phenyl xantphos were synthesised according to literature methods.[6] The secondary phosphines Bu^t_2PH, $(Bu^t)(Cy)PH$, Bu^i_2PH, Pr^i_2PH, Pe^t_2PH, $(Bu^t)(Pe^t)PH$ were synthesised according to the literature method.[6] Cy_2PH and Ph_2PH were purchased from Strem Chemicals and used as supplied. All other reagents, unless detailed, were supplied by the Aldrich Chemical Company and used without further purification.

NMR spectra were recorded on JEOL GX400 series FT NMR spectrometers at ambient temperature (unless otherwise stated). Proton spectra were taken at 400MHz and chemical shifts [δ, (ppm)] are positive to high frequency of $SiMe_4$ unless stated. Carbon spectra were taken at 100MHz and chemical shifts were referenced by using the ^{13}C resonance of the solvent as an internal standard, but are reported with respect to $SiMe_4$. Phosphorus spectra were taken at 31MHz and chemical shifts are referenced by using the ^{31}P resonance of TMP as a calibration standard (chemical shift 140.00ppm).

Infa red spectra were recorded on a Nicolet 60SX FTIR instrument over the range 4000-400 cm^{-1} at a resolution of 2 cm^{-1}.

GC-MS were run under the following standard chromatography conditions (unless stated):- 25 metre CPSil 19 capillary column, 1.2 mm film thickness, Helium carrier gas 5psi, injector temperature 250°C, oven program 50°C for 4 minutes rising to 200°C at 20°C/min and holding at 200°C.

The mass spectra were obtained at 70eV on a VG Mass Lab TRIO 1 bench top quadrapole mass spectrometer. All two sector mass spectrometry experiments were performed on a VG Analytical Ltd. ZAB-2SE mass spectrometer of reverse geometry. LSIMS (FAB +ve ion, FAB -ve ion) experiments were performed using the standard VG dedicated LSIMS ion source. A 35KV caesium ion gun, operating at 30KeV incident energy was used to bombard the sample. Matrices used were either m-nitrobenzyl alcohol(mNBA) or glycerol. Field desorption experiments were carried out using 13mm emitters and manual increase of the emitter current to a maximum of 80mA.

Microanalyses were obtained from the I.C.I. micro analytical laboratory and from Durham University.

3.3 Synthesis of Phosphine Ligands

3.3.1 Synthesis of [o–$C_6H_4(CH_2PBu^t_2)_2$] (1)

This material was synthesised by a variation of the literature preparation.[7] To a solution of o–$C_6H_4(CH_2Br)_2$ (7.5g, 28.0mmol) in dry degassed acetone (10ml) was added dropwise the phosphine Bu^t_2PH (56.0mmol). The reaction mixture was stirred for 24 hours, during which time a white precipitate formed, which thickened over time making stirring difficult. To this mixture was added degassed water (30ml) in which the white solid dissolved, followed by aqueous sodium acetate (14.0g, 170.0mmol). The mixture was stirred for a further 2 hours, during which time a separate layer formed on top of the aqueous solution. The reaction mixture was extracted with diethyl ether (3 X 50 ml) and the ether extracts dried over magnesium sulphate before being evaporated to dryness to leave the product as a white solid. Yield 4.0g (36%). NMR (CD_2Cl_2): $^{31}P\{^1H\}$, δ 23.5 (s) ppm; ^1H, δ 7.44 (m, 2H, aromatic), 6.95 (m, 2H, aromatic), 2.95 (d, 4H, J 2.4 Hz, CH_2), 1.04 (d, 36H, J 10.7 Hz, CH_3) ppm; ^{13}C, δ 26.96 (dd, J 24.5 Hz, 6.2 Hz, CH_2), 30.01 (d, J 13.3 Hz, CH_3), 32.15 (d, J 23.0 Hz, quaternary), 125.38 (s, aromatic), 131.27 (d, J 15.3 Hz, aromatic), 139.56 (d, J 12.2 Hz, aromatic) ppm.

3.3.2 Synthesis of [*o*-$C_6H_4(CH_2PPr^i_2)_2$] (2)

The product was synthesised in a similar manner to the *tert*-butyl analogue **(1)**. Yield 11.7g (62%). NMR (CD_2Cl_2): $^{31}P\{^1H\}$, δ 0.4 (s) ppm; ^1H, δ 7.08 (m, 2H, aromatic), 6.95 (m, 2H, aromatic), 2.94 (d, 4H, J 2.4 Hz, CH_2), 1.65 (m, 4H, CH), 0.98 (m, 24H, CH_3) ppm; ^{13}C, δ 19.62 (d, J 12.2 Hz, CH_3), 19.91 (d, J 12.2 Hz, CH_3), 23.76 (d, J 15.3 Hz, CH), 28.49(dd, J 21.45 Hz, 7.6 Hz, CH_2), 125.85 (s, aromatic), 131.01 (d, J 7.7 Hz, aromatic), 138.11 (s, aromatic) ppm.

3.3.3 Synthesis of [*o*-$C_6H_4(CH_2P(Bu^t)(Cy))_2$] (3)

The product was synthesised in a similar manner to the *tert*-butyl analogue **(1)**. Yield 5.6g (25%). NMR (CD_2Cl_2):$^{31}P\{^1H\}$, δ 11.4 (s), 11.2 (s) ppm;^1H, δ 7.3 (μ, 2H, aromatic), 7.0

(m, 2H, aromatic), 2.96 (s, 4H, CH_2), 1.4-1.6(br, 22H, Cy CH and CH_2), 1.0-1.35(m, 18H, CH_3) ppm.

3.3.4 Synthesis of [*o*-$C_6H_4(CH_2P(Bu^t)(Pe^t))_2$] (4)

The product was synthesised in a similar manner to the *tert*-butyl analogue **(1)**. Yield 3.2g, (27%). NMR (CD_2Cl_2): $^{31}P\{^1H\}$, δ 19.5(s) ppm; ^1H, δ 7.5 (m, 2H, aromatic), 6.95, (m, 2H, aromatic), 2.94 (s, 4H, CH_2), 1.40-1.0 (m, 44H, CH_2 and CH_3) ppm.

3.3.5 Synthesis of [*o*-$C_6H_4(CH_2PPe^t_2)_2$] (5)

The product was synthesised in a similar manner to the *tert*-butyl analogue **(1)**. Yield 2.7g, (22%). NMR (CD_2Cl_2):$^{31}P\{^1H\}$, δ 20.0 (s) ppm; ^1H, δ 7.5 (m, 2H, aromatic), 6.95, (m, 2H, aromatic), 2.94 (s, 4H, CH_2), 1.45 (m, 8H, CH_2), 1.05 (m, 24H, CH_3), 0.8, (m, 12H, CH_3) ppm.

3.3.6 Synthesis of [*o*-$C_6H_4(CH_2PCy_2)_2$] (6)

The product was synthesised in a similar manner to the *tert*-butyl analogue **(1)**. Yield 13.9g (50%). NMR (CD_2Cl_2):$^{31}P\{^1H\}$, δ -5 (s) ppm; ^1H, δ 7.2 (m, 2H, aromatic), 7.0 (m, 2H, aromatic), 2.96 (s, 4H, CH_2), 1.4-1.6 (br, 44H, CH_2) ppm.

3.3.7 Synthesis of [4-nitro-*o*-$C_6H_4(CH_2P(Bu^t)_2$] (7)

The product was synthesised in a similar manner to the *tert*-butyl analogue **(1)**. The material was recrystalised from methanol to yield crystals suitable for a single crystal X-ray diffraction study. The sample decomposed on storage and no attempt was made to resynthesise this material. No spectroscopic data has therefore been collected on this compound. Crystal data for **7**: $C_{24}H_{43}NO_2P_2$, M = 439.5, triclinic, space group P-1, a = 8.8024(8), b = 11.1937(11), c = 14.4535(14) Å, α = 108.079(3), β = 95.683(2), γ = 101.607(2)^0 V = 1306.0(2) Å^3, Z = 2, T = 160 K; 9923 data measured, 5684 unique, Rint = 0.0184, 274 refined parameters, R = 0.0613, $wR2$ = 0.1275.

P(1)-C(9)	1.868(2)	P(2)-C(21)	1.891(2)
P(1)-C(4)	1.885(2)	P(2)-C(17)	1.889(2)
P(1)-C(8)	1.892(2)	P(2)-C(16)	1.,8572(19)
C(15)-C(16)	1.519(3)	C(10)-C(9)	1.507(3)
C(10)-C(9)-P(1)	120.06(14)	C(15)-C(16)-P(2)	118.01(13)
C(10)-C(15)-C(16)	120.03(16)	C(15)-C(10)-C(9)	121.98(17)

Table 3.1 Bond lengths (Å) and angles (°) for [4-nitro-*o*-$C_6H_4(CH_2P(Bu^t)_2$](7)

Figure 3.1 The Crystal Structure of [4-nitro-*o*-$C_6H_4(CH_2P(Bu^t)_2$]

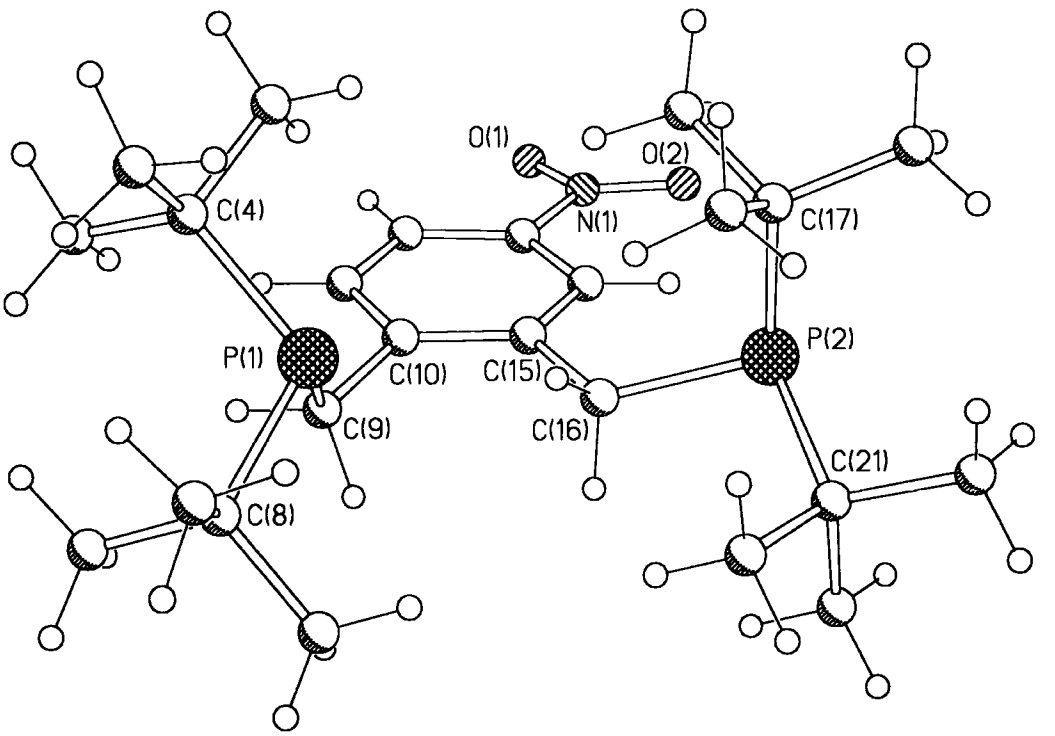

3.3.8 Synthesis of [*o*-$C_6H_4(CH_2PPh_2)_2$] (8)

To a stirred solution of α,α'dibromo-o-xylene (10g, 0.038moles) in diethyl ether was added lithium diphenylphosphide (0.076 moles), generated by treating diphenylphosphine with butyllithium in hexane at room temperature. The reaction mixture was stirred overnight at room temperature followed by heating to the reflux temperature for 2 hours. The solvent

was removed and the residue purified by recrystallisation from hot methanol to yield the product as a white solid. Yield 12.6g (70%) NMR (CD_2Cl_2): $^{31}P\{^1H\}$, δ -14.6(s) ppm; ^1H, δ 7.5-7.8 (m, 20H, aromatic), 7.3 (m, 2H, aromatic), 7.0 (m, 2H, aromatic), 2.96 (s, 4H, CH_2) ppm.

3.3.9 Synthesis of 2,3-[$C_{10}H_6(CH_2PBu^t_2)_2$] (9)

To a stirred solution of 2,3-dimethylnaphthalene (3.0g, 0.019moles) in heptane was added butyllithium (0.077moles) and tmeda (8.8g, 0.077moles). The reaction was stirred for 96 hours, during which time a precipitate developed. The solution was filtered and the solid resuspended in heptane (100 ml) before the addition of di-*tert*-butylchlorophosphine (6.8g, .038 moles) and stirring for a further 24 hours. A second precipitate was observed to form, and this was filtered before removal of the heptane under vacuum. The product was isolated by recrystallisation from methanol. Yield 3.5g (42%) NMR (CD_2Cl_2):$^{31}P\{^1H\}$, δ 24.0 (s) ppm; ^1H, δ 7.94(m, 2H, aromatic), 7.66 (m, 2H, aromatic), 7.30 (m, 2H, aromatic), 3.18 (s, 4H, CH_2), 1.09 (d, 36H, J 10.7 Hz, CH_3) ppm.

3.3.10 Synthesis of 1,8-[$C_{10}H_6(CH_2P^tBu_2)_2$] (10)

The product was synthesised in a similar manner to the 2,3-naphthyl analogue **(9)**. NMR (CD_2Cl_2):$^{31}P\{^1H\}$, δ 34.0 (s) ppm; ^1H, δ 7.95 (m, 2H, aromatic), 7.55 (m, 2H, aromatic), 7.27 (m, 2H, aromatic), 3.65 (s, 4H, CH_2), 0.98 (d, 36H, J 10.7 Hz, CH_3)ppm.

3.3.11 Synthesis of [{1(di-*tert*-butylphosphorylmethyl), 2(di-*tert*-butylphosphinomethyl)}benzene] (11)

During the synthesis and subsequent analysis of **(1)** crystals formed in the NMR tube. These crystals were characterised by single crystal X-ray diffraction and were shown to be the monophosphine oxide of **(1)**. Crystal data for **11**: $C_{24}H_{44}OP_2$, M = 410.5, monoclinic, space group $P2_1/c$, a = 12.3600(10), b = 10.6211(9), c = 19.3962(17) Å, β = 99.818(2)^0 V = 2509.0(4) Å^3, Z = 4, T = 160 K; 17543 data measured, 5794 unique, Rint = 0.0194, 257 refined parameters, R = 0.0418, $wR2$ = 0.0922.

P(1)-C(9)	1.8728(13)	P(2)-C(21)	1.8560(13)
P(1)-C(4)	1.8965(14)	P(2)-C(17)	1.8567(13)
P(1)-C(8)	1.8928(13)	P(2)-C(16)	1.,8224(12)
C(15)-C(16)	1.5176(16)	C(10)-C(9)	1.5172(18)
C(10)-C(9)-P(1)	117.49(9)	C(15)-C(16)-P(2)	120.92(9)
C(10)-C(15)-C(16)	119.02(11)	C(15)-C(10)-C(9)	121.98(11)

Table 3.2 Bond Lengths (Å) and Angles (°) for C_6H_3-1-($CH_2P(O)Bu^t_2$)-2-($CH_2PBu^t_2$) (11)

Figure 3.2 Crystal Structure of C_6H_3-1-($CH_2P(O)Bu^t_2$)-2-($CH_2PBu^t_2$) (11)

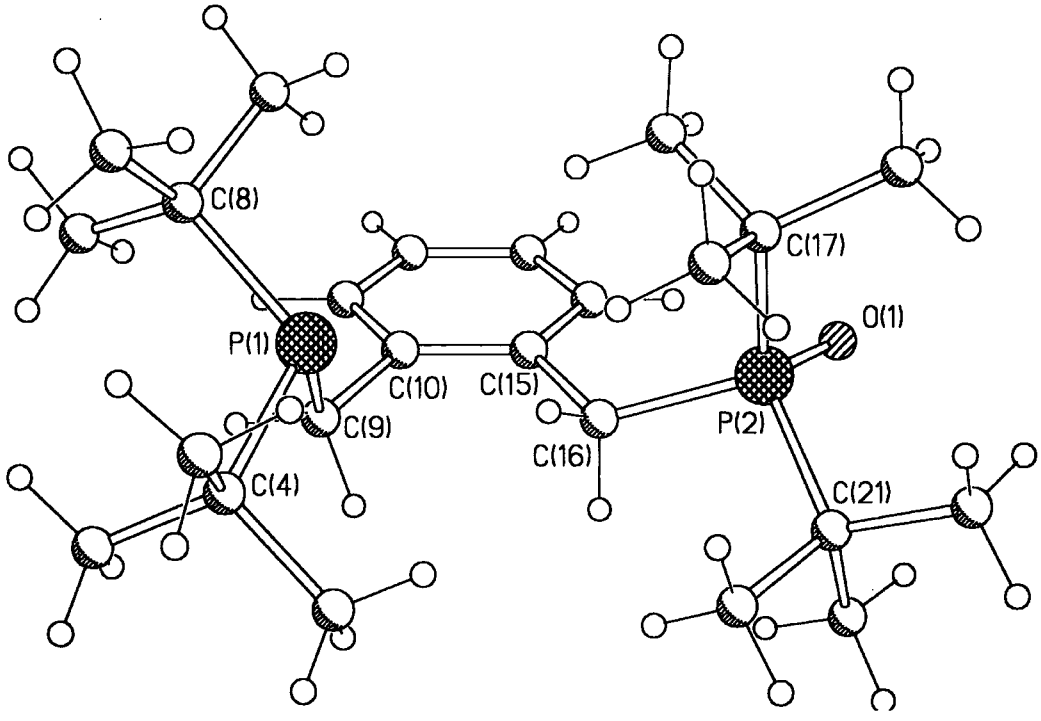

3.4 Synthesis of Palladium (0) Complexes

3.4.1 General Procedure for the Synthesis of DBA Complexes

To the palladium complex [$Pd_2(dba)_3$] (5g, 5.47mmol) dissolved in thf (200ml) was added the diphosphine (10.94mmol) as a solution in thf (100ml). The deep purple colour of

the [$Pd_2(dba)_3$] changed to bright orange after stirring for 1 hour. The reaction solution was stirred for a further 16 hours during which no further colour change occurred. The reaction was fine-filtered to remove any palladium metal, and the solvent removed under reduced pressure to yield an orange sticky gum. This was washed with cold hexane (-30^{0}C) followed by cold ether (-30^{0}C). The washings were discarded and the remaining solid dried under reduced pressure to yield the product as an orange powder. Further purification by recrystallisation as described below gave crystals suitable for X-ray diffraction.

3.4.2 Synthesis of[*o*-$C_6H_4(CH_2PBu^t_2)_2$ Pd (dba)] (12)

Yield 2.56g (32%). Found: C, 67.14; H, 8.0. $C_{41}H_{58}OP_2Pd$ requires C, 67.03; H, 7.90. Crystals suitable for a single crystal X-ray study were obtained by recrystallisation from hot nonane (for data see Figure 3.3. and Table 3.3). Crystal data for **12**: $C_{41}H_{58}OP_2Pd$, M = 735.21, triclinic, space group P-1, a = 9.264(2), b = 11.482(3), c = 19.466(4) Å, α = 97.72(2), β = 93.63(2), γ = 112.725(12)^0 , V = 1877.5(7) Å^3, Z = 2, T = 160 K; 8043 data measured, 5889 unique, Rint = 0.0343, 447 refined parameters, R = 0.0526, $wR2$ = 0.1092.

I.R. (KBr discs, cm^{-1}): ν (CO) 1643 vs.

NMR (d^8-toluene, 293K): $^{31}P\{^1H\}$, δ 48.1 (br), 49.9 (br) ppm; ^1H, δ 6.8-7.4 (br, aromatics + alkene CH), 3.10 (br CH_2), 1.2 (br, CH_3); ^{13}C, δ 31.4 (m, CH_3), 32.0 (br, CH_2), 37.2 (br, quaternary), 64.0(br, alkene CH), 73.0(br, alkene CH), 125-145(m, aromatics), 191.7 (s, carbonyl) ppm.

NMR (d^8-toluene, 193K): $^{31}P\{^1H\}$, δ 42.7 (s), 45.7 (s), 46.5 (s), 47.8 (s), 49.1 (d, J 7.1Hz), 50.1 (s), 51.3 (d, J 7.2Hz) ppm; ^1H, δ 6.9-8.3 (br, aromatics), 5.5(br, alkene CH), 5.1(br, alkene CH), 5.0(br, alkene CH), 4.9(br, alkene CH), 4.7(br, alkene CH), 2.5-3.2(br, CH_2), 1.6(br, CH_3), 1.4(br, CH_3), 1.1(br, CH_3), 0.9(br, CH_3), 0.5(br, CH_3) ppm; ^{13}C, δ 31.0 (m, CH_3), 32.0(br, CH_2), 37.2(br, quaternary), 63.0(br, alkene CH), 71.5(m, alkene CH), 73.0(m, alkene CH), 74.5(m, alkene CH), 125-145(m, aromatics), 190.0(s, carbonyl), 191.0(s, carbonyl), 192.0(s, carbonyl) ppm.

NMR (xylene, 353K): $^{31}P\{^{1}H\}$, δ 51.2 (s), 49.9 (s) ppm.

NMR (xylene, 373K): $^{31}P\{^{1}H\}$, δ 51.6 (br), 50.5 (br) ppm.

NMR (xylene, 393K): $^{31}P\{^{1}H\}$, δ 51.4 (br) ppm.

NMR (xylene, 403K): $^{31}P\{^{1}H\}$, δ 51.7 (br) ppm.

NMR (xylene, 413K): $^{31}P\{^{1}H\}$, δ 52.0 (s) ppm.

NMR (xylene, 423K): $^{31}P\{^{1}H\}$, δ 52.2 (s) ppm.

NMR (CD_2Cl_2, 193K): $^{31}P\{^{1}H\}$, δ 42.8 (d, J 7.6 Hz), 46.8 (d, J 7.0 Hz), 46.9 (d, J 6.8 Hz), 49.5 (d, J 13.2 Hz), 51.5 (d, J 7.8 Hz), 52.9 (d J 13.2 Hz) ppm; ^{1}H, δ 7.0-8.0 (br, aromatics), 4.7 (m, alkene CH), 4.5 (m, alkene CH), 4.35 (m, alkene CH), 4.3 (m, alkene CH), 4.1 (m, alkene CH), 3.2-3.5 (br CH_2), 1.6(br, CH_3), 1.4 (br, CH_3), 1.1 (br, CH_3), 0.81 (br, CH_3), 0.65 (d, J 13.4 Hz, CH_3), 0.31 (d, J 18.4 Hz, CH_3), 0.068 (d, J 18.7 Hz, CH_3) ppm; ^{13}C, δ 30.7 (br, CH_3), 32.6 (br, CH_2), 35.0-38.0 (m, quaternary), 60.7 (d, J 31.6 Hz, alkene CH), 61.3 (d, J 29.9 Hz, alkene CH), 72.0 (d, J 21.8 Hz, alkene CH), 73.1 (br, alkene CH), 125-145 (m, aromatics), 190.4 (s, carbonyl), 192.4 (s, carbonyl), 193.1 (s, carbonyl) ppm.

Mass Spectrum(FAB + ion, mNBA matrix): M/z 734 [(10%), $(M)^+$], 500 [(50%), $(M\text{-dba})^+$].

P(1)-Pd	2.367(2)	P(2)-Pd	2.3540(14)
Pd-C(7)	2.157(5)	Pd-C(8)	2.150(5)
C(7)-C(8)	1.423(8)	P(1)-Pd-P(2)	103.99(5)
C(7)-Pd-C(8)	38.6(2)	C(7)-Pd-P(2)	108.7(2)
C(8)-Pd-P(1)	108.9(2)		

Table 3.3 Bond Lengths (Å) and Angles (°) for [*o*-$C_6H_4(CH_2PBu^t_2)_2$ Pd (dba)] (12)

Figure 3.3 The Crystal Structure of [*o*-$C_6H_4(CH_2PBu^t_2)_2$ Pd (dba)] (12)

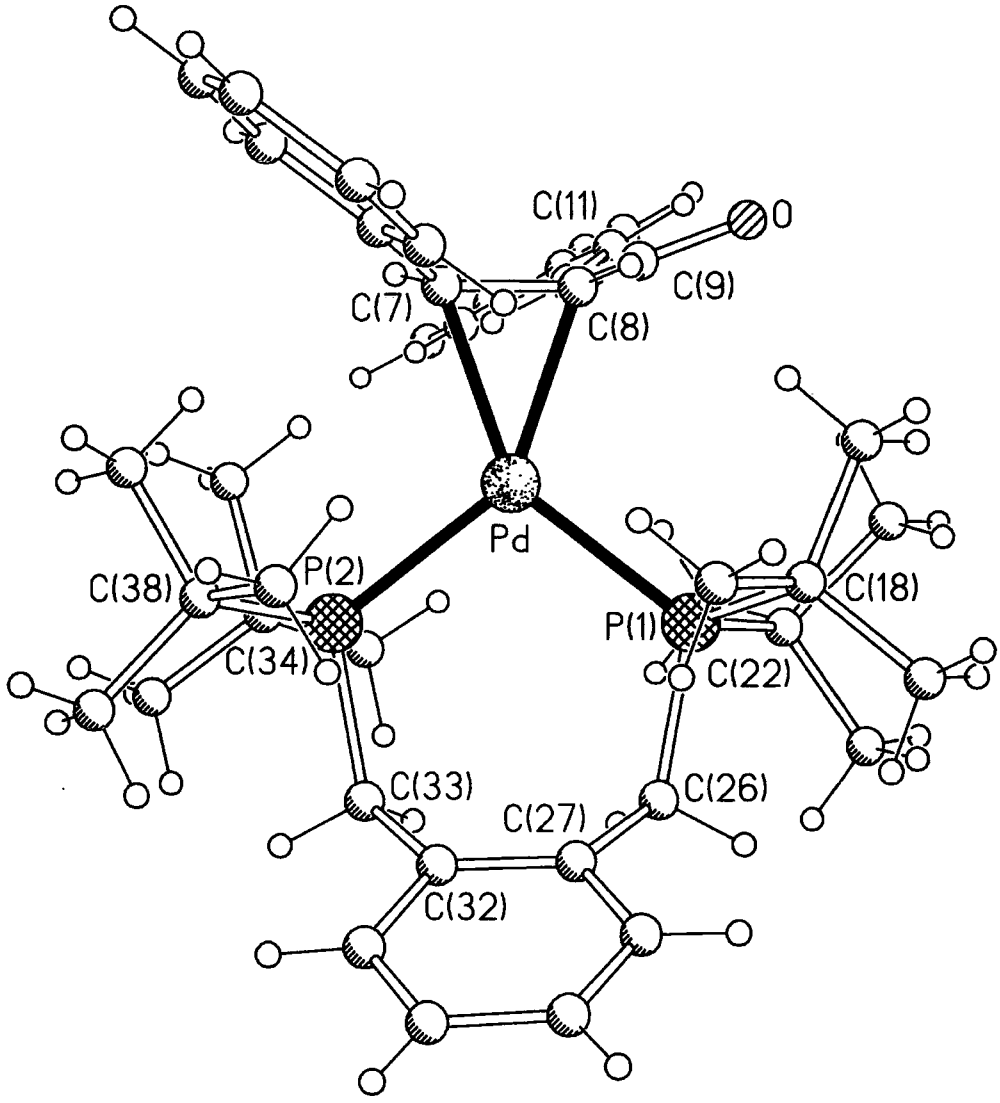

3.4.3 Synthesis of [*o*-$C_6H_4(CH_2PPr^i_2)_2$ Pd (dba)] (13)

Yield 3.0g (40.0%). Found: C, 72.97; H, 6.81. $C_{37}H_{50}OP_2Pd$ requires C, 65.48; H, 7.37 %. Crystals suitable for a single crystal X-ray study were obtained by recrystallisation from hot nonane (for data see Figure 3.4, and Table 3.4). Crystal data for **13**: $C_{37}H_{51}OP_2Pd$, M = 680.12, triclinic, space group P-1, a = 9.1626(11), b = 13.858(2), c = 14.353(2) Å, α =

81.331(3), β = 78.5110(10) γ = 77.523(3)^0 , V = 1732.7(4) Å^3, Z = 2, T = 205 K; 10165 data measured, 6930 unique, Rint = 0.063, 384 refined parameters, R = 0.0834, $wR2$ = 0.1799.

I.R (KBr discs, cm^{-1}): ν (CO) 1651 vs

NMR (d^8 toluene, 293K): $^{31}P\{^1H\}$, δ 29.4(br) ppm; ^1H, δ 7.0-8.0 (br, aromatics + alkene CH), 5.35 (br, alkene CH), 5.05 (br, alkene CH), 3.0 (br, CH_2), 1.85 (br, *iso*-propyl CH), 1.5-0.5 (br, CH_3) ppm; ^{13}C, δ 20.8 (br, CH_2), 26.8 (br, CH_3), 29.6 (br, quaternary), 56.9 (br, alkene CH), 67.5 (br, alkene CH), 123-145 (m, aromatics) 188.8 (s, carbonyl) ppm.

NMR (d^8-toluene, 193K): $^{31}P\{^1H\}$, δ 29.7 (s), 29.5 (s), 27.0 (br), 26.5 (br), 26.0 (br), 24.9 (br) ppm; ^1H, δ 7.0-8.0 (aromatics), 5.6 (br, alkene CH), 5.4 (br, alkene CH), 5.0 (br, alkene CH), 2.6-3.0 (br, CH_2), 1.85 (br, *iso*-propyl CH), 1.7-0.5 (br, CH_3) ppm.

NMR (d^8-toluene, 273K): $^{31}P\{^1H\}$, δ 29.3 (br), 27.2 (br) ppm.

NMR (d^8-toluene, 298K): $^{31}P\{^1H\}$, δ 29.4 (br) ppm.

NMR (d^8-toluene, 323K): $^{31}P\{^1H\}$, δ 29.5 (br), 28.7 (br) ppm.

NMR (d^8-toluene, 353K): $^{31}P\{^1H\}$, δ 28.0 (s) ppm.

NMR (CD_2Cl_2, 293K): ^1H, δ 7.0-8.0 (aromatics), 4.9 (br, alkene CH), 4.7 (br, alkene CH), 3.3 (br, CH_2), 2.2 (br, *iso*-propyl CH), 1.7 (br, *iso*-propyl CH) 1.5-0.5 (br, CH_3) ppm.

Mass Spectrum (FAB + ion, mNBA matrix): M/z 678 [(5%), $(M)^+$], 444 [(30%), $(M\text{-dba})^+$].

P(1)-Pd	2.3167(14)	P(2)-Pd	2.2937(14)
Pd-C(7)	2.137(5)	Pd-C(8)	2.142(5)
C(7)-C(8)	1.426(7)	P(1)-Pd-P(2)	104.35(5)
C(7)-Pd-C(8)	38.9(2)	C(7)-Pd-P(2)	104.8(2)
C(8)-Pd-P(1)	111.9(2)		

Table 3.4 Bond Lengths (Å) and Angles (°) for [*o*-$C_6H_4(CH_2PPr^i_2)_2$ Pd(dba)] (13)

Figure 3.4 The Crystal Structure of [*o*-$C_6H_4(CH_2PPr^i_2)_2$ Pd (dba)] (13)

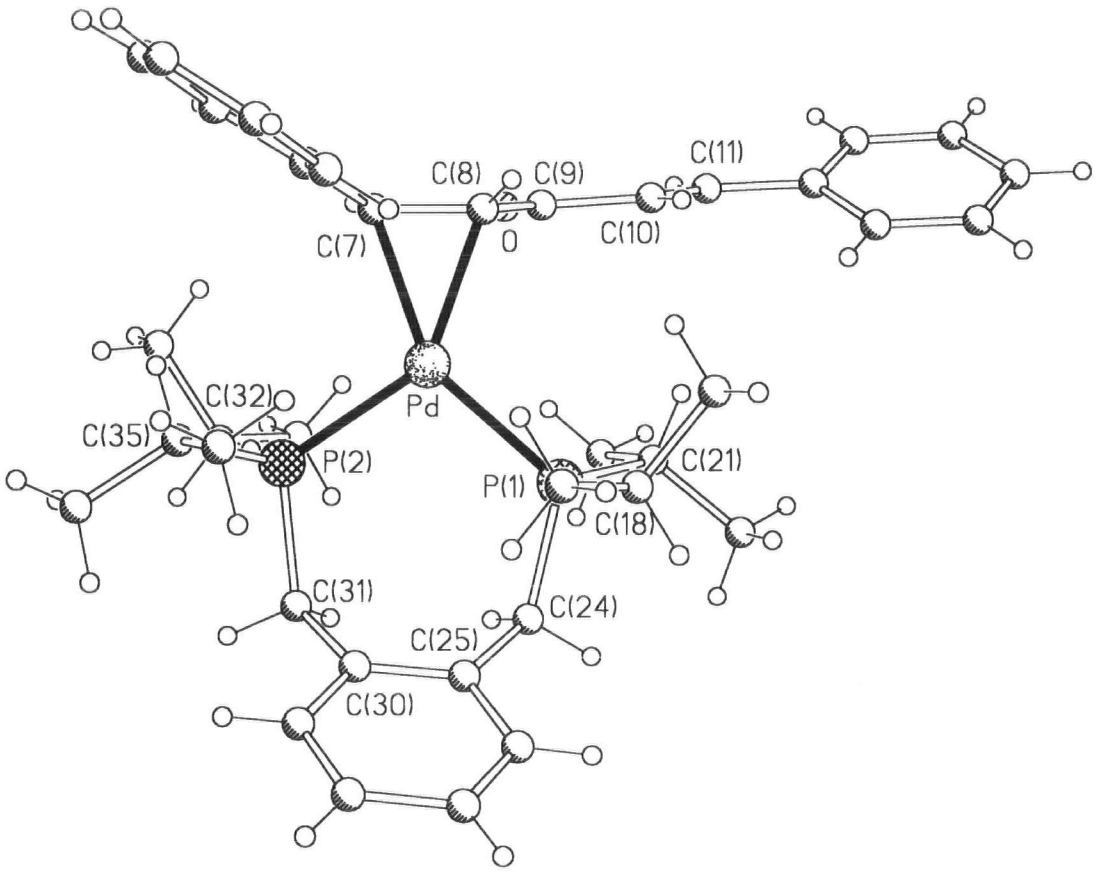

3.4.4 Synthesis of [*o*-$C_6H_4(CH_2PCy_2)_2$ Pd (dba)] (14)

Yield 5.5g (60.0%). Found: C, 71.37; H, 7.57 . $C_{49}H_{66}OP_2Pd$ requires C, 69.8; H, 7.84 %. Crystals suitable for a single crystal X-ray study were obtained by recrystallisation from hot toluene (for data see Figure 3.5, and Table 3.5). Crystal data for **14**: $C_{49}H_{66}OP_2Pd$, M = 838.21, triclinic, space group P-1, a = 9.9570(4), b = 12.5908(5), c = 47.5159(19) Å, α = 85.618(2), β = 88.919(2), γ = 77.405(2)^0 , V = 5796.6(4) Å^3, Z = 4, T = 160 K; 35204 data measured, 25488 unique, Rint = 0.0204, 1283 refined parameters, R = 0.0763, $wR2$ = 0.1454.

I.R (KBr discs, cm^{-1}): ν (CO) 1637 vs

NMR (d^8-toluene, 293K): $^{31}P\{^1H\}$, δ 19.3 (br) ppm; ^1H, δ 7.0-8.0 (br, aromatics + alkene CH), 5.2 (br, alkene CH), 5.05 (br, alkene CH), 3.10 (br, CH_2), 0.7-2.2 (br, CH_2) ppm.

NMR (d^8-toluene, 193K): $^{31}P\{^1H\}$, δ 23.8 (d, J= 43.2 Hz), 21.51 (d, J = 43.2 Hz), 20.5(d, J = 39.3 Hz), 19.2 (d, J = 43.2 Hz), 18.2 (br), 15.5 (br) ppm; ^1H, δ 6.7-8.2 (br, aromatics), 5.5 (br, alkene CH), 5.2 (br, alkene CH), 4.8 (br, alkene CH), 2.5-3.1 (br CH_2), 2.0-1.0 (br, CH_2) ppm.

NMR (CD_2Cl_2, 298K): ^1H, δ 6.8-7.8 (aromatics), 4.6 (br, alkene CH), 4.5 (br, alkene CH), 3.2 (br, CH_2), 1.8-2.1 (br, cyclohexyl CH_2), 0.3 (br, cyclohexyl CH_2).

Mass Spectrum(FAB + ion, mNBA matrix): M/z 838 [(2%), $(M+H)^+$], 605 [(20%), $(M\text{-dba})^+$].

P(1)-Pd	2.3177(10)	P(2)-Pd	2.3087(10)
Pd-C(7)	2.130(4)	Pd-C(8)	2.149(4)
C(7)-C(8)	1.433(6)	P(1)-Pd-P(2)	104.19(4)
C(7)-Pd-C(8)	39.14(15)	C(7)-Pd-P(2)	106.20(11)
C(8)-Pd-P(1)	110.40(11)		

Table 3.5 Bond Lengths (Å) and Angles (°) for [*o*-$C_6H_4(CH_2PCy_2)_2$ Pd (dba)] (14)

Figure 3.5 The Crystal Structure of [*o*-$C_6H_4(CH_2PCy_2)_2$ Pd (dba)] (14)

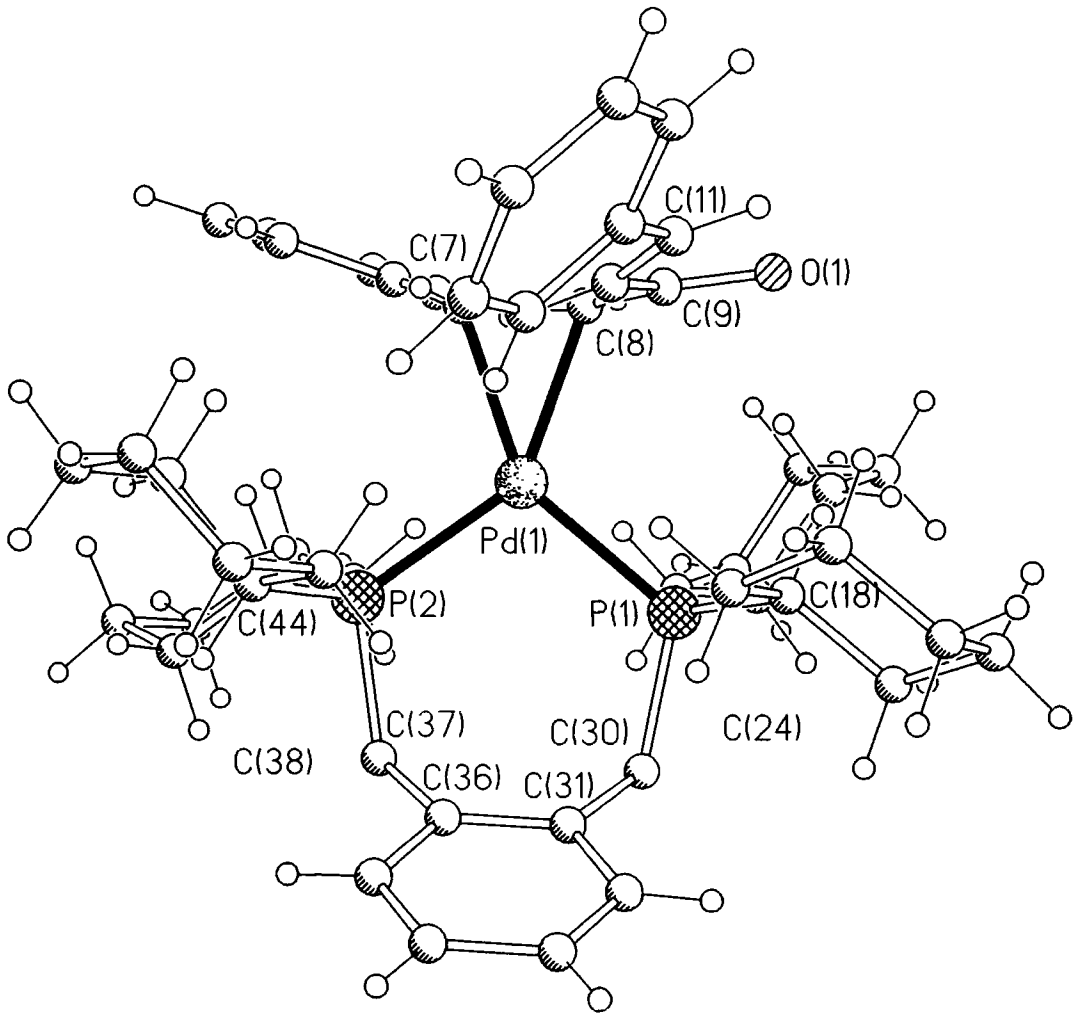

3.4.5 Synthesis of [*o*-$C_6H_4(CH_2P(Bu^t)(Cy))_2$ Pd (dba)] (15)

Yield 4.0g (46.0%). Found: C, 69.96; H, 7.86 . $C_{45}H_{62}OP_2Pd$ requires C, 68.7; H, 7.89 %.

I.R (KBr discs, cm^{-1}): ν (CO) 1644 vs

NMR (d^8-toluene, 293K): $^{31}P\{^1H\}$, δ 38.8 (br), 35.6 (br), 35.0 (br), 31.5 (br) ppm; ^1H, δ 7.0-8.0 (br, aromatics + alkene CH), 5.2 (br, alkene CH), 4.9 (br, alkene CH), 3.1 (br, CH_2), 3.3 (br, CH_2), 2.0-1.0 (br, CH_2, and CH_3) ppm.

NMR (d^8-toluene, 193K): $^{31}P\{^1H\}$, δ 38.7 (br), 37.4 (br), 36.8 (br), 35.8 (br), 34.8 (br), 33.9 (br), 31.2 (br), 30.4 (br), 29.2 (br), 28.3 (br) ppm; ^1H, δ 7.0-8.0 (br, aromatics + alkene CH), 5.5 (br, alkene CH), 5.2, (br, alkene CH), 4.9 (br, alkene CH), 3.1 (br, CH_2), 2.8 (br CH_2), 1.0-2.0 (br, CH_2, and CH_3) ppm.

NMR (d^8-toluene, 203K): $^{31}P\{^1H\}$, δ 38.9 (br), 37.5 (br), 37.4 (br), 36.8 (br), 36.1 (br), 34.9 (br), 34.8 (br), 32.5 (br), 31.5 (br), 30.7 (br), 29.2 (br), 28.5 (br) ppm.

NMR (d^8-toluene, 243K): $^{31}P\{^1H\}$, δ 39.2 (br), 37.8 (br), 36.3 (br), 35.4 (br), 32.6 (br), 31.6 (br), 29.1 (br) ppm.

NMR (d^8-toluene, 273K): $^{31}P\{^1H\}$, δ 38.7 (br), 35.0 (br), 31.0 (br) ppm.

Mass Spectrum (FAB + ion, mNBA matrix): M/z 787 [(4%), $(M+H)^+$], 552 [(60%), $(M\text{-dba})^+$].

Mass Spectrum (Electrospray + ion): M/z 552[(10%), $(M\text{-dba})^+$], 584 [(5%), $(L_2PdO_2)^+$], 787 [(8%), $(M+H)^+$], 1168 [(1%), 2x $(L_2PdO_2)^+$], 1136 [(2%), $(L_2Pd + L_2PdO_2)^+$].

Recrystallisation of the original sample led to the isolation of two fractions, the first dark orange in colour and the second pale yellow/orange.

Fraction 1. Found: C, 69.90; H, 7.80. $C_{45}H_{62}P_2OPd$ requires C, 68.7; H, 7.89 %.

NMR (d^8-toluene, 193K): $^{31}P\{^1H\}$, δ 40.8 (br), 39.7 (br), 38.9 (br), 38.7 (br), 37.8 (br), 36.7 (br), 35.5 (br), 35.4 (br), 34.1 (br), 33.2 (br), 32.1 (br) ppm.

Fraction 2. Found: C, 70.00; H, 7.88. $C_{45}H_{62}P_2OPd$ requires C, 68.7; H, 7.89 %.

NMR (d^8-toluene, 193K): $^{31}P\{^1H\}$, δ 40.9 (br), 39.7 (br), 38.8 (br), 37.8 (br), 36.7 (br), 35.5 (br), 35.4 (br), 34.4 (br), 33.0 (br), 32.1 (br) ppm.

3.4.6 Synthesis of [*o*-$C_6H_4(CH_2PPe^t_2)_2$ Pd (dba)] (16)

Yield 2.6g, (30%). Found: C, 67.58; H, 8.41. $C_{48}H_{66}OP_2Pd$ requires C, 68.35; H, 8.35 %.

I.R. (KBr discs, cm^{-1}): ν (CO) 1646 vs.

NMR (d^8-toluene, 298K): $^{31}P\{^1H\}$, δ 58.5 (br), 56.0 (br) ppm; ^1H, δ 7.0-8.0 (br, aromatics + alkene CH), 3.1-3.4 (br, CH_2), 0.9-1.9 (br, CH_2, and CH_3) ppm.

NMR (d^8-toluene, 193K): $^{31}P\{^1H\}$, δ 61.0 (br), 60.2 (br), 58.5 (br), 57.9 (br), 57.6 (br), 54.3 (br), 53.7 (br), 51.7 (br), 50.5 (br), 48.5 (br) ppm.

Mass Spectrum (FAB + ion, mNBA matrix): M/z 791 [(1%), $(M+H)^+$], 556 [(100%), $(M\text{-dba})^+$].

Mass Spectrum (Electrospray + ion): M/z 556 [(32%), $(M\text{-dba})^+$], 588 [(10%), $(L_2PdO_2)^+$], 1176 [(5%), 2x $(L_2PdO_2)^+$], 1144 [(5%), $(L_2Pd + L_2PdO_2)^+$].

The attempted recrystallisation of **(16)** from thf layered with pentane resulted in the formation of a small quantity of pale blue crystals suitable for X-ray structural analysis. These crystals turned out to be a dioxygen complex and their structure will be discussed in chapter 5.0.

3.4.7 Synthesis of [*o*-$C_6H_4(CH_2P(Pe^t)(Bu^t))_2$ Pd (dba)] (17)

Yield 2.6g (30%). Found: C, 68.39; H, 7.92. $C_{43}H_{62}OP_2Pd$ requires C, 67.7; H, 8.13%.

I.R. (KBr discs, cm^{-1}): ν (CO) 1639 vs.

NMR (d^8-toluene, 298K): $^{31}P\{^1H\}$, δ 54.0 (br), 52.0 (br) ppm; ^1H, δ 7.0-8.0 (br, aromatics + alkene CH), 3.1-3.4 (br, CH_2), 0.9-1.9 (br, CH_2, and CH_3) ppm.

NMR (d^8-toluene, 193K): $^{31}P\{^1H\}$, δ 57.2 (br), 56.0 (br), 54.5 (br), 53.5 (br), 53.0 (br), 52.5 (br), 51.7 (br), 51.2 (br), 50.2 (br), 49.8 (br), 47.8 (br), 46.6 (br), 46.2 (br) ppm.

Mass Spectrum (FAB + ion, mNBA matrix): M/z 763 [(1%), $(M+H)^+$], 528 [(100%), $(M\text{-dba})^+$].

Mass Spectrum (Electrospray + ion): M/z 528 [(20%), $(M\text{-dba})^+$], 560 [(20%), $(L_2PdO_2)^+$], 1120 [(5%), $2x(L_2PdO_2)^+$], 1088 [(5%), $(L_2Pd + L_2PdO_2)^+$].

3.4.8 Synthesis of [*o*-$C_6H_4(CH_2PPh_2)_2$ Pd (dba)] (18)

Yield 2.7g (30.0%). Analysis calculated for $C_{49}H_{42}OP_2Pd$: C, 72.20; H, 5.16. Found: C, 72.21; H, 5.45. Crystals suitable for a single crystal X-ray study were obtained by recrystallisation from thf layered with diethyl ether (for data see Figure 3.6, and Table 3.6). Crystal data for **18**: $C_{49}H_{42}OP_2Pd$, M = 815.17, monoclinic, space group $P2_1/c$, a = 8.6608(2), b = 32.6232(8), c = 13.8956(3) Å, β = 95.309(2)^0, V = 3909.26(16) Å^3, Z = 4, T = 160 K; 20772 data measured, 8326 unique, Rint = 0.0264, 485 refined parameters, R = 0.0326, $wR2$ = 0.0778.

I.R. (KBr discs, cm^{-1}): ν (CO) 1639 vs.

NMR (d^8 toluene, 298K): $^{31}P\{^1H\}$, δ 16.0 (br), 12.0 (br) ppm; ^1H, δ 6.8-8.0 (br, aromatics + alkene CH), 4.7 (br, alkene CH), 3.7 (br, CH_2) ppm.

NMR (CD_2Cl_2, 298K): ^1H, δ 6.8-8.0 (br, aromatics + alkene CH), 4.7 (br, alkene CH), 3.7 (br, CH_2) ppm.

Mass Spectrum (FAB + ion, mNBA matrix): M/z 815 [(5%), $(M+H)^+$], 580 [(20%), $(M\text{-dba})^+$].

Mass Spectrum (Electrospray + ion): M/z 815 [(30%), $(M+H)^+$], 1395 [(20%), $(L_2Pd(dba) + L_2Pd)^+$], 1629 [(3%), $2x(L_2Pd(dba)^+$].

P(1)-Pd	2.3094(5)	P(2)-Pd	2.2852(5)
Pd-C(7)	2.1407(19)	Pd-C(8)	2.1654(19)
C(7)-C(8)	1.415(3)	P(1)-Pd-P(2)	104.623(17)
C(7)-Pd-C(8)	38.37(7)	C(7)-Pd-P(2)	100.00(5)
C(8)-Pd-P(1)	116.94(5)		

Table 3.6 Bond Lengths (Å) and Angles (°) for [*o*-$C_6H_4(CH_2PPh_2)_2$ Pd(dba)] (18)

Figure 3.6 The Crystal Structure of [*o*-$C_6H_4(CH_2PPh_2)_2$ Pd (dba)] (18)

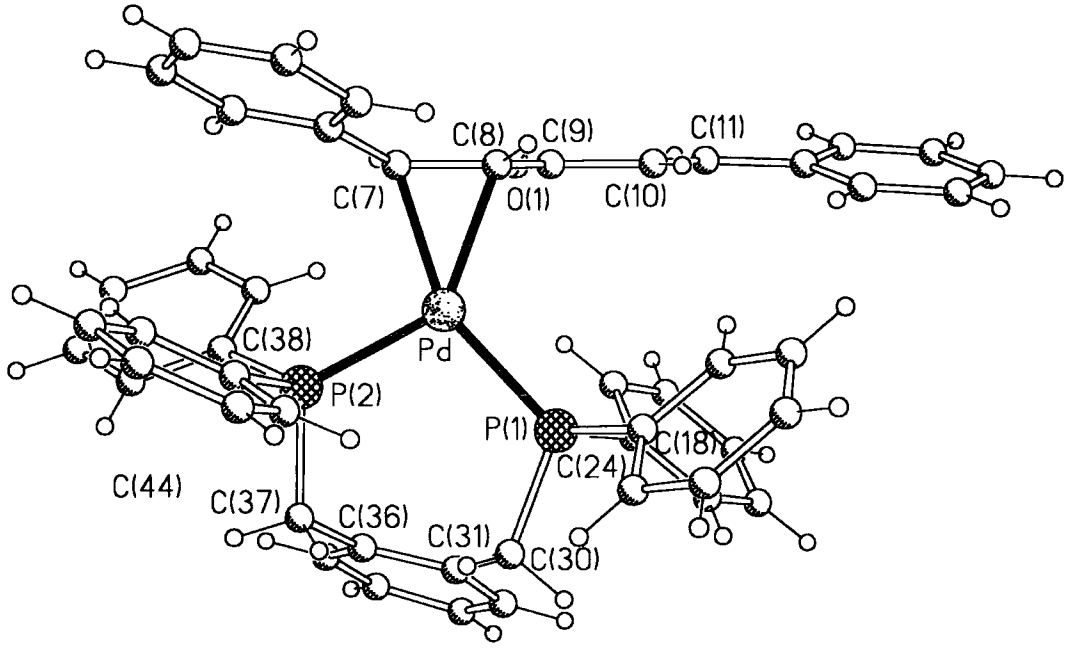

3.4.9 Synthesis of [1,2-$C_2H_4(PBu^t_2)_2$ Pd (dba)] (19)

Yield 3.0g (42%). Found: C, 64.08; H, 8.23. $C_{35}H_{54}OP_2Pd$ requires C, 63.8; H, 8.2%.

I.R. (KBr discs, cm^{-1}): ν (CO) 1652 vs

NMR (d^8-toluene, 298K): $^{31}P\{^1H\}$, δ 85.6 (br), 81.3 (br)ppm; ^1H, δ 6.8-8.0 (br, aromatics + alkene CH), 5.5 (br, alkene CH), 5.1 (br, alkene CH), 1.7-0.7 (br, CH_2 ethyl bridge and CH_3) ppm.

NMR (d^8-toluene, 193K): $^{31}P\{^1H\}$, δ 85.7 (s), 82.0 (s), 81.2 (s), 78.8 (s) ppm.

Mass Spectrum (FAB + ion, mNBA matrix): M/z 659 [(15%), $(M+H)^+$], 424 [(100%), $(M\text{-dba})^+$].

Mass Spectrum (Electrospray + ion): M/z 425 [(22%), $(M\text{-dba})^+$], 457 [(40%) $(L_2PdO_2)^+$], 659 [(30%), $(M+H)^+$], 915 [(20%), $2x(L_2PdO_2)^+$], 1085 [(18%), $(L_2Pd(dba)+L_2Pd)^+$].

3.4.10 Synthesis of [1,3-$C_3H_6(PBu^t_2)_2$ Pd (dba)] (20)

Yield 1.8g, (25%). Found: C, 65.33; H, 8.18. $C_{36}H_{56}OP_2Pd$ requires C, 64.19; H, 8.32%.

I.R. (KBr discs, cm^{-1}): ν (CO) 1640 vs.

NMR (d^8-toluene, 298K): $^{31}P\{^1H\}$, δ 43.3 (br), 43.7 (br) ppm; ^1H, δ 7.0-8.0 (br, aromatics + alkene CH), 5.4-5.2 (br, alkene CH), 1.9-0.7 (br, CH_2 propyl bridge and CH_3) ppm.

NMR (d^8-toluene, 193K): $^{31}P\{^1H\}$, δ 44.2 (s), 41.4 (s), 40.1 (s), 38.3 (s) ppm.

NMR (d^8-toluene, 253K): $^{31}P\{^1H\}$, δ 45.3 (vbr), 42.0 (vbr), 39.9 (vbr) ppm.

NMR (d^8-toluene, 273K): $^{31}P\{^1H\}$, δ 42.4 (br) ppm.

NMR (d^8-toluene, 283K): $^{31}P\{^1H\}$, δ 42.9 (br) ppm.

NMR (d^8-toluene, 293K): $^{31}P\{^1H\}$, δ 43.3 (br), 43.7(br) ppm.

NMR (d^8-toluene, 323K): $^{31}P\{^1H\}$, δ 44.0 (s), 44.4 (br) ppm.

NMR (d^8-toluene, 353K): $^{31}P\{^1H\}$, δ 44.7 (s), 45.2 (s) ppm.

NMR (d^8-toluene, 373K): $^{31}P\{^1H\}$, δ 44.9 (s), 45.4 (s) ppm.

Mass Spectrum (FAB + ion, mNBA matrix): M/z 673 [(10%), $(M+H)^+$], 438 [(100%), $(M\text{-dba})^+$], 1114 [(30%), $(L_2Pd(dba)+L_2Pd)^+$].

3.4.11 Synthesis of [1,3-$C_3H_6(PPh_2)_2$ Pd (dba)] (21)

Yield 3.0g, (37%). Found: C, 69.86; H, 5.28. $C_{44}H_{40}OP_2Pd$ requires C, 70.2; H, 5.32 %. Crystals suitable for a single crystal X-ray study were obtained by recrystallisation from thf layered with diethyl ether (for data see Figure 3.7 and Table 3.7). Crystal data for **21**: $C_{44}H_{40}OP_2Pd$, M = 753.10, monoclinic, space group $P2_1/c$, a = 9.1401(4), b = 41.0250(16), c = 9.7145(4) Å, β = 92.380(2)^0 , V = 3639.5(3) Å^3, Z = 4, T = 160 K; 29743 data measured, 8641 unique, Rint = 0.0409, 440 refined parameters, R = 0.0623, $wR2$ = 0.0810.

I.R. (KBr discs, cm^{-1}): ν (CO) 1639 vs.

NMR (d^8-toluene, 313K): $^{31}P\{^1H\}$, δ 11.0 (s), 7.0 (s) ppm; ^1H, δ 7.0-8.0 (br, aromatics), 1.8-1.4 (br, CH_2 propyl bridge) ppm.

NMR (d^8-toluene, 313K): $^{31}P\{^1H\}$, δ 11.0 (s), 7.0 (s) ppm.

NMR (d^8-toluene, 333K): $^{31}P\{^1H\}$, δ 11.0 (s), 7.0 (s) ppm.

NMR (d^8-toluene, 353K): $^{31}P\{^1H\}$, δ 11.0 (s), 7.0 (s) ppm.

Mass Spectrum (FAB + ion, mNBA matrix): M/z 753 [(18%), $(M+H)^+$], 518 [(100%), $(M\text{-dba})^+$], 1036 [(10%), 2x$(L_2Pd)^+$], 1271 [92%), $(L_2Pd(dba + L_2Pd)^+$].

Mass Spectrum (Electrospray + ion): M/z 518 [(5%), $(M\text{-dba})^+$], 550 [(20%) $(L_2PdO_2)^+$], 753 [(10%), $(M+H)^+$], 1271 [(8%), $(L_2Pd(dba)+L_2Pd)^+$].

P(1)-Pd	2.2942(7)	P(2)-Pd	2.2747(8)
Pd-C(7)	2.128(3)	Pd-C(8)	2.141(3)
C(7)-C(8)	1.421(4)	P(1)-Pd-P(2)	94.96(3)
C(7)-Pd-C(8)	38.88(11)	C(7)-Pd-P(2)	108.20(8)
C(8)-Pd-P(1)	117.96(8)		

Table 3.7 Bond lengths (Å) and Angles (°) for [1,3-$C_3H_6(PPh_2)_2$ Pd (dba)] (21)

Figure 3.7 The Crystal Structure of [1,3-$C_3H_6(PPh_2)_2$ Pd (dba)] (21)

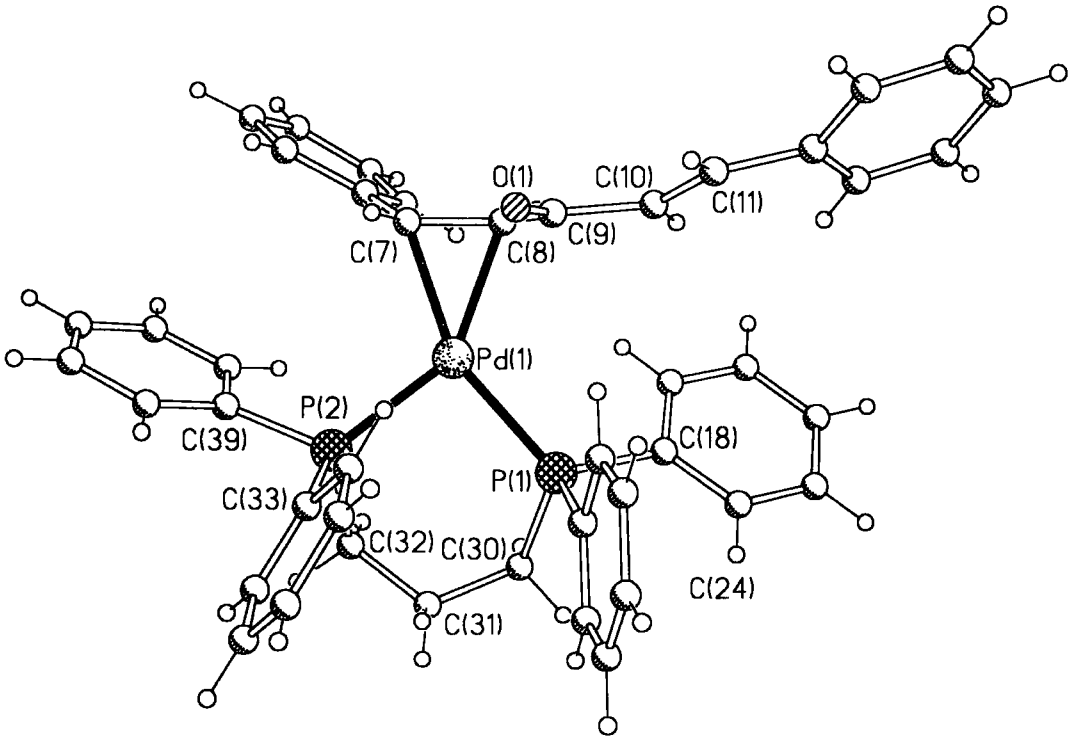

3.4.12 Synthesis of [$(PPh_3)_2$ Pd (dba)] (22)

Yield 3.8g, (40%). Found: C, 71.14; H, 5.15. $C_{53}H_{44}OP_2Pd$ requires C, 73.61; H, 5.09 %. Crystals suitable for a single crystal X-ray study were obtained by recrystallisation from thf layered with diethyl ether (for data see Figure 3.8 and Table 3.8). Crystal data for **22**: $C_{57}H_{52}OP_2Pd$, M = 864.33, monoclinic, space group $P2_1/c$, a = 14.7553(13), b = 18.6845(17), c = 17.6057(16) Å, β = 102.678(2)^0 , V = 4735.5(7) Å^3, Z = 4, T = 160 K; 28416 data measured, 8332 unique, Rint = 0.0870, 609 refined parameters, R = 0.1160, $wR2$ = 0.1438.

I.R. (KBr discs, cm^{-1}): ν (CO) 1645 vs.

NMR (d^8-toluene, 313K): $^{31}P\{^1H\}$, 23.8 (s), 25.6 (s) ppm; ^1H, δ 7.0-8.0 (br, aromatics).

Mass Spectrum (FAB + ion, mNBA matrix): M/z 864 [(1%), $(M+H)^+$], 630 [(10%), $(M\text{-dba})^+$].

P(1)-Pd	2.3295(16)	P(2)-Pd	2.3280(15)
Pd-C(7)	2.160(5)	Pd-C(8)	2.169(6)
C(7)-C(8)	1.405(8)	P(1)-Pd-P(2)	115.11(6)
C(7)-Pd-C(8)	37.9(2)	C(7)-Pd-P(1)	98.77(16)
C(8)-Pd-P(2)	108.55(16)		

Table 3.8 Bond Lengths (Å) and Angles (°) for $[(PPh_3)_2Pd(dba)]$ (22)

Figure 3.8 The Crystal Structure of $[(PPh_3)_2Pd(dba)]$

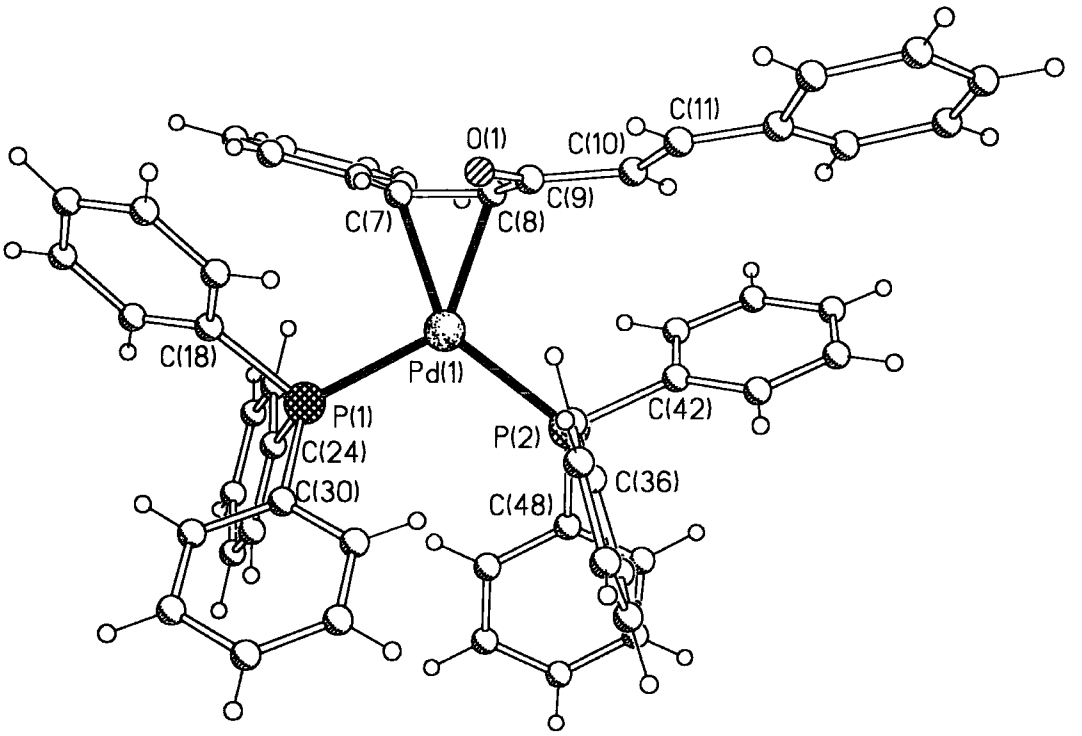

3.4.13 Synthesis of [$C_{10}H_6(2,3,CH_2PBu^t_2)_2Pd(dba)$] (23)

Yield 4.2g (50%). Found: C, 68.01; H, 7.65. $C_{45}H_{60}OP_2Pd$ requires C, 68.8; H, 7.65%.

I.R. (KBr discs, cm^{-1}): ν (CO) 1643 vs.

NMR (d^8 toluene, 293K): $^{31}P\{^1H\}$, δ 52.59(br), 50.9 (br) ppm;^1H, δ 6.8-7.4 (br, aromatics + alkene CH), 3.10 (br CH_2), 1.4 (br, CH_3) ppm.

Mass Spectrum(FAB + ion, mNBA matrix): M/z 785 [(2%), $(M+H)^+$], 550 [(50%), $(M\text{-dba})^+$], 1334 [(10%), $(L_2Pd(dba)+L_2Pd)^+$].

The attempted recrystallisation of **(23)** from thf layered with pentane resulted in the formation of a small quantity of orange crystals suitable for x-ray structural analysis. This recrystallisation was attempted twice and, in both cases, these crystals turned out to be a dioxygen complex. The formation and structural characterisation of these complexes is discussed in chapter 5.0.

3.4.14 Synthesis of [(DPEphos)Pd(dba)] (24)

Yield 4.80g (50%). Found: C, 69.63; H, 4.99. $C_{53}H_{42}O_2P_2Pd$ requires C, 72.4; H, 4.78%. Crystals suitable for a single crystal X-ray study were obtained by recrystallisation from thf layered with heptane (for data see Figure 3.9 and Table 3.9). Crystal data for **24**: $C_{53}H_{42}O_2P_2Pd$, M = 878.10, monoclinic, space group I2/a, a = 21.5459(15), b = 21.2456(15), c = 23.0254(15) Å, β = 111.643(2)^0 , V = 9796.9(12) Å^3, Z = 8, T = 160 K; 30978 data measured, 11741 unique, Rint = 0.0471, 601 refined parameters, R = 0.0878, $wR2$ = 0.1158.

NMR (d^8-toluene, 293K): $^{31}P\{^1H\}$, δ 13.8 (s), 8.1 (s) ppm; ^1H, δ 7.0-8.0 (br, aromatics) ppm.

Mass Spectrum(FAB + ion, mNBA matrix): M/z 878 [(2%), $(M)^+$], 644 [(15%), $(M\text{-dba})^+$].

P(1)-Pd	2.3449(8)	P(2)-Pd	2.3160(8)
Pd-C(37)	2.155(3)	Pd-C(38)	2.161(3)
C(7)-C(8)	1.415(4)	P(1)-Pd-P(2)	106.92(3)
C(37)-Pd-C(38)	38.28(11)	C(37)-Pd-P(2)	102.08(8)
C(38)-Pd-P(1)	112.67(9)		

Table 3.9 Bond Lengths (Å) and Angles (°) for [(DPEphos)Pd(dba)] (24)

Figure 3.9 The Crystal Structure of [(DPEphos)Pd(dba)] (24)

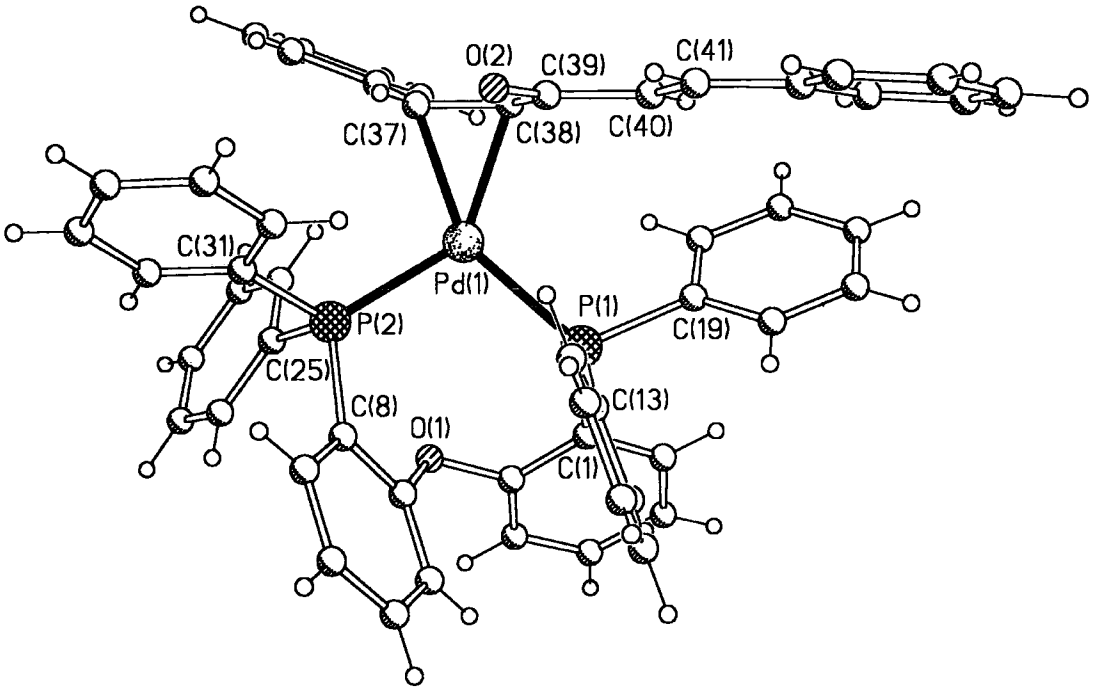

3.4.15 Synthesis of [o–$C_6H_4(CH_2PBu^t_2)_2$ Pt (dba)] (25)

$Pt(dba)_2$ was used in place of $Pd_2(dba)_3$ Yield 2.56g (32%). $C_{41}H_{58}OP_2Pt$ requires C, 59.78; H, 7.05% Found: C, 60.04; H, 7.21%. . Crystals suitable for a single crystal X-ray study were obtained by recrystallisation from thf layered with diethyl ether (for data see Figure 3.10 and Table 3.10). Crystal data for **25**: $C_{41}H_{58}OP_2Pt$, M = 823.90, triclinic, space group P-1, a = 9.2623(5), b = 11.4476(6), c = 19.3459(11) Å, α = 97.976(2), β = 93.121(2), γ

= 112.309(2)^0 , V = 1866.48(18) Å^3, Z = 2, T = 160 K; 14128 data measured, 8516 unique, Rint = 0.0402, 455 refined parameters, R = 0.0547, $wR2$ = 0.0880.

NMR (d^8-toluene, 293K): $^{31}P\{^1H\}$, δ 46.9 (br,J_{Pt-P} 3869 Hz), 44.4 (br, J_{Pt-P} 3298 Hz) ppm; ^1H, δ 6.8-7.4 (br, aromatics + alkene CH), 3.10 (br CH_2), 1.2 (br, CH_3) ppm; ^{13}C, δ 31.4 (m, CH_3), 32.0 (br, CH_2), 37.2 (br, quaternary), 64.0 (br, alkene CH), 73.0 (br, alkene CH), 125-145 (m, aromatics), 191.7 (s, carbonyl) ppm.

Mass Spectrum(FAB + ion, mNBA matrix): M/z 823 [(2%), $(M+H)^+$], 589 [(100%), $(M-dba)^+$], 1412 [(5%), $(L2Pt(dba)+L2Pt)^+$].

P(1)-Pt	2.3070(13)	P(2)-Pt	2.3176(14)
Pt-C(31)	2.128(5)	Pt-C(32)	2.121(5)
C(7)-C(8)	1.426(8)	P(1)-Pt-P(2)	103.69(5)
C(7)-Pt-C(8)	39.2(2)	C(31)-Pt-P(1)	108.84(15)
C(32)-Pt-P(2)	108.40(16)		

Table 3.10 Bond Lengths (Å) and Angles (°) for[o–$C_6H_4(CH_2PBu^t_2)_2Pt(dba)$] (25)

Figure 3.10 The Crystal Structure of [o-$C_6H_4(CH_2PBu^t_2)_2Pt(dba)$]

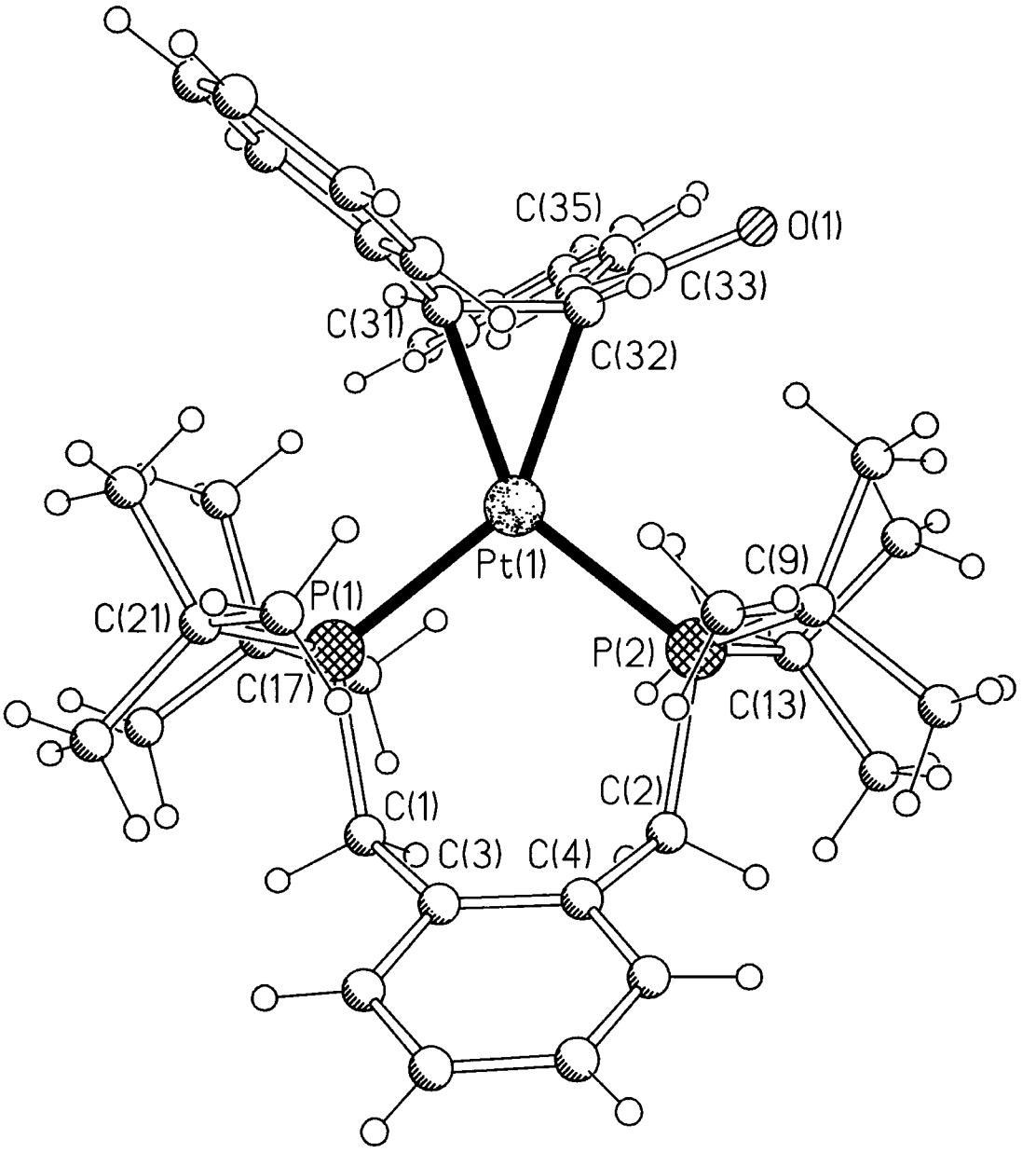

3.4.16 Synthesis of [o-$C_6H_4(CH_2PBu^t_2)_2Pd$(styrene)] (26)

Prepared according to the method of Spencer[21]. Yield 1.1g (85%). $C_{32}H_{52}P_2Pd$ requires C, 63.58; H, 8.61%, Found: C, 63.4; H, 8.8%.

NMR (d^8-toluene, 298K): $^{31}P\{^1H\}$, δ 50.4 (br), 46.5 (br) ppm; ^1H, δ 7.0-7.5 (9H, aromatics), 4.4 (br, 1H, alkene CH), 3.3 (br, 6H, alkene CH, ligand CH_2), 1.4 (br, 36, CH_3) ppm.

NMR (xylene, 193K): $^{31}P\{^1H\}$, δ 48.4 (d, J, 11.7 Hz), 46.9 (d, J, 11.7 Hz), 44.6 (d, J, 11.7 Hz), 42.9 (d, J, 11.7 Hz) ppm.

NMR (xylene, 233K): $^{31}P\{^1H\}$, δ 49.2 (s), 47.8 (s), 45.6 (s), 43.7 (s) ppm.

NMR (xylene, 273K): $^{31}P\{^1H\}$, δ 50.0 (br), 48.8 (br), 46.5 (br), 44.7 (br) ppm.

NMR (xylene, 313K): $^{31}P\{^1H\}$, δ 50.5 (br), 46.5 (br) ppm.

NMR (xylene, 343K): $^{31}P\{^1H\}$, δ 49.0 (vbr) ppm.

NMR (xylene, 373K): $^{31}P\{^1H\}$, δ 49.7 (s) ppm.

NMR (xylene, 403K): $^{31}P\{^1H\}$, δ 50.5 (s) ppm.

NMR (xylene, 298K after heating): $^{31}P\{^1H\}$, δ 50.3 (br), 46.1 (br) ppm.

The attempted recrystallisation of **(26)** from thf layered with pentane resulted in the formation of a small quantity of colourless crystals suitable for X-ray structural analysis. This recrystallisation was attempted twice and, in both cases, these crystals turned out to be a dioxygen complex. The synthesis of these dioxygen complexes and the structural features of these complexes will be discussed in chapter 5.0.

3.4.17 General Procedure for the Synthesis of Benzoquinone Complexes

To the palladium complex [$Pd_2(dba)_3$] (5g, 5.47mmol) and benzoquinone (1.18g, 10.94mmol) dissolved in thf (200ml) was added the diphosphine (10.94mmol) as a solution in thf (100ml). The deep purple colour of the [$Pd_2(dba)_3$] changed to bright orange after stirring for 1 hour. The reaction solution was stirred for a further 16 hours during which no further colour change occurred. The reaction was fine-filtered to remove palladium metal and the solvent removed under reduced pressure to yield a deep orange/red solid. This was

washed with cold hexane (-30°C) followed by cold ether (-30°C). The washings were discarded and the remaining solid dried under reduced pressure to yield the product as an orange/red powder. Further purification by recrystallisation from the appropriate solvent was carried out as described below to give crystals suitable for X-ray diffraction.

3.4.18 Synthesis of [o-$C_6H_4(CH_2PBu^t_2)_2Pd$(benzoquinone)] (27)

Yield 3.0g (45%). Found: C, 59.72; H, 8.07. $C_{30}H_{48}O_2P_2Pd$ requires C, 59.2; H, 7.89%. Crystals suitable for a single crystal X-ray study were obtained by recrystallisation from thf layered with heptane (for data see Figure 3.11 and Table 3.11). Crystal data for **27**: $C_{30}H_{48}O_2P_2Pd$, M = 609.02, monoclinic, space group $P2_1/n$, a = 8.725(3), b = 16.465(6), c = 21.038(8) Å, β = 94.544(7)°, V = 3012.8(19) Å^3, Z = 4, T = 160 K; 15281 data measured, 5301 unique, Rint = 0.1199, 334 refined parameters, R = 0.1137, $wR2$ = 0.1668.

I.R. (KBr discs, cm^{-1}): ν (CO) 1622 vs.

NMR (d^8-thf, 293K): $^{31}P\{^1H\}$, δ 51.4 (s) ppm; ^1H, δ 7.3 (m, aromatics), 7.0 (m, aromatics), 3.5 (br CH_2), 1.2 (d, J, 12.5 Hz, CH_3) ppm; ^{13}C, δ 31.6 (s, CH_2), 32.2 (s, CH_3), 39.2 (s, quaternary), 56.1 (s, CH), 128.1 (s, aromatic),134.97 (s, aromatic), 139.42 (s, aromatic), 192.2 (s, carbonyl) ppm.

NMR (d^8-thf, 193K): $^{31}P\{^1H\}$, δ 52.5 (s) ppm.

Mass Spectrum(FAB + ion, mNBA matrix): M/z 608[(5%), $(M)^+$], 500 [(60%), $(M\text{-}BQ)^+$].

P(1)-Pd	2.3556(19)	P(2)-Pd	2.364(2)
Pd-C(1)	2.179(7)	Pd-C(2)	2.187(7)
C(7)-C(8)	1.425(10)	P(1)-Pd-P(2)	104.53(7)
C(7)-Pd-C(8)	38.1(3)	C(1)-Pd-P(2)	108.5(2)
C(2)-Pd-P(1)	108.0(2)		

Table 3.11 Bond Lengths (Å) and Angles (°) for [o-$C_6H_4(CH_2PBu^t_2)_2$ Pd (benzoquinone)] (27)

Figure 3.11 The Crystal Structure of [o–$C_6H_4(CH_2PBu^t_2)_2$ Pd(benzoquinone)] (27)

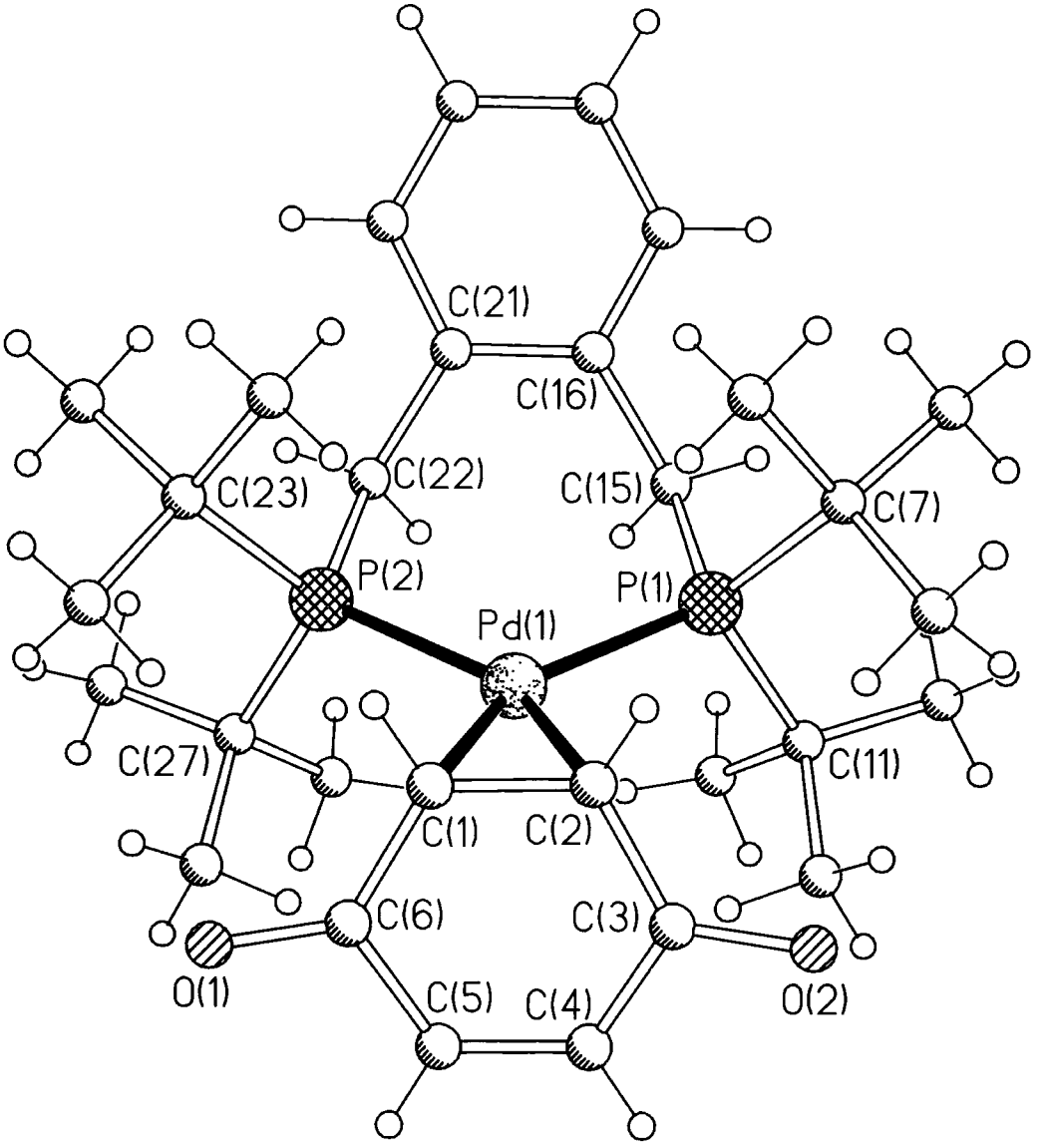

3.4.19 Synthesis of 1,8-[$C_{10}H_6(CH_2PBu^t_2)_2$ Pd (benzoquinone)] (28)

Yield 4.0g (55%). Found: C, 61.05; H, 7.55. $C_{34}H_{50}O_2P_2Pd$ requires C, 62.0; H, 7.59%.

I.R. (KBr discs, cm^{-1}): ν (CO) 1635 vs.

NMR (d^8-thf, 293K): $^{31}P\{^1H\}$, δ 69.5 (s) ppm; ^1H, δ 7.0-8.0 (m, aromatics), 3.9 (br CH_2), 1.2 (d, J, 13.2 Hz, CH_3) ppm.

Mass Spectrum(FAB + ion, mNBA matrix): M/z 668 [(4%), $(M)^+$], 550 [(20%), $(M\text{-}BQ)^+$].

3.4.20 Synthesis of [1,4-$C_4H_8(PBu^t_2)_2$ Pd (BQ)] (29)

Yield 3.2g (52%). Found: C, 47.2; H, 8.48. $C_{22}H_{48}O_2P_2Pd$ requires C, 47.1; H, 8.5%. Crystals suitable for a single crystal X-ray study were obtained by recrystallisation from thf layered with heptane (for data see Figure 3.12 and Table 3.12). Crystal data for **29**: $C_{26}H_{48}O_2P_2Pd$, M = 560.98, monoclinic, space group C2/c, a = 14.4257(16), b = 19.843(2), c = 18.835(2) Å, β = 91.218(3)^0 , V = 5390.2(10) Å^3, Z = 8, T = 173 K; 17248 data measured, 6431 unique, Rint = 0.0404, 298 refined parameters, R = 0.0615, $wR2$ = 0.0774.

NMR (d^8-thf, 293K): $^{31}P\{^1H\}$, δ 57.2 (s) ppm; ^1H, δ 1.85 (br, CH_2), 1.80 (br, CH_2), 1.2 (br, CH_2), 1.16 (d, J 12.2 Hz, CH_3) ppm; ^{13}C, δ 23.5 (s, CH_2), 24.3 (s, CH_2), 29.5 (s,CH_3), 35.4(s, quaternary), 128(m, aromatics), 189.4 (s, carbonyl) ppm.

Mass Spectrum(FAB + ion, mNBA matrix): M/z 560 [(5%), $(M)^+$], 452 [(40%), $(M\text{-}BQ)^+$].

P(1)-Pd	2.3572(7)	P(2)-Pd	2.3759(7)
Pd-C(23)	2.155(3)	Pd-C(22)	2.183(3)
C(22)-C(23)	1.411(4)	P(1)-Pd-P(2)	104.52(3)
C(22)-Pd-C(23)	37.97(10)	C(23)-Pd-P(1)	106.75(8)
C(22)-Pd-P(2)	109.77(8)		

Table 3.12 Bond Lengths (Å) and Angles (°) for [1,4-$C_4H_8(PBu^t_2)_2$ Pd(BQ)] (29)

Figure 3.12 The Crystal Structure of [1,4-$C_4H_8(PBu^t_2)_2$ Pd (BQ)] (29)

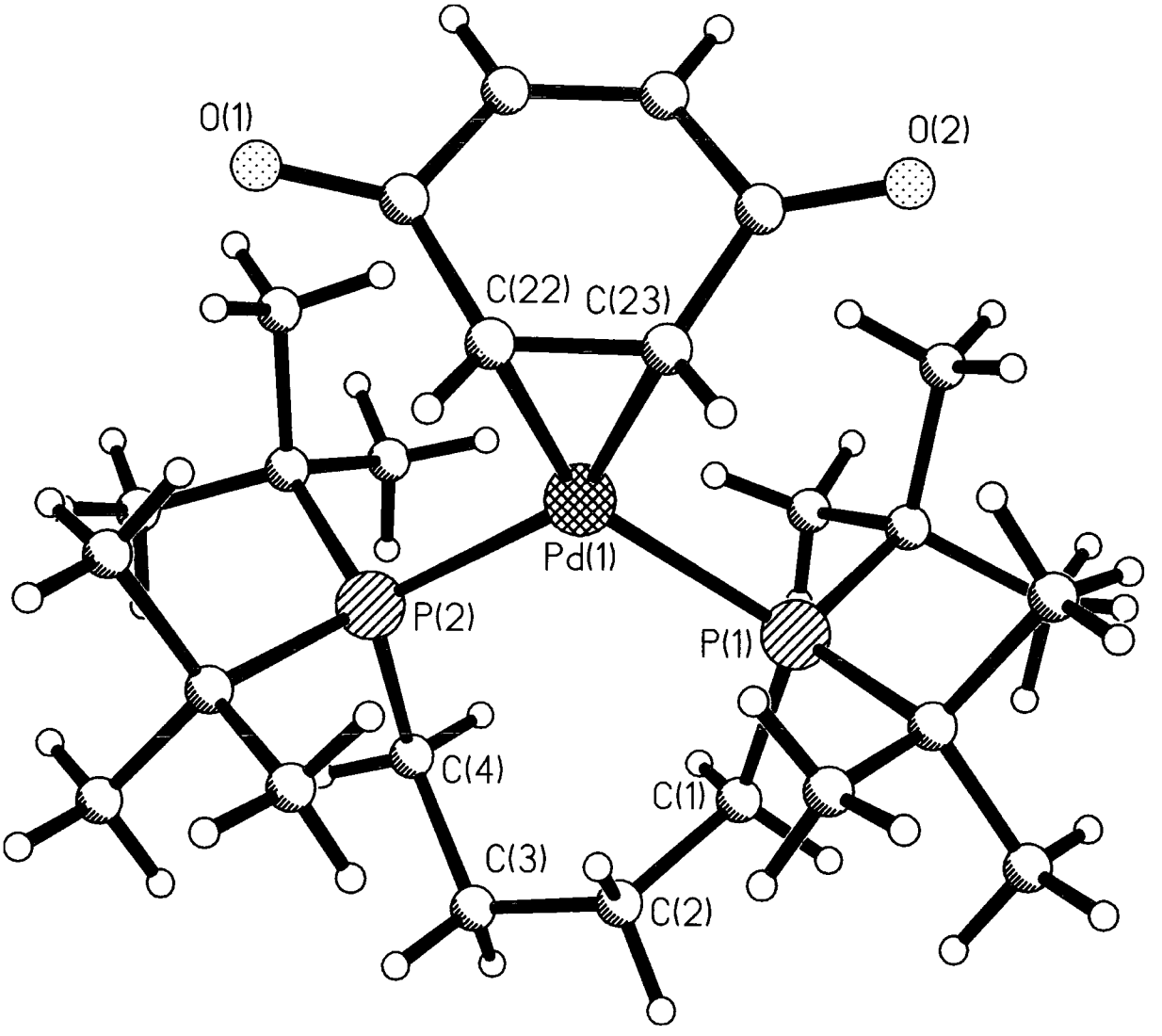

3.4.21 Synthesis of [o-$C_6H_4(CH_2PCy_2)_2$Pd(benzoquinone)] (30)

Yield 6.2g (80%). Found: C, 64.2; H, 7.75. $C_{38}H_{56}O_2P_2Pd$ requires C, 64.0; H, 7.86%.

I.R. (KBr discs, cm^{-1}): ν (CO) 1608 vs.

NMR (CD_2Cl_2, 293K): $^{31}P\{^1H\}$, δ 23.0 (s) ppm; ^1H, δ 1.2 (br, CH_2), 1.7 (br, CH_2), 3.1 (br CH_2), 5.0-5.8 (br,CH), 7.0-8.0 (m, aromatics) ppm.

Mass Spectrum(FAB + ion, mNBA matrix): M/z 712[(5%), $(M)^+$], 604 [(40%), $(M\text{-}BQ)^+$].

3.4.22 Synthesis of [o-$C_6H_4(CH_2PPh_2)_2$Pd(benzoquinone)] (31)

Yield 5.6g (75%). Found: C, 66.26; H, 4.69. $C_{38}H_{32}O_2P_2Pd$ requires C, 66.27; H, 46.5%.

I.R. (KBr discs, cm^{-1}): ν (CO) 1617 vs.

NMR (CD_2Cl_2, 293K): $^{31}P\{^1H\}$, δ 18.65 (s) ppm; ^1H, δ 3.7 (br CH_2), 5.0-5.4 (br, CH), 7.0-8.0 (br, m, aromatics) ppm. ^{13}C, δ 35.7 (s, CH_2), 116.32 (s, aromatic),126.58 (s, aromatic),128.75 (s, aromatic),130.70 (s, aromatic),131.63 (s, aromatic),133.17 (s, aromatic),133.49 (br, aromatic),143.24 (s, aromatic), 185.32 (s, carbonyl) ppm.

Mass Spectrum(FAB + ion, mNBA matrix): M/z 688 [(6%), $(M)^+$], 580 [(25%), $(M\text{-}BQ)^+$].

3.4.23 Synthesis of [1,3-$C_3H_6(PBu^t_2)_2$ Pd (benzoquinone)] (32)

Yield 5.6g (75%). Found: C, 54.51; H, 8.30. $C_{25}H_{46}O_2P_2Pd$ requires C, 54.84; H, 8.41%. Crystals suitable for a single crystal X-ray study were obtained by recrystallisation from thf layered with heptane (for data see Figure 3.13 and Table 3.13). Crystal data for **32**: $C_{25}H_{46}O_2P_2Pd$, M = 546.96, orthorhombic, space group Cmca, a = 19.5904(11), b = 14.0585(8), c = 18.8785(11) Å, $\alpha = \beta = \gamma = 90.0(0)^0$, V = 5199.4(5) $Å^3$, Z = 8, T = 160(2) K; 15942 data measured, 3267 unique, Rint = 0.0278, 148 refined parameters, R = 0.0262, $wR2$ = 0.0550.

I.R. (KBr discs, cm^{-1}): ν (CO) 1617 vs.

NMR (CD_2Cl_2, 293K): $^{31}P\{^1H\}$, δ 44.1 (s) ppm; ^1H, δ 1.11 (d, J= 12.7Hz, $^tBu\text{-}CH_3$), 1.3 (br, CH_2), 1.56 (br, CH_2), 5.29 (s, CH), 5.40 (br, CH) ppm; ^{13}C, δ 26.5 (s, CH_2), 30.0 (s, CH_2), 30.2 (s, CH_3), 30.6 (s, quaternary), 191.1 (s, carbonyl) ppm.

Mass Spectrum(FAB + ion, mNBA matrix): M/z 547[(5%), $(M)^+$], 439 [(40%), $(M\text{-}BQ)^+$].

P(1)-Pd	2.3307(4)	P(2)-Pd	2.3307(4)
Pd-C(1)	2.1633(14)	Pd-C(1A)	2.1633(14)
C(1)-C(1A)	1.434(3)	P(1)-Pd-P(2)	99.658(19)
C(1)-Pd-C(1A)	38.70(8)	C(1)-Pd-P(1)	109.70(4)
C(1A)-Pd-P(2)	109.70(4)		

Table 3.13 Bond Lengths (Å) and Angles (°) for [1,3-$C_3H_6(PBu^t_2)_2Pd(BQ)$] (32)

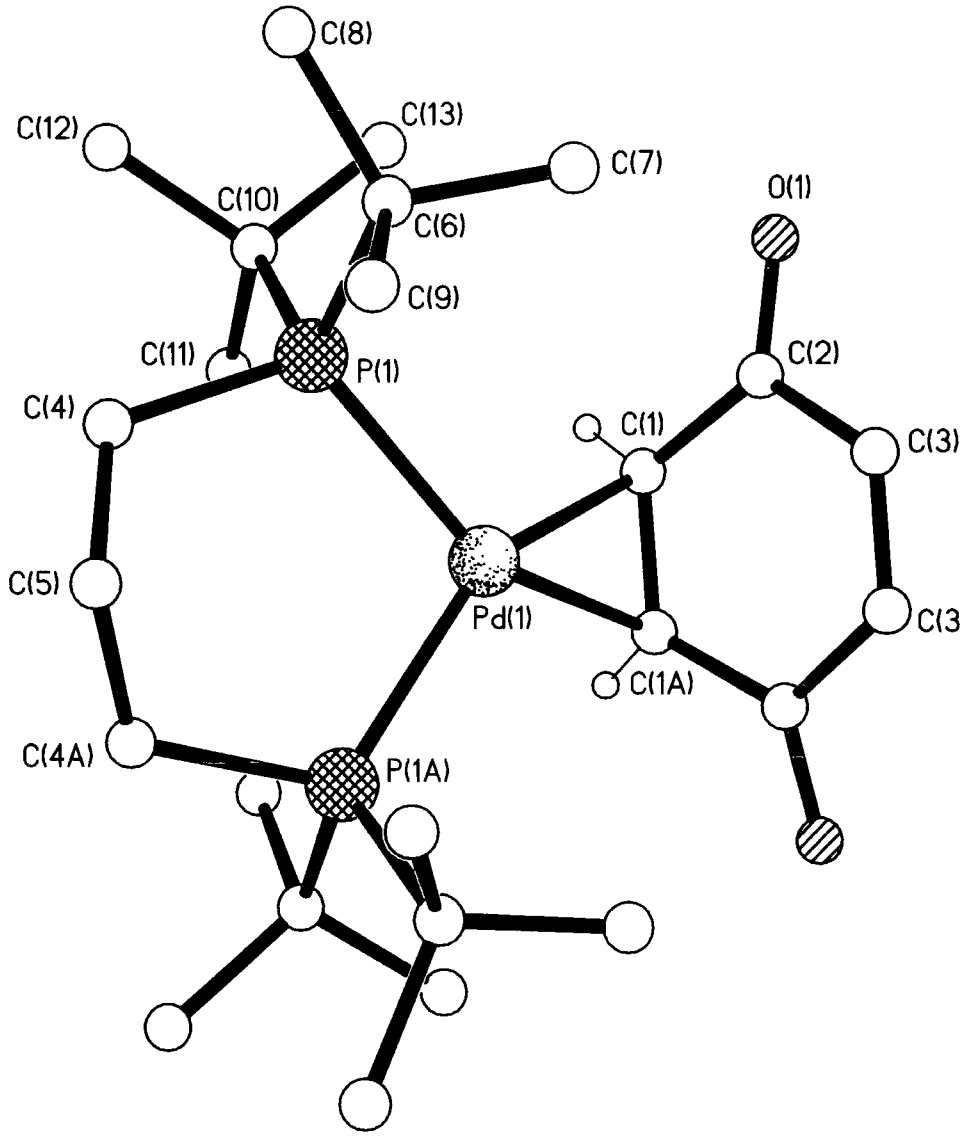

Figure 3.13 The Crystal Structure of [1,3-$C_3H_6(PBu^t_2)_2$Pd(BQ)] (32)

3.4.24 Synthesis of [2,3-$C_{10}H_6(CH_2PBu^t_2)_2$ Pd (benzoquinone)] (33)

Yield 5.0g (70%). Found: C, 61.88; H, 7.26. $C_{34}H_{48}O_2P_2Pd$ requires C, 62.19; H, 7.30%.

I.R. (KBr discs, cm^{-1}): ν (CO) 1623 vs.

NMR (CD_2Cl_2,, 293K): $^{31}P\{^1H\}$, δ 53.7 (s) ppm; ^1H, δ 1.24 (d, J= 12.7Hz, ^tBu-CH_3), 3.5 (br, ligand CH_2), 4.6 (br, CH), 7.36 (m, aromatics), 7.67 (m, aromatics), 7.79 (s, aromatics) ppm. ^{13}C, δ 30.17 (s, CH_2), 30.71 (s, CH_3), 37.98 (s, quaternary), 75.0 (vbr, CH), 116.34 (s, aromatic),126.46 (s, aromatic),127.16 (s, aromatic),128.72 (s, aromatic),129.33 (s, aromatic),131.75 (s, aromatic),135.56 (s, aromatic),143.50 (s, aromatic), 192.2 (s, carbonyl) ppm.

Mass Spectrum(FAB + ion, mNBA matrix): M/z 656[(5%), $(M)^+$], 548 [(60%), $(M\text{-}BQ)^+$].

3.4.25 Synthesis of [(DPEphos)Pd(benzoquinone)] (34)

Yield 5.0g (70%). Found: C, 66.26; H, 4.69. $C_{42}H_{32}O_3P_2Pd$ requires C, 67.02; H, 4.25 %. Crystals suitable for a single crystal X-ray study were obtained by recrystallisation from thf layered with heptane (for data see Figure 3.14 and Table 3.14). Crystal data for **34**: $C_{43}H_{34}O_3P_2Cl_2Pd$, M = 837.94, triclinic, space group P-1, a = 11.1250(8), b = 11.3119(8), c = 16.6951(12) Å, α = 76.549(2), β = 79.842(2), γ = 64.592(2)^0, V =1838.7(2) Å^3, Z = 2, T = 160(2) K; 13115 data measured, 8213 unique, Rint = 0.0340, 466 refined parameters, R = 0.0752, $wR2$ = 0.1131.

I.R. (KBr discs, cm^{-1}): ν (CO) 1625 vs.

NMR (CD_2Cl_2,, 293K): $^{31}P\{^1H\}$, δ 18.2 (s) ppm; ^1H, δ 5.25 (s, 4H, CH), 6.40 (m, 2H, aromatic), 6.76 (m, 2H, aromatic), 6.86 (m, 2H, aromatics), 7.15 (m, 10H, aromatics), 7.25 (s, 12H, aromatics) ppm. ^{13}C, δ 105.04(s, coordinated CH), 120.89(s, aromatic), 124.88(s, aromatic), 128.57 (s, aromatic), 130.12 (s, aromatic), 131.81 (s, aromatic), 134.10 (s, aromatic), 134.17 (s, aromatic), 134.23 (s, aromatic), 134.83 (s, aromatic), 158.97 (s, aromatic), 185.42 (s, carbonyl) ppm.

Mass Spectrum(FAB + ion, mNBA matrix): M/z 752[(8%), $(M)^+$], 644 [(30%), $(M\text{-}BQ)^+$].

P(1)-Pd	2.3152(10)	P(2)-Pd	2.3294(10)
Pd-C(1)	2.164(4)	Pd-C(2)	2.175(4)
C(1)-C(2)	1.422(5)	P(1)-Pd-P(2)	105.66(3)
C(1)-Pd-C(2)	38.26(14)	C(1)-Pd-P(1)	107.13(11)
C(2)-Pd-P(2)	109.01(11)		

Table 3.14 Bond Lengths (Å) and Angles (°) for [(DPEphos) Pd(benzoquinone)] (34)

Figure 3.14 The Crystal Structure of [(DPEphos)Pd(benzoquinone)] (34)

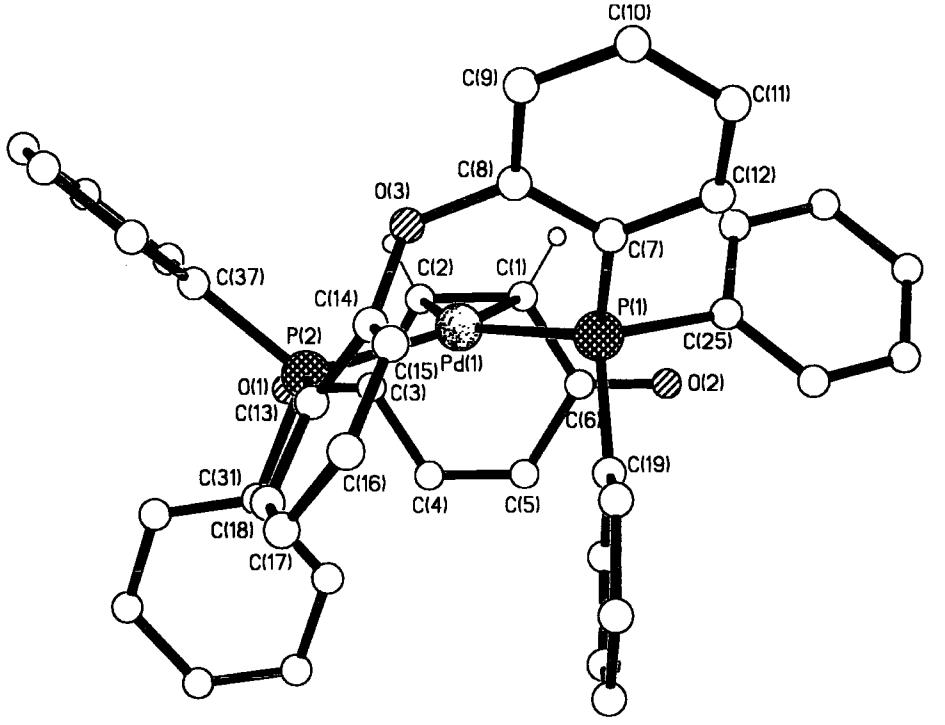

3.4.26 Synthesis of [(xantphos)Pd(benzoquinone)] (35)

Yield 5.0g (70%). Found: C,68.30; H, 5.80. $C_{45}H_{36}O_3P_2Pd$ requires C, 68.18; H, 5.68%. Crystals suitable for a single crystal X-ray study were obtained by recrystallisation from thf layered with heptane (for data see Figure 3.15 and Table 3.15). Crystal data for **35**: $C_{46}H_{38}O_3P_2Cl_2Pd$, M = 878.00, monoclinic, space group $P2_1/c$, a = 8.8641(6), b = 18.4696(12), c = 24.3678(16) Å, β = 99.155(2)^0 , V =3938.6(5) Å^3, Z = 4, T = 160(2) K;

21584 data measured, 7678 unique, *R*int = 0.0679, 495 refined parameters, $R = 0.0964$, $wR2 = 0.0968$.

NMR (CD_2Cl_2,, 293K): $^{31}P\{^1H\}$, δ 16.9 (s) ppm; ^1H, δ 1.58 (s, 6H, CH_3), 4.88 (s, 4H, CH), 6.40 (m, 2H, aromatic), 7.02 (m, 4H, aromatic), 7.09 (m, 20H, aromatics), 7.20 (m, 4H, aromatics), 7.43 (s, 2H, aromatics) ppm. ^{13}C, δ 27.61 (s, CH_3), 36.39 (s, quaternary), 103.76 (s, coordinated CH), 124.54 (s, aromatic), 126.60 (s, aromatic), 128.47 (s, aromatic), 129.86 (s, aromatic), 131.23 (s, aromatic), 134.09 (s, aromatic), 134.16 (s, aromatic), 134.22 (s, aromatic), aromatic), 155.75 (s, aromatic), 185.87 (s, carbonyl) ppm.

Mass Spectrum(FAB + ion, mNBA matrix): M/z 792[(6%), $(M)^+$], 644 [(100%), $(M\text{-}BQ)^+$].

P(1)-Pd	2.3576(11)	P(2)-Pd	2.3499(11)
Pd-C(1)	2.143(4)	Pd-C(2)	2.165(4)
C(1)-C(2)	1.405(6)	P(1)-Pd-P(2)	106.73(4)
C(1)-Pd-C(2)	38.06(15)	C(1)-Pd-P(1)	107.21(13)
C(2)-Pd-P(2)	107.59(12)		

Table 3.15 Bond Lengths (Å) and Angles (°) for [(xantphos)Pd(benzoquinone)] (35)

Figure 3.15 The Crystal Structure of [(xantphos)Pd(benzoquinone)] (35)

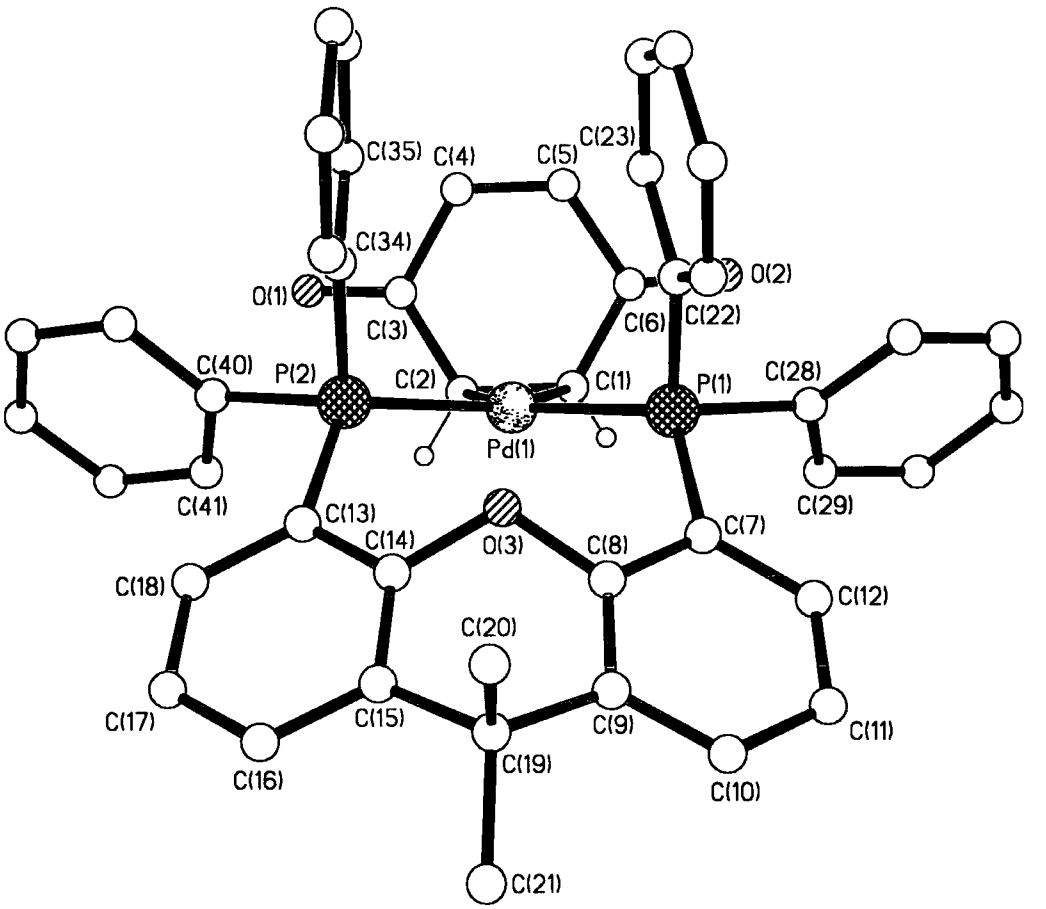

3.4.27 Synthesis of [(dppf)Pd(benzoquinone)] (36)

Yield 5.0g (70%). Found: C, 62.66; H, 4.21. $C_{40}H_{32}O_2P_2FePd$ requires C, 62.50; H, 4.16%.

NMR (CD_2Cl_2, 293K): $^{31}P\{^1H\}$, δ 24.05 (s) ppm; ^1H, δ 4.68 (d, J= 1.46Hz, 4H, C_pH), 4.81 (t, J= 1.95Hz, 4H, C_pH), 5.83 (s, 4H, alkene CH), 7.90 (m, 10H, aromatic), 8.06 (m, 10H, aromatic) ppm; ^{13}C, δ 27.61(s, CH_3), 72.7(s, C_p), 75.0(m, C_p) 104.91 (s, coordinated

CH), 128.56 (s, aromatic), 130.42 (s, aromatic), 134.16 (s, aromatic), 134.23 (s, aromatic), 134.30 (s, aromatic), 184.92 (s, carbonyl) ppm.

Mass Spectrum(FAB + ion, mNBA matrix): M/z 769[(25%), $(M+H)^+$], 660 [(100%), $(M-BQ)^+$].

3.4.28 General Procedure for the Synthesis of TCNE Complexes

To the palladium complex $[Pd_2(dba)_3]$ (5g, 5.47mmol) and tcne (1.40g, 10.94mmol) dissolved in toluene (200ml) was added the diphosphine (10.94mmol) as a solution in toluene (100ml). The solution was stirred overnight and a yellow/green precipitate formed. This was removed by filtration and washed twice with diethyl ether (50ml) before drying.

3.4.29 Synthesis of [o-$C_6H_4(CH_2PBu^t_2)_2$ Pd (tcne)] (37)

Yield 1.4g (90%). Found: C, 57.36; H, 7.05; N, 9.05. $C_{30}H_{44}N_4P_2Pd$ requires C, 57.3; H, 7.00; N, 8.91 %.

NMR (CD_2Cl_2, 293K): $^{31}P\{^1H\}$, δ 53.66 (s) ppm; ^1H, δ 7.4 (2H, m, aromatics), 7.2 (2H, m, aromatics), 3.6 (4H, br CH_2), 1.4 (br, 36H, CH_3) ppm.

3.4.30 Synthesis of [o-$C_6H_4(CH_2PPh_2)_2$ Pd (tcne)] (38)

Yield 1.4g (90%). Found: C, 64.48; H, 4.15; N, 7.70. $C_{32}H_{28}N_4P_2Pd$ requires C, 64.4; H, 3.95; N, 7.9%.

NMR (CD_2Cl_2, 293K): $^{31}P\{^1H\}$, δ 13.08 (s) ppm; ^1H, δ 3.7 (br CH_2), 7.0-8.0 (br, m, aromatics) ppm. δ ^{13}C, δ 35.35 (br, CH_2), 113.6 (s, coordinated CH), 129.59 (s, aromatic), 132.04 (s, aromatic), 132.48 (s, aromatic), 133.41 (s, aromatic), 143.26 (s, aromatic) ppm.

3.4.31 Synthesis of [(DPEphos)Pd(tcne)] (39)

Yield 1.4g (90%). Found: C, 65.15; H, 3.70; N, 7.40. $C_{42}H_{28}N_4OP_2Pd$ requires C, 65.28; H, 3.63; N, 7.25%.

NMR (CD_2Cl_2, 293K): $^{31}P\{^1H\}$, δ 12.99 (s) ppm; δ ^{13}C, δ 114.04 (s, coordinated CH), 125.55 (s, aromatic), 129.36 (s, aromatic), 129.40 (s, aromatic), 131.41 (s, aromatic), 133.29 (s, aromatic), 133.90 (s, aromatic), 133.96 (s, aromatic), 134.02 (s, aromatic), 134.89 (s, aromatic), 159.05 (s, aromatic) ppm.

3.5 Discussion

3.5.1 Phosphine Synthesis

The phosphine ligands **1-8** detailed above were synthesised according to the method of Shaw and Moulton.[7] In this method, the secondary phosphine was reacted with 1,2-dibromo-o-xylene in acetone to yield the diphosphonium bromide as a precipitate. This material was then treated with an excess of sodium acetate in degassed water to liberate the desired phosphine as a precipitate which was extracted into ether. In all cases, except for the synthesis of 1,2-bis(dicyclohexylphosphinomethyl)benzene, the yield of the desired product was less than 50% based on the secondary phosphine.

The main byproduct has been identified in the synthesis of 1,2-bis(di-*tert*-butylphosphinomethyl)benzene and shown to be the result of an internal cyclisation reaction (see scheme 3.1). The cyclised byproduct does not react with sodium

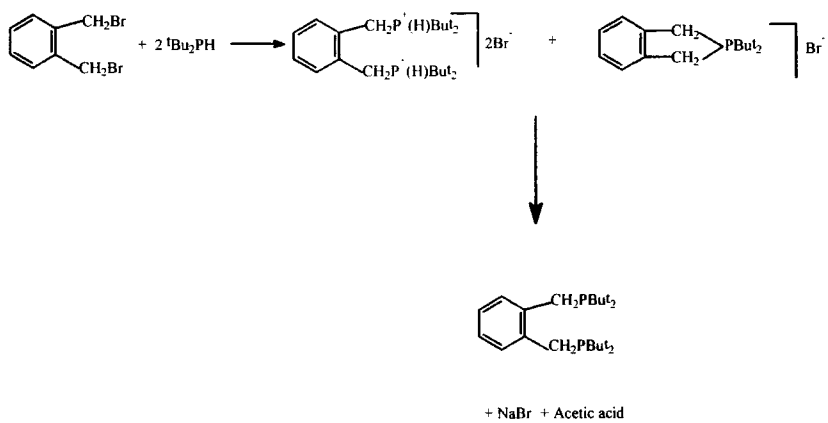

Scheme 3.1

acetate to liberate a monophosphine, and thus this ionic product remains in solution in the synthesis, allowing for easy separation of the desired product from the byproduct. The formation of byproduct was thought to occur via the elimination of HBr from the mono-phosphonium salt followed by cyclisation to form the internal phosphonium salt (scheme 3.2).

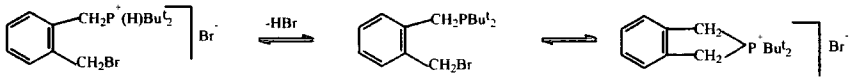

Scheme 3.2

The addition of the alkyl halide to di-*tert*-butylphosphine in excess should give increased yields of the diphosphonium salt, and hence the desired phosphine. This has not proven to be the case; the yield of phosphine never exceeds 40%. This is believed to be due to the basicity of the phosphines themselves which promote HBr elimination when present in excess, and this counteracts the benefit of increased phosphine which promotes diphosphonium salt formation.

The formation of large quantities of the cyclised material in the synthesis of 1,2-bis(di-*tert*-butylphosphinomethyl)benzene make this a very inefficient synthesis, considering the expense of the di-*tert*-butylphosphine starting material. The synthesis of these materials via attack of lithium phosphide intermediates on 1,2-dibromo-o-xylene and 1,2-dichloro-o-xylene has been tried according to scheme 3.3.

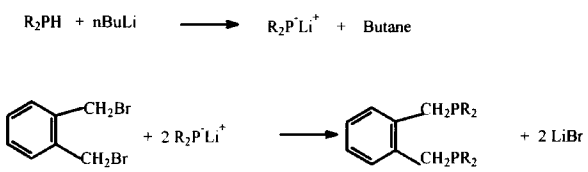

Scheme 3.3

This route works well for the phenyl and cyclohexyl substituted phosphines but, for the di-*tert*-butyl and di-*tert*-pentyl substituted phosphines, a complicated mixture of products is obtained. It would appear in the *tert*-butyl case, because of the steric bulk and electron-donating nature of the groups on phosphorus, that the phosphide anions are very strong bases, similar in nature to lithium diethylamide. The abstraction of protons from, for example, the methylene groups of the xylene precursors competes effectively with the nucleophillic substitution reaction and leads to the complex mixture of products. This is not

the case for Cy_2PLi and Ph_2PLi where nucleophillic substitution is the favoured reaction pathway.

The third procedure for the synthesis of the naphthyl phosphines was used primarily because the alkyl halides necessary to synthesize these materials via the phosphonium salt route are not commercially available. The selective deprotonation of several dimethylnaphthalenes and benzenes has been reported to be complete in 2 hours using pentylsodium/TMEDA mixtures in pentane.[8] We have found the use of butyllithium/TMEDA to be less efficient, but the di-lithio species precipitates from the reaction solvent and can be harvested for reaction with chlorophosphine.

3.5.1.1 Phosphine Crystallographic Data

A brief perusal of the X-ray data for the free phosphine ligands **(7, 11)** indicates that, in both cases, the bond lengths and angles are not unusual for tertiary phosphine ligands.[4] In both cases, the methylene groups act like an elbow to allow the phosphorus atoms to move away from each other. Taking **(7)** as an example, the lone pair on the phosphorus atom P2 points away from the phosphorus atom P1, whose lone pair points toward P2 rather than away. One might anticipate that the phosphorus atoms would orientate themselves on either side of the benzene ring to minimize steric repulsions.

Given the orientation of the lone pairs in the ground state, it seems reasonable to anticipate that this family of ligands could form bridging metal complexes rather more easily than many other chelating phosphines. We can see from the experimental section, and also from later work, all zerovalent palladium alkene complexes of ortho-xylene based ligands contain phosphine ligands coordinated as chelates. No examples of bridging phosphines have been isolated or evidence found for their presence in solution.

For chelation of the phosphine ligands to occur rotation about the carbon-phosphorus bond takes place to orientate both phosphorus lone pairs such that they can interact with available metal d-orbitals. There is, presumably, a significant energy barrier to overcome for which the driving force is chelation.[10] It is still surprising that the chelate effect alone can

account for the complete absence of bridging complexes, especially when the chelate ring size formed in this case is a relatively large seven membered one.

3.5.2 Phosphine Palladium (0) Complexes

The addition of stoichiometric equivalents of bidentate phosphine ligand and $Pd_2(dba)_3$ result in the formation of complexes of general formula [(P-P)Pd(dba)], where the phosphine is coordinated in a chelate fashion to a single palladium atom. The isolated yields of analytically pure samples of these species are relatively low (20-40%), in all cases being due to the difficulty of removing dba from the target compound. An analysis by ^{31}P NMR of the reaction solution 1,2-bis(di-*tert*-butylphosphinomethyl)benzene and $Pd_2(dba)_3$ in thf reveals the presence of signals attributable to the above product, with no evidence for the free ligand. This result suggests that the coordination reaction is quantitative, and supports the suggestion that the low yields are a result of the work up procedure. The reaction of $Pd(dba)_2$ with diop has been studied by Amatore et al in some detail[11], and it has been shown that the reaction of $Pd(dba)_2$ with 1 equivalent of diop {4,5-bis(diphenylphosphino)methyl-2,2'dimethyl-1,3 dioxolane} results in the formation of $[Pd(diop)_2]$ at short reaction times (10 mins), whilst at long reaction times (4 hours), a complex forms in which the two phosphorus atoms are not equivalent. This complex has been assigned as the [(P-P)Pd(dba)] complex where the phosphine is chelating and the dba is coordinated η-2 via one of its alkene moieties. Undoubtedly, the ability to form the bisphosphine species $[Pd(diop)_2]$ is related to the steric bulk of the phosphine, and no evidence has been found for the formation of these species with the bulky dialkylphosphines employed in this study. In the work of Amatore et al, the reaction of $Pd(dba)_2$ with an excess of binap {1,1'-bis(diphenylphosphino)binapthalene}shows no evidence for the formation of $[Pd(binap)_2]$; only the complex [(binap)Pd(dba)] is indicated by ^{31}P NMR. This reaction is believed to be under steric control. In the present study, where the formation of the bisphosphine species might be anticipated, for example, with the phenyl substituted phosphines, the long reaction times favour the formation of the observed [(P-P)Pd(dba)] complex, in agreement with the published literature.[11]

The complexes appear to be air-stable in the solid state and are all orange powders. The stability of the compounds in solution depends on several factors which include the

structure of the phosphine ligand, the nature of coordinated alkene, solvent type , the presence of oxygen and the temperature of the solutions. The formation of oxygen complexes will be discussed in chapter 5.0 which deals with the formation and characterisation of these materials.

The dba ligand is readily displaced by benzoquinone (bq) and tetracyanoethene (tcne) simply by stirring the dba complex in the presence of the more π acidic alkene. The increased propensity of the tcne/bq to back-accept electron density from palladium (0) leads to more stable complexes, and hence drives these reactions in favour of the tcne/bq complexes. The dba ligand itself, though, appears to be quite strongly held, as evidenced by variable temperature NMR experiments on (**12**), where the dba is not dissociated until temperatures in excess of 100^0C.

3.5.3 Spectroscopic Analysis

3.5.3.1 Mass Spectroscopy

A strong molecular ion is observed in the FAB +ve ion mass spectrum of all the palladium (0) alkene complexes. The major ion, though, corresponds to the $[(P\text{-}P)Pd]^+$ fragment which results from the loss of alkene. This ion is the most intense ion in the spectrum in many cases. Also evident are what are most likely cluster ions, which, by mass, correspond to $[(P\text{-}P)Pd(alkene)Pd(P\text{-}P)]^+$. The formation of cluster ions is a common phenomenon in FAB spectra and, in this case, they are suggested to be formed by the association of $[(P\text{-}P)Pd]^+$ with the target compound [(P-P)Pd(dba)]. Single crystal X-ray data and multi-nuclear solution NMR data indicate they do not correspond to dimers of the type $[\{Pd(P\text{-}P)\}_2(alkene)]$, reported to be formed with tributylphosphine and benzoquinone[12] e.g. $[\{Pd(PBu_3)\}_2(p\text{-}C_6H_4O_2)]$.

The loss of alkene, particularly dba, from complexes, appears to be enhanced in the electrospray mass spectrum where the sample is in solution prior to analysis. An interesting feature of the electrospray data is the absence of a molecular ion in many cases, and the presence of ions corresponding to $[(P\text{-}P)Pd(O_2)]$. The formation of oxygen complexes is not new,[13] with examples known for platinum and palladium with triphenylphosphine. A number of these oxygen complexes have been produced in this study and been the subject of single

crystal X-ray studies, as they readily crystallise in the neck of an NMR tube whereas the zerovalent palladium dba complexes remain in solution. One suggested mechanism for the formation of the oxygen complexes involves dissociation of the dba in solution to give a 14 electron species which then reacts with molecular oxygen. This dissociation of dba has been shown to occur using electrochemistry for complexes of the type [(P-P)Pd(dba)] to generate 14 electron [(P-P)Pd], where (P-P) = binap, diop, dppf, dppe, dppm, dppp.[11] The kinetics of the dba dissociation are shown to be dependent on the nature of the phosphine ligand, with increased bite angle favouring the formation of the 14 electron species. The ready crystallisation of these oxygen complexes has allowed the ligand geometry on coordination to palladium to be studied where the crystallization of the dba complexes has not proved possible. This data will be discussed in detail in chapter 5.0.

3.5.3.2 I.R. Spectroscopy

The carbonyl of the coordinated dba and benzoquinone ligands is readily detected by I.R. but no clear correlation exists between the expected ligand basicity and the position of the carbonyl absorption in the I.R. spectrum. Conventional wisdom suggests the variations in electron density at the metal centre resulting from coordination to ligands of differing basicity can be detected by spectroscopic changes in other ancillary ligands coordinated to the metal.[14] The classic ancillary ligand is carbon monoxide where changes in the CO stretching frequency reflect the balance between σ–donation and π–back acceptance for a given phosphine ligand.[15] The absence of a correlation in this study is suggested to be due to the conjugated π-electron system in the alkenes used in this study, of which the carbonyl forms a part. That the phosphine ligand is having an electronic effect on the metal centre, if not a predictable one, is demonstrated by the variation in the carbonyl stretching frequency between complexes.

3.5.3.3 ^{31}P NMR Spectroscopy

The NMR of the complexes [(L-L)Pd(alkene)] **12-38** have been studied, but much of the data leading to an understanding of the solution behavior of these complexes has come from a study of **12** where (L-L) = 1,2-bis(di-*tert*-butylphosphinomethyl)benzene.

The ^{31}P NMR of **(12)** at room temperature in toluene shows 2 broad resonances at 48ppm and 50ppm, indicative of exchange processes occurring within the molecule, not resolved on the NMR time scale. On cooling to -80^{0}C, 7 sharp signals are resolved from the broad resonances. The integration of this spectrum is consistent with there being 3 major conformational species and 1 minor one, giving rise to 8 signals in total. In this case, one of the peaks from the minor species is coincident with one of the major species.

The observations from the VT ^{31}P NMR can be rationalised with reference to published literature.[16] The complex [(L-L)Pd(dba)] where (L-L) = 1,1-bis(diphenylphosphinomethyl)- 2,2'-biphenyl has been synthesised and its ^{31}P NMR spectrum recorded. On cooling to -70^{0}C, 8 doublets are present in the ^{31}P NMR spectrum which are assigned to 4 conformational isomers, each isomer having inequivalent phosphorus centres. These conformational isomers are proposed to result from the restricted motion in both the biphenyl bridge and the coordinated dba. In the dba, rotation about the carbon-carbon bond (to which the carbonyl carbon is attached nearest to the coordinated alkene), is suggested to be restricted.

The following model has been developed on the basis of the above literature and the solid state structure to rationalize the solution multinuclear NMR data. The bonding interaction between the metal and the dba comprises an interaction between a π–orbital of the alkene and an empty d orbital on the metal. The π–orbital on the alkene is located above and below the plane of the carbon-carbon σ bond, and presents itself to the metal such that the substituents on the alkene are above and below the MC_2 plane. The alternative would be that the metal approaches in the same plane as the alkene. The single crystal X-ray study shows the former bonding arrangement is present in the solid state. This is illustrated in Figure 3.16 and Figure 3.17 which show the likely structures frozen out on cooling to 193K in a non-coordinating solvent. The molecule is illustrated in plan view in Figure 3.16 and as a schematic in figure 3.17 looking down the carbon-carbon bond of the coordinated dba. Four conformers are thought to be possible, these are suggested to be a result of freezing out i) two possible dispositions of the aromatic ring of the phosphine ligand relative to the dba and ii) two different orientations of the dba carbonyl resulting from a low energy barrier to rotation about the carbon-carbon bond between the coordinated alkene carbon and the carbonyl

carbon. The broadness in the spectra recorded at room temperature is thought to be due to the latter process as molecular modeling calculations suggest that the ligand aromatic ring flipping is a high energy process and unlikely to occur.[17] The broadness may also be due to an exchange process where the alkene moieties exchange. This process is suggested to occur for η^2 coordinated alkenes such as benzoquinone.[18] In these cases it is perhaps easier to envisage a rolling type exchange of the alkene. On cooling we slow down or even freeze out completely this exchange thus observing the conformers. On warming the rate of exchange increases such that we do not observe the inter conversion and the signals sharpen.

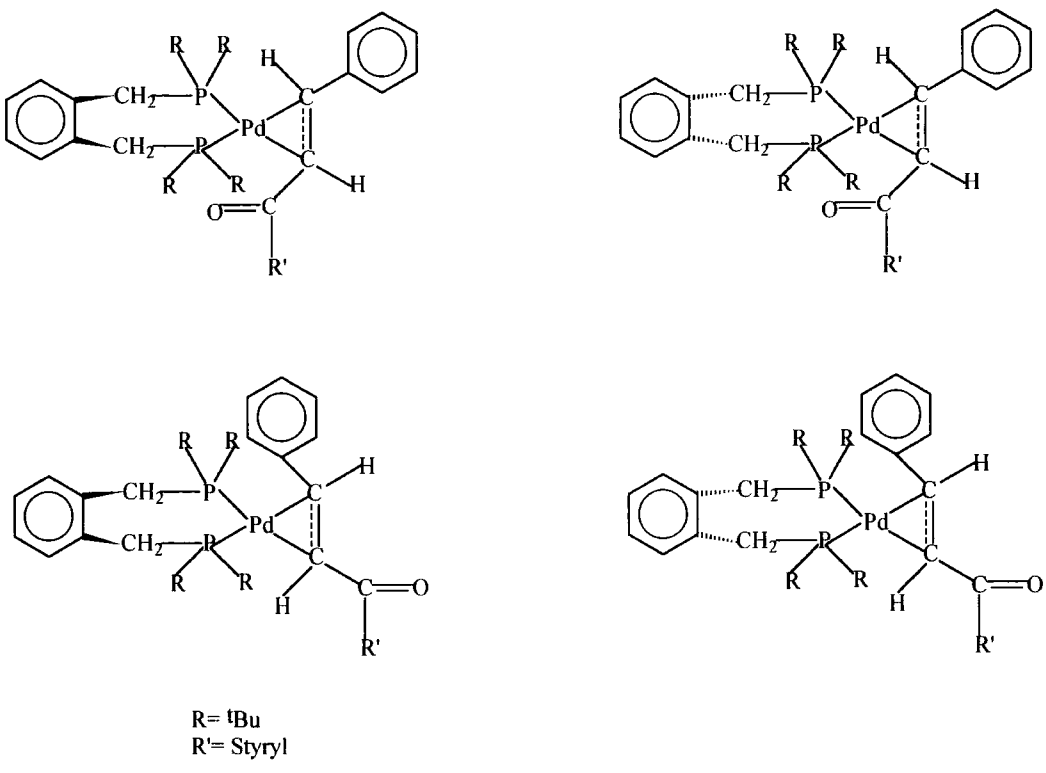

R= ^{t}Bu
R'= Styryl

Figure 3.16 Possible Conformations of (12) on Cooling to -80^{0}C

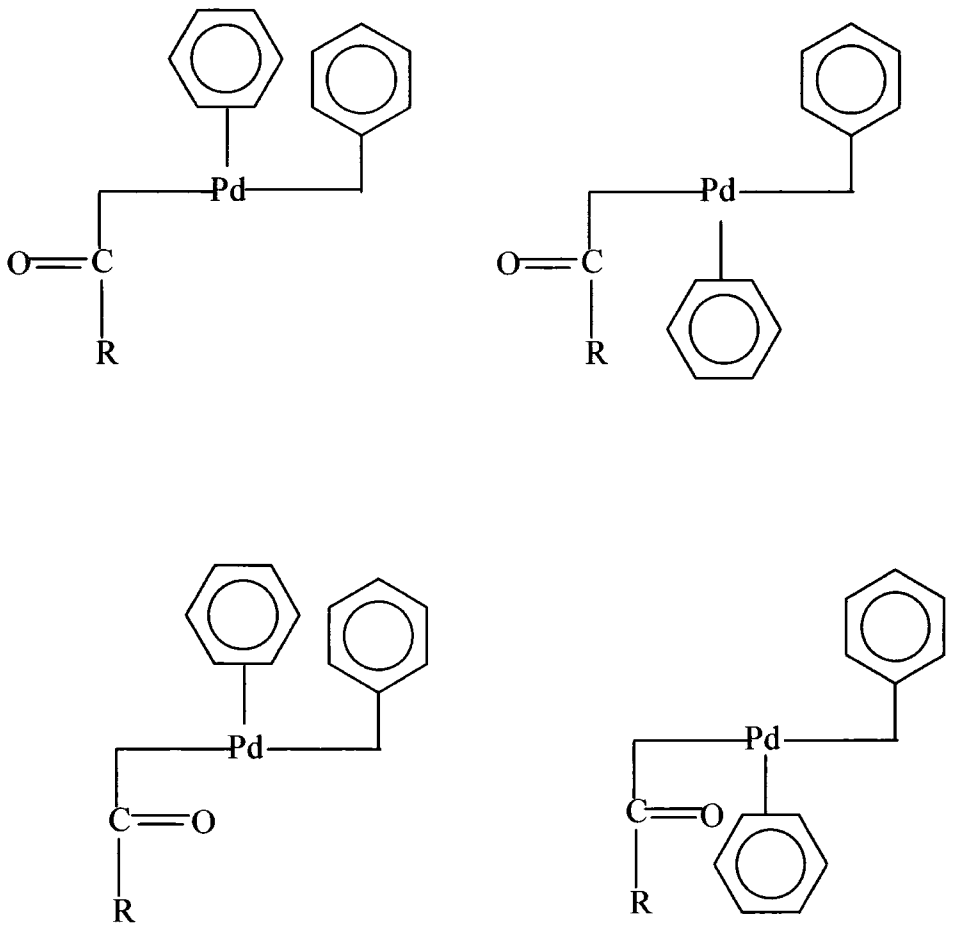

R= Styryl

Figure 3.17 Schematic Illustrating the Possible Conformations of (12) Frozen Out on Cooling to -80^{0}C

If the above model is correct, the ^{31}P NMR data recorded in toluene show the thermodynamic similarity of three of the possible four conformers. It seems likely that the structure where the ligand benzene ring and the carbonyl fragment are in closest proximity is the thermodynamically disfavoured conformer.

Other evidence for this model of the solution state NMR behavior comes from the study of other complexes of the form [(L-L)Pd(dba)], where (L-L) = 1,3-bis(di-*tert*-butylphosphino)propane **(20)**, 1,2-bis(di-*tert*-butylphosphino)ethane **(19)**, 1,3-bis(diphenylphosphino)propane **(21)**, 1,3-bis(dicyclohexylphosphino)propane,[19] 1,2-bis(dicyclohexylphosphino)ethane[19] and the complexess [(L-L)Pd(styrene)] **(26)**,

[(L-L)Pd(BQ)] **(27)** and [(L-L)Pd(tcne)] **(37)**. The ^{31}P NMR data recorded in toluene at 193K, 298K and 373K are presented in Table 3.16 and discussed below.

When (L-L) = 1,2-bis(di-*tert*-butylphosphino)ethane **(19)** the possibility of different conformations relating to the ligand backbone is absent. The room temperature spectrum consists of two relatively sharp signals. The signals might be expected to be sharper due to the reduced bite angle of the ethane bridged phosphines[20] and therefore steric demands imposed by the *tert*-butyl groups of the ligand would be less. Hence the barrier to rotation of the dba carbonyl would be reduced or the rate of inter-conversion of the two possible degenerate η^2 alkene species is now faster than is observable on the NMR time scale.

On cooling to -80^{0}C the ^{31}P NMR spectrum develops to give four signals, two major peaks of equal area and two minor peaks of equal area. This spectrum is consistent with the presence of two conformational isomers arising from the dba, with one isomer being thermodynamically favoured.

When (L-L) = 1,3-bis(di-*tert*-butylphosphino)propane **(20)** the room temperature ^{31}P spectrum consists of two broad resonances one of which is significantly broader than the other. Here we might expect increased broadness of the signals when compared to the ethane bridged phosphine. The bite angles typically for propane bridged chelating phosphines[20] are 6-10 degrees larger than for ethane bridged analogues and therefore the ligand is more sterically demanding for a given substituent on phosphorus. The barrier to conformer inter-conversion would therefore be higher, and consequently, at a given temperature the ^{31}P NMR signals broader. Cooling to -80^{0}C in this case only produces four signals, assigned to two conformational isomers consistent with a symmetrical chelate bridge or one in which the barrier to inter-conversion is very low and hence not frozen out at -80^{0}C. This is most likely true of the propane bridge where the inter conversion of chair and boat conformers of the six membered ring which the propane bridge forms a part of, is not frozen on cooling.

Finally, the complex [(L-L)Pd(styrene)] **(26)** has been studied[21] where (L-L) = 1,2-bis(di-*tert*-butylphosphinomethyl)benzene. The complex was made as a dba free catalyst source. The room temperature ^{31}P NMR consists of two broad resonance's very similar to the dba complex. Heating to 60^{0}C sharpens these signals and cooling to -80^{0}C reveals four

signals (two each of equivalent area), assigned to two conformational isomers, half the number found for the dba complex. This might be expected given that only one of the two proposed inter conversions is possible in the styrene complex. The absence of dba has reduced the number of possible conformational isomers. Here, the conformers are suggested to result from the two possible orientations of the benzene ring of the backbone relative to the coordination of the styrene i.e. the benzene ring of the styrene points up with the ligand backbone or points down away from the ligand backbone.

The VT ^{31}P NMR of mixed substituent phosphines of formula $C_6H_4(CH_2PR^1R^2)$ where stereoisomers are fixed on coordination to palladium, also supports the proposed NMR interpretation. The room temperature ^{31}P NMR spectra of the complex of the above mixed substituent ligand where R^1= *tert*-butyl and R^2= *tert*-pentyl consists, of two broad resonances very similar in nature to those observed for the complex [(L-L)Pd(dba)] where (L-L) = 1,2-bis(di-*tert*-butylphosphinomethyl)benzene. On cooling to -80^{0}C the spectrum complicates dramatically and becomes very complex, but is presumably the result of freezing out conformers of the different possible stereo-isomers e.g. RR RS SR SS.

The ^{31}P NMR spectra of the benzoquinone and tcne complexes is a sharp singlet at all temperatures studied. This supports the hypothesis that the benzene ring flipping is actually a high energy process and is not observed. In the benzoquinone complex **(27)** one would expect to see two signals at -80^{0}C if the ring flipping were occurring.

Heating all of the above complexes results in an initial sharpening of the ^{31}P NMR signals as the rate of inter-conversion of the conformers increases such that on the NMR time scale it is no longer detectable under the conditions used. In non-polar solvent (toluene\xylene), the dba does not dissociate from the palladium in the 1,2-bis(di-*tert*-butylphosphinomethyl)benzene complex until >373K. The same is not true of the styrene complex, where dissociation of styrene is observed at 353K. This weaker coordination of styrene can be rationalised on the basis of the likely reduced back donation into the π^* anti bonding orbital as a result of less electron withdrawing substituents on the alkene i.e. styrene versus dba as predicted by the Dewar, Chatt, Duncanson model. The most important point to realize from this brief study is that the chelate ring remains intact at temperatures well above those employed for the catalytic reactions. This is not to say that the

chelate ring remains intact in the catalytic reactions but if ligand dissociation occurs it is not simply a result of thermal breakdown.

Ligand	Alkene Complex	Temp = 193K	Temp = 298K	Temp = 373K
Boxylyl (1)	dba	51.3(d, J=7.2), 50.1(s), 49.1(d, J=7.2), 47.8(s), 46.5(s), 45.7(s), 42.7(s)	49.9 (br), 48.1 (br)	51.6 (br), 50.5 (br)
Boxylyl (1)	BQ	52.5	52.5	52.5
Boxylyl (1)	tcne	53.6	53.6	53.6
Boxylyl (1)	Styrene	48.4 (s), 46.9 (s), 44.6 (s), 42.9 (s)	50.4 (br), 46.5 (br)	49.7 (s)
dbu'pe	dba	85.7 (s), 82.0 (s), 81.2 (s), 78.8 (s)	85.6 (br), 81.3 (br)	83.5 (d, J 17.0), 79.8 (d, J 17.0)
dcpe	dba		55.7 (br), 54.0 (br)	54.8 (s), 53.5 (s)
dcpp	dba		19.4 (br), 17.4 (br)	20.4 (d, J 24.4), 18.2 (d, J 24.4)
dppp	dba		11.0 (s), 7.0 (s). recorded at 313K	11.0 (s), 7.0 (s). recorded at 353K
dbu'pp	dba	44.2 (s), 41.4 (s), 40.1 (s), 38.3 (s)	43.3 (br), 43.7 (br)	44.7 (s), 45.2 (s)

Table 3.16 ^{31}P NMR Data of Selected Palladium(0) Alkene Complexes

3.5.3.4 ^{1}H and ^{13}C NMR Spectroscopy

The ^{1}H and ^{13}C NMR spectrum of complex **12** dissolved in toluene and dichloromethane also has temperature dependent features as shown in Table 3.17 and 3.18 below. The key features are;

1) In the ^{1}H spectrum, the *tert*-butyl methyl resonance's appear as a single broad feature in toluene and as three broad signals in dichloromethane. On cooling to 193K in both solvents these signals increase in complexity, with the appearance of new signals at 0.5ppm in toluene and 0.068, 0.31, and 0.65ppm in dichloromethane. The appearance of signals to high field on cooling has been observed by Spencer et al in the related complexes [(L-L)Pd(styrene)][21] where (L-L) = 1,2-bis(di-*tert*-butylphosphinomethyl)benzene. The shift to high field of one of the tertiary butyl groups has been explained on the basis that one of the alkyl groups on the phosphine lies above the aromatic ring of styrene which induces the high field shift in the ^{1}H NMR. These kinds of interaction are also possible for dba which has two phenyl groups. The observation of coupling on these high field signals in dichloromethane and not in the toluene mirrors the ^{31}P NMR findings. The ^{31}P NMR of **(12)** in dichloromethane at $-80^{0}C$ gives rise to 6 doublets whereas the same spectrum recorded in toluene gives rise to two doublets and five singlets. This probably reflects the differing rates of exchange reactions in the two solvents, with the limiting spectra not reached in toluene at $-80^{0}C$.

2) In the ^{1}H spectrum, the signals assigned to the coordinated dba CH's appear as two broad humps in dichloromethane, whereas the same region of the spectrum is clear in toluene suggesting that the various exchange processes are occurring at different rates in the two solvents. Cooling both samples to 193K results in the development of several new resonance's between 4.7 and 5.5ppm in the toluene solution and increased complexity in the same region in dichloromethane solution. The alkene CH signals of non coordinated *trans trans* dba appear as two doublets at 6.8 and 7.8ppm, the coupling is a relatively large $^{3}J(H\text{-}H)$ *trans* vicinal coupling. The move to low field of these dba protons on coordination can be rationalised with reference to the Dewar, Chatt, Duncanson model[22] for alkene bonding to transition metals. The filled π orbital of the alkene overlaps with an empty d orbital on the metal to form the σ component of the bond. At the same time a filled d orbital on the metal

overlaps with the π^* anti-bonding orbital on the alkene resulting in the donation of electron density from the metal to the alkene. The degree of donation and back acceptance are influenced by the oxidation state of the metal and the substituents on the alkene. The palladium in this case is electron rich d^{10} Pd(0) and wants to off load electron density. The substituents on the dba are electron withdrawing and as such the π^* anti bonding orbital on the alkene is depleted of electron density. The net effect is a donation of electron density from the metal to the alkene resulting in a lengthening of the carbon-carbon bond and a disruption of the delocalisation of electrons in the conjugated dba molecule. The coordinated dba becomes more alkane like and the protons resonate at higher frequency in the ^{1}H NMR. Supporting evidence for these assignments comes from the synthesis of the complex $[Pt(CH_2{=}CHCOOCH_2Ph)(PPh_3)_2]$ by Chaloner et al[23] where the benzylpropenoate alkene protons resonate between 3.5 and 3.5 ppm to higher field on coordination to the metal in the same manner as dba in the above complex.

3) The carbon NMR shown in Table 3.0 below indicates the presence of three distinct carbonyl species at 193K suggesting that three major species are present which is consistent with the ^{31}P NMR.

4) The carbon signals of the coordinated dba are broad at room temperature and on cooling fine structure develops. If only one conformer were present at 193K then we would expect to see each carbon atom as a doublet of doublets consisting of a larger P-C *trans* coupling (24-30 Hz)[24] and a smaller P-C *cis* coupling (3-7 Hz). In fact because of the presence of conformers we see complex multiplets, in dichloromethane however we can discern the larger *trans* P-C coupling.

Table 3.17 ^{1}H NMR Data For The Complex (12) [(L-L)Pd(dba)]

	DCM solvent at room temperature	DCM solvent at 193K	Toluene solvent at room temperature	Toluene solvent at 193K
tert-butyl CH_3	0.9(br),1.2(br), 1.5(br)ppm	0.068(d,J=18.7 Hz), 0.31(d, J=18.4Hz), 0.65(d, J=13.4Hz)ppm	1.4(br)ppm	0.5(br), 0.9(br), 1.1(br), 1.4(br), 1.6(br)ppm
Ligand CH_2	3.5(br)ppm	3.2-3.5(br)ppm	3.3(br)ppm	2.5-3.2(br)ppm
Coordinated dba CH	4.3(br), 4.6(br)ppm	4.1(m), 4.3(m), 4.35(m), 4.5(m), 4.7(m)ppm	not observed	4.7(br), 4.9(br), 5.0(br), 5.1(br), 5.5(br)ppm
aromatics and dba	6.8-7.8(br)ppm	6.8-7.8(br)ppm	7.0-8.0(br)ppm	6.9-8.3(br)ppm

Table 3.18 Selected ^{13}C NMR Data for the Complex [(L-L)Pd(dba)]

	DCM solvent at 193K	Toluene solvent at room temperature	Toluene solvent at 193K
Coordinated dba CH	60.7(d, J=31.6Hz), 61.3(d, J=29.9Hz), 72.0(d, J=21.8Hz), 73.1(m)ppm	73(br), 64(br)ppm	71.5(m), 73(m), 74.5(m), 63(br,m)ppm
carbonyl	193.1(s), 192.4(s), 190.4(s)ppm	191.7(s)ppm	190(s), 191(s), 192(s)ppm

The ^{1}H NMR data for the complexes **2-35** are listed in the experimental section of chapter 3. In all cases they are consistent with the proposed structure but due to the exchange processes detailed earlier little precise information can be extracted. In all cases the dba CH protons appear as broad humps where observed in the region 4.8-5.2ppm. Cooling the solutions to -80^{0}C reveals greater complexity in this region of the spectrum, consistent with

the proposed model but the resolution remains poor. The same situation is found in the carbon NMR where long acquisition times are not sufficient to reveal the coordinated alkene carbon signals as anything other than broad humps. The absolute chemical shift of these coordinated alkene carbon atoms and the magnitude of any P-C coupling can be extremely useful measures of the electronic modification of the metal centre by phosphine ligands. As the phosphines become more electron releasing to the metal we might expect to see this influence the metal interaction with other ligands such as alkenes. It is in an attempt to offset this lack of solution data that the single crystal X-ray study of a range of these complexes [(L-L)Pd(alkene)] has been performed and the influence of the phosphine ligand on the palladium-alkene parameters in the solid state studied.

The benzoquinone complexes [(L-L)Pd(BQ)] **(27-36)** have similar features in the proton NMR to the dba complexes with some notable differences. The complex [o–$C_6H_4(CH_2P^tBu_2)_2$ Pd (benzoquinone)] **(27)** has a very similar ^1H NMR to that of the equivalent dba complex. The coordinated alkene CH protons are not observed in the room temperature ^1H spectrum, and are evident as broad unresolved features even at 193K. The interesting feature of the ^1H spectra of the benzoquinone complex **(27)** is the absence of the CH protons of the non-coordinated part of the benzoquinone molecule. This suggests either (i) a rapid exchange in solution between two adegenerate η^2-quinone palladium structures, or (ii) a solution inter-conversion between η^2 and η^4-bound benzoquinine.

Work reported in the literature on the complex $[Pt(BQ^*)(C_2H_4)PR_3]$ (where BQ* = benzoquinone and substituted benzoquinones) which was established as having η^2-bonded benzoquinone in the solid state exhibits NMR characteristics suggesting low energy dynamic behaviour on the part of the quinone ligands.[25] In the complex $[Pt(BQ)(C_2H_4)PCy_3]$ where BQ = 2,6-dimethyl-benzo-1,4-quinone fewer resonances than anticipated for the quinone ligand were observed. Most notably, signals in the ^{13}C NMR for the non coordinated alkene moiety of the BQ ligand were absent. This was interpreted as evidence for dynamic processes involving the quinone ligands. It was concluded on the basis of the η^2 bonding confirmed by X-ray crystallography for the complex $[Pt(BQ^*)(C_2H_4)PCy_3)]$ where BQ* = 2,3,5,6-tetramethyl-benzo-1,4-quinone that this dynamic process was most likely a rapid inter conversion between η^2-bonded species.

The BQ 1,2-bis(di-*tert*-butylphosphinomethyl)benzene complex **(27)** has been characterized by single crystal x-ray diffraction in this study and η^2-bonding of the quinone ligand established in the solid state. As mentioned above, the ^{1}H NMR shows no signals attributable to CH protons of the non-coordinated alkene, the CH protons of the coordinated alkene are barely distinguishable at room temperature as a very broad feature. The ^{13}C NMR reveals a broad feature at ~65ppm indicative of η^2-bonding. The large upfield shift on coordination to transition metals is expected[26]. There are also no signals attributable to CH of the non-coordinated alkene evident in the ^{13}C NMR spectrum of this compound.

It seems reasonable then to suggest that a rapid equilibrium is occurring in solution to explain the above NMR features. The benzoquinone complex [2,3-$C_{10}H_6(CH_2PBu^t_2)_2$ Pd (benzoquinone)] **(33)** has very similar NMR features to **(27)** as would be anticipated, for this structurally similar complex.

Spectral features appear to change for less sterically demanding ligands. The ^{1}H NMR spectrum of [1,3-$C_3H_6(PBu^t_2)_2$ Pd (benzoquinone)] **(32)** has both a broad and a sharp feature in the region where we observe coordinated alkene CH. We associate the broad feature with dynamic exchange as discussed above. The sharp feature is a triplet and exhibits coupling (2 Hz) which could be either ^{2}J(P-C) or ^{3}J(P-H) coupling.

The presence of this sharp feature alongside a broad feature indicates two different complexes are present. The nature of this second species is suggested by the work of Stone et al discussed previously,[25] where η^4 quinone bonding has been established by X-ray crystallography. Several points are worthy of note from this work: (i) The carbon signals of the η^4-bonded quinone CH's are only shifted ~25ppm to highfield as opposed to the ~60ppm shift observed for the η^2 bonded complex; (ii) The CH protons appear as sharp signals in the ^{1}H NMR suggesting either very rapid exchange or no exchange; (iii) The complexes of benzoquinones vary in their propensity to form η^2-bound complexes. This seems to be related to the steric bulk of the quinone ligand with bulkier quinones, e.g. Naphthoquinone favouring η^2-coordination and smaller symmetrical benzoquinones forming η^4-species.

The NMR spectra of several of the BQ complexes synthesized in this study can be explained with reference to η^4-bound benzoquinone. The complex [1,3-$C_3H_6(PBu^t_2)_2$ Pd (benzoquinone)] **(32)** has, as mentioned, sharp signals assigned to coordinated alkene CH. The ^{13}C NMR spectra also has a signal at 102.4ppm similar to that exhibited by reported η^4-bound quinones. No evidence of a broad resonance around 65ppm is found, but the signal/noise ratio in this case is not ideal.

The complexes [o–$C_6H_4(CH_2PCy_2)_2$ Pd (benzoquinone)] **(30)** and [o–$C_6H_4(CH_2PPh_2)_2$ Pd (benzoquinone)] **(31)** both exhibit broad and sharp signals in the ^1H NMR attributable to coordinated alkene CH. The ^{13}C spectrum is inconclusive with a weak signal at 104ppm discernible in the ^{13}C NMR of the Phenyl complex, but no evidence for η^2 bonding in the RT spectrum.

The picture clarifies in the case of the dpephos, Xantphos and dppf benzoquinone complexes **(34,35,36)**. Here, the ^1H NMR gives a sharp signal which integrates to be 4 protons, no broad features are observed. The ^{13}C NMR gives a very strong signal around 100 ppm in all cases similar to that found for reported η^4-bound quinone complexes.

It is suggested then that across the range of ligands studied, we have a change in preference of the quinone ligand bonding mode. In the more sterically demanding situation **(27, 33)** only η^2-bonding is observed in the X-ray structure. The broadness of the solution NMR is suggestive of rapid interchange presumably between the two possible possible η^2-structures. The interchange can be envisaged as a flipping or rolling of the quinone ligand. It may be that this inter conversion goes via an η^4-state but this would appear not to be the case given the observed NMR for the complexes of less bulky phosphine ligands where the presence of η^2- and η^4-bonded quinone is indicated in solution. As we decrease steric bulk we reach a point where η^4-bonding is exclusively favoured in the case of the dpephos, Xantphos and dppf ligands. This switch in bonding can be correlated with the total cone angle discussed in section 3.5.4.8, the latter ligands having much more open structures. It is easy to envisage that the η^4-bonding mode requires more space than does η^2-bonding.

3.5.4 Analysis of Crystallographic Data

3.5.4.1 Ligand Derived Influences in Homogeneous Catalysis

Several complexes of the formula [(L-L)Pd(alkene)] have been synthesised and characterized by single crystal X-ray diffraction in order to gain a better understanding of the coordination chemistry of the diphosphines and to elucidate structural differences thought to control catalyst activity and selectivity. Catalysts can crudely be considered as being made up of a metal bonded to participative and non-participative ligands. The former are those ligands which react together to give products (in this case ethene and carbon monoxide) whilst the latter remain predominantly unchanged during the reaction (in this case phosphines). Despite the nomenclature the latter are much more than passive spectator ligands. The skill lies in the ability to control the course of the reaction between participative ligands by judicious choice of these non-participative ligands. The danger is that no such control can be exerted or that the non participative ligands themselves undergo reaction.

Before considering the differences between complexes of different ligands, there are some general features to be considered.

Taking **12** as a representative example firstly we observe the phosphine ligand is coordinated to the metal in a bidentate fashion with the phosphorus atoms occupying adjacent *cis* coordination sites. In this work there are no examples of alternative coordination modes such as the phosphine acting in a monodentate manner to one metal or bridging two metals. These latter two possibilities would seem to be likely from an inspection of the single crystal X-ray study of the uncoordinated phosphines(**7**, **11**) , where the phosphorus lone pairs point away from each other and are located on opposite sides of the benzene ring. The propane and butane bridged phosphines can also act as monodentate or bridging ligands and examples of these are known.[27]

Secondly the coordination environment around palladium is trigonal planar[28] (Y shaped) as expected for zerovalent complexes of the type ML_2(alkene) (M=Pd or Pt). The alkene C-C axis lies close to the trigonal plane in all cases, dihedral angles being small. Large dihedral angles reflect the steric congestion in the trigonal plane generated by the phosphine ligand and also the rigidity of the benzoquinone compared with dba, which can

more easily relieve steric congestion leaving the C-C moiety in the coordination plane. Benzoquinone on the other hand cannot easily bend away from the steric congestion, and this is reflected in a larger dihedral angle for [(L-L)Pd(BQ)] (**27**) compared to the equivalent dba complex (**12**). The only published X-ray structure for a complex of the type [(L-L)Pd(dba)] is for (L-L) = dppe.[16] This complex has trigonal planar geometry and the dba is coordinated to the metal via one of its alkene moieties in a conventional η^2–fashion as found for the complexes produced in this study. Complexes of the type [(L-L)Pd(BQ)] have not been reported previously but the complexes $[PdL_2(C_6H_4O_2)]$ where L= PBu_3, $P(C_6H_4OMe\text{-}p)_3$, PPh_3 $P(C_6H_4Cl\text{-}p)_3$, $P(OPh)_3$ have been synthesised in which the benzoquinone is bound as a bidentate ligand.[18] In the case of tributylphosphine two inter-convertible complexes $[Pd(PBu_3)_2(p\text{-}C_6H_4O_2)]$ and $[\{Pd(PBu_3)\}_2(p\text{-}C_6H_4O_2)]$ were formed.[18] No evidence for dimer formation has been found in this study for benzoquinone and dba complexes.

Thirdly, for complexes of the xylene derived diphosphines, the xylene ring of the phosphine ligand is located away from the square planar palladium environment. This is a consequence of the coordination of the ligand to the metal and the requirement for tetrahedral angles at the methylene carbons.[29] This displacement of the ring is felt to be partly responsible for the observed increased complexity of the NMR spectra at low temperature (-80^0C) of complexes of xylene backbone phosphine ligands, where two different conformations are frozen out (see section 3.5.3.3.).

The remaining features of the X-ray data will be discussed with reference to the data illustrated in Table 3.19 below. This table forms the basis of the discussion regarding the crystallographic data. Also colour pictures of selected crystallographic data are in appendix 1 and 3 which serve to illustrate the salient features of the complexes discussed in this chapter.

Complex	P-M-P Angle (°)	M-P_{AV} distance (Å)	Alkene C-C distance (Å)	M-C_{AV} distance (Å)	C-M-C Angle (°)	Torsion angle (°)	Dihedral angle (°)
12	103.9	2.36	1.42	2.15	38.58	-139.9	6.8
13	104.3	2.31	1.43	2.14	38.92	150.4	1.7
14	103.9	2.32	1.44	2.15	39.07	-156	3.1
18	104.6	2.29	1.41	2.15	38.37	154.6	2.9
21	94.96	2.28	1.42	2.14	38.87	154.2	3.9
22	115.1	2.33	1.41	2.17	37.86	-159	9.3
24	106.9	2.33	1.42	2.16	38.28	153.7	12.4
25	103.7	2.31	1.43	2.12	39.2	133.3	6.3
27	104.5	2.36	1.43	2.18	38.1	n/a	9.3
29	104.5	2.37	1.41	2.17	37.97	n/a	11.3
32	99.7	2.33	1.43	2.16	38.7	n/a	14.1
34	105.7	2.32	1.42	2.17	38.26	n/a	6.9
35	106.7	2.35	1.41	2.15	38.06	n/a	8.2

Table 3.19 Selected Parameters from X-Ray Crystallography Data

Formally, a ligand can control the course of a reaction by modifying the steric or electronic environment of the active site. Whilst it is usually true that both are in operation there are a number of concepts that can be developed to try and isolate and thus understand these effects. These are discussed under the headings of electronic effects and steric effects below.

3.5.4.2 Electronic Effects

An exact measure of the electron density and its orbital distribution for the palladium centre is very difficult to obtain. Classically this is implied by the examination of structural or spectroscopic properties of ligands bonded to it (both metal ligand and intra-ligand). These will now be considered.

3.5.4.3 Analysis of Coordinated Alkene Carbon-Carbon Bond Length

As mentioned previously the crystallographic data for the dba and benzoquinone complexes indicates that the dba is coordinated to the palladium through one of its alkene double bonds in a well known η^2-manner. The bonding of alkenes to transition metals in this fashion is thought to consist of two different components which reinforce each other in a

synergic process. A forward bonding component results from transfer of electron density in the π bonding molecular orbital of the alkene to a suitable sigma bonding orbital on the metal. The second component a backbonding component results from the transfer of electron density from a filled metal d orbital into the π* anti-bonding molecular orbital of the alkene.

Two major changes occur in the alkene as a result of bonding to a transition metal. Firstly the carbon-carbon bond increases in length.[28] This is as a result of the decrease in electron density in the π bonding molecular orbital and the increase in electron density in the π* anti-bonding molecular orbital of the coordinated alkene. Secondly the substituents on the coordinated alkene bend away from the metal on coordination. This again is a result of changes in electron density in the alkene π and π* molecular orbitals. Back donation of electron density from metal d orbitals into the alkene π* changes the hybridization of the alkene carbon atoms from sp^2 towards sp^3.

Taking complex **(12)** as an example, the carbon-carbon bond length of the coordinated dba is 1.42 Å compared to 1.33 Å for the uncoordinated dba. This bond length is approximately midway between that expected for free alkene (ethene, carbon-carbon = 1.337 Å) and a carbon-carbon single bond (ethane carbon-carbon = 1.534 Å[29]. It is concluded from this analysis (see Table 3.19) that changing the phosphorus substituent on the o-xylene phosphine backbone or changing the bidentate phosphine backbone has no significant effect on the length of the carbon-carbon bond of the coordinated dba. For example within the ortho-xylene derived ligands there is an observed difference of 0.01 Å between the complexes **12** and **18** containing *tert*-butyl and phenyl phosphorus substituents respectively. This observed difference is within the quoted error limits of the crystallographically determined bond lengths. Also there is no significant difference in the observed alkene C-C bond length between complexes containing different alkenes. For the diphosphines 1,2bis(di-tert-butylphosphinomethyl)benzene and DPEphos both a dba and benzoquinone complex have been characterized **(12, 27** and **24, 34)**. There is no significant difference in the alkene C-C bond length observed in these complexes. It may seem surprising that diverse changes in the electronic properties of the phosphines are not manifested in significant differences in the alkene bond length. This is most likely due in some part to the synergic nature of the alkene bonding model proposed. The complex [DPEphosPd(tcne)]

synthesised by van-Leeuwen[30] has a coordinated alkene C-C bond length of 1.48 Å, which is significantly longer than observed in this study and reflects the very much greater degree of back acceptance occurring in complexes of tcne. Classically, these complexes are described as metallocyclopropanes, with the alkene carbon atoms almost sp^3 in nature in their transition metal complexes.

Two other points are worthy of note. Firstly the complex [(dppp)Pd(dba)] **(21)**, which is a precursor to an active co-polymerisation catalyst, has the same coordinated C-C bond length as the complex **(12)** which is a precursor to a very active MeP synthesis catalyst. Secondly the complex $[(PPh_3)_2$ Pd (dba)] **(22)** containing monodentate phosphine ligands shows no significant differences in coordinated alkene C-C bond length to both **12** and **22**. This reinforces the above comments that the nature of the phosphine in these examples has little effect on the coordinated alkene C-C bond length in the ground state.

3.5.4.4 Analysis of Palladium Phosphorus Bond Length

Palladium phosphorus bonds can also be viewed as synergic in nature like the palladium alkene interaction. As well as being σ-donors phosphines can act as π-acceptors, their π-acceptor strengths are dependent on the electronegativity of the phosphorus substituents.

The bond lengths observed in this study all fall within the range of palladium-phosphorus bond lengths previously observed for complexes of this type.[31] Detailed inspection of the palladium-phosphorus bond lengths reveals a trend, with the most sterically demanding and most basic phosphines 1,2-bis(di-*tert*-butylphosphinomethyl)benzene and 1,4-bis(di-*tert*-butylphosphino)butane leading to complexes having the longest palladium phosphorus bond lengths.

Within the ortho-xylene derived phosphines as we decrease steric bulk and decrease electron donation at the phosphorus substituents, we see a shortening of the palladium phosphine bond. Thus we observe a difference of 0.07 Å between the *tert*-butyl complex **(12)** and the phenyl complex **(18)**. It is noteworthy that the catalytic selectivity of catalysts based on these two complexes is very different, with the longest Pd-P bonds present in the most

highly MeP selective catalyst (R=*tert*-butyl). Also noteworthy is the selectivity of catalysts based on the complexes **13** and **14**, where both MeP and co-polymer are produced and the Pd-P bond lengths are intermediary between those of active MeP catalysts and active co-polymerisation catalysts.

One possible explanation of this correlation is that dissociation of one phosphorus occurs in the catalytic cycle and favours termination over propagation. This has some similarites to the mechanism proposed by Drent to explain catalyst selectivity in the methoxycarbonylation of alkenes (see introduction). This mechanism suggests that *cis*-phosphine at all times is required for co-polymer formation and that catalysts based on monodentate phosphine result in MeP formation (chain termination) because *cis-trans* isomerisation occurs which leads to the loss of the *cis*-phosphine condition. The thermodynamically more stable *trans*-phosphine complex is proposed to then readily undergo chain termination in the absence of *cis* coordination sites for insertion reactions to occur.

The remainder of the data is consistent with this idea with the following points worthy of note. 1) The phenyl substituted phosphine ligand complexes which give rise to MeP **(22, 24, 34, 35)** all have significantly longer Pd-P bond lengths than are present in those phenyl substituted ligand complexes which give rise to co-polymer **(18, 21)**. 2) The platinum complex **(25)** does not show any activity for either MeP or co-polymer formation. This is consistent with the known increased kinetic inertness of platinum complexes. It is interesting to note though the shorter Pd-P bond length in the platinum complex relative to the palladium complex, a difference of 0.05 Å. 3) The catalyst based on the ligand 1,4-bis(di-*tert*-butylphosphino)butane **(29)** has the longest Pd-P bond length but gives no MeP under standard testing conditions. The formation of palladium metal is observed very rapidly, indicating that the catalyst quickly decomposed. This result is very interesting for two reasons. Firstly, it supports the suggestion that phosphine labilisation is occurring where long Pd-P bonds are present. Secondly, it indicates that there is something special about the ortho-xylyl backbone which leads to high catalytic activity and less facile decomposition. Inspection of the X-ray data for ortho-xylyl complexes **(12, 13, 14, 18, 25)** reveals the planarity of the chelate ring and the orientation of the phosphorus lone pairs toward the palladium. Modelling studies on the complex **(12)** suggest that if phosphine dissociation at one Pd-P bond does occur the rigidity in the chelate backbone prevents its complete

dissociation. Furthermore the steric bulk of the *tert*-butyl substituents provide a barrier to rotation of the phosphine lone pair away from the metal. The result of these features is that it seems likely that if the Pd-P bond is broken it may be able to easily reform before complete dissociation of the ligand occurs. The same situation is not true of the 1,4-bis(di-*tert*-butylphosphino)butane ligand where the backbone flexibility may be the reason for the rapid decomposition. The propensity of butane bridged diphosphines to form *trans* complexes is well known.[27]

The formation of both MeP and co-polymers by catalysts based on **(13** and **14)** can also be rationalised by the ligand dissociation proposal. The shorter, and hence presumably stronger Pd-P bonds, in these complexes will be less susceptible but not resistant to labilisation, leading to a situation where termination occurs when labilisation occurs and polymerization occurs when it does not.

The relationship between steric bulk of substituents and the electron density at the phosphorus centre makes it difficult to deconvolute the two effects (steric and electronic). The observed trend in bond lengths may be the result of 1) reduced steric repulsions between the phosphorus substituents and the ligand set around palladium and/or 2) electronic effects whereby there is reduced π back bonding in the complex of the *tert*-butyl substituted phosphine. The extent of π back bonding inferred then increases in the series *tert*-butyl < cyclohexyl < *iso*-Propyl < phenyl leading to shorter (stronger) palladium phosphorus bonds for the better π acceptor ligands.

3.5.4.5 Steric Effects

Simply, this is the spatial environment around the metal centre created by the participative and non-participative ligands. The former are dictated by the reaction desired, whilst the latter can be modified for optimum performance.

3.5.4.6 Analysis of P-Pd-P Bite Angle

The bite angle (P-Pd-P) within the series of xylene based phosphines(**12, 13, 14, 18, 25**) is relatively insensitive to changing the steric bulk of the phosphorus substituent. Thus we observe only a 0.7^0 difference in bite angle between complex **12** with bulky *tert*-butyl

substituents and complex **18** which has phenyl substituents at phosphorus. This may be an important observation in terms of stability of the complexes. The *tert*-butyl ligand is clearly more sterically demanding than the phenyl analogue, and this increased steric pressure must manifest itself in some way. Given the inability of the backbone to accommodate variations in steric bulk it is suggested that the most likely mechanism is for the metal to be "pushed" away from the congestion. The result of reducing steric congestion in this way would be a lengthening of the palladium phosphorus bond. A similar lengthening of the palladium phosphorus bond in related complexes has been reported by van-Leeuwen[30]. In van-Leeuwen's study the phosphine ligands illustrated in Figure 3.18 below (A and B) have significantly different calculated natural bite angles but similar observed bite angles in the $L_2Pd(tcne)$ complexes. It is suggested that the palladium bite angle has reached an upper limit and that whilst phosphine B (Figure 3.18) has a natural bite angle of 108.8^0, the Pd(tcne) fragment prefers for electronic reasons a smaller P-Pd-P angle. This smaller bite angle is achieved by lengthening the palladium phosphorus bond from 2.33 to 2.35 Å.

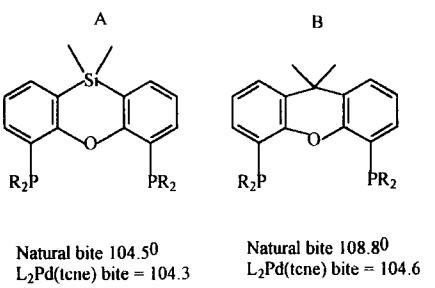

Figure 3.18

The interesting conclusion relevant to this work is the apparent control of bite angle by the alkene palladium fragment. Table 3.20 below shows the natural bite angles calculated for the xylene based ligands whose dba complexes have been characterized by x-ray crystallography in this thesis. We see that for the phenyl phosphine a natural bite angle of 90^0 is calculated which is significantly lower than the experimentally observed P-Pd-P angle in the dba complex **(18)**. The ligands 1,2bis(di-*iso*-propylphosphinomethyl)benzene **(2)** and 1,2bis(dicyclohexylphosphinomethyl)benzene **(3)** also have lower calculated natural bite angles than the bite angles found in their X-ray structures. It should be noted though that the

potential energy wells observed in the bite angle versus energy plots for the above ligands are shallow, suggesting a range of bite angles are accessible.

$C_6H_4(CH_2PR_2)$	Calculated Natural bite angle
R= *tert*-Butyl	105
R= *iso*-propyl	100
R= cyclohexyl	100
R= phenyl	90

Table 3.20 Calculated Natural Bite Angles of Phosphine Ligands of General Formula $C_6H_4(CH_2PR_2)$

The experimentally observed insensitivity of P-Pd-P bite angle to changes in phosphorus substituent is not observed for propane bridged diphosphines. The complexes of dppp have reported bite angles in the range 88^0-95^0 some 5^0-7^0 lower than found for complexes of 1,3-bis(di-*tert*-butylphosphino)propane. This fact is illustrated in Table 3.21 which details the P-M-P angle and Pd-P bond length for a range of palladium and platinum phosphine complexes of propane and ethane bridged phosphines. This data has been obtained from the Cambridge crystallographic database. The flexibility of the propane bridge has been suggested to be important in active catalysts which employ these ligands[32]. Firstly it is suggested that the ligand can move between and adopt stable conformations on changing the oxidation state of the coordinated metal without dissociation from the metal. In the case of palladium this involves the ligand remaining attached to the metal as it changes between trigonal planar palladium (0) and square planar[33] palladium(II). Secondly it is suggested the backbone flexibility is important in minimizing the energy of transition states and hence allowing reactions to proceed more easily.

The bite angle (P-Pd-P) of the complex **(12)** is 103.99^0, some 3-4^0 larger than the equivalent bite angle for **(32)** and 1,3-bis(di-*tert*-butylphosphino)propane complexes of platinum (see Table 3.21). This increase on going from a propane to a xylene backbone is thought to be a contributing factor in explaining the increased rates of reaction. At its most simplistic level the reason for this is that increasing the P-Pd-P angle forces together the reacting groups on the other face of the metal centre.

Further work by Spencer's group[21] also supports the idea that larger bite angles favour faster insertion reactions. His work has sought to probe the structure of protonated platinum and palladium complexes, particularly where the acid contains a non-coordinating anion. Specifically the complexes [(L-L)Pt(C_7H_{10})] and [(L-L)Pd(C_7H_{10})], where 1) C_7H_{10} = norbornene and 2) (L-L)= 1,2-bis(di-*tert*-butylphosphinomethyl)benzene **(1)**, 1,3-bis(di-*tert*-butylphosphino)propane or 1,2-bis(di-*tert*-butylphosphino)ethane . These were reacted with $HBF_4.OEt_2$ to yield cationic complexes of formula $[Pt(C_7H_{11})(L\text{-}L)]^+[Y]^-$ which are stabilized by agostic interaction between the β-C-H of the norbornyl fragment and the metal centre. Spencer further discusses the relationship between the phosphine ligand and the extent of the β-hydrogen agostic interaction in the platinum norbornyl complexes $[Pt(C_7H_{11})(L\text{-}L)]^+[Y]^-$. It is suggested that the chelate ring size and the bulk of the substituents at phosphorus in the phosphine ligand influences the structure adopted. They base their argument on the observed values of J(Pt-H) and J(Pt-P) NMR couplings in respective complexes of different phosphines. The implication that the smaller diphosphines L-L = {$Bu^t_2P(CH_2)_2PBu^t_2$, P-Pt-P 89^0 } favour an alkene hydride type structure (highest values of J(Pt-H) but lowest values of $J(Pt\text{-}P_{trans})$, whilst the larger diphosphines L-L = $o\text{-}C_6H_4(CH_2PBu^t_2)_2$ and $Bu^t_2P(CH_2)_3PBu^t_2$ favour alkyl like structures. The P-Pt-P angles reported for the above are 105^0 (calculated, not derived from X-ray structure) for L-L = $o\text{-}C_6H_4(CH_2PBu^t_2)_2$ and 98-101^0 for L-L = $Bu^t_2P(CH_2)_3PBu^t_2$ with corresponding J(Pt-H) values of 79 and 85Hz as compared to a value of J(Pt-H) of 136Hz for L-L = $Bu^t_2P(CH_2)_2PBu^t_2$. The alkyl structures resulting from the larger bite angles resemble the product of insertion whilst the alkene hydride type structure, resulting from smaller bite angles resemble the pre-insertion product. It might be anticipated that if the product of alkene insertion is favoured for larger large bite angle phosphines, the product of carbon monoxide insertion would also be favoured.

The dpephos based diphosphine palladium (dba) complex **(24)** has a bite angle of 106.9^0 which is 5.5^0 higher than that observed by van-Leeuwen[30] in the equivalent tcne complex of this ligand. This is quite a significant difference especially given the bulk of the dba versus that of tcne. It is suggested from the crystallographic data that the dpephos backbone is very flexible and the benzene rings linked by the ether oxygen can twist across each other. This flexibility in the backbone may allow increased steric repulsion to be

accommodated in preference to significant bond lengthening. This bite angle appears to represent the largest for a complex of type [(P-P)Pd(alkene)], the previous largest bite angle reported being 106.4^0 for the complex [Pd(diop)(C_2H_4)]. [33]

Complex **(22)** which has *cis*-coordinated phosphine ligands has the largest bite angle of all the compounds studied in this work. This high value is thought to be important for catalytic systems of TPP[34] . The *cis*-phosphine complex is proposed to be present in the active catalytic cycle in the TPP system. Its concentration though might be expected to be very small under the conditions of excess phosphine used.[34] This is due to the likely *cis-trans* isomerisation which would be favoured under conditions of high excess phosphine. The suggestion is that the rates observed for the TPP system are generated by a small fraction of the added palladium present in this highly active *cis* phosphine palladium complex (see chapter 1). This activity is due to it having a very large bite angle which increases the rate of insertion reactions.[35]

The analysis of bite angle data also suggests a similarity between the butane bridged catalysts **(29)** and those based on the rigid xylene backbone **(12, 13, 14, 18)**. Clearly given the rapid decomposition observed for catalysts based on the butane bridged phosphine ligand and the selectivity changes observed for the xylene based catalysts, a large bite angle on its own is not sufficient to give active/selective catalysts.

Ligand (L-L)	Complex	P-M-P	Pd-P
$Ph_2P(CH_2)_3PPh_2$	(L-L)Pd$(Cl)_2$	90.58	2.25
$Ph_2P(CH_2)_3PPh_2$	(L-L)Pd$(NCS)_2$	89.32	2.24
$^iPr_2P(CH_2)_3P^iPr_2$	(L-L)Pd(CO)(H)-bridging	97.5	(2.33)(2.37)
$Bu^t_2P(CH_2)_3PBu^t_2$	(L-L)Pt(η-3 styrene)	99.57	2.29
$Bu^t_2P(CH_2)_3PBu^t_2$	(L-L)Pt(acetylene)	100.4	2.27
$Bu^t_2P(CH_2)_3PBu^t_2$	(L-L)Pt$(Cl)_2$-bridging	97.86	2.29
$Bu^t_2P(CH_2)_3PBu^t_2$	(L-L)Pt(H)(OSO_2CF_3)	101.31	(2.37)(2.2)
$Bu^t_2P(CH_2)_3PBu^t_2$	(L-L)Pt$(Et)_2$	97.87	2.32
$Bu^t_2P(CH_2)_3PBu^t_2$	(L-L)Pt$(Cl)_2$	99.07	2.28
$Bu^t_2P(CH_2)_3PBu^t_2$	(L-L)Pt-Pt(L-L)	102.58	2.27
$Bu^t_2P(CH_2)_2PBu^t_2$	(L-L)Pt$(\mu\text{-}H)_2$Pt(L-L)	89.56	2.26
$Pr^i_2P(CH_2)_2PPr^i_2$	(L-L)Pt$(\mu\text{-}H)_2$Pt(L-L)	88.56	2.25
$Pr^i_2P(CH_2)_2PPr^i_2$	Pd$(L\text{-}L)_2$	87.02	2.36
$Cy_2P(CH_2)_2PCy_2$	(L-L)Pd(butadiene)	88.81	2.31
$Cy_2P(CH_2)_2PCy_2$	(L-L)Pd$(Cl)_2$	87.08	2.23
$Ph_2P(CH_2)_2PPh_2$	(L-L)Pd(dba)	87.19	2.29

Table 3.21 Influence of Bridge Length on P-Pd-P Bite Angle in C2 and C3 Bridged Diphosphines

In conclusion the increased activity observed in catalyst solutions on going from 1,3-bis(di-*tert*-butylphosphino)propane based systems to 1,2-bis(di-*tert*-butylphosphinomethyl)benzene systems can in part be rationalised on the basis of the increased P-Pd-P bite angle present in the metal complexes leading to faster insertion reactions. Also the activity of TPP based systems can be understood by proposing very fast insertions occurring in a *cis*-phosphine complex with large bite angle, present in low concentration. These ideas have led to the synthesis of new catalysts based on phenyl ether backbones where it was intended to mimic TPP but in a bidentate ligand thereby maintaining the large bite angle but increasing the concentration of active catalyst by preventing *cis-trans* isomerisation. This approach has been successful in producing MeP selective catalysts based on bidentate phenyl substituted phosphines. It is clear though that the presence of a large bite angle alone is not sufficient to give active/selective catalysts.

3.5.4.7 Analysis of Torsion Angles

Another prominent feature of the series of dba complex structures is the distortion of the dba as it tries to minimize the effects of steric repulsions. This bending and twisting of the dba can be quantified and used as a measure of the steric encroachment of a given ligand. The measure of the dba distortion which has been developed is the torsion angle and it is defined in Figure 3.19 below.

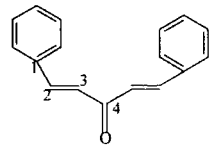

Torsion angle = angle subtended by bonds 1-2 and 3-4 as viewed down bond 2-3

Figure 3.19

In free dba one might expect relatively little torsion strain and the measured torsion angle would approach 180^0. This has been checked using the X-ray crystallographic data for a molecule of dba which was present in the unit cell of a palladium complex as a non interacting co-crystallised component[36]. It may therefore be slightly different to free dba crystallized singly because of solid state packing forces, however the torsion angle determined from this source does indeed come close to 180^0C as expected.

As mentioned above, the torsion angle measured may be considered as reflecting the extent to which the substituents of the coordinated double bond are forced to twist away from the favoured conformation as a result of the steric demands of the phosphine ligand. Consistent with this, complexes of the *tert*-butyl substituted phosphine (**12, 25**) show the greatest torsion angle deviation from 180^0. This can be seen clearly from the single crystal X-ray data and the colour images in appendix 1.

The differences between the other phosphines in this series (Table 3.19) is less marked and is not always in a predictable direction. The phosphine, 1,2-bis(di-*iso*-propylphosphinomethyl)benzene induces a greater change in torsion angle than does 1,2-bis(dicyclohexylphosphinomethyl) benzene in complexes of the type [(L-L)Pd(dba)]. This is not in line with conventional wisdom which ranks the phosphines

tert-Bu_2PH > Cy_2PH > Pr^i_2PH using cone angle[37] as a measure of the steric bulk for the monodentate phosphines.

Inspection of the crystallographic data gives a possible explanation. The cyclohexyl rings of **14** appear to stack and the plane of the cyclohexyl rings faces the plane of one of the phenyl rings of the dba. This slightly unusual apparent stacking of the cyclohexyl and phenyl rings results in **14** being less stericaly demanding in the solid state. In the solution state and in the absence of dba the cyclohexyl groups will most likely adopt an alternative conformation which will occupy a greater volume. The stacking or meshing together of cyclohexyl rings[38] has been observed for the complex $[Pt\{P(cyclohexyl)_3\}_3]$, which on the basis of the large cone angle of the phosphine PCy_3 (170^0) we might not expect to be stable.[39] The X-ray structure shows that the cyclohexyl rings can mesh into each other thus effectively reducing the steric crowding and stabilizing the molecule. Such stacking is well known for aryl phosphines and could contribute to the small deviations in torsion angles observed for the phenyl analogues.

Whilst it is difficult and possibly ill advised to equate ground state X-ray parameters with dynamic catalytic phenomena, it should be recognised that in this case the maximum deviation in the solid state structure (largest torsion angle) correlates with the maximum observed catalytic activity i.e. **(12)**.

3.5.4.8 Analysis of Cone Angles

The table below lists a series of structural parameters calculated from the single crystal X-ray data.

Complex Number	Parallel Pocket Angle[1]	Perpen. Pocket Angle[1]	Internal Cone Angle[1]	Catalyst Selectivity
12	127.8	196.2	151	MeP
13	157.92	277.2	160	MeP/Co-poly
14	150.5	220.3	157	MeP/Co-poly
18	145.44	196.2	172.5	MeP/Co-poly
21	156.2	205.2	176.1	Co-poly
22	133.2	197.3	170	MeP
24	135.7	200.9	171.4	MeP
25	123.1	196.9	147.6	inactive
27				MeP
29	121.3	194.8	148.4	decompose
32	131	215.6	151	MeP
34	117.7	195.1	172.5	MeP
35	114.8	195.5	174.5	MeP

1. See text section 3.5.4.8 for definition

Table 3.22 Selected Steric Parameters Calculated from X-ray Data

The different phosphine ligands employed in this study form complexes in which the steric environment around palladium differs. The analysis of cone angle is an attempt to quantify these steric differences and relate them to the known activities and selectivities observed in the catalysis. Three parameters have been measured and the data listed in Table 3.22 above. These are 1) total cone angle 2) in plane pocket angle 3) perpendicular pocket angle. These quantities have been evaluated from experimentally-determined X-ray data in the following way (a visual representation is shown in appendix 2). The non phosphine ligands are removed from the data and the palladium atom and the two chelating phosphine atoms are used to define a triangle with the transition metal at the apex. A sphere is then constructed around the palladium atom which defines the origin, with dimensions such that it completely contains the van der Waals surfaces of each atom (including H atoms) in the

complex. The particular radius of each sphere is not important so long as it wholly contains the complex. The van der Waals surfaces of each atom are then projected onto the sphere surface, each point being mapped along an axis from the transition metal origin. This leads to a coded representation describing where, and in how large a region, the central metal atom is accessible from a remote observers point of view. For example, bulky phosphine ligands which encroach around the palladium yield surfaces that show only small regions of accessibility. For the total cone angle analysis, the surface area of the patch corresponding to visible palladium is calculated and used to define a conical (spherical) surface on the sphere. The steric congestion can then be measured by the apex angle of the cone formed. For the in plane and perpendicular pocket angle analysis, the maximum arc length of the patch is measured both in the plane and perpendicular to the plane containing the PdP_2 fragment. The angles subtended by the arcs define the interior cone angles or pocket angles which give a measure of the cavity size at the active palladium centre in two dimensions. This analysis is similar to that proposed by Barron (see introduction). The perpendicular pocket angle data has been included but in all cases these values are in excess of 180^0. This reflects the situation that the phosphorus substituents do not intertwine and that directly above and below the metal is a narrow channel even for the most sterically demanding ligands.

When we look at the data in Table 3.22 three main features can be identified.

1) All of the complexes which lead to MeP selective catalysts have a parallel pocket angle of less than 136.0^0. Thus the monodentate phosphine complex **22** and the complexes based on the phenyl substituted diphosphines **24**, **34**, **35** have a similar steric environment in the P-Pd-P plane to the very active catalysts based on ^{t}butyl phosphines. This suggests that selectivity is governed by accessibility of the metal centre and/or competition between insertion and termination reactions. It seems likely that below a certain threshold value termination reactions are always favoured. It is not unreasonable to suggest that below a certain threshold steric congestion induces phosphine labilisation leading to termination as discussed earlier. In support of this is the similarity in terms of the spatial environment around palladium, of the pre-catalysts **18** and **21** both of which give rise to catalysts which are selective for the formation of ethene/CO co-polymers.

2) The complex based on the four carbon butane bridged ligand **(29)** looks similar in terms of steric congestion imposed at the metal centre to the complex **12**. This again points to a special property of the xylene backbone which is responsible for its activity. The platinum complex not surprisingly also has similar steric parameters to the palladium analogue. The inactivity of this platinum complex to date is perhaps less surprising given the known differences in reactivity between platinum and palladium. Classical study of homogeneous palladium catalysis often utilizes the synthesis of platinum analogues for which it is possible to isolate catalytic model complexes for individual study due to the known reduced reactivity.

3) The 3-dimensional total cone angle does not correlate well with selectivity. The phenyl substituted diphosphines which are MeP selective have total cone angles in excess of 170^0 as compared to 150^0 for the *tert*-butyl complexes. This raises an important point, that it is the ability of the phenyl group to orientate itself in a particular direction which is important in governing selectivity. This orientation would appear to be governed by the ligand backbone in bidentate phosphines, the steric disposition of which prevents the phenyl substituents from feathering or stacking to completely reduce steric interactions.

The analysis performed by Barron[42] *et al* correlates pocket angles (for the complexes [(P-P)Pd(CO^{t}Bu)(Cl)] where (P-P) = dppe, dppp, dppb, dmpe, dcpe) with activity in the ethene/CO co-polymerisation reaction. The two phosphines, which result in highest activity (dppp and dcpe), have similar in plane pocket angles. It is suggested that there is an optimum size for the active catalytic centre and that the most sterically crowded species during the catalytic cycle is the ethylene complex [(P-P) Pd (CH_2=CH_2)(COR)]$^+$, formed as an intermediate prior to alkene insertion. In order for the above alkene insertion/acyl migration to occur, the ethene must be coplanar with the migrating acyl group. Thus, it is in the ligand plane that steric hindrance becomes a controlling factor in ethene coordination/insertion.

Further, they propose that if the internal cone angle of the [(P-P)Pd] moiety is sufficiently small (i.e. n=4), then ethene is precluded from complexation, there being insufficient space available. Barron et al[42] argue that, for the co-polymerisation of ethene, the in-plane pocket angle is the important parameter in determining activity. The phosphine ligands dcpe and dppp are both active co-polymerisation catalysts and, whilst the former has

an ethane bridge and the latter a propane bridge, they have similar in plane pocket angles in palladium complexes. The data collected in this study do not contradict the ideas of Barron, but they further suggest that the steric environment in the palladium square plane is important in governing catalyst selectivity as well as playing a role in activity.

An impression of the substrate channel can be obtained if the crystallographic data for the 1,2-bis(di-*tert*-butylphosphinomethyl)benzene palladium dba complex is viewed as a space-filling model, which utilizes the van der Waals size of each atom (see appendix 3). What also becomes apparent from these views is the lack of accessibility of the palladium from any other direction than head on. The formation of five coordinate intermediates where the fifth ligand is proposed to interact with the dz^2 orbital on palladium, which has orbitals above and below the P-Pd-P plane, would appear to be disfavoured on steric grounds. The same would not appear to be true for 1,3-bis(diphenylphosphine)propane palladium dba, where the total cone angle approaches 180° and the approach of substrate molecules from above and below looks feasible. This is also borne out by inspection of the crystallographic data with the dba fragment removed, where the metal can be seen to be much more open and accessible. The perpendicular pocket angle data in this case is not a suitable parameter to describe the steric environment, full examination of the crystallographic data being required. The relative accessibility of the dz^2 orbital on palladium and the ability to form five coordinate intermediates could be factors which may be important in determining whether a given catalyst will form methylpropionate or co-polymer. Five coordinate intermediates have been suggested to be viable intermediates in the ethene/co co-polymerisation from modelling studies.[41]

The initial alkene insertion into a palladium-hydride bond is proposed to result in an agostic complex. The formation of an alternating co-polymer requires that this complex captures a CO molecule and inserts it into a Pd-C bond. Since the fourth ligand position of the square plane is occupied by an agostic bond, it is suggested the CO molecule adds to one of the free apical positions. In the modelling studies,[41] the five coordinate complex was found not to constitute a stationary point on the potential energy surface. Instead, it relaxed during a geometry optimization into a four coordinate square planar compound.

Another feature proposed by Drent and others[34] to occur in the co-polymerisation of ethene which might be expected to be influenced by the increasing steric bulk of the ligands is the ability of the growing polymer chain to internally coordinate to the palladium centre. This is proposed to play a role in ensuring that double insertions of ethene and CO do not occur in the growing polymer chain. The chelate ring formed as a result of this internal coordination would be expected to be coplanar with the P-Pd-P plane. This can only be a factor in the methoxycarbonyl mechanism where it is possible that the absence of the intra molecular stabilization allows methanol to effectively compete at the metal centre to terminate the cycle after one CO/ethene insertion, resulting in methyl proportionate formation rather than co-polymer. In the hydride mechanism the acyl intermediate has no oxygen atom capable of chelating in the above manner. Barron[42] *et al* have suggested the formation of stable chelates of this type to explain the lack of activity of dppe and dmpe which give rise to large in plane pocket angles at palladium. The formation of stable chelates is proposed to oppose the insertion of the next monomer unit (CO) by blocking the required coordination site at palladium and thus inhibiting polymerization. The magnitude of this effect will depend on the coordination strength of the carbonyl group to the palladium centre.

The authors argue[42] that, for complexes in which the phosphines have a small pocket angle (i.e. dcpe, dppp), the phosphines substituents may inhibit or even preclude chelation as a consequence of the steric repulsion between the substituents on phosphorous and the carbonyl. In contrast, complexes containing phosphorus with a large pocket angle (i.e. dmpe) will have significantly less steric hindrance and chelation may become so strong that insertion of the next monomer is inhibited completely; therefore chain propagation cannot occur. Modelling studies and structural data[34, 41] support the suggestion that the growing polymer chains are stabilized by the carbonyl group interacting with the metal centre.

In conclusion, we have identified a structural parameter calculated from experimental X-ray data which correlates structural features of complexes with MeP selectively in the methoxycarbonylation of ethene. This inplane pocket angle also links bulky alkyl and phenyl substituted diphosphines with monodentate phosphine ligands. The proposed relationship is based on the known reactivity of square planar palladium(II) compounds and the known requirements for insertion reactions in a range of homogeneous catalytic processes.

3.6 Conclusions

A number of new phosphine ligands have been synthesised and characterized. These and others have been utilized to synthesize a range of palladium(0) alkene complexes. The phosphine ligands chosen in this study all readily form complexes with $Pd_2(dba)_3$. The complexes have the formula [(P-P)Pd(dba)] where the bidentate phosphine binds as a chelate ligand to a single palladium atom. The environment around the palladium is essentially trigonal planar, with only small dihedral angles between P_2Pd and PdC_2 planes observed. The solution behavior of the complexes can be rationalised with reference to a model which postulates fluxional behavior in the dba moiety, detected by the solution NMR data obtained for a range of related complexes.

The dba can be readily displaced from these alkene complexes by electron withdrawing alkenes such as benzoquinone and tetracyanoethylene. Unlike dba, benzoquinone can bond to the palladium via one or both of its alkene substituents, the bonding mode adopted being dependent on the steric congestion enforced by the phosphine ligand. Very sterically demanding ligands such as **(1)** give rise to η^2-bonding whereas less sterically demanding ligands (eg. dppf) give rise exclusively to η^4-bonding. The two modes of bonding do not rapidly inter-convert, as signals attributable to both modes are present in cases **(6, 8)** where the steric demands of the ligand are intermediate.

3.7 References

1. Chapter 1 and references therein
2. E. Drent, EP 0, 271, 144, **1988**
3. R.P. Tooze, G.R. Eastham, K. Whiston and X.L. Wang; WO 96/19434
4. F. R. Hartley, *The Chemistry of Organophosphorus Compounds Volume 1*, J. Wiley & Sons, 1994.
5. C. Amatore, E. Carre, A. Jutand and M. A. B'Barki, *Organometallics*, **1995**, 14, 1818.
6. M. Kranenburg, Y. E. M. van der Burgt, P. C. J. Kamer, P. W. N. M. van Leeuwen, K. Goubitz and J. Fraanje, *Organometallics*, **1995**, 14, 3081.
   F. R. Hartley, "*The chemistry of organophosphorus compounds*" volume 1, chapter 7. J.Wiley & Sons, **1994.**
7. J. Moulton and B. L. Shaw, *J. Chem. Soc. Chem. Comm*; **1976**, 365.
8. J. Klein, A. Medlik and A. W. Meyer, *Tetrahedron*, **1976**, 32, 51.
9. G. R. Eastham and R. P. Tooze I. C. I. internal report and patent in draft.
10. R. P. Houghton, "*Metal Complexes In Organic Chemistry*", page 60. Cambridge University Press, 1979.
    R.H. Crabtree, "*The Organometallic Chemistry of Transition Metals*", page 2. J. Wiley & Sons, New York, 1988.
    C. Masters, "*Homogeneous Transition Metal Catalysis-a gentle art*", page 11. Chapman and Hall, 1981.
11. C. Amatore, G. Broeker, A. Jutand and F. Khalil, *J. Am. Chem. Soc.*, **1997**, 119, 5176-5185.
12. H. Minematsu, S. Takahashi and N. Hagihara, *J. Organomet. Chem.*, **1975**, 91, 389.
13. J. S. Valentine, *Chem. Rev.*, **1973**, 73, 3, 235.
14. C. A. Tolman, D. J. English and L. E. Manzer, *Inorg. Chem.*, **1974,** 14, 2353.
15. J.P. Collman, L.S. Hegedus, R.G. Norton and R.G. Finke, "*Principles and Applications of Organotransition Metal Chemistry*", University Science Books, Mill Valley (CA) USA, 1987.
    R.H. Crabtree, "*The Organometallic Chemistry of Transition Metals*", J. Wiley & Sons, New York, 1988.

P. M. Maitlis, P. Espinet, M. J. H. Russell, " *Complexes of Palladium (0), Comprehensive Organometallic Chemistry I*".

16. W. A. Herrmann, W. R. Thiel, C. Brosmer, K. Ofele, T. Priermeier and W. J. Scherer, *J. Organomet. Chem.*, **1993**, 461, 51.
17. J. Kendrick and T. Griffin personal communication.
18. H Grennberg, A Gogoll and Jan-E Buckvall, *Organometallics*, **1993**, 12, 1790.

    M. J. Chetcuti, J. A. K. Howard, M. Pfeffer, J. L. Spencer and F. G. A. Stone, *J. Chem. Soc. Dalton. Trans.*, **1980**, 276.

    M. J. Chetcuti, J. A. K. Howard, M. Pfeffer, J. L. Spencer, F. G. A. Stone and P. Woodward, *J. Chem. Soc. Dalton. Trans.*, **1980**, 284.

    A. J. Deeming, I. P. Rothwell, *J. Chem. Soc. Dalton. Trans.*, **1978**, 1497.
19. G. R. Eastham and R. P. Tooze I. C. I. internal report
20. Data from Cambridge Crystallographic Database.
21. N. Carr, B. L. Dunne, L. Mole, A. G. Orpen and J. L. Spencer, *J. Chem. Soc. Dalton. Trans.* **1991**, 863.

    N. Carr, L. Mole, A. G. Orpen and J. L. Spencer,*J. Chem. Soc. Dalton Trans.* **1992**, 2653.

    F. M. Conroy-Lewis, L. Mole, A. D. Redhouse, S. A. Lister and J. L. Spencer, *J. Chem. Soc. Chem. Comm.* **1991**, 1601.

    L. E. Crascall, J. L. Spencer,*J. Chem. Soc. Dalton. Trans.* **1992**, 3445.
22. J.P. Collman, L.S. Hegedus, R.G. Norton and R.G. Finke, "*Principles and Applications of Organotransition Metal Chemistry*", University Science Books, Mill Valley (CA) USA, 1987.

    R.H. Crabtree, "*The Organometallic Chemistry of Transition Metals*", J. Wiley & Sons, New York, 1988.
23. P. A. Chaloner, S. E. Davies and P. B. Hitchcock, *J. Organomet. Chem.*, **1997**, 527, 145.
24. P. A. Chaloner, S. E. Davies and P. B. Hitchcock, *J. Organomet. Chem.*, **1997**, 527, 145.
25. M. J. Chetcuti, J. A. K. Howard, M. Pfeffer, J. L. Spencer, F. G. A. Stone and P. Woodward, *J. Chem. Soc. Dalton. Trans.*, **1980**, 284.

26. J.P. Collman, L.S. Hegedus, R.G. Norton and R.G. Finke, "*Principles and Applications of Organotransition Metal Chemistry*", University Science Books, Mill Valley (CA) USA, 1987.

27. Y. Ben-David, M. Portnoy and M. Milstein, J.*Chem.Soc. Chem. Comm.*, **1989**, 1816.
Y. Ben-David, M. Portnoy and M. Milstein, *J. Am. Chem. Soc.*, **1989**, 111, 8742.
Y. Ben-David, M. Portnoy and M. Milstein, *Organometallics*, **1972**, 11, 1995.
Y. Ben-David, M. Portnoy and M. Milstein, *Organometallics,* **1993**, 12, 4734.
M. Portnoy and M. Milstein, *Organometallics*, **1993**, 12, 1655.
M. Portnoy, F. Frolov and M. Milstein, *Organometallics*, **1991**, 10, 3960.

28. J.P. Collman, L.S. Hegedus, R.G. Norton and R.G. Finke, "*Principles and Applications of Organotransition Metal Chemistry*", University Science Books, Mill Valley (CA) USA, 1987.
R.H. Crabtree, "*The Organometallic Chemistry of Transition Metals*", J. Wiley & Sons, New York, 1988.
P. M. Maitlis, P. Espinet, M. J. H. Russell, *Complexes of Palladium (0), Comprehensive Organometallic Chemistry 1.*

29. J. McMurray, "*Organic Chemistry*" 3rd Ed. Brookes/Cole Publishing.

30. M. Kranenburg, J. G. P. Delis, P. C. J. Kamer, P. W. N. M. van Leeuwen, K. Vrieze, N. Veldman, A. L. Spek, K. Goubitz and J. Fraanje, *J. Chem. Soc. Dalton. Trans.*, **1997**, 1839.

31. C. P. Casey and G. T. Whitekar, *Isr. J. Chem.*, **1990**, 30, 299.
C. P. Casey, G. T. Whitekar, M. G. Melvilleand L. M. Petrovich, *J. Am. Chem. Soc.*, **1992**, 114, 5535.

32. G. P. C. M. Dekker, C. J. Elsevier, K. Vrieze and P. W. N. M. van-Leeuwen, *Organometallics*, **1992**, 11, 1598.

33. M. Hodgson, D. Parker, R. J. Taylor and G. Ferguson, *J. Chem. Soc. Chem. Comm.*, **1987**, 1309.

34. E. Drent and P.H.M. Budzelaar, *Chem. Rev.*, **1996**, 96, 663.
E. Drent, J.A.M. van Broekhowen and M.J. Doyle, *J. Organomet. Chem.*, **1991**, 417, 235.

35. J. M. Brown, P. J. Guiry, *Inorganica Chimica Acta*, **1994**, 220, 249.

36. X-Ray structure [$oC_6H_4(CH_2P^tBu_2)_2Pd(COC_2H_5)(Cl)$] chapter 6 this thesis.

37. C. A. Tolman, *Chem. Rev.*, **1977**, 77, 313.

38. C. Masters, "*Homogeneous Transition Metal Catalysis-A Gentle Art*", Chapman and Hall

39. J.P. Collman, L.S. Hegedus, R.G. Norton and R.G. Finke, "*Principles and Applications of Organotransition Metal Chemistry*", University Science Books, Mill Valley (CA) USA, 1987.

40. J.P. Collman, L.S. Hegedus, R.G. Norton and R.G. Finke, "*Principles and Applications of Organotransition Metal Chemistry*", University Science Books, Mill Valley (CA) USA,1987.

41 P. Margl and T. Ziegler, *J. Am. Chem. Soc.*, **1996**, 118, 7337.

42. Y. Koide, S. G. Bott and A. R. Barron *Organometallics*, **1996**, 15, 2213.

.

CHAPTER 4.0

The Interaction of Phosphine Palladium(0) Alkene Complexes with Protic Acids

4.1 Introduction

In chapter 1, catalytic results were reported for a related series of palladium phosphine complexes. These results showed a remarkable sensitivity to the structure of the phosphine ligand. In chapter 2 structural features arising from this variation of the ligand were analysed in order to explain this structure-activity relationship. This present chapter now focuses on the activation process, whereby the zerovalent palladium complexes react with acids to give active complexes, and attempts to provide answers to the following questions

1) Can the differences in activity/selectivity of the different phosphine palladium complexes be explained by differences in the reaction pathway of the pre-catalysts with acids?

2) What species are present at the beginning of the reaction and what can this tell us about the mechanism of the reaction?

4.2 Experimental

The general conditions outlined in chapter 2 apply.

4.3 Reaction of DBA Complexes with Acid

4.3.1 Reaction of [o–$C_6H_4(CH_2PBu^t_2)_2Pd(dba)$] (12) with Toluenesulphonic Acid

To the palladium complex [$L_2Pd(dba)$] (50mg) and the acid (10 equivalents) in a 10ml NMR tube was added 2 ml of the chosen solvent (see Table 4.1). When the tube was shaken to ensure complete dissolution of the contents, a deep red colour was immediately observed

which changed to a pale yellow colour after standing overnight. The sample was analysed after 24 hours by ^{31}P NMR at room temperature (see Table 4.1). The reaction of **(12)** with toluenesulphonic acid in methanol and dichloromethane was also characterized by ^{1}H NMR and these results are presented in Table 4.2 .

Solvent	dcm	MeOH	CH_3CN	toluene	acetone	thf	$CHCl_3$
δ(ppm)	68.2	69.7	68.5	68.4	69.7	69.5	69

Table 4.1 **^{31}P NMR Analysis of the Reaction Between p-Toluenesulphonic Acid and (12)**

	d^4MeOH	CD_2Cl_2
tert-Butyl-CH_3	1.55(d, J=15.63Hz)	1.63(d, J=15.63Hz)
p-TsOH-CH_3	2.37(br)	2.5(br)
ligand CH_2	3.68(br)	3.82(br)
Aromatics	7.0-8.0	7.0-8.0

Table 4.2 **^{1}H NMR Analysis of the Reaction Between p-Toluenesulphonic Acid and (12)**

4.3.2 Reaction of Complexes [(L-L)Pd(dba)] with Methanesulphonic Acid in Methanol

General Procedure

The complex [(L-L)Pd(dba)] (30 mg) was added to 2.0ml methanol in a 10ml NMR tube. To this was added methanesulphonic acid (5 molar equivalents) which resulted in the immediate formation of a deep red colour. The samples were analysed immediately by multinuclear NMR at room temperature and in some cases at -80^{0}C.

4.3.2.1 [o-$C_6H_4(CH_2PBu^t_2)_2$Pd(dba)] (12) + 5 CH_3SO_3H

NMR (d^4-methanol, 298K): $^{31}P\{^{1}H\}$, δ 63.0(br), 40.0(br) ppm.

NMR (d^4-methanol, 193K): $^{31}P\{^{1}H\}$,δ 63.92 (d, J=48.2Hz), 57.93 (d, J=48.1Hz), 42.41 (d, J=48.1Hz), 37.31 (d, J=48.2Hz) ppm.

4.3.2.2 [o-$C_6H_4(CH_2PPr^i_2)_2Pd(dba)$] (13)+ 5 CH_3SO_3H

NMR (d^4-methanol, 298K): $^{31}P\{^1H\}$,δ 42.2(s), 39.1(br), 34.2(d, J=34Hz), 21.6(br), 18.0(d, J=34Hz) ppm.

4.3.2.3 [o-$C_6H_4(CH_2PCy_2)_2Pd(dba)$] (14)+ 5 CH_3SO_3H

NMR (d^4-methanol, 298K): $^{31}P\{^1H\}$,δ 32.1(d, J= 83.0 Hz), 25.7(d, J= 70.8 Hz), 15.0(br), 13.7(br) ppm.

NMR (d^4 methanol, 193K): $^{31}P\{^1H\}$,δ 30.4(d, J= 80.6 Hz), 24.7(d, J= 75.7 Hz), 23.2(d, J= 68.4 Hz), 13.1(d, J= 68.4 Hz), 12.6(d, J= 78.2 Hz), 9.0(d, J= 73.2 Hz) ppm.

4.3.2.4 [1,3-$C_3H_6(PPh_2)_2Pd(dba)$] (21)+ 5 CH_3SO_3H

NMR (d^4-methanol, 298K): $^{31}P\{^1H\}$,δ 5.80(d, J=90.4Hz), 7.20(d, J=78.2Hz), 10.50(d, J=75.7Hz), 15.5(d, J=95.2Hz) ppm.

NMR (d^4-methanol, 193K): $^{31}P\{^1H\}$,δ 5.50(d, J= 92.8 Hz), 7.43(d, J= 78.1 Hz), 9.50(d, J= 78.1Hz), 15.1(d, J=92.8 Hz) ppm.

4.3.2.5 [1,3-$C_3H_6(PBu^t_2)_2Pd(dba)$] (20)+ 5 CH_3SO_3H

NMR (d^4-methanol, 298K): $^{31}P\{^1H\}$,δ 54.63(br), 52.0(d, J=53.7Hz), 44.4(br), 37.0(d, J=53.7Hz) ppm.

NMR (d^4-methanol, 298K): ^1H, δ 0.85-1.5(br, 36H, ^{t}Bu-CH_3), 1.85(br, 2H, CH_2), 2.02(br, 2H, CH_2), 2.30(br, 2H, CH_2), 2.77(s, 3H, CH_3SO_3), 5.05(br, 1H, benzyl CH), 7.0-8.0(br,m, 10H, aromatics) ppm.

4.3.4 Reaction of Complexes [(L-L)Pd(dba)] with Methanesulphonic Acid in Diethyl Ether

To the palladium complex [(L-L)Pd(dba)] (1.0g)dissolved in diethyl ether (100 ml) was added the neat acid (5 molar equivalents) via a Pasteur pipette, which resulted in the immediate formation of a red purple precipitate. Stirring was continued for a further 30

minutes with no further change observed before the precipitate was removed by filtration and dried under reduced pressure to yield the product as a crisp powder.

4.3.4.1 [o-$C_6H_4(CH_2PBu^t_2)_2Pd(dba)$] (12)

Synthesis of $[dbaH]^+[MeSO_3]^-.MeSO_3H^-$ (40)

A red purple solid was isolated yield (1.0g). Analysis. Found: C, 55.64; H, 6.7 %.

After ether wash Analysis. Found: C, 58.2; H, 7.5 %.

NMR spectrum recorded immediately:

NMR (CD_2Cl_2, 298K): $^{31}P\{^1H\}$,δ 63.0(br), 40.0(br) ppm.

NMR (CD_2Cl_2, 193K): $^{31}P\{^1H\}$,δ 63.92(d, J=48.2Hz), 57.93(d, J=48.1Hz), 42.41(d, J=48.1Hz), 37.31(d, J=48.2Hz) ppm.

NMR spectrum recorded after 24 hours:

NMR (CD_2Cl_2, 298K): $^{31}P\{^1H\}$,δ 67.5(s) ppm.

NMR (CD_2Cl_2, 193K): $^{31}P\{^1H\}$,δ 68.0(s), 67.0(s) ppm.

Recrystallisation of this solid from dichloromethane layered with diethyl ether led to the isolation of red blocks and these were identified as $[dbaH]^+[MeSO_3]^-.MeSO_3H^-$ (for data see Figure 4.1 and Table 4.3) and not the anticipated palladium containing complex. There were insufficient crystals present to allow spectroscopic studies to be undertaken. Crystal data for : $C_{19}H_{22}O_7S_2$, M = 426.49, monoclinic, space group $P2_1/n$, a = 7.8585(6), b = 12.0834(10), c = 21.2594(17) Å, β = 96.256(2), V = 2006.7(3) Å^3, Z = 4, T = 160 K; 12160 data measured, 4545 unique, Rint = 0.0377, 264 refined parameters, R = 0.0356, $wR2$ = 0.0899.

S(1)-O(2)	1.5438(14)	S(1)-O(3)	1.4310(13)
S(1)-O(4)	1.4222(13)	S(1)-C(18)	1.7513(18)
S(2)-O(5)	1.4536(13)	S(2)-O(6)	1.4649(12)
S(2)-O(7)	1.4255(14)	S(2)-C(19)	1.742(2)
C(1)-O(1)	1.2970(19)	O(1)-H-0(5)	

Table 4.3 Bond Lengths (Å) and Angles (°) for $[DBA\text{-}H]^+[CH_3SO_3]^-.CH_3SO_3H$

Figure 4.1 The Crystal Structure of $[dbaH]^+[MeSO_3]^-$.MeSO3H

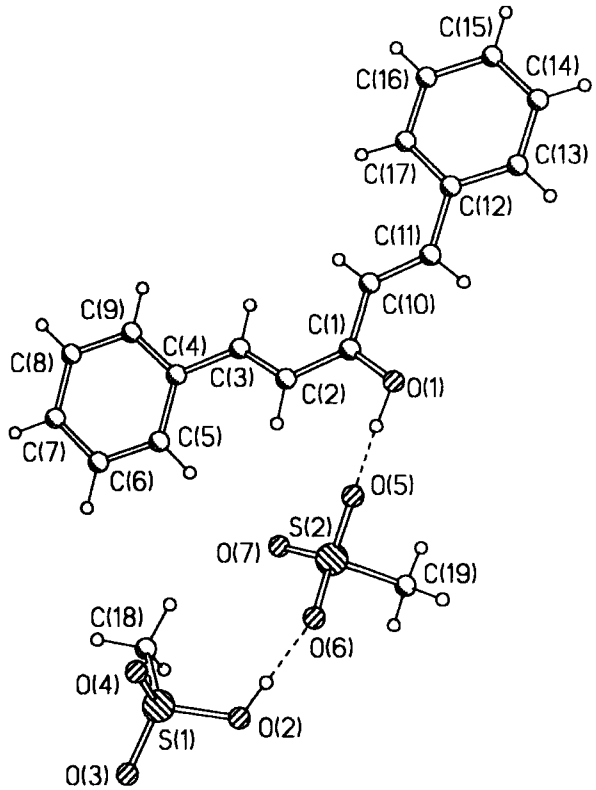

4.3.4.2 $[o\text{-}C_6H_4(CH_2PPe^t{}_2)_2Pd(dba)]$ (17)+ 5 CH_3SO_3H

A red/purple solid was isolated Yield (1.0g). Analysis. Found: C, 64.68; H, 7.49 %.

NMR spectrum recorded immediately:

NMR (CD_2Cl_2, 298K): $^{31}P\{^1H\}$,δ 73.0(s), 66.0(br), 50.5(br) ppm.

NMR spectrum recorded after 24 hours:

NMR (CD_2Cl_2, 298K): $^{31}P\{^1H\}$,δ 73.0(s) ppm.

4.3.4.3 $[o\text{-}C_6H_4(CH_2PCy_2)_2Pd(dba)]$ (14)+ 5 CH_3SO_3H

An orange solid was isolated Yield (1.1g). Analysis. Found: C, 56.35; H, 6.98 %.

NMR spectrum recorded immediately:

NMR (CD_2Cl_2, 298K): $^{31}P\{^1H\}$,δ 41.0(s), 29.0(br), 22.7(br), 12.5(br) ppm.

NMR spectrum recorded after 24 hours:

NMR (CD_2Cl_2, 298K): $^{31}P\{^1H\}$,δ 41.0(s) ppm.

4.3.4.4 [1,3-$C_3H_6(PPh_2)_2Pd(dba)$] (21)+ 5 CH_3SO_3H

An orange solid was isolated Yield (1.0g). Analysis. Found: C, 57.07; H, 4.91 %.

NMR spectrum recorded immediately:

NMR (CD_2Cl_2, 298K): $^{31}P\{^1H\}$,δ 14.8(s), 12.8(d, J= 92.8 Hz), 9.3(d, J= 78.1 Hz), 5.5(d, J= 78.1Hz), 5.3(d, J= 90.3Hz) ppm.

NMR spectrum recorded after 24 hours:

NMR (CD_2Cl_2, 298K): $^{31}P\{^1H\}$,δ 14.8(s) ppm.

4.3.4.5 [1,3-$C_3H_6(PBu^t_2)_2Pd(dba)$] (20)+ 5 CH_3SO_3H

A red/purple solid was isolated Yield (1.0g). Analysis. Found: C, 52.87; H, 7.19%.

NMR spectrum recorded immediately:

NMR (CD_2Cl_2, 298K): $^{31}P\{^1H\}$,δ 57.8 (d, J=58.6Hz), 53.2 (d, J=58.6Hz), 44.2 (d, J=58.6Hz), 35.9 (d, J=58.6Hz) ppm.

NMR spectrum recorded after 24 hours:

NMR (CD_2Cl_2, 298K): $^{31}P\{^1H\}$,δ 70.2(s) ppm.

4.3.4.6 [o-$C_6H_4(CH_2PPh_2)_2Pd(dba)$] (7)+ 5 CH_3SO_3H

A orange solid was isolated Yield (1.0g). Analysis. Found: C, 53.6; H, 4.6 %.

NMR spectrum recorded immediately:

NMR (CD_2Cl_2, 298K): $^{31}P\{^1H\}$,δ 26.8(s), 24.9(d, J= 83.0 Hz), 18.4(d, J= 68.3 Hz), 13.2(d, J= 65.9 Hz), 11.7(d, J= 80.5 Hz) ppm.

NMR spectrum recorded after 24 hours:

NMR (CD_2Cl_2, 298K): $^{31}P\{^1H\}$,δ 26.8(s) ppm.

4.3.5 Synthesis Of [*o*-$C_6H_4(CH_2PBu^t_2)_2Pd(OH_2)_2]^{2+}$ 2[OTs]$^-$ (41)

Method 1

To the palladium complex **(12)** (1.0g)dissolved in diethyl ether (100 ml) was added the neat acid (5 molar equivalents) via a Pasteur pipette, which resulted in the immediate formation of a red/purple precipitate. Stirring was continued for a further 30 minutes (no further change observed) before the precipitate was removed by filtration and dried under reduced pressure to yield the product as a crisp powder. A red/purple solid was isolated (1.0g). Analysis. Found: C, 63.58; H, 7.02.

NMR (CD_2Cl_2, 298K): $^{31}P\{^1H\}$,δ 63.0(br), 40.0(br) ppm.

Recrystallisation of this solid from dichloromethane layered with diethyl ether led to the isolation of yellow crystals which were identified as the bis-aquo compound $[o\text{-}C_6H_4(CH_2PBu^t_2)_2Pd(OH_2)_2]^{2+}$ 2[OTs]- (for data see Figure 4.2 and Table 4.4). Crystal data for **(41)**: $C_{38}H_{62}O_8P_2PdS_2$, M = 879.34, monoclinic, space group $P2_1/n$, a = 14.6760(12), b = 15.7127(13), c = 17.3890(14) Å, β = 90.593(2), V = 4009.7(6) Å^3, Z = 4, T = 160 K; 22881 data measured, 9170 unique, Rint = 0.0669, 474 refined parameters, R = 0.0667, $wR2$ = 0.1675.

P(1)-Pd	2.3030(14)	P(2)-Pd	2.2876(13)
Pd-O(1)	2.125(3)	Pd-O(2)	2.109(4)
P(1)-Pd-P(2)	101.01(5)	O(1)-Pd-O(2)	82.25(14)
O(1)-Pd-P(1)	89.81(10)	O(2)-Pd-P(2)	86.92(10)
O(1)-O(3)		O(1)-O(6)	
O(2)-O(4)		O(1)-O(7)	

Table 4.4 Bond Lengths (Å) and Angles (°) for $[o\text{-}C_6H_4(CH_2PBu^t_2)_2Pd(H_2O)_2]^{2+}$ 2[OTs]$^{2-}$

Method 2

This complex could also be prepared in the following way: To the palladium complex **(12)** (1.0g, 0.014moles) dissolved in thf (100 ml) was added the neat acid (5 molar equivalents) via a Pasteur pipette, which resulted in the immediate formation of a deep red/purple coloration. Stirring was continued for a further 30 minutes at which point water (0.5ml, 0.028moles) was added. Stirring was continued for a further 2 hours during which time the solution changed from red to yellow in colour. The solvent was removed under reduced pressure and the solid washed twice with ether (50 ml) before drying to leave a yellow solid 0.96g (80%). $C_{38}H_{65}P_2S_2O_8Pd$ requires C, 51.7; H, 7.37 %. Found: C, 50.37; H, 7.59

NMR (CD_2Cl_2, 298K): $^{31}P\{^1H\}$,δ 69.2(s) ppm; ^1H, δ 1.45 (s, 36H, ^{t}Bu-CH_3), 2.28 (s, 6H, OTs-CH_3), 3.1 (br, 4H, CH_2), 3.8 (br, 4H, H_2O), 7.0-8.0 (br,m, 12H, aromatics) ppm.

NMR (CD_2Cl_2, 193K): $^{31}P\{^1H\}$,δ 69.2(s) ppm.

Figure 4.2 **The Crystal Structure of $[o\text{-}C_6H_4(CH_2PBu^t_2)_2Pd(OH_2)_2]^{2+}$ 2[OTs]$^-$ View 1 with OTs Anions Omitted.**

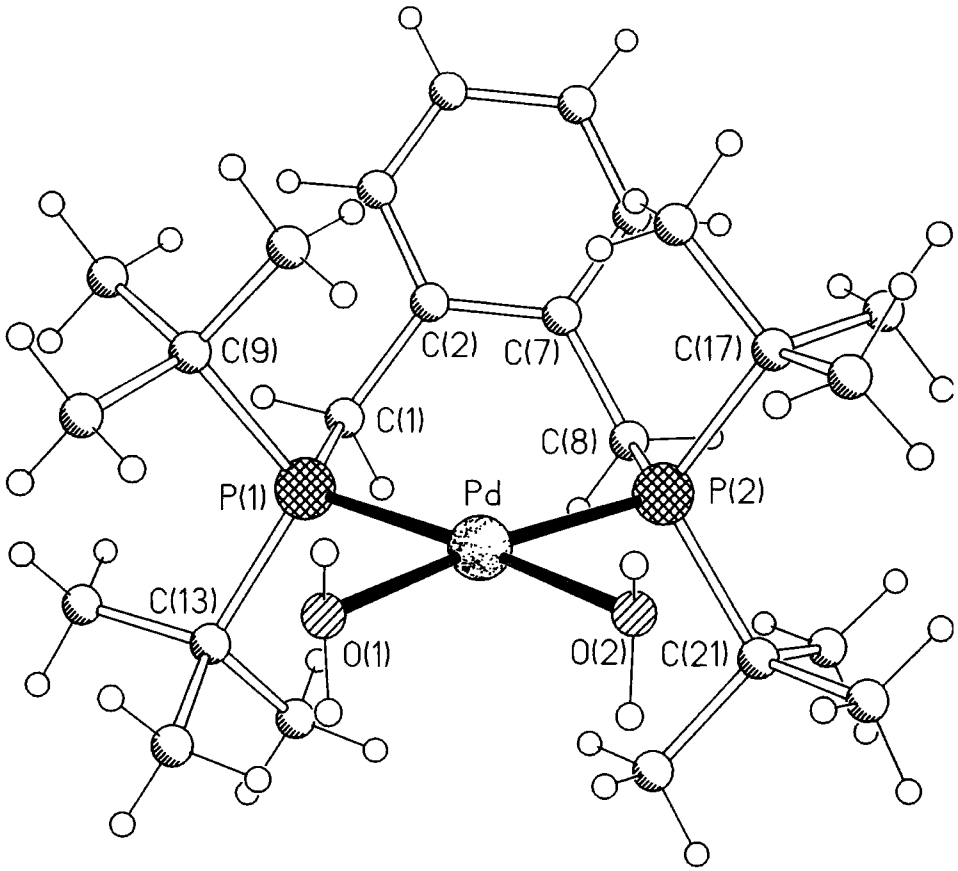

Figure 4.2 **The Crystal Structure of $[o\text{-}C_6H_4(CH_2PBu^t_2)_2Pd(OH_2)_2]^{2+}$ 2[OTs]$^-$ View 2**

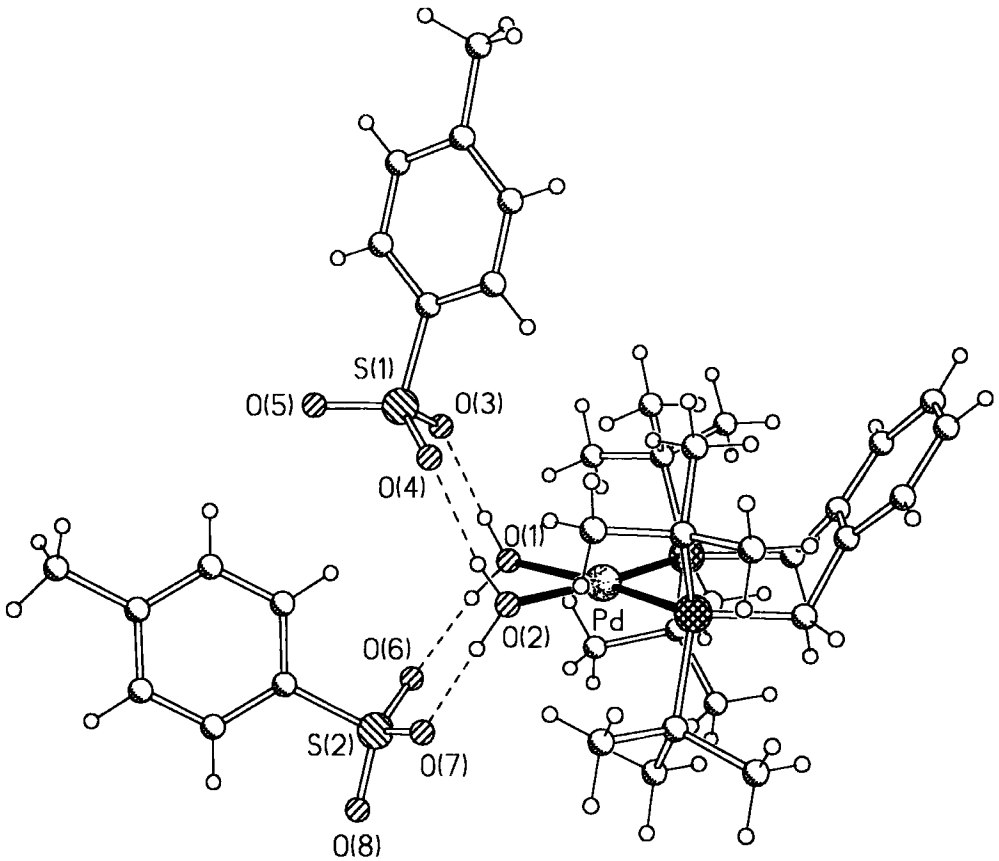

4.3.6 Synthesis of $[o\text{-}C_6H_4(CH_2PBu^t_2)_2Pd(OH_2)_2]^{2+}$ 2[BF4]- (42) and $[dbaH]^+[BF4]^-$ (43)

To the palladium complex **(12)** (0.1g) dissolved in diethyl ether (100 ml) was added the neat acid (5 molar equivalents) via a Pasteur pipette, this resulted in the immediate formation of a precipitate. Stirring was continued for a further 30 minutes (no further change observed) before the precipitate was removed by filtration and dried under reduced pressure

to yield the product as a crisp powder. Further purification by recrystallisation from the appropriate solvent was carried out as indicated to give crystals suitable for X-ray diffraction.

A red/purple solid was isolated (90 mg). Analysis found: C, 63.58; H, 7.02 %. Recrystallisation of this solid from dichloromethane layered with diethyl ether led to the isolation of two different crystal types both of which proved suitable for structural determination. The first of these were yellow blocks and were identified as the bis-aquo compound $[o\text{-}C_6H_4(CH_2PBu^t_2)_2Pd(OH_2)_2]^{2+}$ $2[BF_4]^-$ (for data see Figure 4.3 and Table 4.5). Crystal data for **(42)**: $C_{24}H_{48}B_2F_8O_2P_2Pd$, $M = 710.58$, monoclinic, space group $P2_1/n$, $a = 10.4611(7)$, $b = 15.3279(11)$, $c = 19.3458(13)$ Å, $\beta = 99.040(2)$, $V = 3063.5(4)$ Å^3, $Z = 4$, $T = 160$ K; 16289 data measured, 6103 unique, Rint = 0.0429, 377 refined parameters, $R = 0.0311$, $wR2 = 0.0801$.

P(1)-Pd	2.2923(7)	P(2)-Pd	2.3018(7)
Pd-O(1)	2.154(2)	Pd-O(2)	2.159(2)
P(1)-Pd-P(2)	100.4(2)	O(1)-Pd-O(2)	82.03(8)
O(1)-Pd-P(1)	87.66(6)	O(2)-Pd-P(2)	90.30(6)
O(1)-F(3)		O(1)-F(7)	
O(2)-F(2)		O(2)-F(6)	

Table 4.5 Bond Lengths (Å) and Angles (°) for $([o\text{-}C_6H_4(CH_2PBu^t_2)_2PdOH_2)_2]^{2+}$ $2[BF_4]^-$

The second crystal type were red blocks and these were identified as $[dbaH]^+[BF_4]^-$ (for data see Figure 4.4 and Table 4.6). There were insufficient crystals present to allow spectroscopic studies to be undertaken. Crystal data for **(43)**: $C_{34}H_{30}B_2F_8O_2$, $M = 644.20$, triclinic, space group P-1, $a = 8.075(2)$, $b = 8.426(2)$, $c = 13.186(4)$ Å, $\alpha = 101.297(7)^0$, $\beta = 95.774(7)$, $\gamma = 116.529(6)$, $V = 768.9(4)$ Å^3, $Z = 1$, $T = 160$ K; 4164 data measured, 2794 unique, Rint = 0.0781, 211 refined parameters, $R = 0.0765$, $wR2 = 0.1900$.

B(1)-F(1)	1.388(4)	B(1)-F(2)	1.377(4)
B(1)-F(3)	1.385(4)	B(1)-F(4)	1.421(3)
C(9)-O(1)	1.313(3)	H(1)-F(4)	1.76

Table 4.6 Bond Lengths (Å) and Angles (°) for $[DBA\text{-}H]^+$ $[BF_4]$

Figure 4.3 The Crystal Structure of $[o-C_6H_4(CH_2PBu^t_2)_2Pd(OH_2)_2]^{2+}$ 2[BF4]$^-$

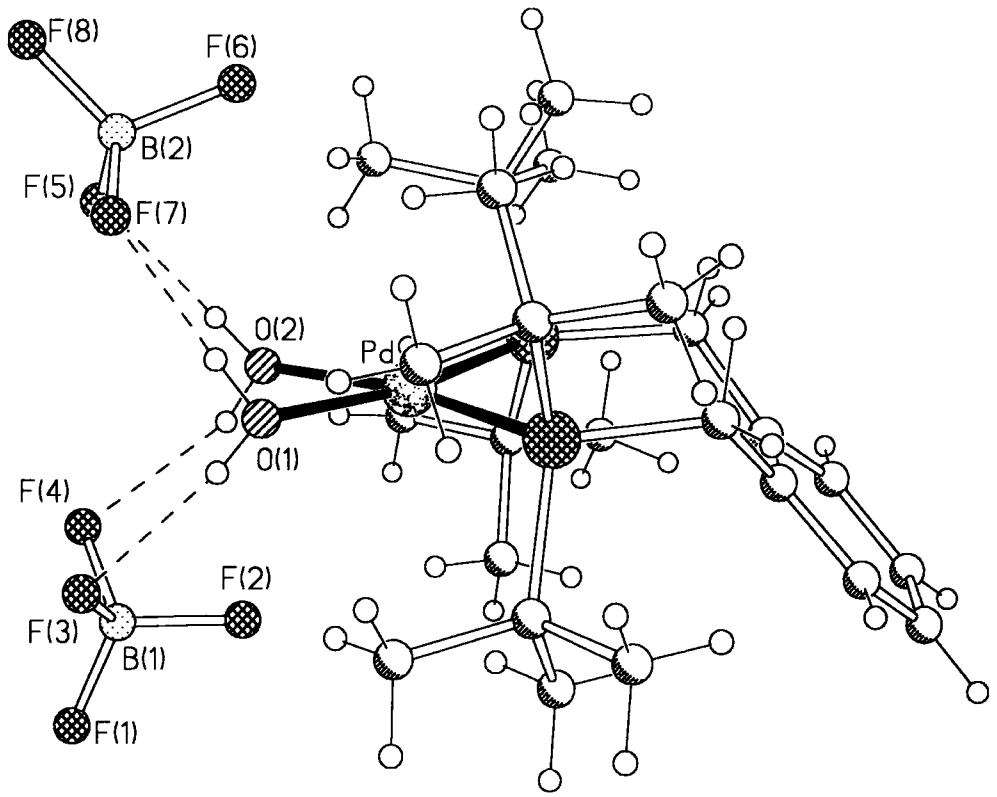

Figure 4.4 The Crystal Structure of $[dbaH]^+[BF_4]^-$

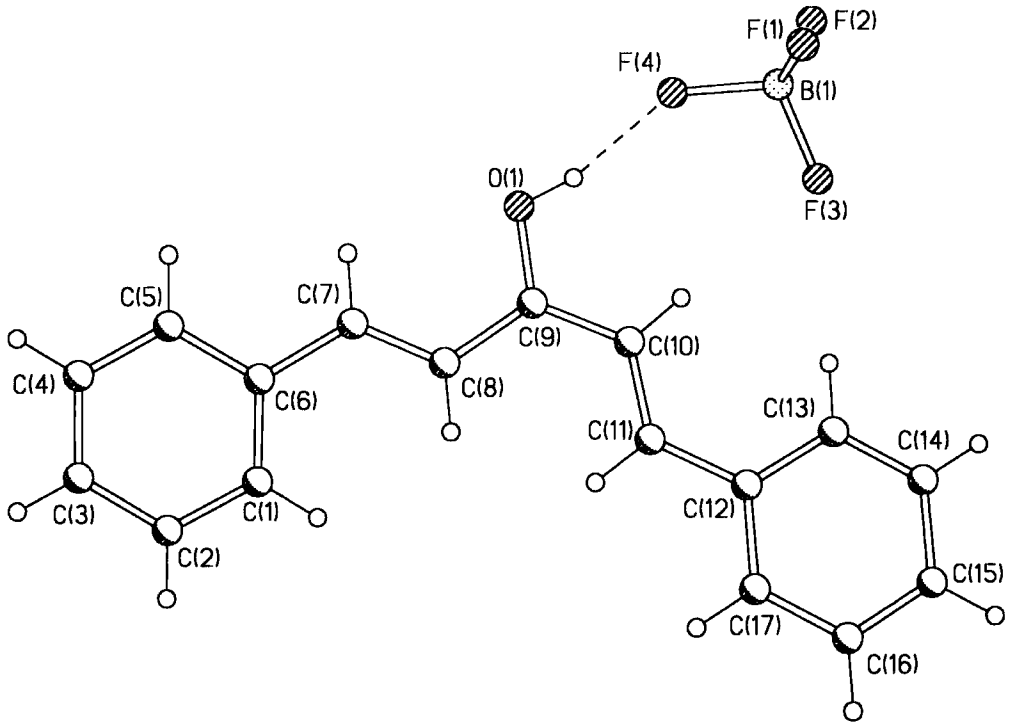

4.3.7 Synthesis of $[o\text{-}C_6H_4(CH_2PPr^i_2)_2Pd(CH_3SO_3)_2]$ (44)

To the palladium complex **(13)** (1.0g, 0.0014moles) dissolved in thf (100 ml) was added the neat acid (10 molar equivalents) via a Pasteur pipette, which resulted in the immediate formation of a deep red/purple coloration. Stirring was continued overnight before removal of the solvent under reduced pressure to yield an orange red gum. This material was recrystallised from dichloromethane, layered with diethyl ether, to yield yellow crystals of $[o\text{–}C_6H_4(CH_2P^iPr_2)_2\ Pd(CH_3SO_3)_2.\ 2\ thf]$ 0.71g (80%) suitable for structural determination (for data see Figure 4.5 and Table 4.7). Crystal data for **(44)**: $C_{30}H_{58}O_8P_2PdS_2$, $M = 879.34$, monoclinic, space group $P2_1/n$, $a = 9.8188(9)$, $b = 15.0712(14)$, $c = 24.739(2)$ Å,

β = 96.108(3), V = 3640.1(6) Å^3, Z = 4, T = 160 K; 22487 data measured, 8396 unique, Rint = 0.0731, 398 refined parameters, R = 0.0430, $wR2$ = 0.0833.

P(1)-Pd	2.2476(8)	P(2)-Pd	2.2467(9)
Pd-O(1)	2.117(2)	Pd-O(4)	2.131(2)
P(1)-Pd-P(2)	99.17(3)	O(1)-Pd-O(4)	87.05(9)
O(1)-Pd-P(1)	87.38(6)	O(4)-Pd-P(2)	87.10(7)

Table 4.7 Bond Lengths (Å) and Angles (°) for [o–$C_6H_4(CH_2PPr^i_2)_2Pd(CH_3SO_3)_2$. 2 thf]

Figure 4.5 The Crystal Structure of [o–$C_6H_4(CH_2PPr^i_2)_2Pd(CH_3SO_3)_2$. 2 thf] (Solvent Molecules Omitted)

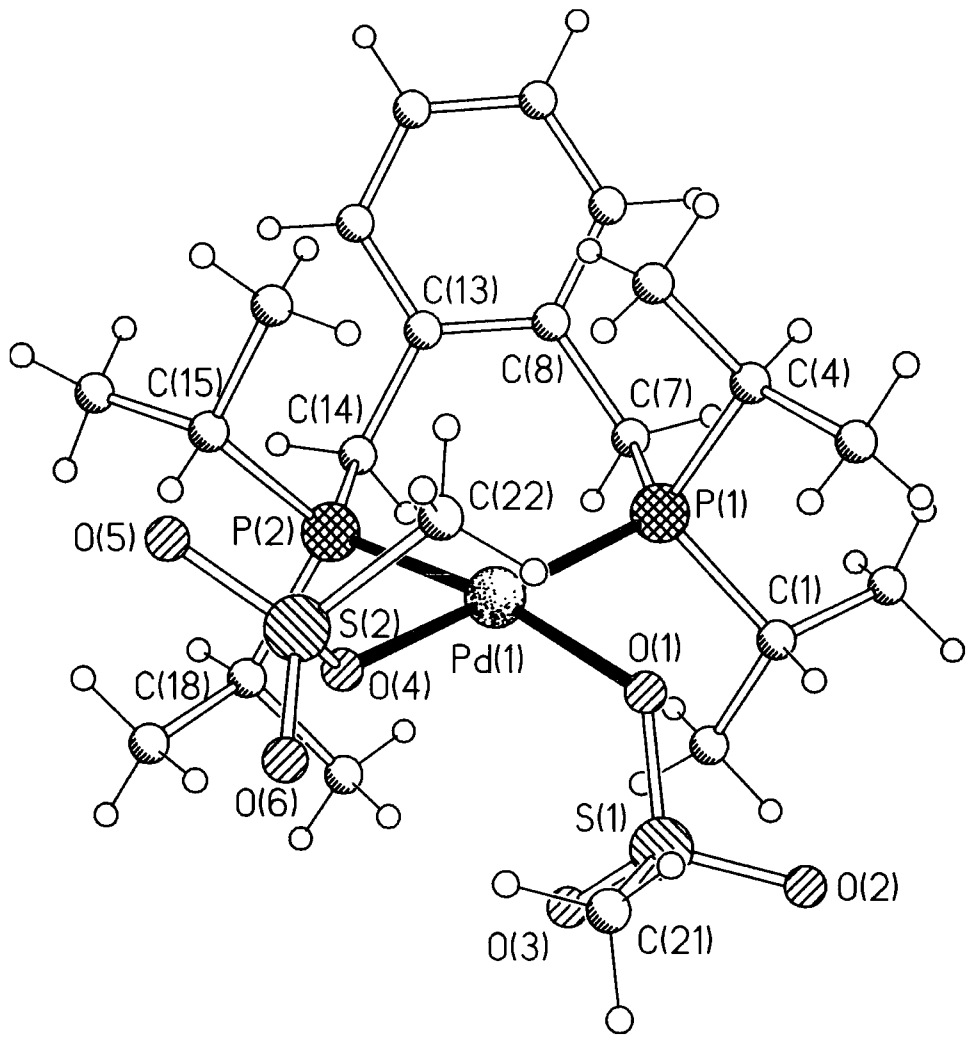

4.3.8 Reaction of Complexes [(L-L)Pd(benzoquinone)] with Methanesulphonic Acid in Methanol

The catalyst testing reported in chapter 1.0 of this thesis showed a difference in activity between palladium(0) pre-catalysts incorporating dba and those incorporating benzoquinone. A notable difference between the complexes occurs in preparing solutions for catalysis, and is the absence for benzoquinone complexes of the red coloured intermediates that are formed on reacting the dba complexes with sulphonic acids. The reaction of a range of palladium(0) BQ complexes with methanesulphonic acid have been studied to understand the differences, and relate them to the different catalytic effects.

General Procedure

The complex [(L-L)Pd(benzoquinone)] (30 mg) was added to a 10ml NMR tube and dissolved in 2.0ml d^4-methanol. To this was added methanesulphonic acid (5 molar equivalents) which resulted in an almost immediate change in colour from orange to pale yellow. The sample was analysed immediately by multinuclear NMR at room temperature. In all cases a portion of the NMR sample was analysed by GC for the presence of hydroquinone (comparison of retention time with reference standard material).

4.3.8.1 [o–$C_6H_4(CH_2PBu^t_2)_2$Pd(benzoquinone)] (27)

NMR (d^4 methanol, 298K): $^{31}P\{^1H\}$, δ 67.5 (s) ppm, ^1H, δ 1.41 (d, J= 15.62Hz, 36H, Bu^t-CH_3), 2.75 (br, 6H, $CH_3SO_3^-$), 3.55 (br, 4H, ligand CH_2), 7.21 (m, 2H, aromatic), 7.34 (m, 2H, aromatic) ppm; ^{13}C, δ 26.4 (d, $J_{(P-C)}$= 20Hz, ligand CH_2), 30.7 (s,^tBu-CH_3), 39.4 (s,$CH_3SO_3^-$), 41.8 (d, $J_{(P-C)}$16.9Hz, Bu^t-quaternary), 131.9 (s, aromatic CH), 133.3 (s, aromatic CH), 149.9 (d, $J_{(P-C)}$=4.6Hz, aromatic CH) ppm.

NMR (d^4-methanol, 193K): $^{31}P\{^1H\}$,δ 68.0 (s), 67.0 (s) ppm.

Mass Spectrum(FAB + ion, mNBA matrix): M/z 595 [(100%), $(M-CH_3SO_3)^+$].

GC Analysis; Hydroquinone detected.

4.3.8.2 [o–$C_6H_4(CH_2PCy_2)_2Pd$(benzoquinone)] (30)

NMR (d^4-methanol, 298K): $^{31}P\{^1H\}$, δ 50.67 (s) ppm; ^1H, δ 1.2-2.1 (br, 44H, CH_2), 2.70 (br, 6H, $CH_3SO_3^-$), 3.8 (br, 4H, CH_2) ppm.

GC Analysis; Hydroquinone detected

4.3.8.3 [o–$C_6H_4(CH_2PPh_2)_2Pd$(benzoquinone)] (31)

NMR (d^4-methanol, 298K): $^{31}P\{^1H\}$, δ 26.7 (s) ppm; ^1H, δ 2.74(br, 6H, $CH_3SO_3^-$), 4.5 (br, 4H, CH_2), 7.0-8.2 (br, m, aromatics) ppm.

Mass Spectrum(FAB + ion, mNBA matrix): M/z 675 [(48%), $(M\text{-}CH_3SO_3)^+$].

GC Analysis; Hydroquinone detected

4.3.8.4 [1,3-$C_3H_6(PBu^t_2)_2Pd$(benzoquinone)] (32)

NMR (d^4-methanol, 298K): $^{31}P\{^1H\}$, δ 69.2, ^1H, δ 1.64(d, J= 15.14 Hz, 36H, ^{t}Bu-CH_3), 1.98 (br, 2H, CH_2), 2.15 (br, 4H, CH_2), 2.74 (br, 6H, $CH_3SO_3^-$) ppm.

Mass Spectrum(FAB + ion, mNBA matrix): M/z 533 [(100%), $(M\text{-}CH_3SO_3)^+$].

GC Analysis; Hydroquinone detected

4.3.8.5 [2,3-$C_{10}H_6(CH_2PBu^t_2)_2$ Pd (benzoquinone)] (28)

NMR (d^4-methanol, 298K): $^{31}P\{^1H\}$, δ 71.5 (s) ppm; ^1H, δ 1.72(d, J= 15.14 Hz, 36H, ^{t}Bu-CH_3), 2.90(br, 6H, $CH_3SO_3^-$), 4.13(br, 4H, ligand CH_2), 7.65(m, 2H, aromatic), 7.98(m, 2H, aromatic), 8.21(m, 2H, aromatic) ppm.

Mass Spectrum(FAB + ion, mNBA matrix): M/z 645 [(100%), $(M\text{-}CH_3SO_3)^+$].

GC Analysis; Hydroquinone detected

4.3.8.6 [(DPEphos)Pd(benzoquinone)] (34)

NMR (d^4-methanol, 298K): $^{31}P\{^1H\}$, δ 25.1 (s) ppm; ^1H, δ 2.90 (br, 6H, $CH_3SO_3^-$), 6.77 (m, 2H, aromatic), 7.18 (m, 2H, aromatic), 7.42 (m, 2H, aromatic), 7.65 (m, 4H, aromatic), 7.75 (m, 18H, aromatic) ppm.

Mass Spectrum(FAB + ion, mNBA matrix): M/z 739 [(25%), $(M\text{-}CH_3SO_3)^+$].

GC Analysis; Hydroquinone detected

4.3.8.7 [1,4-$C_4H_8(PBu^t_2)_2$ Pd (benzoquinone)] (29)

NMR (d^4-methanol, 298K): $^{31}P\{^1H\}$, δ 83.76 (s) ppm.

Mass Spectrum(FAB + ion, mNBA matrix): M/z 547 [(2%), $(M\text{-}CH_3SO_3)^+$].

GC Analysis; Hydroquinone detected

4.3.8.8 [(dppf)Pd(benzoquinone)] (36)

NMR (d^4-methanol, 298K): $^{31}P\{^1H\}$, δ 45.4 (s) ppm; ^1H, δ 2.90 (br, 6H, $CH_3SO_3^-$), 4.68 (s, 4H, C_p), 4.86 (s, 4H, C_p), 7.67 (br, 8H, aromatic), 7.79(br, 4H, aromatic), 7.99(m, 8H, aromatic) ppm.

GC Analysis; Hydroquinone detected

4.3.9 Reaction of Complexes [(L-L)Pd(tcne)] with Methanesulphonic Acid in Dichloromethane

The tetracyanoethylene (tcne) complexes evaluated in chapter 1.0 all proved to be completely inactive as catalysts in the methoxycarbonylation of ethene. The activation of a series of these complexes with methanesulphonic acid is studied to see if these protonation reactions can explain the lack of activity.

General Procedure

The complex [L_2Pd(tcne)] (30 mg) was added to a 10ml NMR tube and dissolved in 2.0ml CD_2Cl_2. To this was added methanesulphonic acid (5 molar equivalents) which resulted in no colour change. The sample was analysed immediately by multinuclear NMR at room temperature.

4.3.9.1 [o–$C_6H_4(CH_2PBu^t_2)_2$ Pd (tcne)] (37)

NMR (CD_2Cl_2, 298K): $^{31}P\{^1H\}$, δ 54.0 (s) ppm.

4.3.9.2 [o–$C_6H_4(CH_2PPh_2)_2$ Pd (tcne)] (38)

NMR (CD_2Cl_2, 298K): $^{31}P\{^1H\}$, δ 18.65 (s), ppm.

4.3.9.3 [(DPEphos)Pd(tcne)] (39)

NMR (CD_2Cl_2, 298K): $^{31}P\{^1H\}$, δ 17.9 (s) ppm.

4.5 Discussion

4.5.1 Reaction of [o–$C_6H_4(CH_2PBu^t_2)_2Pd(dba)$] with Methanesulphonic Acid

The addition of 1 equivalent of methanesulphonic acid to **(12)** results in a very complex ^{31}P NMR spectrum. At room temperature a number of broad resonances are evident. On cooling to 193K these sharpen considerably, but the spectrum is very complex with in excess of 30 signals observed. In addition to signals with the correct chemical shift for the starting material there are a number of other resonances. The spectrum is too complex to determine unequivocally the nature of any other products. When five molar equivalents of methanesulphonic acid are used a very different picture emerges. The ^{31}P NMR spectrum recorded immediately shows two broad resonances at δ (P)= ca. 63 ppm and 40 ppm at room temperature. At 193K these are resolved into four doublets, where the coupling constants are similar. The observation is that the starting material **(12)** which has a ^{31}P NMR spectrum which consists of four approximately equal intensity doublets in methanol at 193K reacts to give a product whose 193K ^{31}P NMR spectrum also consists of four doublets. The four doublets in the product spectrum whilst having different chemical shifts and coupling constants to **(12)**, are present in approximately the same ratio as those in the starting material.

The reaction solution is allowed to warm to room temperature and the ^{31}P NMR monitored at hourly intervals over the next 24 hours. This reveals the development of a resonance at δ (P)= ca. 65ppm, which after 24 hours is the major signal in the spectrum. No other new signals are evident and the species giving rise to this room temperature ^{31}P NMR singlet would appear to be the final product of the reaction between **(12)** and 5 equivalents of methanesulphonic acid in methanol. Cooling this reaction solution to 193K resolves this singlet into 2 distinct peaks of equal intensity, with no phosphorus-phosphorus coupling observed.

The initial product of protonation can be isolated by carrying out the addition of methanesulphonic acid to **(12)** dissolved in diethyl ether. Under these conditions the product of reaction separates as a precipitate which gives an identical ^{31}P NMR spectrum when dissolved in methanol to that obtained when the complex is formed in-situ in methanol (ca.

63 ppm and 40 ppm). Analytical data suggest the compound formed is $[oC_6H_4(CH_2PBu^t_2)_2Pd(\eta^3\text{-dbaH})]^+ [OSO_2CH_3]^-$ (see scheme 4.1), present as two conformational isomers. The evidence for this assignment is discussed below, with a proposed reaction scheme illustrated in Scheme 4.3.

The reaction of $[o\text{-}C_6H_4(CH_2PBu^t_2)_2Pd(\eta^2\text{-}CH_2{=}CHPh)]$ with HBF_4 in diethyl ether has been reported by Spencer[1] *et al* and reviewed in the introduction to this work. The product of reaction is the compound $[o\text{–}C_6H_4(CH_2PBu^t_2)_2Pd(\eta^3\text{-MeCHPh})]^+ [BF_4]^-$ (see scheme 4.1) in which the cationic species formed on protonation of the styrene complexes is stabilized by an η^3-benzyl linkage. Stabilization in this manner is peculiar to the styrene complexes which can adopt this linkage. The protonation of ethene and norbornene complexes results in complexes which are stabilized by a β- CH agostic interaction[2]. By analogy, it is suggested that the complex $[o\text{-}C_6H_4(CH_2PBu^t_2)_2Pd(\eta^2\text{-dba})]$ **(12)** is also able to adopt an η^3-benzyl linkage to stabilize cationic species resulting from protonation with methanesulphonic acid.

The close comparison of the NMR data for $[o\text{–}C_6H_4(CH_2PBu^t_2)_2Pd(\eta^3\text{-MeCHPh})]^+ [BF_4]^-$ and $[oC_6H_4(CH_2PBu^t_2)_2Pd(\eta^3\text{-dbaH})]^+ [OSO_2CH_3]^-$ is shown in Tables 4.8 and 4.9 below, with the atom numbering scheme illustrated in Figure 4.6. The NMR data are consistent with η^3-benzyl structures, where two conformational isomers are frozen out at 193K. The presence of conformational isomers results from the independent reaction of the isomers present in the dba complex **(12)**, to give conformationally different species. The isomers arise as a result of the steric interaction of the carbonyl containing fragment of the dba with the bulky *tert*-butyl groups of the phosphine ligand and also the relative dispositions of the ligand aromatic ring. A similar model to that proposed in chapter 2 to explain the VT NMR of **(12)** is applicable here.

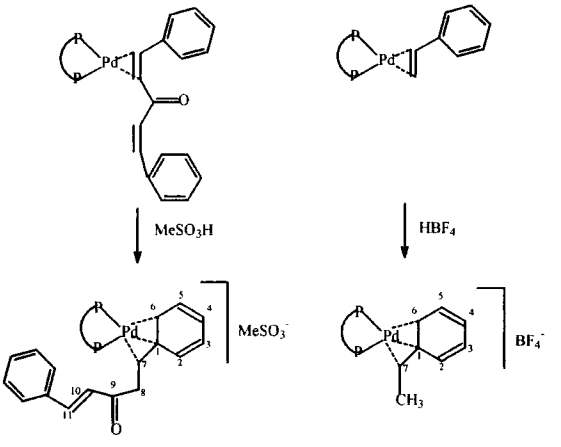

Scheme 4.1

Several points can be made from the comparison of the NMR data in Tables 4.8 and 4.9.

1) The signals present in the 193K ^{1}H and ^{13}C NMR indicative of the η^2-dba coordination, have disappeared, suggesting an alternate bonding mode of the dba and ruling out the possibility that the acid is simply protonating the carbonyl of the dba in these isolated complexes. This does not rule out the possibility that the carbonyl oxygen is the initial site of protonation which has not been detected due to rapid intra molecular proton transfer leading to the observed products occurring. This mechanism has been suggested for the protonation of zerovalent benzoquinone complexes[3].

2) The benzylic proton in the styrene complexes is reported as a multiplet at 5.25ppm, whilst we observe two broad signals at δ 5.0 and 5.2ppm consistent with the presence of two conformational isomers.

3) The aromatic carbon atoms C1 and C6 are identified in all the complexes protonated by Spencer,[4] except for $[o\text{-}C_6H_4(CH_2PBu^t_2)_2Pd(\eta^3\text{-}MeCHPh)]^+$ $[BF_4]^-$ for which only C1 is observed. Our results also support this feature two CH signals are observed at δ 119.2 and 118.9ppm assigned to C1 of the proposed conformational isomers.

4) Two CH signals are identified at δ 81.3 and 81.9ppm and these are assigned to one of the carbon atoms of the uncoordinated alkene. Again we see two signals associated with the presence of two conformational isomers frozen out at 193K.

The presence of the η^3-benzyl bonding mode has been established by Spencer from a single crystal X-ray study[2] of $[Pt(\eta^3\text{-}MeCHC_6H_4Br\text{-}4)\text{-}\{Bu^t_2P(CH_2)_3PBu^t_2\}]^+ [BF_4]^-$. In all other cases, attempts to recrystallise the reaction products from the protonation reactions failed. This is consistent with our work where attempts at recrystallisation have resulted either in decomposition or the isolation of unexpected complexes. Spencer *et al* report that $[o\text{-}C_6H_4(CH_2PBu^t_2)_2Pd(\eta^3\text{-}MeCHPh)]^+ [BF_4]^-$ decomposes in CH_2Cl_2 above 250K to give uncharacterized species.

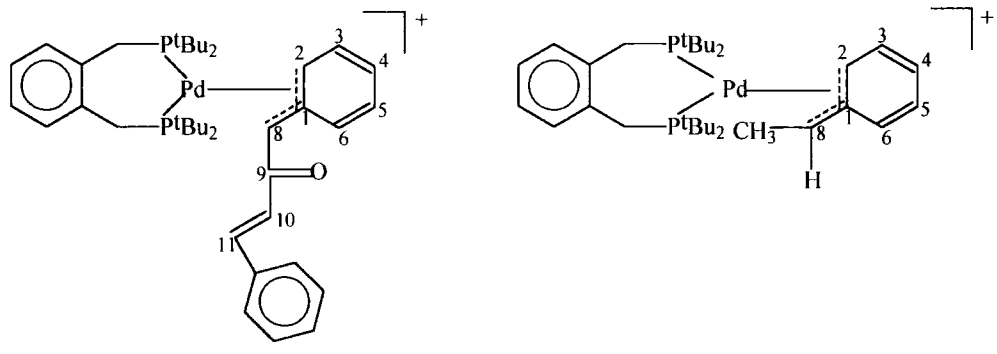

Figure 4.6 Labelling Scheme for Comparison Of NMR Data

Assignment	[*o*-$C_6H_4(CH_2PBu^t_2)_2Pd$ (η^3-MeCHPh)]$^+$ $[BF_4]^-$ (ppm).	[*o*-$C_6H_4(CH_2PBu^t_2)_2Pd$ (η^3-dbaH)]$^+$ $[MeSO_3H]^-$ (ppm).
C_{2-6}	127.6-135.5	125.0-145.0
C_1	119.0(d, J(P-C)=6Hz)	118.9(s), 119.2(s)
C_7	51.7(dd, $J(P-C)_{Trans}$ 42Hz, $J(P-C)_{Cis}$ 13Hz)	57.3(m)
C_8	N/A	not identified
C_9	N/A	177.0(s), 178.1(s)
C_{10}	N/A	81.3(s), 81.9(s)
C_{11}	N/A	not observed
Bu^t-CH_3	30.4(br), 31.1(d, J(P-C) 3Hz)	31.4(br), 32.5(br)
Bu^t-quaternary	37.0(br), 40.9(d, $J_(P-C)$ 8Hz)	38(d, J(PC) 7.5Hz), 38.4(d, J(PC) 6.5Hz), 38.8(d, J(PC) 11.2Hz), 39.3(d, J(PC) 5.1Hz), 39.6(br), 40.2(d, J(PC) 9.3Hz), 41.3(d, J(PC) 5.5Hz)
$CH_3SO_3^-$	N/A	15.9(s)

Table 4.8 **Comparison of ^{13}C NMR Data for [o-$C_6H_4(CH_2PBu^t_2)_2Pd(\eta^3$-MeCHPh)]$^+$ $[BF_4]^-$ and [o-$C_6H_4(CH_2PBu^t_2)_2Pd(\eta^3$-dbaH)]$^+$ $[MeSO_3]^-$**

Assignment	[*o*-$C_6H_4(CH_2PBu^t_2)_2Pd$ (η^3-MeCHPh)]$^+$ $[BF_4]^-$ (ppm).	[*o*-$C_6H_4(CH_2PBu^t_2)_2Pd$ (η^3-dbaH)]$^+$ $[MeSO_3H]^-$ (ppm).
Styrene CH_3	1.77(d, J=10Hz)	N/A
Ligand CH_2	3.28-4.0(br,m)	3.3-4.2(br)
Bu^t-CH_3	0.64(d, 9H, J=13.1Hz), 1.37(d, 18H, J=13.1), 1.44(d, 9H, J=14.6Hz)	0.5(br, 9H), 1.0-2.1(br, 27H)
Styrene CH	5.25(m, 1H)	N/A
Dba CH	N/A	5.0(m), 5.2(m)
Dba CH_2	N/A	not identified
Aromatics	7.2-7.7(m, 4H)	7.0-8.2(br,m)

Table 4.9 **Comparison of ^1H NMR Data for [o-$C_6H_4(CH_2PBu^t_2)_2Pd(\eta^3$-MeCHPh)]+ $[BF_4]$- and [o-$C_6H_4(CH_2PBu^t_2)_2Pd(\eta^3$-dbaH)]+ $[MeSO_3]$-**

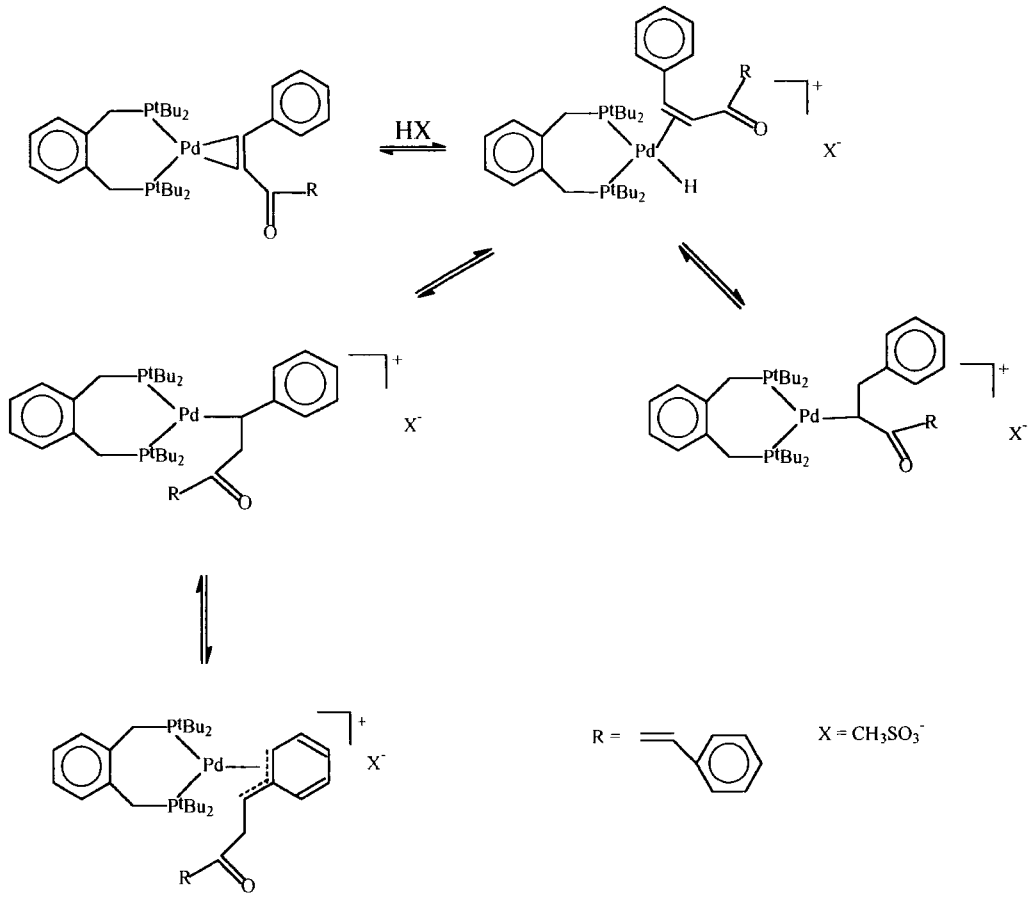

Scheme 4.2

Mechanism of Formation of η^3-benzyl Complexes

The solid isolated from the reaction of **(12)** with methanesulphonic acid in diethyl ether has been characterized by C, H, N analysis along with the solids isolated from the reaction of **(12)** with p-TsOH and HBF_4. These data is given in Table 4.10, and confirm the composition of the initial reaction product to be $[o\text{-}C_6H_4(CH_2PBu^t_2)_2Pd(\eta^3\text{-}dbaH)]^+ [X]^-$, where X = OTs, BF_4. For methanesulphonic acid the C, H, N data supports the structure $[o\text{-}C_6H_4(CH_2PBu^t_2)_2Pd(\eta^3\text{-}dbaH)]^+ [MeSO_3]^-$. $MeSO_3H$ where another molecule of methanesulphonic acid is associated with the protonated complex. The presence of this second mole of acid is only indicated for methanesulphonic acid. Further evidence for this comes from two sources. Firstly, the attempted recrystallisation of the solid isolated from the reaction of **(12)** with methanesulphonic acid, where red crystals of $[dbaH]^+[MeSO_3]^-$ $.MeSO_3H$ are recovered (see section 4.3.4.1). This material is also synthesised from the

reaction of dba with an excess of methanesulphonic acid in pentane, where the product precipitates from the reaction solution. Secondly the work of Zacchini[5] *et al* discussed earlier, has shown that the anion in the complex illustrated in Figure 4.5.5 has a molecule of methanesulphonic acid hydrogen bonded to a methanesulphonate anion in the same manner. Thus the presence of a molecule of methanesulphonic acid hydrogen bonded to the methanesulphonate anion is not unprecedented for this acid.

In the protonated alkene complex $\{[dbaH]^+[MeSO_3]^- .MeSO_3H\}$ isolated in this study, the molecule of methanesulphonic acid is hydrogen bonded via one of the oxygen atoms of the sulphonate anion. It is suggested that this interaction is weak and the molecule of acid is easily displaced on ether washing. Further complementary evidence for the presence of methanesulphonic acid comes from the results obtained for catalyst tests performed with the solids before and after ether washing (comparative studies in laboratory autoclave). The solid isolated, and not washed prior to catalyst testing, exhibits high initial activity in the absence of any added acid and has a higher overall turnover number (6200 moles MeP/mole complex/hr). This is compared to the ether washed sample which displays a much lower initial activity and a much lower overall TON (2250 moles MeP/mole complex/hr). The difference in activity can be attributed to the extra acid present in the unwashed sample.

Reaction	Found	Required for [*o*-$C_6H_4(CH_2PBu^t_2)_2Pd(\eta^3\text{-dbaH})]^+$ $[X]^-$	Required for [*o*-$C_6H_4(CH_2PBu^t_2)Pd(\eta^3\text{-dbaH})]^+$ $[X]^-$. [HX]
(12) + $MeSO_3H$	C, 55.6%, H, 6.7%	C, 60.8%, H, 7.4%	C, 55.7%, H, 6.9%
(12) + $MeSO_3H$ precip washed with ether	C, 58.2%, H, 7.5%	C, 60.8%, H, 7.4%	C, 55.7%, H, 6.9%
(12) + þTsOH	C, 63.58%, H, 7.0%	C, 63.6%, H, 7.2%	C, 61.3%, H, 6.7%
(12) + HBF_4	C, 56.68%, H, 6.6%	C, 57.1%, H, 6.7%	C, 54.9%, H, 6.5%

Table 4.10 C, H, N Data for Reaction Products of (12) with Acid

4.5.2 Identification of $[oC_6H_4(CH_2PBu^t_2)_2Pd(solv)(X)]^+$ $[X]^-$, the Second Protonation Product

The reaction solution from the addition of 5 equivalents of methanesulphonic acid to **(12)** was allowed to warm to room temperature and the ^{31}P NMR monitored at hourly intervals over the next 24 hours. This revealed the development of a resonance at δ (P)= ca. 65ppm, which after 24 hours is the major signal in the spectrum. No other new signals are evident and the species giving rise to this room temperature ^{31}P NMR singlet would appear to be the final product. Cooling the reaction solution to 193K resolved the singlet into 2 distinct peaks of equal intensity, with no phosphorus-phosphorus coupling observed.

The NMR evidence is inconclusive as to the precise nature of the final product of reaction between **(12)** and methanesulphonic acid. Scheme 4.3 below shows the second step reaction and the two most likely products. The available evidence is discussed below.

The final product of reaction between **(12)** and methanesulphonic acid might be expected to be the neutral species [o-$C_6H_4(CH_2PBu^t_2)_2Pd(MeSO_3)_2$], where both sulphonate anions are covalently bonded to the metal centre. Interaction between palladium(0) complexes and strong acids in this manner is well documented[7]. Indeed the reaction of **(13)** with an excess of methanesulphonic acid leads to the formation of $[oC_6H_4(CH_2PPr^i_2)_2Pd(MeSO_3)_2]$ which has been identified by X-ray diffraction (see Figure 4.5).

Indeed the room temperature NMR data is consistent with the structure being $[o\text{-}C_6H_4(CH_2PBu^t_2)_2Pd(MeSO_3)_2]$ or $[o\text{-}C_6H_4(CH_2PBu^t_2)_2Pd(solvent)_2]^{2+}$ $2[(MeSO_3)_2]^{2-}$, the ^{31}P NMR shows a single resonance indicative of both phosphorus atoms being equivalent. The reaction of **(12)** with excess p-TsOH has been studied in more detail (see Table 4.1, 4.2). The room temperature NMR data is consistent with the formation of $[o\text{-}C_6H_4(CH_2PBu^t_2)_2Pd(OTs)_2]$. The reaction has been carried out in a range of solvents and in all cases the reaction product has a single ^{31}P NMR resonance around 68ppm.

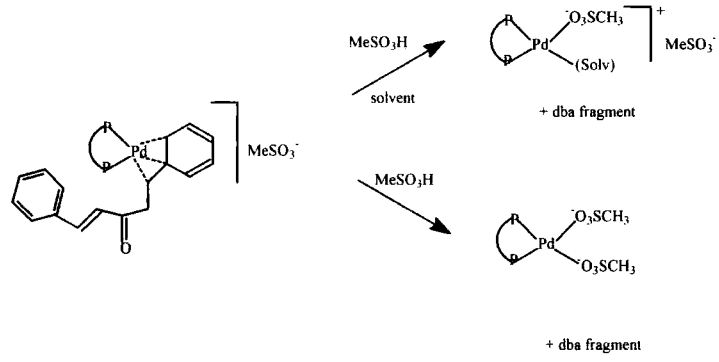

Scheme 4.3

The absolute chemical shift observed is consistent with the above assignment. This has been confirmed by the reaction of $[o\text{-}C_6H_4(CH_2PBu^t_2)_2Pd(Cl)_2]$ with an excess of silver tosylate. The chemical shift observed for the dichloride (35ppm) disappears and a new signal at 68ppm is seen, identical with that observed for the reaction of **(12)** with an excess of the acid. The uncertainty over the precise assignment of the complex comes from the observation that on cooling to 193K the ^{31}P NMR spectrum in methanol develops to 2 equal intensity resonances with no P-P coupling observed. In dichloromethane, the ^{31}P NMR spectrum on cooling remains as a single resonance. The above two possibilities can account for this behavior (scheme 4.2). Firstly the complex $[o\text{-}C_6H_4(CH_2PBu^t_2)_2Pd(MeSO_3)_2]$ could freeze out different conformations of the sulphonate methyl groups relative to the two possible dispositions of the ligand benzene ring. The proposal of the existence of conformational isomers seems reasonable given the known steric bulk of the ligand. The question mark over this proposal is the observation of solvent dependent behavior and the observation that the ratio of the peaks on cooling is always 1:1, this seems peculiar. It might be reasonably expected that the ratio of the conformational isomers would vary. The second proposal takes account of the 1:1 ratio observed which suggests the signals arise from 2 inequivalent phosphorus atoms in the same molecule, the complex

$[o\text{-}C_6H_4(CH_2PBu^t_2)_2Pd(MeSO_3)(solv)]^+[MeSO_3]^-$ being frozen out on cooling to 193K. Literature precedent exists for the displacement of weakly coordinating anions by solvent specifically water, when present in stoichiometric quantites[8]. The presence of these very small quantities of water could arise from the sulphonic acid; methanesulphonic acid and þ-TsOH are both hygroscopic the latter also crystallising with a molecule of water of crystallization which cannot easily be removed. The reactions illustrated in scheme 4.4 below have been reported for the complex $[(dppp)Pd(O_3SCF_3)_2]$ by Stang et.al[8]

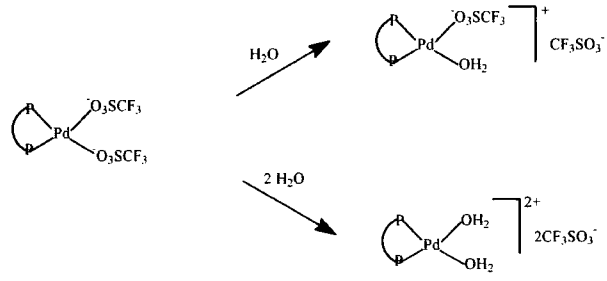

Scheme 4.4

Both the mono aquo and bis-aquo complexes above have been the subject of single crystal x-ray studies. The formation of the mono aquo is from the addition of exactly one equivalent of water, whilst an excess gives rise to the bis-aquo-complex. This serves to illustrate the ease with which these non coordinating anions can be displaced by water in these complexes.

This coordination of water to a palladium(II) centre has also been demonstrated by Leoni *et al* according to scheme 4.5 below[9].

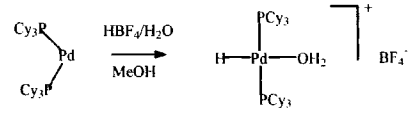

Scheme 4.5

In the above example the affinity of the palladium(II) centre for water in the presence of a coordinating solvent in excess is demonstrated. The ^{31}P NMR of the above aquo hydride is reported to be a singlet when recorded in acetone at both room temperature and 183K, suggesting the exchange processes in the complex are not frozen out even at these extreme temperatures.

The complex $[(dppp)Pd(thf)(OTs)]^+[OTs]^-$ has also been synthesised[10] and characterized by single crystal X-ray diffraction. This is an example of a coordinating solvent occupying a vacant coordination site in preference to a sulphonate anion. Whilst numerous examples of solid state structures exist with water bound to a palladium(II) centre it seems likely that the methanol solvent in reactions reported here is coordinating to the metal centre and is responsible for the observed low temperature NMR . In support of this is the synthesis and characterization by single crystal X-ray diffraction of the complex illustrated in scheme 4.6 below by Zacchini[11] *et al.* In this complex the sulphonate anion is acting as a bidentate ligand and its ^{31}P NMR spectrum is reported to be identical to that observed for the second protonation product. It is suggested that in coordinating solvent the coordinated sulphonate is monodentate with solvent occupying the vacant coordination site. In non coordinating solvent the bidentate sulphonate remains intact and only one ^{31}P NMR signal is observed at all temperatures.

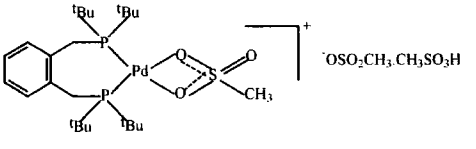

Figure 4.7

4.5.3 Reaction of (3), (5), (7), (11), (12) with Methanesulphonic Acid

4.5.3.1 $[o\text{-}C_6H_4(CH_2PCy_2)_2Pd(dba)]$ (14)

The reactions of **(14)** with methane sulphonic acid in a) methanol (section 4.3.2) and b) ether (section 4.3.4) has been followed by ^{31}P NMR and the spectra suggest a similar reaction profile to that suggested for the reaction of **(12)** with methanesulphonic acid. The key features of the analysis are 1). The C,H,N analysis of the precipitate isolated from the reaction of **(14)** with methanesulphonic acid in ether is consistent with a complex having the

formula $C_{51}H_{72}P_2S_2O_7Pd$, which corresponds to $[o\text{-}C_6H_4(CH_2PCy_2)_2Pd(\eta^3\text{-}dbaH)]^+$ $[MeSO_3]^-$. $[MeSO_3H]$ (see Table 4.5.4). 2) The ^{31}P NMR of **(14)** at 193K reveals signals which can be assigned to 3 main conformers. The VT ^{31}P NMR spectrum of the dba complex **(14)** contains signals associated with three of the four suggested conformational isomers as the major species present. In line with the behavior observed by **(12)** we also see 6 doublets in the ^{31}P NMR spectrum of the initial protonation species in approximately the same ratio suggesting that each isomer reacts to form an independent species which is not interconvertable. 3) When the complex $[o\text{-}C_6H_4(CH_2PCy_2)_2Pd(\eta^3\text{-}dbaH)]^+$ $[MeSO_3]^-$. $[MeSO_3H]$ is dissolved in $CDCl_3$ and monitored by ^{31}P NMR after standing overnight, only a single resonance is observed which can be assigned to the complex $[o\text{-}C_6H_4(CH_2PCy_2)_2Pd(MeSO_3)_2]$, resulting from the reaction of $[o\text{-}C_6H_4(CH_2PCy_2)_2Pd(\eta^3\text{-}dbaH)]^+$ $[MeSO_3]^-$ with further acid (scheme 4.6). This assignment is based on the analysis obtained from the synthesis and isolation of $[oC_6H_4(CH_2PCy_2)_2Pd(OTs)_2]$ reported in Chapter 4 of this thesis. Further work is required to determine the precise nature of the dba fragment formed in this reaction, but the anticipated product would be benzylidene(ethylbenzyl)ketone resulting from the hydrogenation of the coordinated alkene moiety.

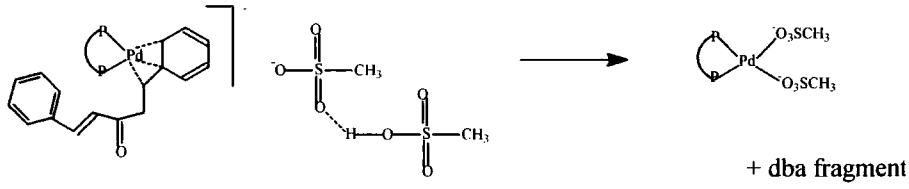

Scheme 4.6

(P-P) Complex	Found (%)	Required for $[(P\text{-}P)Pd(\eta^3\text{-}dbaH)]^+ [X]^- . [HX]$	Required for $[(P\text{-}P)Pd(\eta^3\text{-}dbaH)]^+ [X]^-$
$oC_6H_4(CH_2PCy_2)_2$ **(14)**	C, 56.3 H, 6.98	C, 56.5 H, 7.5	
$oC_6H_4(CH_2PBu^t_2)_2$ **(17)**	C, 64.68 H, 7.49	C, 57.6 H, 7.4	C, 62.4 H, 7.5
$Bu^t_2P(CH_2)_3PBu^t_2$ **(20)**	C, 52.87 H, 7.19	C, 52.9 H, 7.19	
$Ph_2P(CH_2)_3PPh_2$ **(21)**	C, 57.07 H, 4.91	C, 58.35 H, 4.86	

Table 4.11 C, H, N Data for Reaction Products of [(L-L)Pd(dba)] Complexes with Acid

One interesting feature of the ^{31}P NMR data is the observation at room temperature of two sharp doublets and two broader resonance's. This is in contrast to the reaction of **(12)** with methanesulphonic acid where only broad signals are observed. It is suggested in the case of the less sterically demanding cyclohexyl ligand that two of the conformers of η^3-benzyl species formed have significantly different exchange rates because of steric congestion. The synthesis of $[(\eta^3\text{-syn-}\alpha\text{-ethylbenzyl})Pd(TMEDA)]^+ [B(3,5\text{-}(CF_3)_2\text{-}C_6H_3)_4]^-$ has been reported by Gatti[12] *et al* and NMR studies have shown that the $[(\eta^3\text{-R-}\alpha\text{-benzyl})Pd(L)_2]^+$ moiety undergoes two dynamic processes in solution, illustrated in scheme 4.7. The processes are 1) η^3-η^1 coordination of the benzyl group and 2) ligand exchange of coordination sites. It seems likely that due to the steric bulk of the dba and the phosphine ligand the exchange reactions of the type illustrated below occur at different rates for the conformational isomers present. Thus for two isomers, the rate of exchange is slow relative to the NMR time scale such that broad signals are observed like those observed for the ^{t}butyl complex. For the second isomer the exchange is either not occurring or is fast relative to the NMR time scale such that sharp signals are observed. Cooling this sample down and recording the ^{31}P NMR spectrum reveals sharp signals which we can assign to the remaining conformers.

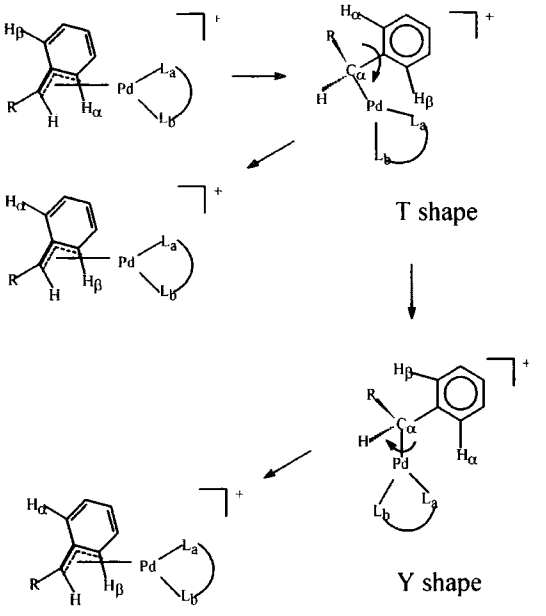

Scheme 4.7 Mechanism of exchange in η^3-benzyl complexes

4.5.3.2 [o-$C_6H_4(CH_2PPr^i_2)_2Pd(dba)$] (13)

The addition of methanesulphonic acid to **(13)** has been followed in methanol (section 4.3.2) and the data is found to be consistent with the reaction pathway proposed for the reaction of **(12)**. As with the cyclohexyl derivative **(14)** at room temperature two sharp doublets and two broad signals are observed in the ^{31}P NMR spectrum suggesting species with different barriers to exchange.

Reaction of **(13)** with an excess of methanesulphonic acid surprisingly does not lead to the formation of bis-aquo complexes.

The reaction product after recrystallisation from dichloromethane is the bis-methanesulphonate where both anions are covalently bonded to the metal centre. The absence of the bis-aquo-complex is not only a consequence of reduced steric congestion in the ligand, as the compounds have been shown to form readily with dppp, but more likely, because of the smaller size of the methanesulphonate anion. The main features of this complex **(44)** from the crystallographic study are:

1) The coordination environment around palladium is essentially square planar. The Pd-P bond lengths are 2.25Å which are significantly reduced from those found in the zerovalent Pd-alkene complex, this reflects the more electrophillic nature of the palladium(II) compared to palladium(0) . These bond lengths are within the range expected for *cis* phosphines coordinated to Pd(II)[13] and are similar to complexes of dppp, [(dppp)Pd(Cl)$_2$] 2.25Å, [(dppp)Pd(NCS)(SCN)] 2.26Å, [(dppp)Pd(NCS)$_2$] 2.24Å. The similar selectivity of palladium complexes of these two ligands in the carbonylation of ethylene, where both give co-polymers is considered to be a reflection of the similar geometries.

2) Similar to the bis-aquo complexes, the bite angle is significantly reduced in the Pd(II) oxidation state (4^0 less than dba complex).

Interestingly the ^{31}P NMR spectra of this complex mimics that of the *tert*-butyl complex resulting from interaction of **(12)** with $MeSO_3H$. The ^{31}P NMR exhibits a single resonance at RT in methanol and 2 equal intensity signals at -80°C, with a single resonance observed at all temperatures in dichloromethane. This suggests anion dissociation in solution and points to the formation of [(L-L)Pd(solv)(X)]$^+$ [X]$^-$ type species, where expected coupling is not observed as the exchange is still rapid.[14]

4.5.3.3 [(Bu$^t_2$P(CH$_2$)$_3$PBu$^t_2$)Pd(dba)] (20)

The addition of methanesulphonic acid to **(20)** has been followed in methanol (section 4.3.2) and the data is consistent with the reaction pathway proposed for the reaction of **(12)**. As with the cyclohexyl derivative **(14)** at room temperature two sharp doublets and two broad signals are observed suggesting species with different barriers to exchange. The ^{1}H NMR data is also consistent with the formation of [(Bu$^t_2$P(CH$_2$)$_3$PBu$^t_2$)Pd(η^3-dbaH)]$^+$ [$MeSO_3$]$^-$. The ^{31}P NMR of the product of reaction of **(20)** with methanesulphonic acid in ether contains sharp signals at room temperature. This sample has been analysed in CD_2Cl_2 and may reflect the different behavior of these compounds in coordinating and non coordinating solvents.

4.5.3.4 [(Ph$_2$P(CH$_2$)$_3$PPh$_2$)Pd(dba)] (21)

The addition of methanesulphonic acid to **(21)** has been followed in methanol (section 4.3.2) and the data is consistent with the reaction pathway proposed for the reaction of **(12)**.

Unlike the cyclohexyl derivative **(14)** at room temperature where two sharp doublets and two broad signals are observed all the signals for this reaction are sharp suggesting either no exchange or very fast exchange processes. The C, H, N data (Table 4.5.4) is consistent with the formation of $[(Ph_2P(CH_2)_3PPh_2)Pd(\eta^3\text{-dbaH})]^+$ $[MeSO_3]^-.MeSO_3H$ as seen for other bidentate phosphine complexes reacting with methanesulphonic acid in ether. This change from the appearance of very broad NMR signals with bulky phosphines to sharp signals with less bulky phenyl phosphines is interesting in the context of the observed catalyst testing data. For example the position of the equilibrium may lie right over toward the η^3 complex and very slow η^3-η^1 exchange will limit the activation of the pre-catalyst. This also provides an explanation of the lag times where slow activation means that the maximum concentration of active catalyst is present some time into the experiment. The stability of η^3-styrene complexes is reported by Drent and Budzelaar[15] as responsible for the lack of activity of specific palladium phosphine catalysts in CO/styrene co-polymerisation.

4.5.4 Formation of Bis-Aquo Complexes

There is significant interest in late transition metal aquo-complexes in the recent literature. One reason for this is because of the role of aquo complexes in the formation of metal-OH bonds which are implicated in several reactions such as Wacker oxidation[16], the water gas shift reaction[16, 17] and alkene hydrocarbonylation.[17] More specifically the water gas shift reaction is invoked by Drent[15] and others[18, 19] to explain the formation of palladium hydride from complexes such as $[(P\text{-}P)Pd(X)_2]$, where X is a non-coordinating anion such as BF_4^-. The reaction of **(12)** with an excess of toluenesulphonic acid in a range of solvents leads to the formation of $[(L\text{-}L)Pd(OTs)_2]$ irrespective of the solvent used for the reaction. When this reaction is carried out in thf and water is added, the bis-aquo-complex $[(L\text{-}L)Pd(OH_2)_2]^{2+}$ $2[OTs]^-$ is formed. It seems likely that in the coordinating solvents the species formed are $[(L\text{-}L)Pd(solv)_2]^{2+}$ $2[OTs]^-$ or $[(L\text{-}L)Pd(solv)(OTs)]^+$ $OTs]^-$. In wet thf water readily displaces the solvent and coordinating anions to give the bis-aquo complexes.

The ready formation of aquo complexes has been reported by others,[20] for example the controlled addition of 1 equivalent of water to anhydrous $[(dppp)Pd(OTf)_2]$ leads initially to the isolation of the mono aquo complex $[(dppp)Pd(OH_2)(OTf)]^+$ $[OTf]^-$. Addition of a

second equivalent of water then leads to the formation of $[(dppp)Pd(OH_2)_2]^{2+}$ $2[OTf]^-$. Also the complex $[(dppp)Pd(solv)(OTs)]^+$ $[OTs]^-$ has been reported to form by reacting $[(dppp)Pd(OAc)_2]$ with þ-$TsOH.H_2O$ in methanol.[6]

The surprising result in this study is the formation of bis-aquo complexes from the η^3-dba derivatives on attempted recrystallisation, which occurs for both þ-TsOH and HBF_4, and could involve the reaction of the η^3 dba derivative with excess acid present. A proposed mechanism is illustrated in Scheme 4.8. The C, H, N data (Table 4.10) for the solids isolated from these reactions suggest that excess acid is not present in the case of the above two acids, but in both examples the yields of the crystalline products were not determined. Perhaps also relevant in the work of Spencer[1] is the reported slow decomposition of the η^3-styryl complex of the ligand **(1)** to uncharacterized species in dichloromethane. The η^3-benzyl complex may react via an alternative mechanism which does not require additional acid to be present.

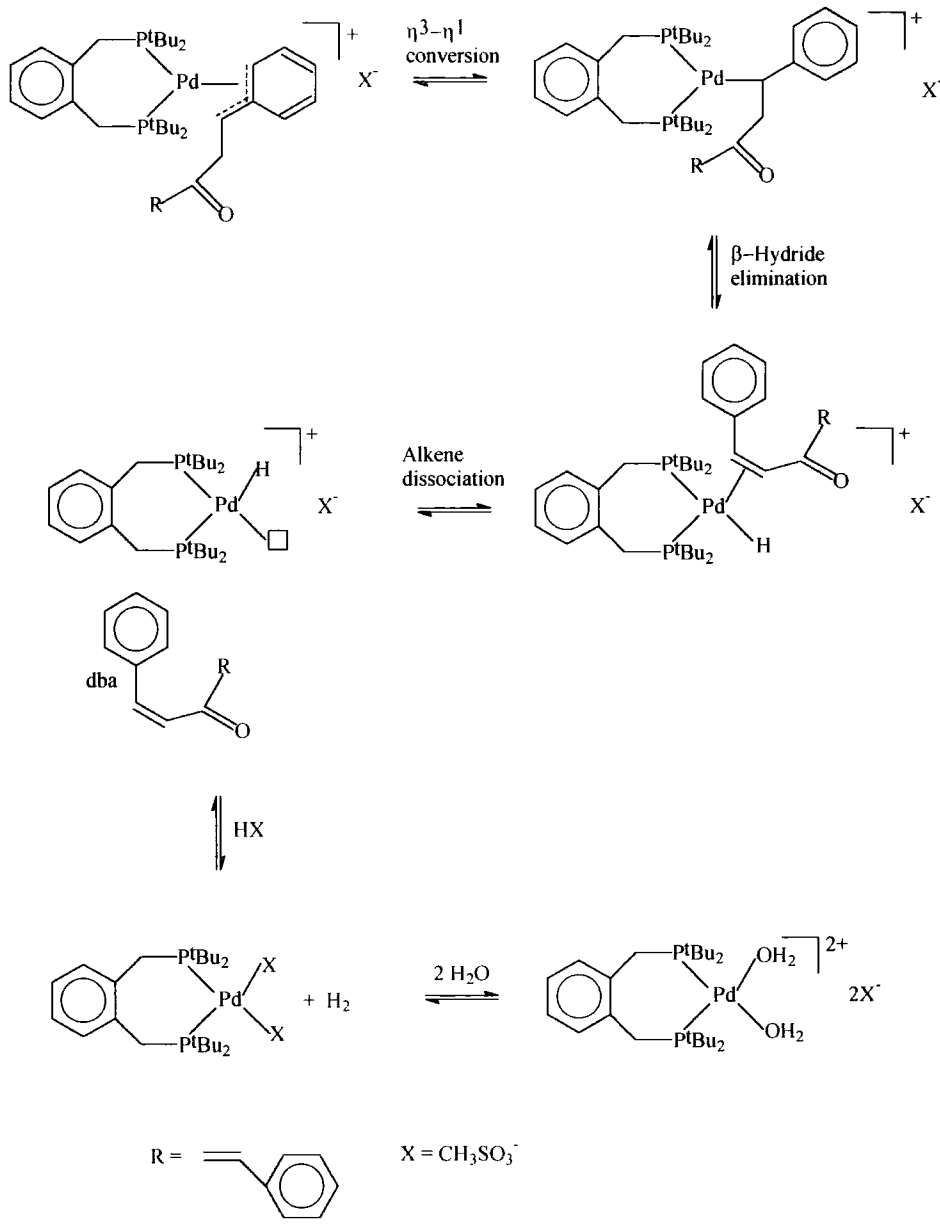

Scheme 4.8 Proposed Mechanism of Formation of Aquo Complexes

The X-ray structures of the bis-aquo complexes **(41, 42)** have several interesting features. In both complexes, the Pd(II) atom has a distorted square planar coordination. Two *cis*-sites are occupied by the phosphine ligand while the remaining two sites are taken up by two coordinated water molecules.

The P-Pd-P bond angles 101.0^0, 100.4^0, are both smaller than those observed in the Pd(O) alkene complexes, but are very much larger than those reported in the dppp aquo

complexes.[20] These bite angles are even smaller than those observed for the Pd(II) oxygen complex **(26b)** where a reduction in bite angle was observed with increase in oxidation state. This decrease in bite angle is likely to be a result of the complex trying to attain square planar geometry favoured for palladium(II) compounds. The optimum P-Pd-P angle in these complexes would be 90^0 as opposed to 120^0 in the zerovalent trigonal planar species.[17] Clearly the rigid xylene backbone and the bulky phosphorus substituents prevent attainment of 90^0 bite angles but a reduction towards this value for palladium(II) is not surprising.

The O1-Pd-O2 bite angles are 82.25^0 and 82.03^0, which is significantly smaller than observed for the $[(dppp)Pd(OH_2)_2]^{2+}$ $2[OTf]^-$ complex where this angle is 87.66^0. This presumably reflects the increased steric congestion imposed by the larger bite angle in complexes of **(1)**.

The Pd-P bond lengths of 2.29Å, 2.30Å both cases are in the normal range for *cis* chelated phosphines They are some 0.06Å shorter than the Pd(O) alkene complexes which reflects the more electrophillic nature of the palladium on oxidation and the increased deshielding of the phosphorus atoms.

The Palladium oxygen distances of 2.12, 2.10Å in $[o\text{-}C_6H_4(CH_2PBu^t_2)_2Pd(OH_2)_2]^{2+}$ $2[OTs]^-$ and 2.15, 2.16Å in $[o\text{-}C_6H_4(CH_2PBu^t_2)_2Pd(OH_2)_2]^{2+}$ $2[BF_4]^-$ compare favourably with those of related complexes, e.g. $[(dppp)Pd(OH_2)_2]^{2+}$ $2[OTf]^-$ where Pd-O = 2.13 and 2.14Å and $[(dppp)Pd(OH_2)(OTf)]^+$ $[OTf]^-$ where Pd-O = 2.16Å. This would again appear to support the idea that complexes which give co-polymer and those which give MeP are similar electronically (ground state indications). In the above examples, both ligands in Pd(II) complexes have affinity for H_2O, but the interaction of water with the metal centre is similar, as judged by metal-oxygen bond length.

Particularly noteworthy in these complexes are the hydrogen bonding patterns. Taking the tosylate complex $[o\text{-}C_6H_4(CH_2PBu^t_2)_2Pd(OH_2)_2]^{2+}$ $2[OTs]^-$, both coordinated water molecules are doubly hydrogen bonded to the tosylate counterions. Interestingly, the two water molecules are each hydrogen bonded to different tosylates rather than the same one (see Figure 4.3.5.1). The same situation is also found in the BF_4 complex where each water

molecule is doubly hydrogen bonded but each contains two hydrogen bonds to different BF_4 anions. The role of hydrogen bonding in the formation of aquo transition metal complexes has long been recognised[16] and is important in stabilizing the solid state structures of these molecules.

In the tosylate complex the S-O bond distance of the hydrogen bonded oxygen's is longer than the S-O bond distance of the non hydrogen bonded oxygen. The situation is similar in the BF_4 complex where the B-F bond lengths are longer where a hydrogen bond exists between the coordinated water and the fluorine atom.

The length of the O-H...O hydrogen bond is between 1.8 and 2.0Å which is comparable to that found for the above mentioned dppp aquo-complexes.

4.5.5 Reaction of Benzoquinone Complexes with Methanesulphonic Acid

In contrast to the reaction of the dba complexes with methanesulphonic acid, the benzoquinone complexes react rapidly to give the expected $[(L\text{-}L)Pd(X)_2]$ species, where X= methanesulphonate. Several points can be made with reference to this reaction. 1) The starting complex exhibits ^1H NMR signals characteristic of η^2-alkene bonding to palladium. These are completely absent after reaction with methanesulphonic acid indicating that complete reaction of the starting material has occurred. 2) The complex [(Bipy)Pd(BQ)] has been reported in the literature[22] and its reaction with sulphonic acids shown to lead to the formation of $[(Bipy)Pd(X)_2]$ and hydroquinone. The formation of hydroquinone is observed in all cases studied here suggesting a common reaction pathway. 3) The reaction is complete in a matter of minutes in all cases, in contrast to the dba complexes which require 24 hours for complete reaction to occur. It is this feature of the benzoquinone complexes which is of interest from a general mechanistic point of view. In the usual catalyst testing protocol the dba pre-catalyst is dissolved in the reaction solvent, acid is added and the solution added to the autoclave before heating to 80^0C under vacuum. At this point the reaction gases are added and the catalysis begins. Clearly, we do not know the extent of the activation of the dba pre-catalyst complex at this point. However the use of the benzoquinone complex allows the synthesis of $[(L\text{-}L)Pd(X)_2]$ rapidly and in 100% yield and thus a comparison of the activity of the two complexes will give an indication of the importance of the η^3- benzyl species as a

catalytic intermediate. It is suggested that the η^3- benzyl species has a rapid route into the hydride mechanism via carbonylation/methanolysis of the palladium alkyl formed by η^3-η^1 equilibrium exchange (see Scheme 4.8). It is further suggested that the extent of this equilibrium exchange is dependent on the steric bulk of the phosphine ligand, and in some circumstances the η^3- benzyl species is rate limiting. The catalysis results support the above suggestion with lower activities observed for benzoquinone complexes where the catalysts are selective for MeP. The implications for the catalysis of the different activation processes will be discussed at the end of this chapter.

The reaction of [(COD)Pd(BQ)] with a range of acids has been reported[23] and the products formed shown to depend on the acid strength. Using methanesulphonic acid, the reaction proceeds according to the reaction scheme shown below to give the Pd(II) bis methanesulphonate species.

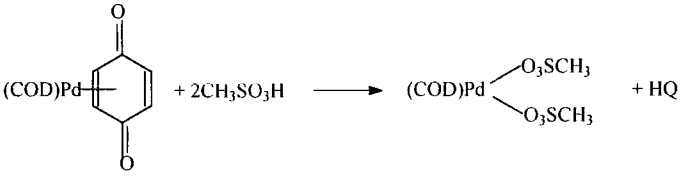

Scheme 4.9

This is consistent with our findings, where the reaction with methanesulphonic acid followed by ^{31}P NMR, shows a product having a down field shift compared with the starting complex (section 4.3.8). A new signal at δ 67ppm is observed similar to that found for the bis-aquo-complex $[(L\text{-}L)Pd(H_2O)_2]^{2+}$ $2[OTs]^-$ and also similar to the second species formed from the reaction of **(12)** with 10 equivalents of methanesulphonic acid (section 4.3.4). The chemical shift value and its proximity to similar compounds characterized by single crystal X-ray diffraction suggest a Pd(II) species of the type $[(L\text{-}L)Pd(X)_2]$. Interestingly, the ^{31}P NMR at -80° reveals two signals identical to those observed in section 4.3.4 for the second species formed in the reaction of the dba complex **(12)** with methanesulphonic acid showing these to be the same compound.

The room temperature ^1H and ^{13}C NMR are also consistent with the formation of $[(L\text{-}L)Pd(MeSO_3)_2]$ with only one *tert*-butyl environment indicated and only 3 aromatic carbon signals detected, indicating a symmetrical molecule.

Analysis of the reaction product by mass spectrometry reveals the major ion to be m/z 595 due to loss of one methanesulphonate anion from the target molecule. This is perhaps not surprising given the poorly coordinating nature of the anions.

4.5.5.1 Reaction of Benzoquinone Complexes 28-36 with Methanesulphonic Acid

The reaction of all the BQ complexes synthesised in this study is similar to that described for the *tert*-butyl complex **(27)**. This is supported by the multinuclear NMR characterization where signals are consistent with the formation of $[L\text{-}L)Pd(X)_2]$ species. Mass spectral detection of an intense ion corresponding to loss of a methanesulphonate anion from the proposed product, and the detection of hydroquinone by GC-MS in all cases further supports the proposed reaction scheme.

As mentioned previously, the rapid formation of $[(L\text{-}L)Pd(X)_2]$ via this route allows us to evaluate the role of the dba/acid intermediate as a pre-catalyst able to enter the catalytic cycle. This may be important for the phenyl substituted ligands where the increased π acidity and reduced steric bulk may lead to differences in the stability/reactivity of the η^3-benzyl species.

It is also clear from this study that the mode of coordination of the benzoquinone to palladium does not change the nature of the species formed in the reaction with acid, with complexes of the type $[(L\text{-}L)Pd(X)_2]$ always being formed as the final reaction product. The complexes proposed to have η^2-bonding of benzoquinone (e.g. **27**) react to give the same products as those proposed to have η^4 bonding (eg. **36**). On the basis of this, we might conclude that the role of BQ as an additive in catalytic reactions would then be independent of the phosphine ligand bound to palladium. This would not appear to be the case with the catalysis carried out with complexes of **(12)** showing no benefit from running in the presence of benzoquinone. The co-polymerisation catalysts based on dppp developed by Shell[24] on the other hand, all operate more favourably in the presence of benzoquinone.

The proposed role of BQ is twofold, firstly it is suggested that Pd(O) intermediates are trapped by benzoquinone and secondly, it is suggested that benzoquinone quenches palladium hydride, thereby pushing the catalysis into the methoxycarbonyl mechanism. With respect to

the trapping of Pd(0) intermediates our evidence (Chapter 2.0) is that η^4-bound BQ complexes are stable and are not exchanging with η^2-bound species. There is also literature evidence to suggest that no exchange between bound and free quinone occurs in these η^4-complexes.[23]

It seems reasonable to propose that the trapping of Pd(0) intermediates by benzoquinone occurs more favourably in situations where it can form stable η^4-bound complexes. These complexes can then be reoxidised via the mechanism proposed by Backvall et al[23] generating [(L-L)Pd(X)$_2$] and hydroquinone. The benzoquinone can interact with Pd(O) complexes of more bulky phosphines in an η^2-manner (see X-ray data for **(27)**) but this may be less efficient leading to decomposition rather than trapping.

It is not possible to comment on the role of benzoquinone in quenching hydrides as the benzoquinone has been reduced in the activation process to hydroquinone and therefore the catalyst testing is not carried out in the presence of benzoquinone.

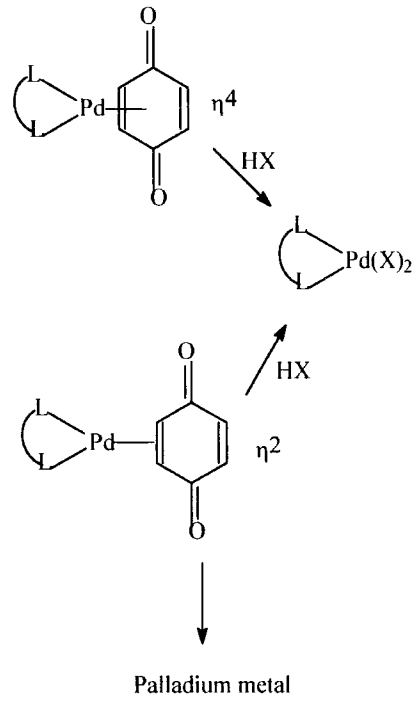

Scheme 4.10
Proposed Mode of Action of Benzoquinone

Another feature of these complexes, revealed by reaction of both the dba and benzoquinone complexes with acid, are the changes in deshielding of the phosphorus atoms following oxidation of the palladium.

Phosphine	^{31}P NMR of [(L-L)Pd(alkene)] complex[2](ppm)	^{31}P NMR of [(L-L)Pd(X)$_2$] complex(ppm)	Chemical shift difference (ppm)
dppp[1]	11.0, 7.0	14.8	5.5
xantphos	16.9	23.2	6.3
dpephos	18.2	25.1	6.9
[$C_{10}H_6$-2,3($CH_2PBu^t_2$)$_2$]	53.7	71.5	17.8
1,3-C_3H_6(PBu^t_2)$_2$	44.1	69.2	19.1
[*o*-C_6H_4(CH_2PPh_2)$_2$]	18.7	26.7	8
[*o*-C_6H_4(CH_2PCy_2)$_2$]	23	50.7	27.7
1,4-C_4H_8(PBu^t_2)$_2$	57.2	83.7	26.5
[*o*-C_6H_4($CH_2PBu^t_2$)$_2$]	51.4	67.5	16.1

1. data for alkene = dba. 2. data presented for alkene = benzoquinone unless otherwise stated

Table 4.12 Differences between ^{31}P NMR Shifts for Pd(II) and Pd(0) Complexes

Data in Table 4.12 show the difference in chemical shift between Pd(II) and Pd(0) complexes on oxidation for those complexes containing *tert*-butyl substituents to be on average 19.9ppm compared to an average chemical shift change of 7.0ppm for the phenyl substituted ligands. The average for the phenyl substituted compounds does not include the values for dppf where the presence of a second metal atom may significantly effect the degree of σ donation and π back acceptance of electrons.

The differences in chemical shift for different phosphorus substituent do not seem to be influenced by the diphosphine backbone and are presumably a consequence of the π acidity of the phenyl substituents bound to phosphorus. This π acidic behavior of phenyl substituted phosphines is well established and contributes to increased stability in metal complexes. The increased π acidity results in shorter metal-phosphorous bond lengths, a feature we have discussed in chapter 2 of this thesis as contributing to shorter Pd-P bond lengths in Pd(O) alkene complexes.

If we compare *tert*-butyl substituted phosphine complexes with phenyl substituted phosphine complexes, the degree of π back acceptance of electrons from the metal is expected to be greater for the phenyl complexes with little or no back acceptance occurring for the *tert*-butyl substituted phosphine complexes. Consequently when the *tert*-butyl substituted phosphine palladium(0) complexes are oxidised and the metal centre becomes more electrophillic the phosphorus atoms become deshielded to an even greater extent. The ^{31}P NMR shift to low field is a measure of the degree of phosphorus deshielding.

This increased deshielding as a result of the weak π-acceptor properties of the *tert*-butyl substituted phosphines may have an effect in the catalytic reactions of palladium phosphine complexes. The phenyl substituted diphosphine complexes will have shorter Pd-P bonds and hence increased stability over the *tert*-butyl liganded complexes. This will be discussed more fully later in this thesis.

4.5.6 Reaction of TCNE Complexes with Methanesulphonic acid

No reaction is observed by NMR between the [(L-L)Pd(TCNE)] complexes **39-41** with methanesulphonic acid in methanol. Only signals attributable to the starting complex are observed. TCNE complexes are often synthesized for their known stability. The presence of electron withdrawing substituents results in strong bonding of the alkene to the metal. Three factors are perhaps relevant here:

The reaction with acid may require dissociation of the alkene from the metal. This has not been shown to be the case for the dba complexes of the type [(L-L)Pd(dba)], where (L-L) = binap or dppf which undergo oxidative addition reactions[28] with phenyl iodide. The reaction has been shown to occur at the intact [(L-L)Pd(dba)] complex albeit at a slower rate than that observed for the 14e-intermediate resulting from alkene labilisation

Both the dba and benzoquinone complexes have carbonyl groups which can become protonated. The reaction of these complexes with acid may require initial protonation of the carbonyl followed by intra molecular delivery of the proton to the metal. The absence of any protonatable group precludes this pathway. The mechanism proposed in the literature for the

reaction of BQ complexes invokes carbonyl group protonation as a first step in the metal oxidation and concomitant production of hydroquinone.

Reaction of the [L-L)Pd(TCNE)] with acid may be precluded in steric grounds. The reported oxidative additions to [(L-L)Pd(dba)] are all with phenyl substituted phosphine ligands where the palladium centre is relatively accessible. The dz^2 orbital is not sterically shielded as it would appear to be in the complexes of **(1)** (see appendix 3).

4.5.7 Protonation of DBA

Two X-ray structures have been determined in this study which contain protonated dba. The crystals in both cases are red blocks and were isolated from reactions where the η^3-benzyl species (red/purple in colour) was the target compound. Several points are worthy of note.

1. Protonation of the carbonyl leads to a lengthening of the C=O bond from 1.23Å in free dba to 1.30Å in protonated dba. The value of the C=O bond length in free dba comes from an X-ray structural determination of the acyl complex where dba was found to co-crystallize. No bonding interactions were found between the dba and the palladium complex. It is therefore assumed that the bond lengths and angles are similar to those expected for non-coordinated dba.

The ready protonation of dba is interesting as it may well represent the first step in the protonation of the (L-L)Pd(dba) complexes. As above, rapid initial protonation of the carbonyl has been suggested as the first step in the reaction of palladium(0) BQ complexes with acid. This is proposed to be followed by intra molecular transfer of the proton to the metal centre. We have not been able to find evidence for this in the protonation of palladium dba complexes. Though the addition of one equivalent of acid gives a complex ^{31}P NMR spectrum.

2. In the complex $[dbaH]^+ [BF_4]^-$ the B-F bond lengths are in the normal range for complexes of this anion. As expected the B-F bond length for the Fluorine which is hydrogen

bonded to the protonated dba is longer than the other B-F bond lengths reflecting this interaction.

A similar situation arises with the sulphonate complex where a lengthening of the S-O distance occurs for both S-O bond lengths where different oxygen atoms interact with i) dba and ii) free sulphonic acid (see Figure 4.1). The non interacting oxygen has a shorter S-O bond length reflecting this non coordinated status. All S-O bond lengths are all within the range expected for sulphonate anions.

3. The alkene C=C bond length would also appear to lengthen slightly from 1.32Å in free dba to 1.35Å when the carbonyl is protonated. this bond lengthening 3 bonds removed from the carbonyl reflects the disruption in the delocalisation of the π system in dba

4. The O-H bond length in the complex where the dba has been protonated with HBF_4 is shorter than the O-H bond length where methanesulphonic acid is the acid. This reflects the stronger acidity of methanesulphonic acid, over HBF_4 which gives rise to the weaker conjugate base $[dbaH]^+$ $[OSO_2CH_3]^-$, and hence longer O-H bond. A further indication of this is the shorter distance between the hydrogen and the anion, the more acidic proton having a shorter interaction.

4.6 Conclusion

The reaction of several palladium(0) alkene complexes containing bidentate phosphine ligands with the acids CH_3SO_3H, p-TsOH and HBF_4 has been studied and the results are summarized in the diagram below.

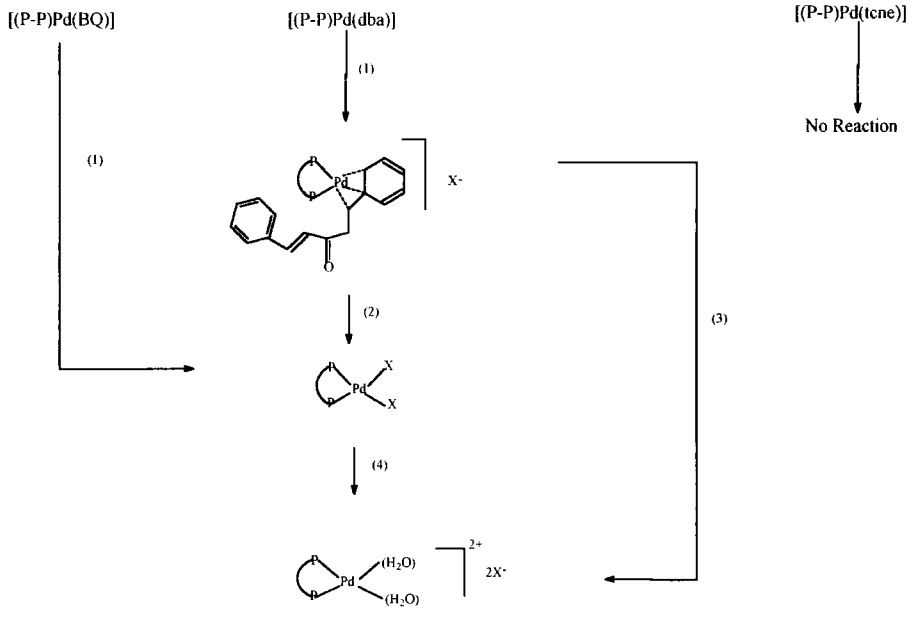

(1) Addition of 5 HX in MeOH or ether, where X = non-coordinating anion
(2) Stir overnight
(3) Recrystallise from dcm/pentane
(4) Addition 2 equivalets H_2O

Summary of interactions of [(P-P)Pd(alkene)] with sulphonic acids

Scheme 4.11

All of the dba complexes form η^3-benzyl complexes on reaction with the acids used in this study. Analysis of the ^{31}P NMR spectra of these complexes reveals very broad room temperature signals for the complexes giving active MeP catalysts **(12)**, with sharp signals found for the complexes giving inactive or co-polymer selective catalysts **(21)**. It is suggested that the broad signals represent the η^3-η^1 exchange known to occur for compounds of this type, and furthermore, that the carbonylation of the η^1-alkyl form represents a rapid route into the hydride mechanism. For the complexes of the phenyl substituted ligands, such as dppp, where the ^{31}P NMR of the derived η^3-benzyl complex consists of sharp signals, it is suggested that the η^3-η^1 exchange is minimal, and the equilibrium is in favour of the η^3 benzyl form. In

this form both available coordination sites at palladium are occupied and further reaction is limited. The work of Spencer[1] supports this idea where the formation of agostic ethyl complexes versus alkene-hydride complexes are reported to be ligand dependent (see introduction). The more sterically demanding ligands favour the agostic ethyl complexes where steric congestion is minimized, whereas the less bulky ligands favour the alkene-hydride structure, which requires more space around the metal.

Reaction of the η^3-benzyl form to give a species $[(L\text{-}L)Pd(solv)(X)]^+ [X]^-$ occurs for all of the η^3-benzyl complexes over a period of 24 hours. Further work is required to determine the differences in rates for this second reaction, though in all cases it seems slow compared to the initial formation of the η^3-benzyl complex. The differences in initial rates are thought to be due to the ability of the η^3-benzyl complexes to be carbonylated. It is anticipated that carbonylation is quickly followed by alcoholysis and formation of a palladium hydride. This palladium hydride is then able to rapidly turnover MeP.

Clearly the species $[(L\text{-}L)Pd(solv)(X)]^+ [X]^-$ can generate catalytic intermediates as judged by the activity of the BQ complex **(27)**, but the reduced initial rates may reflect the kinetics of the formation of either hydride or methoxycarbonyl species from the above species.

The failure to isolate a complex where two sulphonate anions are covalently bound to the metal for the ligand **(1)** is also worthy of comment. A result of this is that all of the complexes isolated in this chapter for this ligand are cationic as is the complex isolated by Zacchini.[11] The same is not true for the ligand **(2)** where two methanesulphonates can fit around the metal centre (see Figure 4.5). The catalytic cycles both invoke cationic species and the ready formation of these with this ligand may play a role in facile activation and reactivity of these pre-catalysts.

4.7 References

1. L. E Crascall and J. L. Spencer, *J. Chem. Soc. Dalton Trans.*, **1992**, 3445.
2. N. Carr, B. J. Dunne, L. Mole, A. G. Orpen and J. L. Spencer, *J. Chem. Soc. Dalton. Trans.*, **1991**, 863.

   N. Carr, L. Mole, A. G. Ospen and J. L. Spencer, *J. Chem. Soc. Dalton. Trans.*, **1992**, 2653.
3. H. Grennberg, A. Gogell and J. E. Backvall, *Organometallics*, **1993**, 12, 1790.
4. L. E. Crascall, S. A. Lister, A. D. Redhouse and J. L. Spencer, *J. Organomet. Chem.*, **1990**, 394, C35.
5. S. Zacchini, B. T. Heaton, J. Iggo, R. Whyman, C. Jacob, Unpublished Results
6. G. R. Eastham and R. P. Tooze, ICI Internal Report
7. V. Gruslin, *Chem. Rev.*, **1996**, 96, 2011.

   V. N. Zudin, U. D. Chinakov, V. M. Nekipelov, V. A. Likholobov and Yu I. Yermakov, *J. Organomet. Chem.*, **1995**, 289, 425.

   J.P. Collman, L.S. Hegedus, R.G. Norton and R.G. Finke, "*Principles and Applications of Organotransition Metal Chemistry*", University Science Books, Mill Valley (CA) USA, 1987.
8. P. J. Stang, D. H. Cao, G. T. Poulter and A. M. Arif, *Organometallics*, **1995**, 1110.

   F. Benetollo, R. Bertoni, G. Bonbieri, L. Toniolo, *Inorganica Chemica Acta*, **1995**, 223, 5.

   P. Leoni, M. Sonnovigo, M. Pasquali, S. Midollini, D. Brago and P. Sabatino, *Organometallics*, **1991**, 10, 1038.
10. G. R. Eastham and R P Tooze, ICI Internal Report
11. S. Zacchini, PhD Thesis Interim Report
12. G. Gatti, J. A. Lopez, C. Mealli and A. Musco, *J. Organomet. Chem.*, **1994**, 483, 77.
13. Cambridge Crystallographic Database
14. J. Brown, *Angew. Chem. Int. Ed.*, **1996**, 35, 657.
15. E. Drent and P. H. M. Budzelaar, *Chem. Rev.*, **1996**, 96, 663.
16. H. E. Bryndza, H. E. Tam, *Chem. Rev.*, **1988**, 88, 1163 & references therein.

17. J.P. Collman, L.S. Hegedus, R.G. Norton and R.G. Finke, *Principles and Applications of Organotransition Metal Chemistry*, University Science Books, Mill Valley (CA) USA, 1987.

R.H. Crabtree, *The Organometallic Chemistry of Transition Metals*, J. Wiley & Sons, New York.

D. Choudhury, D. J. Cole-Hamilton, *J. Chem. Soc. Dalton. Trans.*, **1982**, 1885.

18. V. Zudin, N. Chinakov, D. Nekipelov, M. Rogav, V. A. Likhobolov, Yu I. Ermankov

19. A. Sen, *Adv. Polym. Sci.* **1986**, 73/74, 125

B. Milani, *J. Chem. Soc. Dalton. Trans.*, **1994**, 1903.

B. Milani, *J. Chem. Soc. Dalton. Trans.*, **1996**, 3139

20. P. J. Stang, D. H. Cao, G. T. Poulter and A. M. Arif, *Organometallics*, **1995**, 1110.

F. Benetollo, R. Bertoni, G. Bonbieri, L. Toniolo, *Inorganica Chemica Acta*, **1995**, 223, 5.

P. Leoni, M. Sonnovigo, M. Pasquali, S. Midollini, D. Brago and P. Sabatino, *Organometallics*, **1991**, 10, 1038.

21. M. Kranenburg, J. G. P. Delis, P. C. J. Kamer, P. W. N. M. van Leeuwen, K. Vrieze, N. Veldman, A. L. Spek, K. Goubitz and J. Fraanje, *J. Chem. Soc. Dalton Trans.*, **1997**, 1839 and references therein.

22. M. Hiramatsu, K. Shirozaki, T. Fujinami and S. Sakai, *J. Organomet. Chem.*, **1983**, 246, 203.

23. H. Grennberg, A. Gogoll and Ju-E. Buckvall, *Organometallics*, **1993**, 12, 1790.

24. E. Drent, EP 0, 271, 144, 1988

E. Drent, P.H.M. Budzelaar and W.W. Taylor, EP 0, 386, 833, 1996

E. Drent and P.H.M. Budzelaar, EP 0, 386, 348, 1990

E. Drent, P.H.M. Budzelaar, W.W. Taylor and J Staperasma, EP 0, 441, 447, 1991

E. Drent, EP 0, 495, 547, 121, 965, 1984

E. Drent, EP 0, 274, 795, 181, 014, 1986

E. Drent, US 5, 210, 280, 235, 865, 1987

25. E Drent and P H M Budzelaar, *Chem. Rev.* **1996**, 96, 663.

26. C. A. Tolman, D. J. English and L. E. Manzer, *Inorg. Chem.*, **1974,** 14, 2353.

27. M. Kronenberg, J. G. P. Delis, P. C. J. Konar, P. W. N. M. Van Leeuwen, K. Urieze, N. Veldman, A. L. Spek, K. Groubitz and J. Eraanze, *J. Chem. Soc. Dalton. Trans.*, **1997**, 1838.

28. C. Amatore, G. Broeker, A. Jutand and F. Khalil, *J. Am. Chem. Soc.*, **1997**, 119, 5176.

CHAPTER 5.0

Reactions of Palladium (0) Alkene Complexes and Pre-Catalyst Solutions with Individual Reaction Components and Impurities

5.1 Introduction

Results reported in Chapter 2 demonstrate the sensitivity of the catalysis to the nature of the phosphine ligand with catalyst activity and selectivity affected by small changes in ligand structure. In the Chapter 3 possible explanations were presented for these results via an analysis of the ground state structures of the palladium complexes of these ligands. In Chapter 4 this was extended by considering the activation of the catalysts using sulphonic acid to assess if the observed differences could explain the catalysis results.

In this chapter we consider a small number of the phosphine ligands in more detail. We explore the coordination chemistry with a range of palladium(II) complexes to complement the palladium(0) coordination chemistry reported in chapter 3. Furthermore, we study the reactions of these pre-catalyst solutions with CO and oxygen in an attempt to understand the rapid decomposition observed for certain of these pre-catalyst complexes.

Finally the results of deuterium labeling studies, which seek to further define the mechanism of the methoxycarbonylation reaction, are presented.

5.2 Experimental

The general conditions outlined in Chapter 2 apply

5.3 Reaction of Pre-Catalyst Solutions with CO

General Procedure

1) dba Complexes

To the complex [$L_2Pd(dba)$] (30 mg) was added methanol (30ml) followed by methanesulphonic acid (20 molar equivalents). An immediate deep red solution formed on addition of the acid and this solution was added to a glass Bucchi autoclave, as described in chapter 2. The autoclave was charged with 4 bar carbon monoxide and heated to 80^0C for 1 hour. At the end of this time the autoclave was cooled, and the pressure vented before the contents were removed, via syringe, under a stream of nitrogen Any solid was separated and analysed for palladium content, and the solutions were submitted for analysis by multinuclear NMR.

2) Benzoquinone Complexes

To the complex [$L_2Pd(BQ)$] (30 mg) was added methanol (30ml) followed by methanesulphonic acid (20 molar equivalents). The pale yellow coloured solution produced was added to the autoclave and the procedure described above followed.

3) Acetate Complexes

To the complex [$L_2Pd(OAc)_2$] (30 mg) was added methanol (30ml) followed by methanesulphonic acid (20 molar equivalents). The pale yellow coloured solution produced was added to the autoclave and the procedure described above followed.

5.3.1 [o-$C_6H_4(CH_2PBu^t_2)_2Pd(dba)$] (12) + CO

The general procedure for the reaction of dba complexes with CO outlined above was followed. A black particulate precipitate formed immediately after addition of carbon monoxide, and was isolated, befor washing with methanol. Analysis of this solid shows it to be 97.1% w/w palladium. The solution was sampled for analysis by ^{31}P NMR.

Solution analysis:

NMR (methanol, 298K): $^{31}P\{^1H\}$, δ 50.6(br) ppm.

NMR (methanol, 298K): ^{31}P, δ 47.5 (d, J_{P-H} 470Hz) ppm.

5.3.2 [*o*-$C_6H_4(CH_2PBu^t_2)_2Pd(BQ)$] (27) + CO

The general procedure for the reaction of benzoquinone complexes with CO outlined above was followed. As for the dba complex, a black particulate precipitate formed

immediately after addition of carbon monoxide. The solution was sampled for analysis by ^{31}P NMR.

Solution analysis:

NMR (methanol, 298K): $^{31}P\{^{1}H\}$, δ 50.6(br) ppm.

NMR (methanol, 298K): ^{31}P, δ 47.5 (d, J_{P-H} 470Hz) ppm.

5.3.3 [*o*-$C_6H_4(CH_2PPr^i_2)_2Pd(OAc)_2$] (51) + CO

The general procedure for the reaction of acetate complexes with CO outlined above was followed with the exception that no methanesulphonic acid was added. A clear yellow solution was isolated from the autoclave and was analysed by ^{31}P NMR.

NMR (methanol, 298K): $^{31}P\{^{1}H\}$, δ 20.6(s) ppm.

NMR (methanol, 298K): ^{31}P, δ 20.9(br) ppm.

The reaction was repeated according to the method outlined for the reaction of acetate complexes with CO, this time with added methanesulphonic acid. A clear yellow solution was isolated from the autoclave and was analysed by ^{31}P NMR.

NMR (methanol, 298K): $^{31}P\{^{1}H\}$, δ 50.7(s), 20.9(s) ppm.

NMR (methanol, 298K): ^{31}P, δ 50.7 (br), 20.9(br) ppm.

5.3.4 [*o*-$C_6H_4(CH_2PCy_2)_2$ Pd (dba)] (14) + CO

Synthesis of [*o*-$C_6H_4(CH_2PCy_2)_2Pd(H_2O)]^{2+}$ 2[$CH_3SO_3]^-$ (45)

The general procedure for the reaction of dba complexes with CO outlined above was followed. A clear yellow solution was isolated from the autoclave and was analysed by ^{31}P NMR. NMR (methanol, 298K): $^{31}P\{^{1}H\}$, δ 44.2(s), 15.2(s) ppm.

NMR (methanol, 298K): ^{31}P, δ 44.2 (br), 15.2(br) ppm.

The solvent was removed from the sample in vacuo. Attempted recrystallisation from dichloromethane, layered with pentane resulted in the formation of a small quantity of yellow crystals suitable for X-ray structural analysis. These crystals turned out to be [*o*-$C_6H_4(CH_2PCy_2)_2Pd(H_2O)_2]^{2+}$ 2[$CH_3SO_3]^-$. 0.35 CH_2Cl_2. Crystal data for **(45)** :

$C_{35}H_{64.67}Cl_{0.67}O_{10}P_2PdS_{2.67}$, M = 923.06, monoclinic, space group $P2_1/c$, a = 12.0373(5), b = 18.6614(8), c = 19.5579(9) Å, β = 105.443(2)^0 , V = 4234.7(3) Å^3, Z = 4, T = 173 K; 25794 data measured, 10029 unique, Rint = 0.0450, 509 refined parameters, R = 0.0796, $wR2$ = 0.0997.

P(1)-Pd	2.2576(8)	P(2)-Pd	2.2505(8)
Pd-O(1)	2.121(2)	Pd-O(2)	2.139(2)
P(1)-Pd-P(2)	100.10(3)	O(1)-Pd-O(2)	87.33(9)
O(1)-Pd-P(1)	86.33(6)	O(2)-Pd-P(2)	86..25(6)
O(1)-H-O(3)	1.88(2)	O(1)-H-O(6)	1.90(2)
O(2)-H-O(4)	1.92(2)	O(2)-H-O(7)	1.83(2)

Table 5.1 Bond Lengths (Å) and Angles (°) for $[o\text{-}C_6H_4(CH_2PCy_2)_2Pd(H_2O)_2]^{2+}$ $2[CH_3SO_3]^-$. 0.35 CH_2Cl_2 (45)

Figure 5.1 The Crystal Structure of $[o\text{-}C_6H_4(CH_2PCy_2)_2Pd(H_2O)_2]^{2+}$ $2[CH_3SO_3]^-$. 0.35 CH_2Cl_2 (45) Anions omitted.

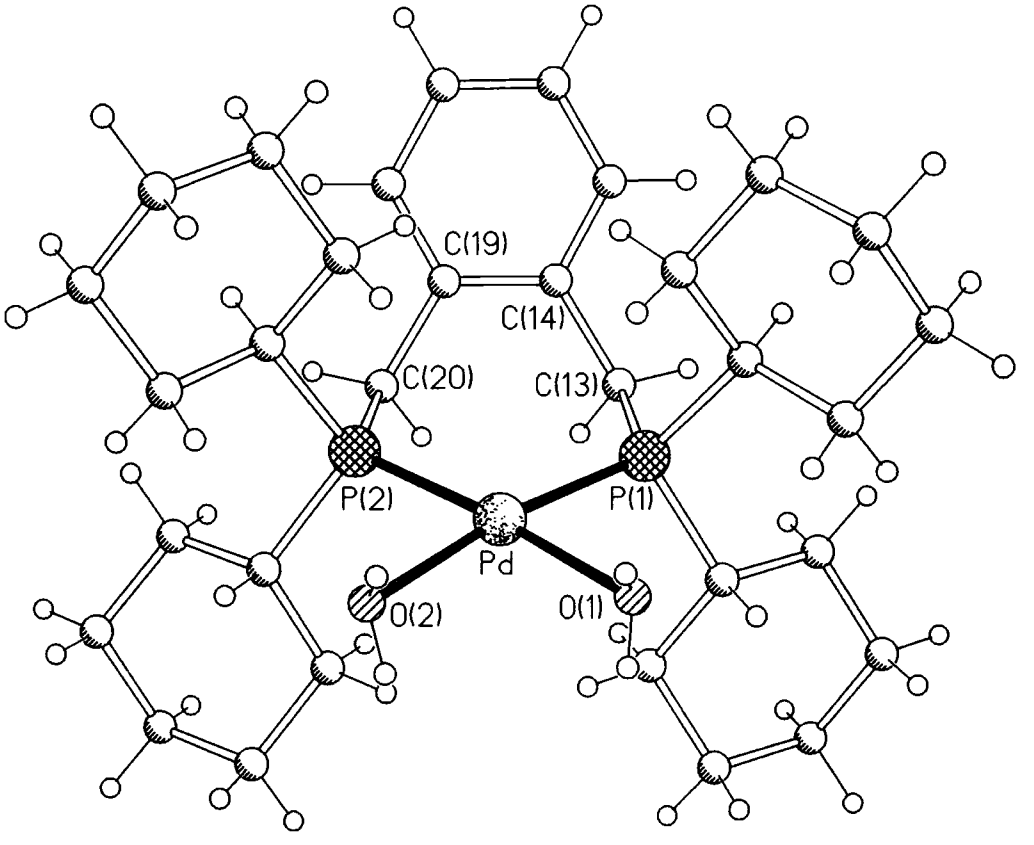

5.3.5 $[o\text{-}C_6H_4(CH_2PPh_2)_2Pd(BQ)]$ (31) + CO

The general procedure for the reaction of benzoquinone complexes with CO outlined above was followed. There was some evidence for the formation of palladium metal but this seemed minimal, with most of the sample recovered as a yellow orange solution which was analysed by ^{31}P NMR.

NMR (methanol, 298K): $^{31}P\{^1H\}$, δ 26.8(s), 19.1(s) ppm.

5.3.6 [(DPEphos)Pd(BQ)] (34) + CO

The general procedure for the reaction of benzoquinone complexes with CO outlined above was followed. A clear yellow orange solution was isolated from the autoclave and was analysed by ^{31}P NMR. There was no evidence for palladium metal formation.

NMR (methanol, 298K): $^{31}P\{^1H\}$, δ 25.1(s), 9.1(s) ppm.

5.4 Reaction of Catalyst Solutions with Ethene

The general procedure for the reaction of dba complexes with CO outlined above was followed with ethene used instead of carbon monoxide.

5.4.1 [*o*-$C_6H_4(CH_2PBu^t_2)_2$ Pd (dba)] (12) + Ethene

A clear yellow solution was removed from the autoclave, with no evidence for decomposition.

NMR (methanol, 298K): $^{31}P\{^1H\}$, δ 71.5 (br), 40.0 (br) ppm.

GC-MS: no evidence for butene or ethene oligomers

5.5 Formation of Dioxygen Complexes

5.5.1 Synthesis of [*o*-$C_6H_4(CH_2PPe^t_2)_2$ Pd(O_2)] (46)

Attempted recrystallisation of the dba complex **(16)** from thf layered with pentane resulted in the formation of a small quantity of pale blue crystals suitable for X-ray structural analysis. These resulted from reaction with adventitious oxygen and turned out to be [*o*-$C_6H_4(CH_2P^tPe_2)_2$ Pd (O_2)] (16b). Crystal data for **(46)**: $C_{28}H_{52}O_2P_2Pd$, M = 589.04, triclinic, space group P-1, a = 7.2378(8), b = 9.2179(10), c = 22.177(3) Å, α = 97.694(3), β = 90.882(3), γ = 101.133(3)^0 , V = 1437.4(3) Å^3, Z = 2, T = 160 K; 10310 data measured, 6271 unique, Rint = 0.0221, 311 refined parameters, R = 0.0380, $wR2$ = 0.0741.

P(1)-Pd	2.2854(7)	P(2)-Pd	2.2856(7)
Pd-O(2)	2.0038(17)	Pd-O(1)	2.0254(17)
O(1)-O(2)	1.445(3)	P(1)-Pd-P(2)	102.79(2)
O(2)-Pd-O(1)	42.04(7)	O(2)-Pd-P(2)	106.59(5)
O(1)-Pd-P(1)	108.59(6)		

Table 5.2 Bond Lengths (Å) and Angles (°) for [*o*-$C_6H_4(CH_2PPe^t_2)_2Pd(O_2)$](46)

Figure 5.2 The Crystal Structure of [*o*-$C_6H_4(CH_2PPe^t_2)_2Pd(O_2)$] (46)

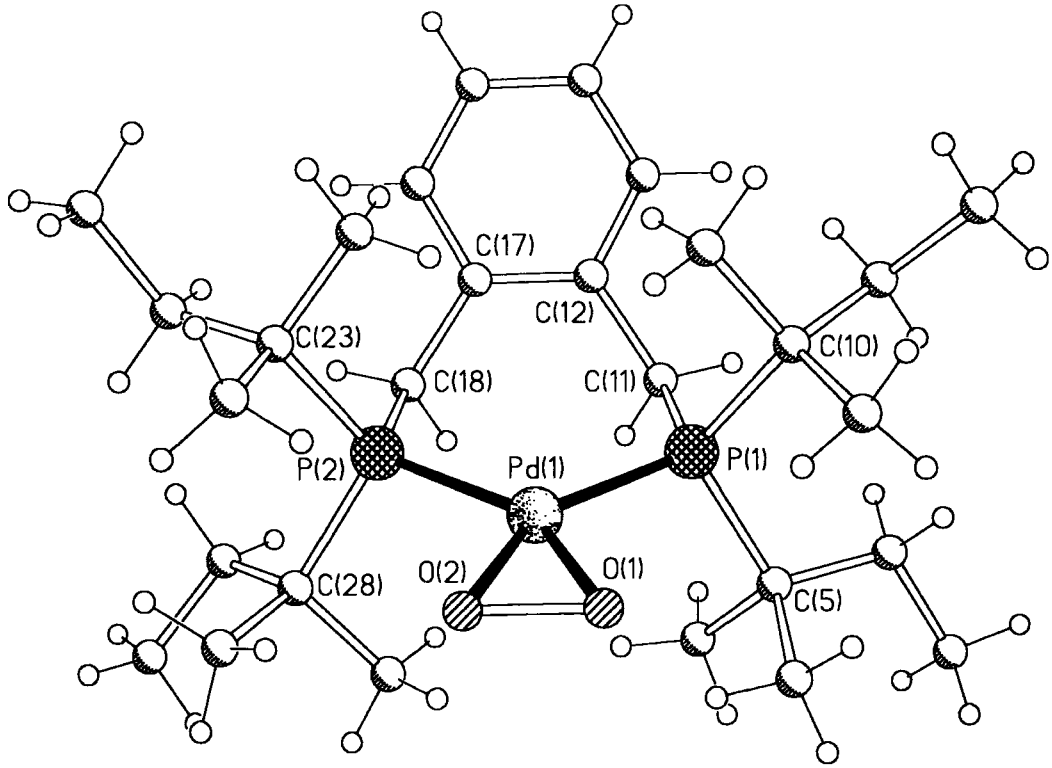

5.5.2 Synthesis of [2,3-$C_{10}H_6(CH_2PBu^t_2)_2Pd(O_2)$] (47)

Attempted recrystallisation of the dba complex **(23)** from thf layered with pentane resulted in the formation of a small quantity of orange crystals suitable for X-ray structural analysis. These crystals resulted from reaction with adventitious oxygen and turned out to be [2,3–$C_{10}H_6(CH_2PBu^t_2)_2Pd(O_2)$] **(47)**. Crystal data for **47**: $C_{28}H_{46}O_2P_2Pd$, M = 582.99, monoclinic, space group $P2_1/c$, a = 17.6034(13), b = 7.2340(6), c = 21.7345(17) Å, β = 91.244(2)^0 , V = 2767.1(4) Å^3, Z = 4, T = 160 K; 17046 data measured, 6546 unique, Rint = 0.0613, 310 refined parameters, R = 0.0669, $wR2$ = 0.0825.

P(1)-Pd	2.2779(9)	P(2)-Pd	2.2825(9)
Pd-O(2)	2.008(2)	Pd-O(1)	2.021(2)
O(1)-O(2)	1.441(3)	P(1)-Pd-P(2)	101.85(3)
O(2)-Pd-O(1)	41.91(9)	O(2)-Pd-P(2)	107.59(7)
O(1)-Pd-P(1)	108.66(7)		

Table 5.3 Bond Lengths (Å) and Angles (°) for [2,3-$C_{10}H_6(CH_2PBu^t_2)_2Pd(O_2)$]

Figure 5.3 The Crystal Structure of [2,3-$C_{10}H_6(CH_2PBu^t_2)_2Pd(O_2)$] (47)

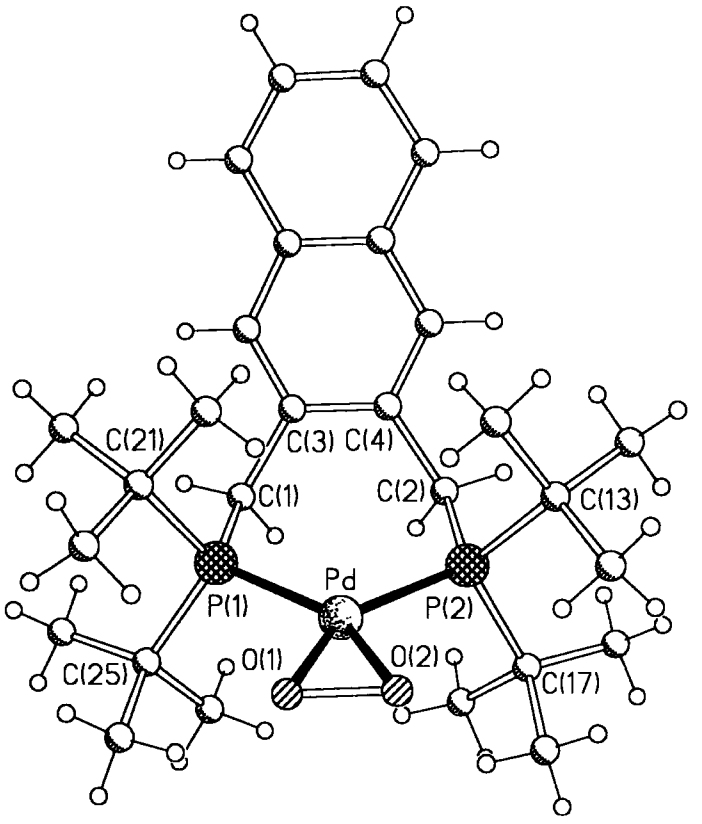

5.5.3 Synthesis of [*o*-$C_6H_4(CH_2PBu^t_2)_2Pd(O_2)$] (48)

Attempted recrystallisation of the styrene complex **(26)** from thf layered with pentane resulted in the formation of a small quantity of colorless crystals suitable for X-ray structural analysis. These resulted from reaction with adventitious oxygen and turned out to be [*o*-$C_6H_4(CH_2PBu^t_2)_2Pd(O_2)$]. $C_{24}H_{44}P_2O_2Pd$ requires: C, 54.1; H, 8.27 %. Found: C, 53.85; H, 8.33 %. Crystal data for **48**: $C_{26}H_{48}O_2P_2Pd$, M = 528.98, monoclinic, space group $P2_1/m$, a = 7.2701(15), b = 19.787(4), c = 8.9669(19) Å, β = 102.177(5)^0 , V = 1260.9(5) Å^3, Z = 2, T = 160 K; 6660 data measured, 2289 unique, Rint = 0.0685, 259 refined parameters, R = 0.0899, $wR2$ = 0.1968.

NMR (d^8 toluene, 298K): $^{31}P\{^1H\}$, δ 60.1 (s) ppm.

I.R (KBr discs, cm^{-1}): ν (O-O) 858 vs

P(1)-Pd	2.234(5)	P(2)-Pd	2.299(6)
Pd-O(2)	2.03(2)	Pd-O(1)	2.00(2)
O(1)-O(2)	1.42(2)	P(1)-Pd-P(2)	102.8(2)
O(2)-Pd-O(1)	41.30(6)	O(2)-Pd-P(2)	106.1(6)
O(1)-Pd-P(1)	109.9(8)		

Table 5.4 Bond Lengths (Å) and Angles (°) for $[o\text{-}C_6H_4(CH_2PBu^t_2)_2Pd(O_2)]$

Figure 5.4 The Crystal Structure of $[o\text{-}C_6H_4(CH_2PBu^t_2)_2Pd(O_2)]$

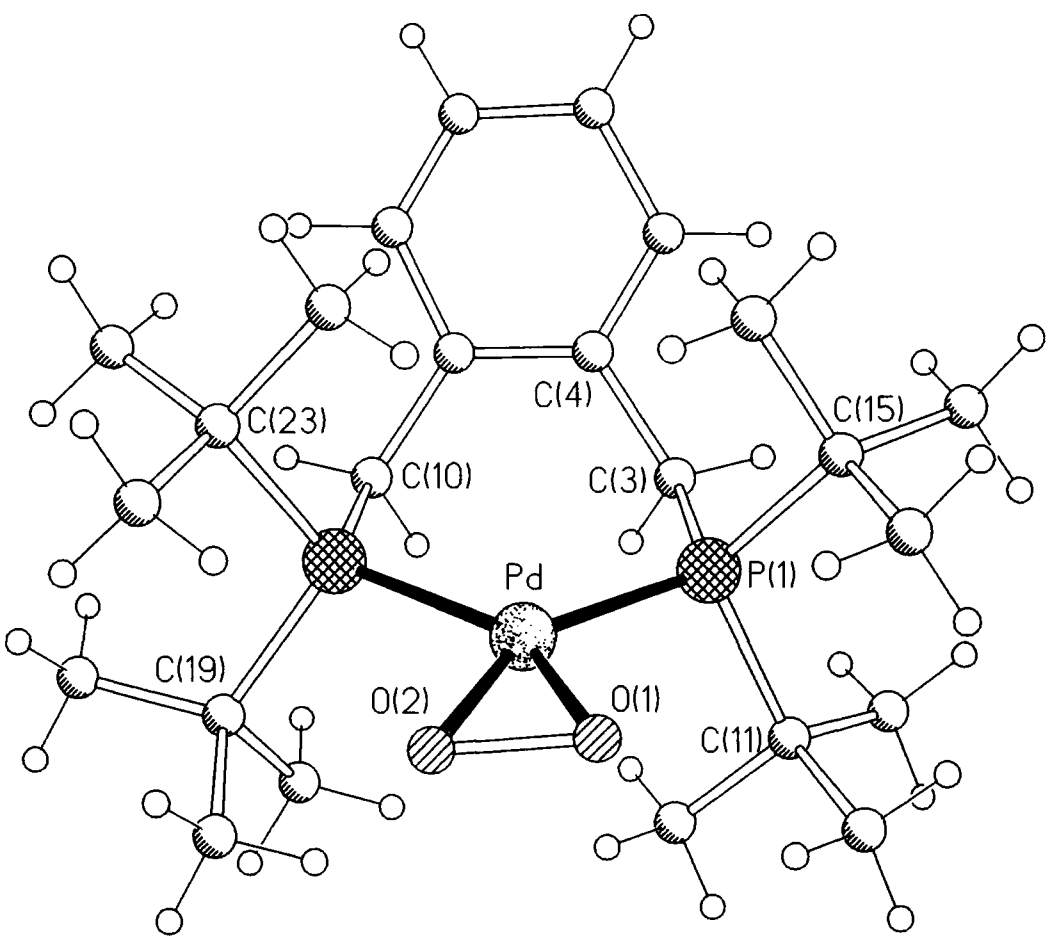

5.6 Coordination Chemistry with Palladium(II) Compounds

5.6.1 Reaction of Phosphines with $[(PhCN)_2Pd(Cl)_2]$

General Procedure

To an orange solution of $[(PhCN)_2Pd(Cl)_2]$ (0.4g, 1.04mmol) in dichloromethane (50 ml) was added the phosphine ligand (1.04mmol) as a solution in dichloromethane. An immediate colour change from orange to yellow occurred. The reaction mixture was stirred for two hours before removal of the solvent in vacuo, followed by washing the residue with cold ether (-30^0C) before drying.

5.6.1.1. o-$C_6H_4(CH_2PBu^t_2)_2$ (1) + $[(PhCN)_2Pd(Cl)_2]$

Yield 0.44g (80.0%).

I.R (KBr disc, cm^{-1}): ν (Pd-Cl) 350 cm^{-1} (m)

NMR (CD_2Cl_2, 293K): ^{31}P {^1H}, δ 40.0 (vbr) ppm; ^1H, δ 7.2-7.4 (br, aromatics), 3.0-3.4 (br, CH_2), 1.2-1.6 (br, CH_3) ppm; ^{13}C, δ 29.72 (br, CH_2), 30.27 (s, CH_2), 30.73 (s, CH_2), 32.00 (s, CH_3), 41.30 (s, quaternary), 42.54 (s, quaternary), 126-145 (m, aromatics) ppm.

Mass Spectrum(electrospray):

M/z 1107 [(3%), $((L\text{-}L)_2Pd_2Cl_3)^+$], 1071 [(10%), $((L\text{-}L)_2Pd_2Cl_2)^+$],1036 [(10%), $((L\text{-}L)_2Pd_2Cl)^+$], 535 [(100%), $((L\text{-}L)PdCl)^+$]

A sample of material from the same reaction was analysed at a lower cone voltage

M/z 1107 [(1%), $((L\text{-}L)_2Pd_2Cl_3)^+$], 1071 [(10%), $((L\text{-}L)_2Pd_2Cl_2)^+$], 821 [(10%, $((L\text{-}L)_3Pd_3Cl_4)^{2+}$], 803 [(15%, $((L\text{-}L)_3Pd_3Cl_3)^{2+}$], 535[(50%), $((L\text{-}L)Pd_2Cl)^+$]

5.6.1.2. o-$C_6H_4(CH_2PPr^i_2)_2$ (2) + $[(PhCN)_2Pd(Cl)_2]$

Synthesis of $[o\text{-}C_6H_4(CH_2PPr^i_2)_2Pd(Cl)_2]$ (49)

Yield 0.48g (90.0%). $C_{20}H_{36}P_2Cl_2Pd$ requires C, 46.60; H, 6.99 %. Found: C, 46.48; H, 6.81 %.

I.R (KBr disc, cm^{-1}): ν (Pd-Cl) 300 cm^{-1} (m)

NMR (CD_2Cl_2, 293K): $^{31}P\{^1H\}$, δ 31.9 (s) ppm; ^1H, δ 7.2-7.3 (br, 4H, aromatics), 3.2 (br,4H, CH_2), 2.9 (br,4H, CH), 3.0 (br,4H, CH_2), 1.5-1.1 (br, 24H, CH_3) ppm; ^{13}C, δ 20.8 (s, CH_3), 26.8 (d, $J_{(P\text{-}C)}$=9.2Hz, CH_2), 26.9 (d, $J_{(P\text{-}C)}$=9.2Hz, CH_2), 28.2 (s, CH), 128.2 (s, aromatic CH), 131.6 (s, aromatic CH), 132.8 (s, aromatic) ppm.

Mass Spectrum(FAB + ion, mNBA matrix): M/z 515 [(5%), $(M)^+$], 481 [(60%), $(M\text{-}Cl)^+$].

5.6.1.3. $Bu^t_2P(CH_2)_3PBu^t_2)_2$ + $[(PhCN)_2Pd(Cl)_2]$

Synthesis of $[(Bu^t_2P(CH_2)_3PBu^t_2)Pd(Cl)_2]$ (50)

Yield 0.45g (86.0%). $C_{19}H_{42}P_2Cl_2Pd$ requires C, 44.70; H, 8.23 %. Found: C, 44.92; H, 8.10 %.

I.R (KBr disc, cm^{-1}): ν (Pd-Cl) 297 cm^{-1} (m)

NMR (CD_2Cl_2, 293K): $^{31}P\{^1H\}$, δ 34.5 (s) ppm.; ^1H, δ 2.3 (br, 2H, CH_2), 2.1 (br, 4H, CH_2), 1.4 (br, 36H, CH_3) ppm.

Recrystallisation from dichloromethane layered with pentane resulted in the formation of a small quantity of yellow crystals suitable for X-ray structural analysis. Crystal data for **(50)**: $C_{22.5}H_{46}P_2Cl_2Pd$, M = 555.83, monoclinic, space group $P2_1/c$, a = 23.0537(16), b = 14.7902(11), c = 16.1896(11) Å, β = 98.175(2)^0 , V = 5464.1(7) Å^3, Z = 8, T = 160(2) K;

28664 data measured, 12313 unique, *R*int = 0.0232, 551 refined parameters, $R = 0.0730$, $wR2 = 0.1342$.

P(1)-Pd	2.3054(13)	P(2)-Pd	2.3026(14)
Pd-Cl(1)	2.3641(14)	Pd-Cl(2)	2.3645(13)
P(1)-Pd-P(2)	98.09(5)	Cl(1)-Pd-Cl(2)	85.44(5)
Cl(1)-Pd-P(1)	88.03(5)	Cl(2)-Pd-P(2)	90.45(5)

Table 5.5 Bond Lengths (Å) and Angles (°) for $[(Bu^t_2P(CH_2)_3PBu^t_2)Pd(Cl)_2]$

Figure 5.5 The Crystal Structure of $[(Bu^t_2P(CH_2)_3PBu^t_2)Pd(Cl)_2]$

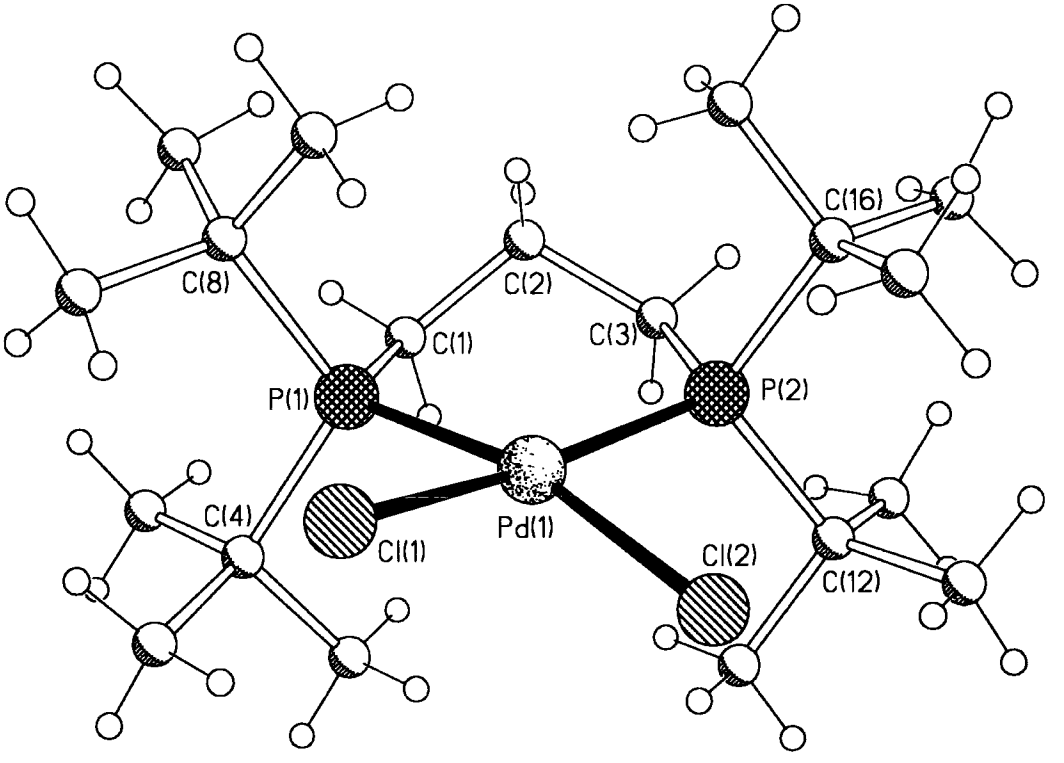

5.6.2. Reaction of Phosphines with Palladium Acetate

General Procedure

To an orange solution of $[Pd(OAc)_2]$ (1.30g, 1.58mmol) in acetone (50 ml) was added the phosphine ligand (1.58mmol) as a solution in acetone (20 ml). The reaction mixture was stirred for 18 hours, during which time a precipitate developed. Petroleum ether (100 ml) was added to complete the precipitation before separation of the solid by filtration and drying in vacuo.

5.6.2.1. o-$C_6H_4(CH_2PBu^t_2)_2$ (1) + $[Pd(OAc)_2]$

Isolated a pale green solid. Yield 0.8g (21.0%).

I.R (KBr disc, cm^{-1}): ν (Pd-OAc) 1540s (C=O) cm^{-1} (m)

NMR ($CDCl_3$, 293K): $^{31}P\{^1H\}$, δ 111.69 (s) ppm; ^1H, δ 6.89 (br, 4H, aromatics), 2.94 (d, 8H, CH_2), 2.0(s, 12H, acetate CH_3), 1.35 (d, 72H, Bu^t CH_3) ppm; ^{13}C, δ 24.03 (s, acetate CH_3), 28.85 (s, CH_3), 31.8 (d, J_{P-C}24.9 Hz CH_2), 35.55 (d,J_{P-C}17.4 Hz quaternary), 130.6(br, aromatic CH), 143.24(s, aromatic), 185.2 (s, acetate C=O)

Mass Spectrum(FD): M/z 724 [(80%)].

Mass Spectrum(FAB + ion, mNBA matrix): M/z 605 [(40%)].

5.6.2.2. o-$C_6H_4(CH_2PPr^i_2)_2$ (2) + $[Pd(OAc)_2]$

Synthesis of $[o\text{-}C_6H_4(CH_2PPr^i_2)_2Pd(OAc)_2]$ (51)

Isolated as an off-white solid. Yield 2.5g (77.0%). $C_{24}H_{42}P_2O_4Pd$ requires C, 51.24; H, 7.47 %. Found: C, 51.52; H, 7.51 %.

I.R (KBr disc, cm^{-1}): ν (Pd-OAc) 1629s (C=O) cm^{-1}

NMR (CD_2Cl_2, 293K): $^{31}P\{^1H\}$, δ 34.3 (s) ppm; ^1H, δ 7.2 (br, 4H, aromatics), 3.2 (br, 4H, CH_2), 2.3 (br, 4H, CH), 1.8 (br, 6H, acetate CH_3), 1.4 (br, 12H, CH_3),1.2 (br, 12H, CH_3) ppm; ^{13}C, δ 18.85 (s, acetate CH_3), 20.2 (s, CH_3), 26.7 (s, CH_2), 27.6 (s, CH), 128.2 (s, aromatic CH), 133.4(s, aromatic CH), 136.1(s, aromatic), 177.0 (s, acetate C=O) ppm.

Mass Spectrum(FAB + ion, mNBA matrix): M/z 504 [(10 %), $(M)^+$], 444 [(40 %), $(M\text{-}Cl)^+$].

5.6.2.3. $Bu^t_2P(CH_2)_3PBu^t_2$ + $[Pd(OAc)_2]$

1. Synthesis of $[(Bu^t_2P(CH_2)_3PBu^t_2)Pd(OAc)_2]$

2. Synthesis of $[\{(Bu^t_2P(CH_2)_3PBu^t_2)Pd(OAc)_2\}_4]$. 10.5 CH_2Cl_2 (52)

Isolated as a yellow green solid. Yield 2.6g (78.0%). $C_{23}H_{48}P_2O_4Pd$ requires C, 49.55; H, 8.62 %. Found: C, 49.61; H, 8.51 %.

I.R (KBr disc, cm^{-1}): ν (Pd-OAc) 1644s (C=O) cm^{-1}

NMR (CD_2Cl_2, 293K): $^{31}P\{^1H\}$, δ 33.34 (s) ppm; ^1H, δ 2.2(br, 2H, CH_2), 1.90(br, 4H, CH_2), 1.78 (br, 6H, acetate CH_3), 1.1-1.4 (br, 36H, CH_3) ppm.

Mass Spectrum(FAB + ion, mNBA matrix): M/z 498 [(5 %), $(M)^+$], 439 [(50 %), $(M\text{-}Cl)^+$].

Recrystallisation from dichloromethane layered with pentane resulted in the formation of a small quantity of yellow crystals suitable for X-ray structural analysis. Crystal data for **(52)**: $C_{102.5}H_{213}P_8Cl_{21}O_{16}Pd$, M = 3119.54, orthorhombic, space group $Pca2_1$, a = 38.530(2), b =19.1969(9), c = 20.3787(10) Å, β = 90.0^0 , V = 15073.2(13) Å^3, Z = 4, T = 180(2) K; 91913 data measured, 33354 unique, Rint = 0.1008, 1420 refined parameters, R = 0.0723, $wR2$ = 0.1407.

P(1)-Pd(1)	2.382(2)	P(8)-Pd(1)	2.403(2)
Pd(1)-O(1)	2.024(5)	Pd(1)-O(3)	2.035(5)
P(1)-Pd-O(1)	89.34(16)	O(1)-Pd-P(8)	91.37(16)
P(8)-Pd-O(3)	89.87(16)	P(1)-Pd-O(3)	88.71(16)

Table 5.6 Bond Lengths (Å) and Angles (°) for $[\{(Bu^t_2P(CH_2)_3PBu^t_2)Pd(OAc)_2\}_4]$. 10.5 CH_2Cl_2 Considering One Palladium Centre Only

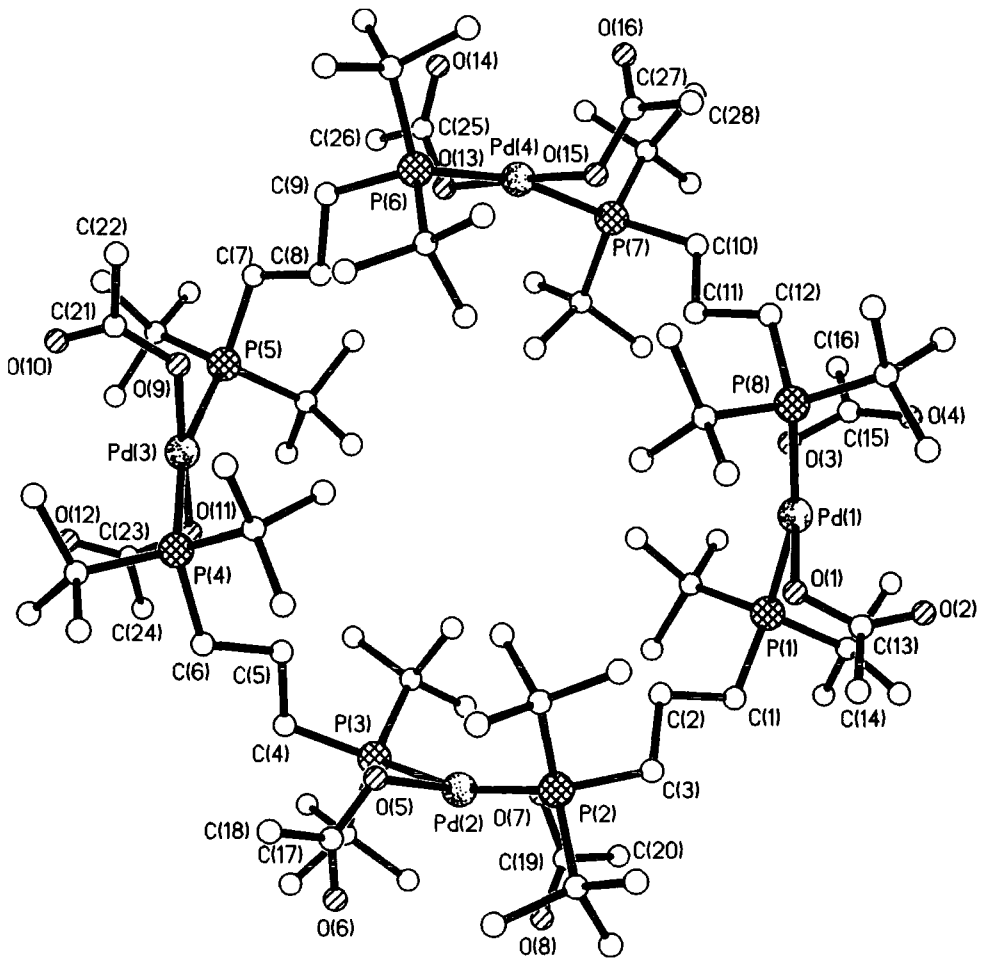

Figure 5.6 The Crystal Structure of $[\{(Bu^t_2P(CH_2)_3PBu^t_2)Pd(OAc)_2\}_4]$. 10.5 CH_2Cl_2

5.7 Reactions of (12) with Propionyl Chloride

5.7.1 Reaction with One Equivalent:

Synthesis of [o-$C_6H_4(CH_2PBu^t_2)_2Pd(Cl)_2$](53) and [o-$C_6H_4(CH_2PBu^t_2)_2Pd(COC_2H_5)(Cl)$] (54)

The dba complex **(12)** (30 mg, 0.04mmol) was dissolved in diethyl ether in an NMR tube and propionyl chloride (3.8mg,0.04mmol) was added via a micro syringe. The solution turned from orange to yellow in colour immediately and the solution was analysed by ^{31}P NMR.

NMR (diethyl ether, 293K): $^{31}P\{^1H\}$, δ 46.0 (br). 35.0 (s), 17.0 (br) ppm.

Removal or the solvent from the sample and recrystallisation from ether layered with pentane led to the isolation of yellow crystals suitable for single crystal X-ray study. Crystal data for **(53)**: $C_{24}H_{44}P_2Cl_2Pd$, M = 571.83, monoclinic, space group $P2_1/c$, a = 9.1581(10), b=19.656(2), c = 15.180(2) Å, β = 101.694(3)^0, V = 2675.8(5) Å^3, Z = 4, T = 160(2) K; 15154 data measured, 5351 unique, R int = 0.0620, 275 refined parameters, R = 0.0556, $wR2$ = 0.0975.

P(1)-Pd	2.3269(10)	P(2)-Pd	2.3084(10)
Pd-Cl(1)	2.3615(10)	Pd-Cl(2)	2.2.3594(10)
P(1)-Pd-P(2)	101.83(4)	P(1)-Pd-Cl(1)	89.95(4)
P(2)-Pd-Cl(2)	88.38(4)	Cl(1)-Pd-Cl(2)	83.67(4)

Table 5.7 Bond Lengths (Å) and Angles (°) for [o-$C_6H_4(CH_2PBu^t_2)_2Pd(Cl)_2$] (53)

When the experiment was repeated crystals formed on the sides of the NMR tube and these were the subject of a single crystal x-ray study. Crystal data for **(54)**: $C_{44}H_{63}P_2ClO_2Pd$, M = 827.73, triclinic, space group P-1, a = 10.2985(7), b=11.3708(7), c = 19.5555(13) Å, α = 90.228(2), β = 96.228(2), γ = 115.134(2)^0, V = 2057.4(2) Å^3, Z = 2, T = 160(2) K; 11286 data measured, 7934 unique, R int = 0.0333, 465 refined parameters, R = 0.0517, $wR2$ = 0.1093.

P(1)-Pd	2.4812(9)	P(2)-Pd	23177(8)
Pd-C(1)	2.010(4)	Pd-Cl	2.4135(9)
P(1)-Pd-P(2)	103.08(3)	P(1)-Pd-Cl	90.40(3)
P(2)-Pd-C(1)	94.10(10)	C(1)-Pd-Cl	77.42(10)

Table 5.8 Bond Lengths (Å) and Angles (°) for [o-$C_6H_4(CH_2PBu^t_2)_2Pd(COC_2H_5)(Cl)$.dba] (54)

Figure 5.7 The Crystal Structure of [o-$C_6H_4(CH_2PBu^t_2)_2Pd(Cl)_2$]

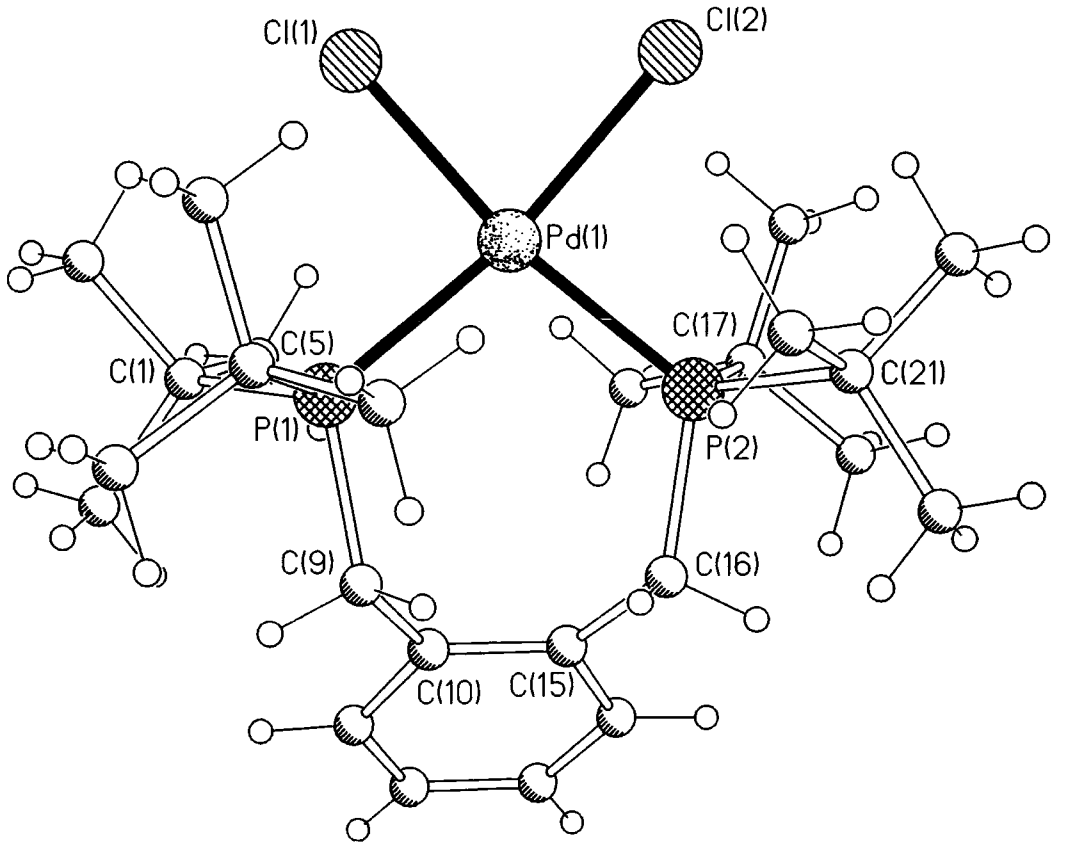

Figure 5.8 The Crystal Structure of [o-$C_6H_4(CH_2PBu^t_2)_2Pd(COC_2H_5)(Cl)$].dba

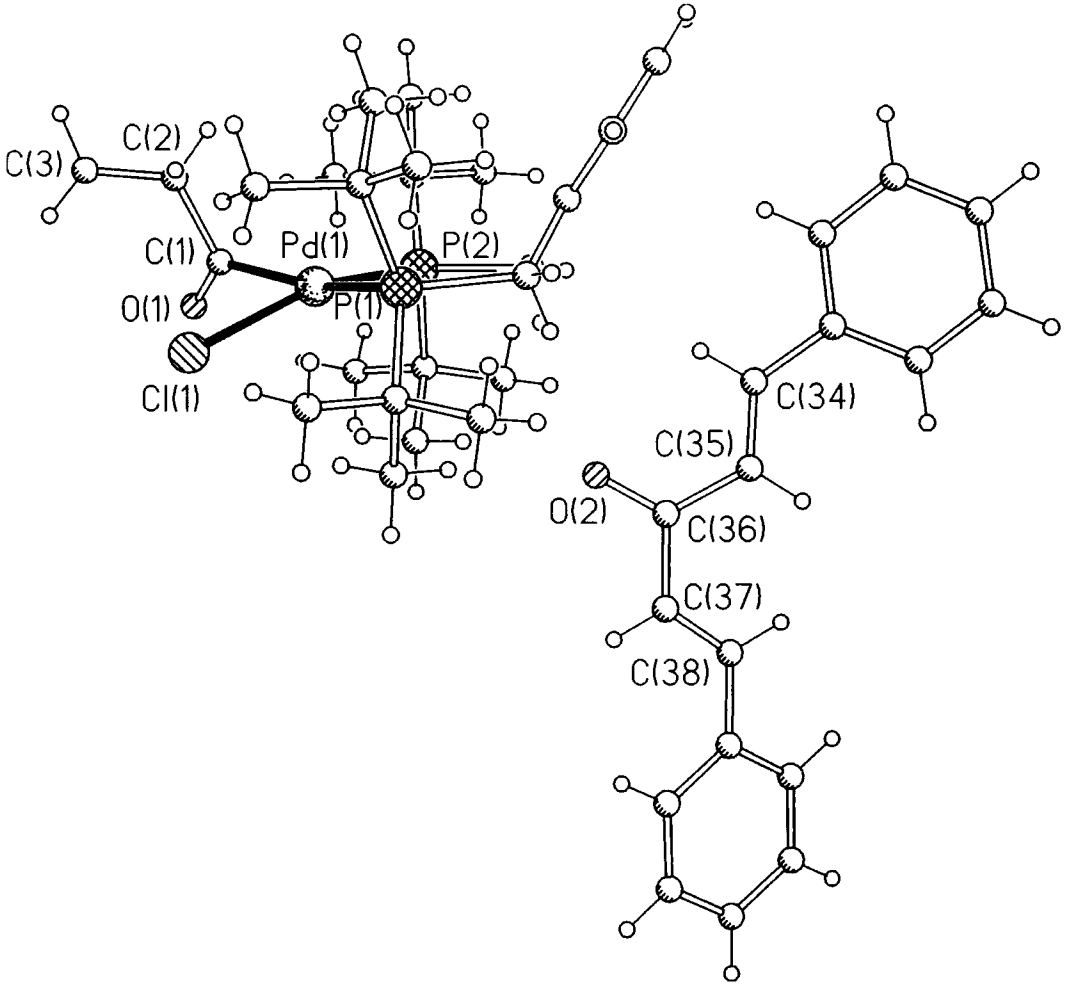

5.7.2 Reaction of (12) with Ten Equivalents of Propionyl Chloride : Synthesis of [o-$C_6H_4(CH_2PBu^t_2)_2Pd(Cl)_2$. CH_2Cl_2] (55)

The dba complex **(12)** (2.0g, 2.72mmol) was dissolved in diethyl ether(100ml) and propionyl chloride (2.6g, 27.2mmol) was added via syringe. The solution turned from orange to yellow in colour immediately and a yellow precipitate began to form after 15 minutes. The reaction mixture was stirred for a further two hours before the precipitate was separated by filtration and dried in vacuo. Yield 1.4g (90%). $C_{24}H_{44}P_2Cl_2Pd$ requires C, 50.43; H, 7.70 %. Found: C, 50.39; H, 7.65 %.

NMR (CD_2Cl_2, 293K): $^{31}P\{^1H\}$, δ 35.0 (s) ppm; ^1H, δ 7.2 (br, 2H, aromatics),7.05 (br, 2H, aromatics), 3.3 (br, 4H, CH_2), 1.4 (d, 36H, $J_{(H-H)}$14.16 Hz, CH_3) ppm. ^{13}C, δ 28.7 (s, CH_2),

30.1 (s, CH_3), 38.8(s, quaternary) 126.5(s, aromatic CH), 131.4(s, aromatic CH), 133.1(s, aromatic) ppm.

Mass Spectrum (electrospray): M/z 535 [(60%), $(M\text{-}Cl)^+$].

Recrystallisation from dichloromethane layered with pentane resulted in the formation of a small quantity of yellow crystals suitable for x-ray structural analysis. Crystal data for **(55)**: $C_{25}H_{46}P_2Cl_4Pd$, M = 656.76, monoclinic, space group $P2_1/c$, a = 7.4876(5), b = 21.9249(14), c = 18.3797(12) Å, β = 95.225(2)^0 , V = 3004.8(3) Å^3, Z = 4, T = 160(2) K; 18660 data measured, 6925 unique, Rint = 0.0261, 302 refined parameters, R = 0.0495, $wR2$ = 0.0988.

P(1)-Pd	2.2968(10)	P(2)-Pd	23240(8)
Pd-Cl(2)	2.3210(13)	Pd-Cl(1)	2.3496(10)
P(1)-Pd-P(2)	102.69(3)	P(1)-Pd-Cl(2)	86.48(5)
P(2)-Pd-Cl(1)	90.63(4)	Cl(1)-Pd-Cl(2)	80.68(6)

Table 5.9 Bond Lengths (Å) and Angles (°) for [o-$C_6H_4(CH_2PBu^t_2)_2Pd(Cl)_2$].$CH_2Cl_2$

Figure 5.9 The Crystal Structure of [o-$C_6H_4(CH_2PBu^t_2)_2Pd(Cl)_2$]. CH_2Cl_2

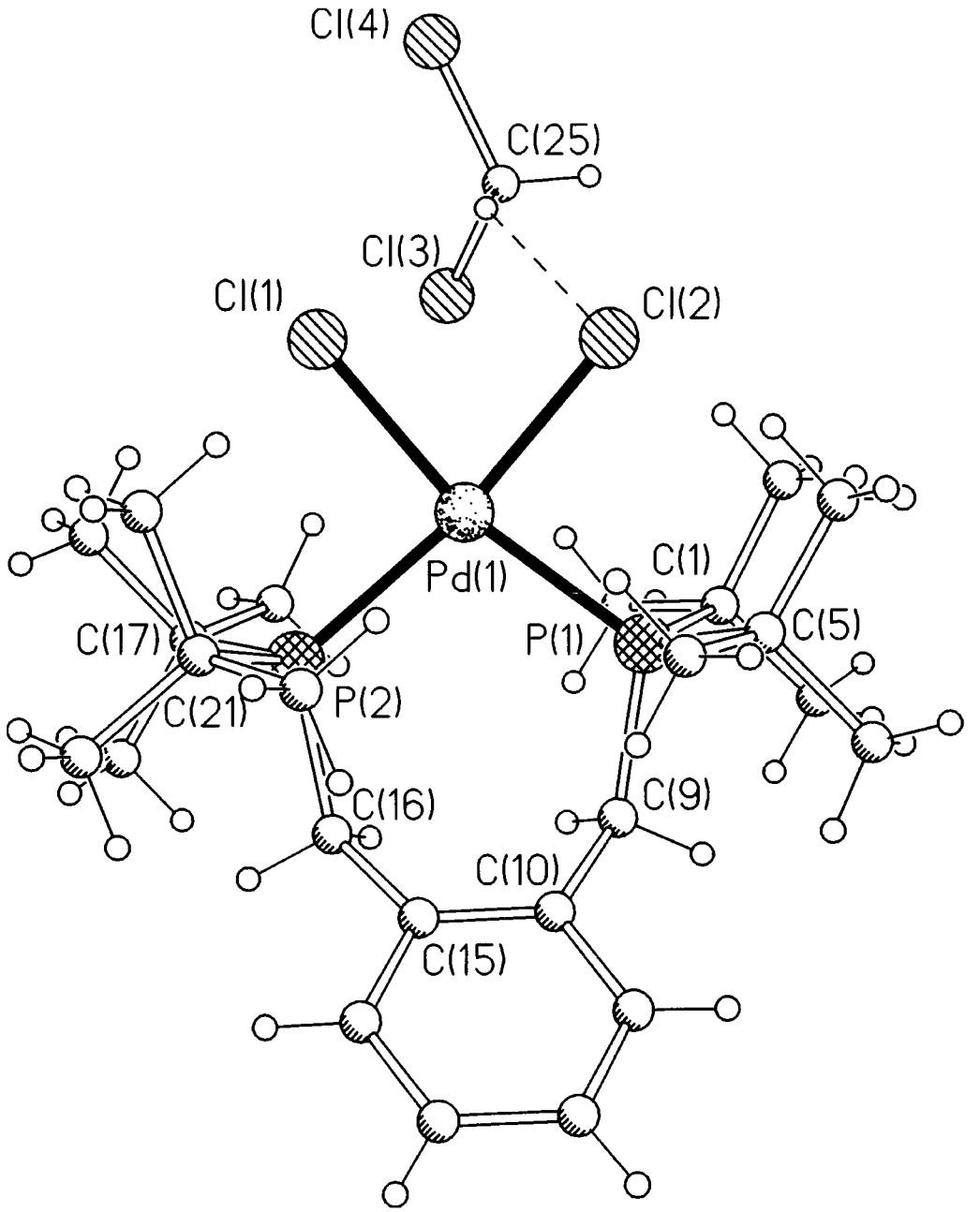

5.8 Discussion

5.8.1 Reactions with Carbon Monoxide

5.8.1.1 Complexes of [o–$C_6H_4(CH_2PBu^t_2)_2$] (1)

Treatment of either of the zerovalent palladium alkene complexes **(12)**, **(27)** with methanesulphonic acid followed by exposure to carbon monoxide causes rapid, visible decomposition. The phosphine ligand remains in solution as the doubly protonated salt o–$C_6H_4(CH_2PHBu^t_2)_2]^{2+}$ $2[CH_3SO_3]^-$, which is not surprising given the basic nature of the dialkyl phosphine and the presence of an excess of methanesulphonic acid. The identification of the solid formed as palladium metal comes from the X-ray fluorescence (XRF) analysis of the precipitate which shows it to be 97.1% palladium by composition. The formation of palladium metal begins within minutes of the addition of CO even at room temperature and is rapidly accelerated by heating the reaction solution. In this study there is no evidence for the formation of complexes of the type [(L-L)Pd(CO)$_2$] or [$Pd_2(\mu\text{-H})(\mu\text{-CO})\{(L\text{-L})\}_2]^+$ $[X]^-$ which are well documented for bidentate phosphine[1] complexes of palladium(II) on reaction with CO. The rapid decomposition under moderate CO pressures parallels the rapid decay of catalytic activity reported in chapter 1 of this thesis, and it is known that lowering the CO pressure and changing the ratio of CO:ethene increases the stability of the catalyst.[2] The implication here is that whilst CO is a requirement for MeP synthesis it also has a role in catalyst decomposition leading to palladium metal.

5.8.1.2 Complexes of [o–$C_6H_4(CH_2PPr^i_2)_2$] (2)

When the corresponding alkene complex of this different ligand **(13)** is treated as above striking differences are observed. No evidence of palladium metal is found even after heating at 80^{0}C and 4 bar CO pressure for 1 hour. It does seem surprising that this relatively small change in the phosphine ligand structure results in such a dramatic change in catalyst properties. We have seen in chapter 2 of this thesis that catalysts derived from this ligand have different selectivities and stability's in the methoxycarbonylation of ethene, with co-polymer being formed by these catalysts. The ^{31}P NMR analysis shows the presence of two species in solution after exposure to CO. Neither of these is the doubly protonated ligand found for the *tert*-butyl ligand. This has been shown by the absence of P-H coupling in the

proton coupled ^{31}P NMR spectrum. The signal at 50.7 ppm which represents approximately 60% of the sample is most likely the compound $[o\text{–}C_6H_4(CH_2PPr^i_2)_2Pd(OH_2)]^{2+}$ $2[(CH_3SO_3)_2]^-$, the water arising from the solvent, reagent grade methanol typically used for the catalytic testing. The affinity of water for palladium(II) centres has been well documented and discussed previously.[3] Also the reaction repeated with the cyclohexyl ligand $o\text{–}C_6H_4(CH_2PCy_2)_2$ **(3)** has led to the isolation of the bis-aquo-complex $[o\text{–}C_6H_4(CH_2PCy_2)_2Pd(OH_2)]^{2+}$ $2[(CH_3SO_3)_2]^-$. The NMR peak at 20.9 ppm which represents approximately 40% of the sample is most likely a palladium(0) carbonyl species or a bridging hydrido carbonyl complex, both of which have been reported to form in reactions of this type[1]. On the basis of chemical shift it seems more likely that the complex is palladium(0) but this is not conclusive. Supporting evidence for the above assignments comes from the reaction of the acetate complex $[o\text{–}C_6H_4(CH_2PPr^i_2)_2Pd(OAc)_2]$ with 4 bar CO at 80^0 C for one hour. In this case the ^{31}P NMR reveals the presence of only one signal at 20.5 ppm attributable to the palladium(0) carbonyl species. The absence of methanesulphonic acid precludes the formation of the bis-methanesulphonate species $[o\text{–}C_6H_4(CH_2PPr^i_2)_2Pd(OSO_2CH_3)_2]$, which gives rise to the high frequency signal at 50.7 ppm.

The important point to highlight for complexes of this ligand is the stability, with respect to decomposition to palladium metal of these catalysts under CO atnospheres. The most active/selective MeP catalysts exhibit instability to CO readily forming palladium metal. The possibility of a link between phosphine labilisation and catalyst activity is again suggested. The most active MeP selective catalysts readily dissociate phosphine from their palladium complexes, whilst the above phosphine which forms some co-polymer in catalysis appears to have improved stability toward phosphine dissociation.

5.8.1.3 Complexes of $[o\text{–}C_6H_4(CH_2PCy_2)_2]$ (6)

Taking the complex $[o\text{–}C_6H_4(CH_2PCy_2)_2Pd(dba)]$ **(14)** and treating it with CO as described in section 5.3 leads to the isolation of the bis-aquo-complex $[o\text{–}C_6H_4(CH_2PCy_2)_2Pd(OH_2)_2]^{2+}$ $2[(CH_3SO_3)_2]^-$ after removal of the solvent and recrystallisation from dichloromethane layered with pentane. The ^{31}P NMR of the solution taken immediately after the reaction reveals the presence of two components whose chemical

shifts are consistent with them being the bis-aquo (δ 44.2ppm) and the palladium(0) carbonyl complex (δ 15.2ppm). The isolation of only the bis-aquo-complex after recrystallisation is most likely due to the reaction of the palladium(0) species with excess methanesulphonic acid. It has also been reported in the literature that the isolation of the compound $[(L\text{-}L)Pd(CO)_2]$ where (L-L) = (S,S)-2,4-bis(diphenylphosphino)pentane was not possible due to the gradual loss of CO from the complex.[4] It is therefore also reasonable to propose that the palladium(0) species decomposes, although no palladium metal is observed even after recrystallisation. In common with the complexes of **(2)**, the complexes of **(3)** exhibit CO stability, but their activity in the methoxycarbonylation of ethylene is minimal, and the selectivity is to co-polymers rather than the desired MeP.

The X-ray structure of **(45)** has several interesting features as discussed for the bis-aquo complexes of the *tert*-butyl substituted ligand **(41, 42)** isolated in chapter 5 of this thesis. The Pd(II) atom has a distorted square planar coordination where the two *cis* sites are occupied by the diphosphine ligand while the remaining two sites are taken up by two coordinated water molecules.

The P-Pd-P bond angle of 100.1^0 is smaller than observed in the Pd(0) alkene complex, but much larger than those reported in the dppp aquo-complexes.[3] This decrease in bite angle is likely to be a result of the complex trying to attain square planar geometry favoured for palladium (II) compounds. The optimum P-Pd-P angle in these complexes would be 90^0 as opposed to 120^0 in the zerovalent trigonal planar species.[6] Clearly the rigid xylene backbone and the bulky phosphorus substituents prevent attainment of 90^0 bite angles but a lowering on oxidation of the metal centre is not surprising.

The O1-Pd-O2 bite angles is 87.33^0, which is comparable to that observed for the $[(dppp)Pd(OH_2)_2]^{2+}$ $2[OTf]^-$ complex[5] where this angle is 87.66^0. This angle, though, is larger than those found in the bis-aquo complexes of the *tert*-butyl ligand **(1)**, and presumably reflects the increased steric congestion imposed by the larger P-Pd-P bite angle in complexes of **(1)**.

The Pd-P bond lengths (2.25Å, 2.26Å) are in the normal range for *cis* chelated phosphines. They are some 0.06Å shorter than the Pd(O) alkene complexes which reflects the more electrophillic nature of the palladium on oxidation and the increased deshielding of the phosphorous atoms. They are also shorter than the bis-aquo complexes of **(1)** again reflecting perhaps the decreased steric congestion and increased π acidity of the cyclohexyl ligand compared to the *tert*-butyl analogue.

The Palladium oxygen distances of 2.12, 2.14 are close to those reported for related complexes, e.g. $[(dppp)Pd(OH_2)_2]^{2+}$ $2[OTf]^-$ where Pd-O = 2.13 and 2.14Å and $[(dppp)Pd(OH_2)(OTf)]^+$ $[OTf]^-$ where Pd-O = 2.16Å.

Particularly noteworthy for this complex is the hydrogen bonding pattern. Both coordinated water molecules are doubly hydrogen bonded to the two methanesulphonate counterions. Interestingly, the two water molecules are each hydrogen bonded to different methanesulphonates rather than the same one. The same situation is found for the bis-aquo complexes of **(1)** reported in this study, and also for all of the bis-aquo complexes reported in the literature. The role of hydrogen bonding in the formation of aquo transition metal complexes has long been recognised,[3] and is important in stabilizing the solid state structures of these molecules.

5.8.1.4 Complexes of $[o\text{–}C_6H_4(CH_2PPh_2)_2]$

Treatment of the complex $[o\text{–}C_6H_4(CH_2PPh_2)_2Pd(BQ)]$ **(31)** with methanesulphonic acid followed by exposure to CO as described in section 5.3 above leads to the formation of clear solutions with no evidence for decomposition to palladium metal. Analysis of the solution by ^{31}P NMR reveals the presence of two species in solution with signals at δ 26.8 and 19.1 ppm respectively. The peak at δ 26.8 ppm can be assigned as the bis-methanesulphonate complex $[o\text{–}C_6H_4(CH_2PPh_2)_2$ Pd $(OSO_2Me)_2]$ by reference to the data in Chapter 4 where the reaction of the benzoquinone complex $[o\text{–}C_6H_4(CH_2PPh_2)_2$ Pd (BQ)] with methanesulphonic acid gave rise to this compound (^{31}P NMR δ 26.8ppm). The peak at δ 19.1ppm is most likely a palladium(0) species. The complex $[o\text{–}C_6H_4(CH_2PPh_2)_2$ Pd (BQ)] reported in Chapter 3 has a ^{31}P NMR signal at δ 18.65ppm.

5.8.1.5 Complexes of [(DPEphos)Pd(BQ)]

Treatment of the above complex with methanesulphonic acid followed by exposure to CO as described in section 5.3 above, leads to clear solutions with no evidence for decomposition to palladium metal. Analysis of the solution by ^{31}P NMR reveals the presence of two species in solution giving peaks at δ 25.1 and 9.1 ppm respectively. The peak at δ 25.1 ppm is assigned to the bis-methanesulphonate complex [(DPEphos)Pd $(OSO_2Me)_2$] also formed in the reaction of the benzoquinone complex [o–$C_6H_4(CH_2PPh_2)_2$ Pd (BQ)] with methanesulphonic acid (^{31}P NMR δ 25.1ppm) as described in Chapter 4. The peak at δ 9.1 is assigned to a palladium(0) species. The complex [(DPEphos)Pd (dba)] reported in Chapter 3 gave rise to ^{31}P NMR signals at δ 13.8 and 8.1ppm respectively.

In summary, it is found that the complex which is the most successful pre-catalyst for high selectivity to MeP, decomposes in excess sulphonic acid when exposed to CO. The complex which is the most successful pre-catalyst for co-polymerisation appears to be stable to ligand dissociation under the same conditions.

5.8.2 Reaction of Catalyst Solutions with Ethene

The pre-catalyst solution comprising [o–$C_6H_4(CH_2PBu^t_2)_2Pd(dba)$] **(12)** + 20 equivalents of methanesulphonic acid was treated with 4 bar ethene at 80^0C for 1 hour. This experiment was conducted to ascertain the stability of this MeP selective pre-catalyst to ethene and to determine if the system was active for the formation of ethene dimers and oligomers. The dimerisation/oligomerisation of ethene is reported for the ethene/CO catalysts based on dppp. This is reported to occur in the complete absence of CO.

The solutions treated with ethene appear to be stable with respect to palladium metal formation for a number of days, this is in contrast to the instability found on treatment with CO. Furthermore using the above composition no evidence for butenes or higher oligomers was found. The solutions removed from the autoclave and analysed by ^{31}P NMR show the presence of a new speciesgiving rise to broad signals (indicative of exchange processes) of equivalent area at δ 71.5 and 40.0 ppm. The absence of ethene oligomerisation in a system which clearly interacts with ethene giving rise to an unidentified complex is interesting. One

plausible explanation is that the steric crowding at the metal centre in complexes of $[o\text{-}C_6H_4(CH_2PBu^t_2)_2]$ **(1)**, does not favour the co-planar transition state required for ethene insertion into a palladium alkyl bond. The oligomerisation activity of less sterically demanding pre-catalysts **(13, 14, 18)** needs to be studied to identify if there is a relationsdhip between cone angle and oligomerisation activity, as has been found for MeP selectivity in the methoxycarbonylation of ethene in this study.

5.8.3. Synthesis of Oxygen Complexes $[L_2Pd(O_2)]$

Several complexes of the type $[L_2Pd(O_2)]$ have been synthesised by other workers.[7] The best known example is the complex $[(PPh_3)_2Pd(O_2)]$, synthesised from $[(PPh_3)_4Pd]$ and oxygen. The mechanism of this reaction is suggested to involve the coordinatively unsaturated species $[(PPh_3)_2Pd]$ formed from $([(PPh_3)_4Pd]$ in solution. In this study, the analysis of solutions of complexes of the type $[L_2Pd(alkene)]$ which have been exposed to air reveals the formation of palladium oxygen complexes in solution. This suggests the likely mechanism of formation is via the coordinatively unsaturated 14e-species $[L_2Pd]$ see Scheme 5.1. This dissociation of alkene has been demonstrated for complexes of the type (L-L)Pd(dba) where L-L = diop, binap and dppf.[8]

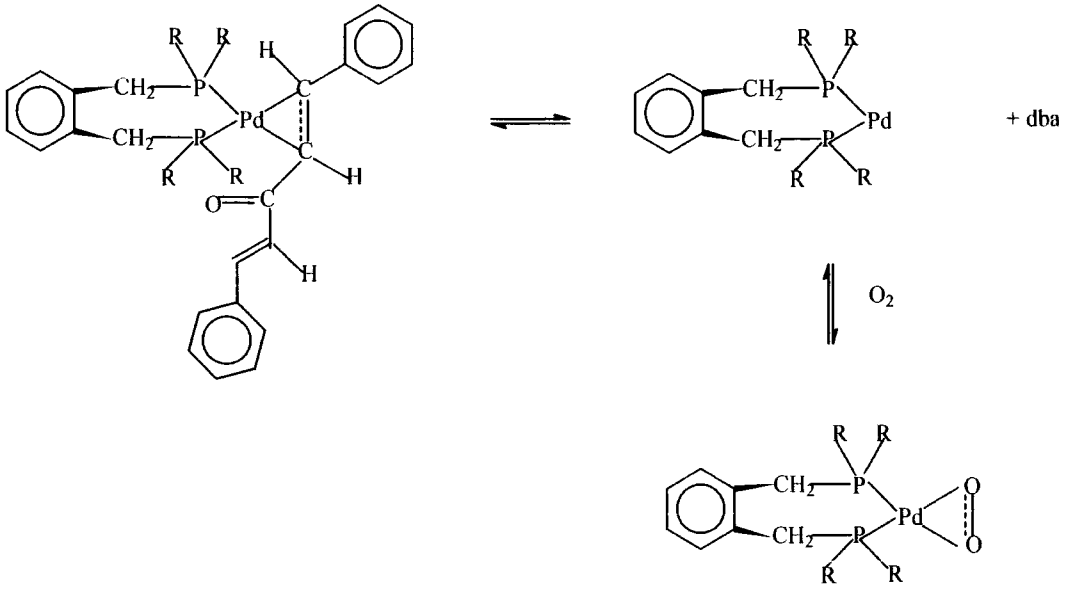

Scheme 5.1
Mechanism Of Formation Of Oxygen Complexes

For the ligand 1,2-bis(di-*tert*-butylphosphinomethyl)benzene, the styrene complex **(26)** has proved impossible to characterize by single crystal X-ray diffraction. Attempts to grow crystals of this compound always led to the formation of the oxygen complex **(48)** via interaction with adventitious oxygen. Under conditions where O_2 is introduced, the oxygen complex forms readily. This formation is much easier from this styrene complex than from the dba **(12)** or benzoquinone **(27)** complex. In these latter examples, the presence of electron withdrawing substituents on the alkene leads to stronger back acceptance of electron density from the metal d orbitals to the π^*-alkene anti-bonding orbitals and hence stronger alkene bonding.

The isolation of oxygen complexes more readily from Pd(0) alkene complexes where alkene bonding is weaker also supports the dissociative mechanism proposed for the formation of these complexes. Supportive evidence for this argument comes from the VT NMR studies reported in chapter 3, where the dissociation of dba from the zerovalent complex in xylene was observed to occur above 100^0C, whereas the dissociation of styrene is observed around 60^0C. Thus the formation of oxygen complexes from the styrene complex would be predicted to be more readily accomplished if alkene decomplexation is a required first step.

The isolation and characterization by X-ray diffraction of oxygen complexes has only been achieved for palladium complexes of bulky dialkyl phosphines in this study. As mentioned above, there is evidence though for the formation of oxygen complexes with non-bulky alkyl phosphine ligands. The compound [(dppp)Pd(dba)] when analysed in dichloromethane solution by electrospray MS generates ions which correspond to the oxygen complex (L-L)Pd(O_2). These ions are not generated by analysis of the solid using FAB as the ionization technique. The inference here again is that dissociation of the alkene occurs in solution as a prerequisite to reaction with oxygen. The increased propensity of the bulky phosphines to form oxygen complexes is then likely to be a result of the equilibrium illustrated in Figure 5.1 being shifted to the right with increasing steric bulk.

5.8.3.1. Crystallographic Features

Taking complex 26b, which contains the 1,2-bis(di-*tert*-butylphosphinomethyl)benzene ligand, several points are worthy of note. Firstly, the oxygen is bound η^2 in a similar manner to alkene complexes. The palladium oxygen bond lengths are identical within the quoted error of the crystallographic study, and are very similar in length to the values reported for the complex $[(PPh_3)_2Pt(O_2)]$ in the literature.[10] The complex has slightly distorted square planar geometry with the angle between the P-Pd-P plane and the O-Pd-O plane being 6.4°. Square planar geometry is expected for Pd(II) compounds of this type[9] and indeed the platinum complex $[(PPh_3)_2Pt(O_2)]$ has this geometry around the metal atom.[10]

Other aspects of the molecule **(48)** are also similar to the above published structure. The Pd-P bond lengths are in the range 2.2 - 2.3Å common for Pd(II) compounds. There is a slight *trans* influence noted with the Pd-P bond lengths differing by as much as 0.06Å in complex **48**. This is also observed for $[(PPh_3)_2Pt(O_2)]$ where the Pt-P bond lengths differ by 0.03Å (2.28 and 2.25Å).

The oxygen-oxygen bond has lengthened significantly on coordination presumably as a result of accepting electron density from the metal into a π^* anti bonding orbital. The bond length is midway between that observed in molecular oxygen (1.208Å) and a single oxygen-oxygen bond. Examples of these complexes such as $[(PPh_3)_2Pt(O_2)]$ are reported in the literature to be very reactive, commonly leading to phosphine oxidation.[11] The dioxygen complexes are also reported to be active oxidizing agents[11]. The oxygen is clearly activated by coordination to the transition metal. No studies on the reactivity of the oxygen complexes made in this work have been carried out, but related studies[12] have shown the oxygen complexes to react with sulphonic acids leading to complexes of the type $[(L\text{-}L)Pd(X_2)]$.

The Pd-P bond lengths in these complexes e.g. **(48)** are significantly shorter than those observed in the Pd(0) alkene complex of the equivalent ligand **(12)**. This is expected for the smaller Pd(II).

The bite angle, P-Pd-P also appears to be reduced in the oxygen complex compared to the Pd(0) alkene complexes (102.8Å compared with 104.0Å). It is expected that a square planar Pd(II) complex would have a smaller bite angle than a trigonal planar Pd(0) complex of the same phosphine ligand. Modeling studies suggest that the optimum bite angle for Pd(II) phosphine complexes is around 94° some 8° smaller than that observed.[13] Palladium zero on the other hand has a reported optimum in excess of 100 °.

The small dihedral angles between P_2Pd and PdO_2 planes suggest that the strain in these complexes is limited. A number of examples exist where strain is relieved by a twisting of the molecule resulting in a large dihedral angle.[14] The absence of a significant twist suggests the molecule is reasonably strain free. A reflection of stability is the lack of evidence of phosphine oxide formation, in the synthesis of these complexes and their study in solution. As mentioned above the reaction of oxygen complexes of this type to form phosphine oxides is well documented, as is the reaction of free phosphines in solution with oxygen gas.

5.8.3.2 Spectroscopy

The ^{31}P NMR signal for the oxygen complexes **(48)** arises at ~60ppm shifted 10ppm to higher frequencies from the alkene complexes **(12, 27, 35)**. This is consistent with increased deshielding of the phosphorus on oxidation of the palladium.

Also, the IR spectra of these complexes exhibit a ν(O-O) band at 858cm^{-1}, similar in frequency to literature values of 830cm^{-1} for $[(PPh_3)_2Pt(O_2)]$ and 880cm^{-1} $[(PPh_3)_2Pd(O_2)]$.[15] These frequencies are also similar to IR absorption bands found by Vaska for iridium-oxygen complexes.[16]

5.8.3.3 Synthesis of $[o\text{–}C_6H_4(CH_2PPe^t_2)_2$ Pd $(O_2)]$ (46) and $[2,3\text{-}C_{10}H_6(CH_2PBu^t_2)_2Pd(O_2)]$ (47)

The crystallographic features of the oxygen complexes **(46** and **47)** are similar to those described above **(48)**. The interesting feature of the ligands $(o\text{–}C_6H_4(CH_2PPe^t_2)_2)$ and

2,3-$C_{10}H_6(CH_2PBu^t_2)_2$ is the apparent increased propensity of the dba complexes **(16, 23)** to form these oxygen complexes when compared to 1,2-bis(*di-tert*-butylphosphinomethyl)benzene (*o*-$C_6H_4(CH_2PBu^t_2)_2$). In both of these cases, several attempts were made to recrystalise the dba complexes **(16** and **23)**. In most cases, only finely-powdered material was obtained. If any oxygen was admitted into the apparatus, formation of the oxygen complex occurred and this recrystallised readily. On a number of occasions, recrystallisation of the oxygen complex of the above two ligands occurred on the sides of the NMR tube of a sample of the dba complex.

The increased propensity to form oxygen complexes suggests that in the palladium complexes **(16** and **23)** the alkene (dba) is more labile than in the 1,2-bis(di-*tert*-butylphosphinomethyl)benzene complex **(12)** thus leading to a higher concentration of the 14e [(L-L)Pd] intermediate species proposed to react with molecular oxygen. The reason for this increased lability could be increased steric congestion.

The di-*tert*-pentyl substituted ligand **(5)** was designed as a slightly less sterically crowded ligand than the di-*tert*-butyl substituted ligand **(1)**. It was hoped that the methylene linkage of the ethyl groups would introduce flexibility allowing the attached methyl groups to bend away from steric pressure around the metal centre. Inspection of the crystallographic data of **16b** shows that this does occur leaving the two methyl groups close to the metal centre. The net result is that oxygen complexes of the two ligands **(46** and **48)** are not very different. The P_2Pd-PO_2 dihedral angle is slightly smaller for the *tert*-pentyl ligand (2.4° versus 4.7 for the *tert*-butyl ligand) suggesting a small effect in reducing steric interactions. This, though, does not explain the observed increased propensity for the *tert*-pentyl ligand to form oxygen complexes. In solution, the situation may be expected to change. With free rotation around the P-C bonds there may be increased interaction between the dba ligand and the -*tert*-pentyl group resulting in increased labilisation of dba.

5.8.4 Coordination Chemistry with Palladium(II) Compounds

5.8.4.1 Reactions with bis(benzonitrile)palladiumdichloride

5.8.4.1.1 $[(PhCN)_2Pd(Cl)_2]$ +(1)

The reaction of the palladium(II) complex with the bulky phosphine ligand **(1)** does not lead to the isolation of the complex $[(L\text{-}L)Pd(Cl)_2]$, where the phosphorus atoms of the bidentate ligand occupy *cis* positions in a square planar palladium(II) complex. This is established by the synthesis of this complex by an alternative route (see 5.7.2) and characterization by single crystal X-ray diffraction and multi nuclear NMR. The compound produced in this reaction contains broad ^{31}P NMR signals shifted some 5ppm to low field from those observed for the *cis* chelate $[(L\text{-}L)Pd(Cl)_2]$. It is suggested that in the complexes formed, the phosphine ligand is bridging palladium atoms rather than chelating a single palladium atom. The remainder of the characterization supports this suggestion with the proton and carbon NMR spectra containing broad features. In particular the methylene CH_2 protons appear as a very broad feature in the ^1H and ^{13}C NMR, indicating numerous inequivalent environments not resolved. Also infrared spectroscopy indicates the presence of the Pd-Cl bond with a band at $350cm^{-1}$, consistent with the presence of *trans* chloride ligands.[17] The mass spectrum of the complex also supports the presence of bridging phosphines. Clearly, if the ligand bridges, then the possibility of quite large clusters exists and the electrospray mass spectrum reveals the formation of ions which can be assigned to dimeric and trimeric palladium species. These species are not indicated in the electrospray spectrum of the monomeric $[(o\text{-}C_6H_4(CH_2PBu^t_2)_2)Pd(Cl)_2]$, indicating that the ions are not mass spectral artifacts.

5.8.4.1.2 $[(PhCN)_2Pd(Cl)_2]$ +(2)

The reaction of the phosphine ligand **(2)** with the palladium(II) complex leads to the isolation of $[(o\text{-}C_6H_4(CH_2PPr^i_2)_2)Pd(Cl)_2]$, where the phosphine acts as a chelate to a single palladium atom. The different behavior of this ligand versus **(1)** is again noteworthy. No evidence for bridging phosphine complexes is found. Spectroscopic data support the formation of the complex $[(o\text{-}C_6H_4(CH_2PPr^i_2)_2)Pd(Cl)_2]$ having *cis* chloride ligands, with the following features worthy of note. 1) The ^{31}P NMR is a sharp singlet. 2) The ^1H and ^{13}C

NMR signals can all be readily assigned. The presence of only two aromatic CH signals in the proton spectra and three aromatic carbons in the carbon spectra is consistent with the symmetrical species [(o–$C_6H_4(CH_2PPr^i_2)_2$)Pd$(Cl)_2$]. 3) The mass spectrum contains ions attributable to the suggested molecular ion minus a chloride. This is a common fragment ion for complexes of this type with the -ve ion spectra containing a large ion corresponding to Cl^-. The other major ion in the spectrum corresponds to the [(o–$C_6H_4(CH_2PPr^i_2)_2$)Pd]$^+$ fragment resulting from loss of the second chloride. There is no evidence for higher mass species such as those found for the ligand **(1)** where bridging complexes are formed. 4) Also infrared spectroscopy indicates the presence of a Pd-Cl bond with a band at 300cm^{-1} , this is consistent with the presence of a dichloride complex with *cis* coordination of the phosphine ligands.[17]

5.8.4.1.3 [(PhCN)$_2$Pd$(Cl)_2$] +1,3-$C_3H_6(PBu^t_2)_2$

The reaction of the phosphine ligand, 1,3-$C_3H_6(PBu^t_2)_2$ with the palladium(II) complex leads to the isolation of the complex [(1,3-$C_3H_6(PBu^t_2)_2$)Pd$(Cl)_2$] where the phosphine acts as a chelate to a single palladium atom. This has been demonstrated by single crystal X-ray diffraction and by spectroscopic characterization, the main features of which are 1) the ^{31}P NMR is a sharp singlet; 2) the mass spectrum contains ions attributable to the suggested molecular ion minus a chlorine which is a common fragment ion for complexes of this type. The -ve ion spectrum contains a large ion current corresponding to Cl^-. The other major ion in the +ve ion spectrum corresponds to the [(1,3-$C_3H_6(PBu^t_2)_2$)Pd]$^+$ fragment resulting from loss of the other chloride. There is no evidence for higher mass species such as those found for the ligand **(1)** where bridging complexes are formed; 3) also infrared spectroscopy indicates the presence of the Pd-Cl bond with a band at 297cm^{-1} , which is consistent with the presence of a dichloride complex with *cis* coordination of the phosphine ligands.[17]

The key features of the X-ray structure are illustrated in Figure 5.8.4.1.3 and selected bond lengths are shown in Table 5.8.4.1.3. Two crystallographically independent molecules are present within the unit cell and the bond lengths and angles differ slightly for each one. The coordination around palladium is approximately square planar but the P_2Pd-PdCl_2 dihedral angle is fairly large being 9^0 and 15^0 respectively for the two molecules. These large twists in the molecules suggests the chelate may not have good stability, but in this example no evidence for the formation of bridging compounds has been found. The same cannot be

said of the analogous acetate complex discussed in section 5.8.4.2.3, below where the formation of a bridging phosphine complex has been identified by single crystal X-ray study. The P-Pd-P bite angle (98.09^0) and the Pd-P bond lengths (2.30 Å) are all within the range anticipated for *cis* phosphine palladium dichloride complexes of this phosphine. The analogous platinum complex has a bite angle of 99.07^0 and a Pt-P average bond length of 2.28 Å, whilst the Pd(dppp) analogue has a bite angle of 90.58^0 and a Pd-P average bond length of 2.24 Å.

The ready formation of *cis* chelating phosphine complexes with this ligand and its similarity to the *iso*-propyl ligand **(2)** rather than the *tert*-butyl ligand **(1)** in this respect seems at odds with the observed activity in the methoxycarbonylation of ethene, where the propane bridged ligand forms complexes which are active catalysts for the formation of MeP. However, the large dihedral angle found for the dichloride, the coordination chemistry observed with palladium acetate and the rapid decomposition observed on reaction with CO, all suggest that chelate bonding is not very strong and phosphine labilisation may well occur in solution.

5.8.4.2 Reactions with Palladium Acetate

5.8.4.2.1 $[Pd(OAc)_2]$ +(1)

The reaction of **(1)** with palladium acetate in acetone leads to the isolation of a pale green compound in relatively low yield. The spectroscopic characterization of this complex is consistent with the structure illustrated in Figure 5.10. This structure has been deduced based on several pieces of analytical data.

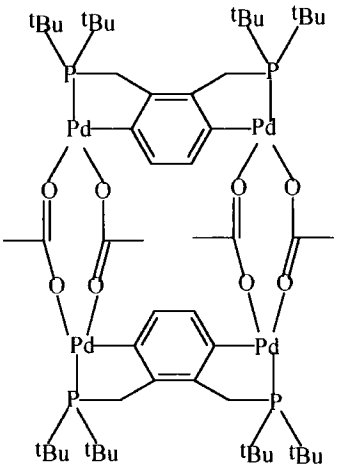

Figure 5.10 Proposed Structure from Reaction of (1) + $Pd(OAc)_2$

1. The ^{31}P NMR exhibits a single resonance at 111.69 ppm indicating only one type of phosphorus environment. The spectrum does not change on cooling to -80^{0}C, indicating that exchange processes are not occurring at room temperature to mask any of the signals. The magnitude of the chemical shift is consistent with a 5 membered palladacycle ring containing phosphorus. The compound illustrated in Scheme 5.2 has been synthesised[18] and characterized by ^{31}P NMR and single crystal X-ray diffraction. This compound has phosphorus in a 5 membered palladacycle ring and the ^{31}P NMR signal is at 105ppm. Also in this compound only one of the phosphorus atoms is in the palladacycle ring, the other is present as a free phosphine moiety which appears in the ^{31}P NMR spectrum as a singlet at 35ppm. Clearly in the reaction carried out in this study the absence of these high field signals indicates that no free phosphine is present in the complex isolated.

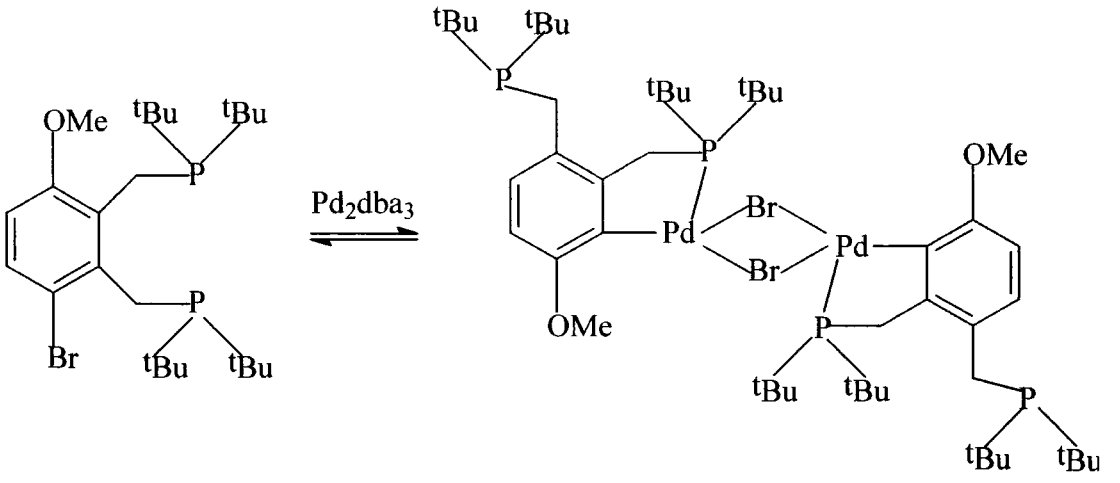

Scheme 5.2

2. The I.R. spectrum is consistent with the presence of bridging acetate ligands,[19] with the C=O stretch observed 60-100cm^{-1} wave numbers lower than observed for unidentate acetate bonding. This is a result of the donation of electron density from the oxygen lone pair to the palladium to form the bridged complex. This leads to an decrease in the bond order of the C=O bond and consequently a lower C=O stretching frequency.

3. No molecular ions ascribed to the tetrameric complex are observed in the mass spectrum of this sample. In the +ve ion FD spectrum the major ion (m/z 724) corresponds to the molecule splitting in half with each palladium retaining one acetate ligand (see Figure 5.11). The +ve ion FAB spectrum contains m/z 605 as a major ion, which corresponds to the loss of two acetates from the above 724 ion, and is again consistent with the tetramer fragmenting initially into two smaller fragments each based around a central xylene with two palladacycle rings. Analysis of the isotope patterns for the two ions discussed above shows them to contain two palladium atoms further supporting the proposed structure.

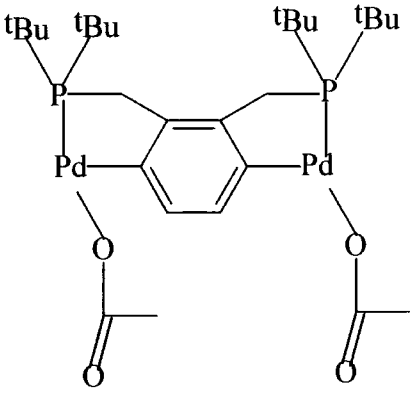

FD Major ion M/Z 724

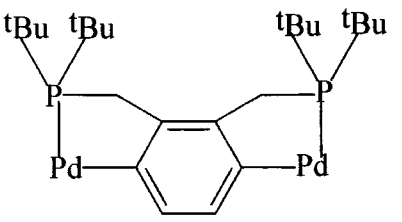

FAB Major ion M/Z 605

Figure 5.11 Major Ions Observed in Mass Spec. Analysis

4. The ^{1}H NMR spectrum is consistent with the proposed structure with the ratio of aromatic CH:methylene CH_2 being 1:2 and the ratio of aromatic CH:acetate CH_3 being 1:3. If aromatic CH activation has not occurred then we would expect the ratio of aromatic CH:methylene CH_2 and aromatic CH:acetate CH_3 to be 1:1 and 1:1.5 respectively.

The formation of this compound is suggested to be driven by the thermodynamic stability of the 5 membered rings formed. Other examples of stable palladacycle ring formation are known with perhaps the best example being the formation of catalysts useful in the Heck reaction.[20] Here mixing palladium acetate with tris-o-tolyphosphine leads to the exclusive formation of the palladacycle product.

5.8.4.2.2 [Pd(OAc)$_2$] +(2)

The reaction of the phosphine ligand **(2)** with the palladium acetate leads to the isolation of the complex [(o–$C_6H_4(CH_2PPr^i_2)_2$)Pd(OAc)$_2$] where the phosphine acts as a chelate to a single palladium atom. The different behavior of this ligand versus **(1)** is again noteworthy. No evidence was found for high frequency ^{31}P NMR signals forming with time, which are indicative of secondary reactions in this reaction . The formation of a precipitate might disfavour further reactions, but the ^{31}P NMR recorded over a period of days suggest that the compound is stable in solution. Spectroscopic data support the formation of the

bis-acetate complex with the following features worthy of note: 1) The ^{31}P NMR is a sharp singlet 2) The ^{1}H and ^{13}C NMR signals can all be readily assigned. The presence of only two aromatic CH signals in the proton spectra and three aromatic carbons in the carbon spectra is consistent with the symmetrical species $[(o\text{–}C_6H_4(CH_2PPr^i_2)_2)Pd(OAc)_2]$. 3) The mass spectrum contains ions attributable to the suggested molecular ion minus an acetate group. This is a common fragment ion for complexes of this type with the -ve ion spectra containing a large ion current corresponding to OAc^-. The other major ion in the spectrum corresponds to the $[(o\text{–}C_6H_4(CH_2PPr^i_2)_2)Pd]^+$ fragment resulting from loss of the other acetate group. There is no evidence for higher mass species such as those found for the ligand **(1)** where bridging complexes are formed.

5.8.4.2.3 $[Pd(OAc)_2]$ +1,3-$C_3H_6(PBu^t_2)_2$

The reaction of the phosphine ligand 1,3-$C_3H_6(PBu^t_2)_2$ with palladium acetate leads to the isolation of the complex $[(1,3\text{-}C_3H_6(PBu^t_2)_2)Pd(OAc)_2]$ where the phosphine acts as a chelate to a single palladium atom. Interestingly, attempted recrystallisation of this material from dichloromethane, layered with pentane, leads to a rearrangement, and the material which crystallizes from solution is the tetramer $[\{(Bu^t_2P(CH_2)_3PBu^t_2)Pd(OAc)_2\}_4]$, where the phosphines are now bridging *trans* phosphines rather than chelating *cis* phosphines. The mass spectrum indicates that the solid initially isolated is the monomeric $[(1,3\text{-}C_3H_6(PBu^t_2)_2)Pd(OAc)_2]$ with ions attributable to the suggested molecular ion minus an acetate group being observed, and also ions attributable to the fragment $[(1,3\text{-}C_3H_6(PBu^t_2)_2)Pd]$, both acetate groups being lost.

The key features of the x-ray structure are illustrated in Figure 5.6. and the bond lengths and angles around one of the palladium centres are shown in Table 5.6. The square planar geometries around the palladium centres are similar with Pd-P bond lengths in the range expected for *trans* palladium phosphine complexes.

In conclusion the tertiary butyl substituted bidentate phosphines studied do not want to be *cis* chelates and adopt *trans* geometry through bridging, made possible by the flexible propane bridge. However the more rigid xyxyl phosphine undergoes facile o-metallation to give novel palladacycles.

5.8.5 Reactions of (12) with Propionyl Chloride

5.8.5.1 Reaction with One Equivalent of Propionyl Chloride: Synthesis of [o–$C_6H_4(CH_2PBu^t_2)_2Pd(COC_2H_5)(Cl)$]

The reaction of 1 equivalent of propionyl chloride with **(12)** led to the formation of two species, as determined by ^{31}P NMR of the reaction solution. The first of these is [o–$C_6H_4(CH_2PBu^t_2)_2Pd(Cl)_2$] **(53)**, and its formation seems surprising given the reaction stoichiometry. The propionyl chloride was distilled prior to use in an attempt to remove traces of HCl which inevitably form from the hydrolysis of the acid chloride in moist air. Three possible routes can be suggested for the formation of the dichloride [o–$C_6H_4(CH_2PBu^t_2)_2Pd(Cl)_2$], and these are illustrated in Scheme 5.3. Formation of palladium(4+) complexes, examples of which are well known,[21] can be invoked to explain each possible route to the observed products.

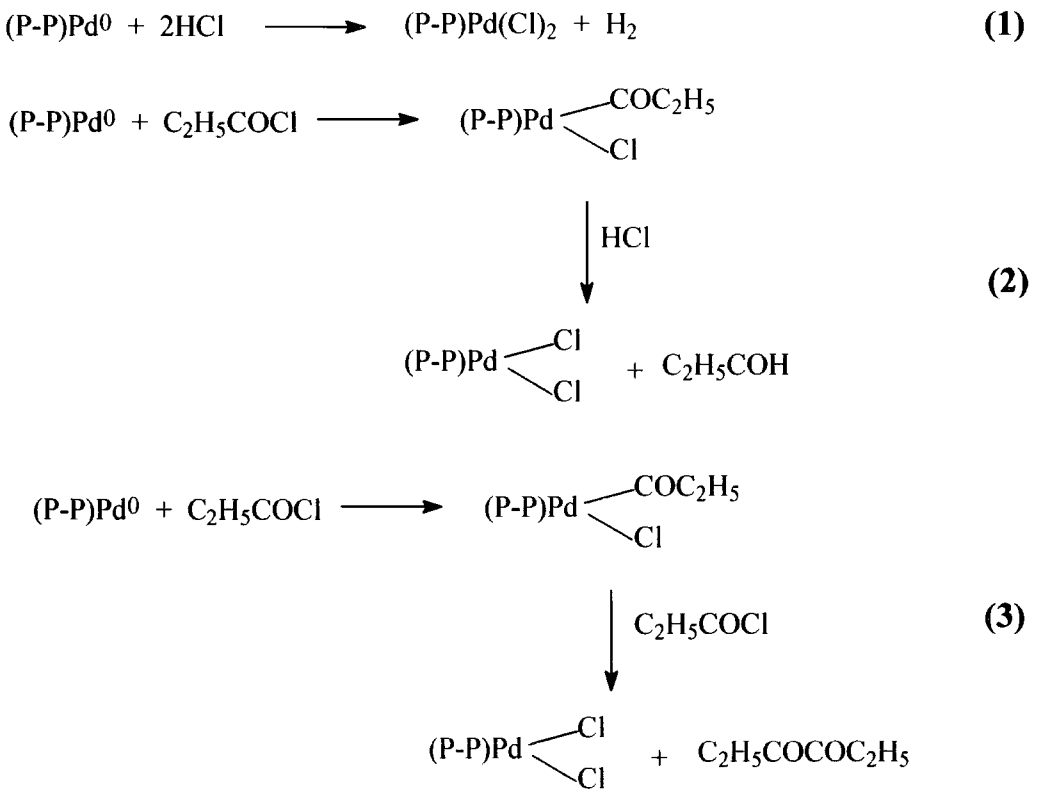

Scheme 5.3
Possible Routes for the Reaction of Pd(0) with Propionyl Chloride

The second species detected is the target acyl complex $[o\text{–}C_6H_4(CH_2PBu^t_2)_2Pd(COC_2H_5)(Cl)]$ **(54)**, formed as a result of the oxidative addition of propionyl chloride to the palladium(0) starting complex. The ^{31}P NMR of the acyl complex appears as two broad signals indicating some fluxional behavior, the nature of which is not immediately obvious. The NMR tube in which this reaction was undertaken was left to stand allowing crystals of the acyl complex to form on the sides of the tube. Further detailed NMR characterization proved impossible as no pure sample of the acyl complex could be isolated.

The features of the X-ray structure of the dichloride complex will be discussed in section 5.8.5 along with the X-ray crystallographic data obtained for a related complex **(55)** obtained via alternative means.

The key features of the X-ray structure of the acyl complex **(54)** are illustrated in Figure 5.8, with the key bond angles and lengths around palladium listed in Table 5.8. The most striking feature from analysis of the X-ray data is the difference in palladium phosphorus bond lengths, with the Pd-P distance *trans* to the acyl ligand being some 0.16Å longer than the phosphorus *trans* to the chloride ligand. This bond length of 2.48Å is extremely long for a metal phosphorus bond. The phenomenon we are observing here is the *trans* influence which is a ground state effect. Ligands can be ranked according to their ability to lengthen bonds to *trans* located groups, and the acyl group ranks high in this series. The related kinetic phenomenon is the *trans* effect which reflects a ligands ability to labilise a group *trans* located. It seems reasonable that the two are interrelated and therefore it is believed that the acyl group leads to labilisation of the phosphorus atom *trans* located in the above complex. This could be the origin of the observed broadening in the ^{31}P NMR, with labilisation of phosphorus giving rise to T or Y shaped intermediates. This has important implications for the catalysis. If it is assumed that this ground-state *trans* influence plays an important role in the overall labilisation of the phosphine ligand (*trans* effect), this bond lengthening may well be the prelude to the bond breaking completely and the phosphine partially dissociating from the metal. This raise two intriguing possibilities, 1) that phosphine labilisation in this manner is an integral part of the mechanism for the synthesis of MeP and ligands which can labilise in this way are what differentiates between the reaction selectivity i.e.. ligands which remain as a chelate at all times lead to co-polymer (this will be further explored in the final chapter of this thesis); and 2) phosphine labilisation is the first step on

the road to catalyst deactivation. Clearly once one phosphorus has dissociated from the metal, it is open to reaction with the other components of the reaction solution eg. H^+. The highly basic alkyl phosphine will readily react with the excess methanesulphonic acid, protonating the phosphine and making re-coordination more difficult.

No other *cis* acyl complexes of palladium or platinum have been reported, presumably due to their instability. The only material characterized crystallographically which shows similar features is the platinum complex $[(1,3\text{-}C_3H_6(PBu^t_2)_2)Pt(H)(OSO_2CF_3)]$. Here the platinum phosphorus bond *trans* to the hydride is 2.37Å, some 0.16Å longer than the platinum phosphorus bond *trans* to the triflate (2.20Å). The hydride ligand is well known as a high *trans* influence ligand although in this example the bond length of 2.37Å is 0.11Å shorter than the observed *trans* influence of the acyl ligand.

A second important feature of the X-ray data is the large distortion from the square planar environment favoured for palladium(II) complexes. The dihedral angle is 24.5^0 significantly larger than has been measured for any of the palladium(II) complexes of **(1)** characterized in this study. This again suggests that a significant amount of strain exists within the molecule and it seems reasonable to propose relief of that strain occurs in solution by phosphine labilisation. Also the palladium chloride distance is longer than observed in the dichloride by some 0.06Å, again indicative of the steric congestion.

The side on view of the molecule (Figure 5.8) shows the disposition of the *tert*-butyl groups above and below the distorted square plane. It can be seen how the methyl groups project above and below the PdP_2 plane preventing access to the dz^2 orbital . The steric bulk of the ligand effectively creates a channel along which the substrates can approach the metal. This steric environment created by the ligand forms the basis of a possible reason for the high selectivity observed for catalysis using these ligands. This has been discussed in Chapter 3 of this thesis where the steric congestion of a range of ligands has been assessed from solid state data. The acyl structure discussed here would seem to support the hypothesis that access to the dz^2 orbital is not possible and further insertions of ethene/CO required for co-polymer synthesis are sterically disfavoured. Modeling work by Cavell et al[22] suggest that five coordinate intermediates are likely in co-polymer syntheses using P-N ligand complexes of palladium.

5.8.5.2 Reaction with Ten Equivalents of Propionyl Chloride: Synthesis of [o-$C_6H_4(CH_2PBu^t_2)_2Pd(Cl)_2$]

The solid isolated from this reaction is confirmed by analytical data and by single crystal X-ray data to be the dichloride [o–$C_6H_4(CH_2PBu^t_2)_2Pd(Cl)_2$], **(55)**. The product from this reaction was recrystallised from dichloromethane, and a molecule of solvent is present in the unit cell of the crystal. The key features of the x-ray data are illustrated in Figure 5.8.3 and the bond lengths and angles around palladium are shown in Table 5.8.3. The molecule of dichloromethane sits between the two chlorine atoms and hydrogen bonds are formed between the hydrogen atoms of the dichloromethane and the chlorine atoms of the palladium complex. This hydrogen bonding has several effects on the ground state structure which are revealed when a comparison is made of the key crystallographic features of the dichloride complex with and without the hydrogen bonding dichloromethane. This comparison is possible because of the single crystal X-ray study of the same dichloride **(53)** but without solvent inclusion obtained from the reaction using 1 equivalent of propionyl chloride with the dba complex **(12)** (section 5.8.5.1). The key features of these X-ray data are illustrated in Figure 5.7 and the bond lengths and angles around palladium are shown in Table 5.8.

The Cl-Pd-Cl angle differs by 3^0 with the smaller angle of 80.68^0 being found in the hydrogen bonded complex. The presence of the molecule of dichloromethane acts to pull the chlorines closer together. Two other consequences of this effect are slightly longer palladium phosphorus bond lengths and a larger P-Pd-P bite angle for this complex. The hydrogen bonding is acting to reduce strain in the molecule with the dihedral angle in the hydrogen bonded complex being 7.9^0 versus 20.8^0 in the absence of the hydrogen bonded dichloromethane. There would clearly seem to be a thermodynamic gain to be derived in the solid state from dichloromethane acting in this way. The reduction of steric strain in palladium(II) complexes of the ligand **(1)** has been observed previously in the dioxygen and bis-aquo complexes, where the presence of H_2O and O_2 leads to complexes in which the dihedral angle is reduced and the distortion in the square planar complexes is reduced (see Table 5.10).

Complex	Dihedral Angle
[*o*-$C_6H_4(CH_2PBu^t_2)_2Pd(COC_2H_5)(Cl)$]	24.5
[*o*-$C_6H_4(CH_2PBu^t_2)_2Pd(Cl)_2$].dcm	7.9
[*o*-$C_6H_4(CH_2PBu^t_2)_2Pd(Cl)_2$]	20.8
[*o*-$C_6H_4(CH_2PBu^t_2)_2$ Pd $(OH_2)_2]^{2+}$ 2[OTs]$^-$	0.8
[*o*-$C_6H_4(CH_2PBu^t_2)_2$ Pd $(OH_2)_2]^{2+}$ 2[BF_4]$^-$	6.8
[*o*-$C_6H_4(CH_2PBu^t_2)_2Pd(O)_2$]	4.7

Table 5.10 Comparison of Dihedral Angles P_2Pd/PdX_2 Palladium(II) Complexes of (1)

5.8.6 Deuterium Labelling Studies

5.8.6.1 Experimental

1. [(L-L)Pd(dba)] + $MeSO_3H$ + CO/ethene + CH_3OD

A typical catalyst solution is made up as follows: The pre-catalyst Pd[L-L]dba (1.36 x 10^{-4} moles) was weighed into a 100ml round bottomed flask in a nitrogen filled glove box. The flask was then removed and connected to a standard vacuum/nitrogen line where CH_3OD (30 ml) was added. The methanol was degassed prior to addition to eliminate oxygen. The acid methanesulphonic acid (0.065g, 6.8 x 10^{-3} moles) was added and the catalyst solution immediately transferred to the nitrogen flushed autoclave. In each experiment, after addition of the reaction solution, the autoclave was heated to 80°C. When at temperature, the autoclave was opened to a cylinder containing a 1:1 mixture of carbon monoxide and ethylene at a pressure of 10bar. The reaction time in this series of experiments was kept at a constant 1 hour. At the end of the reaction the solutions were removed from the autoclave and analysed by ^{13}C NMR. The results are presented below in Table 5.11.

2. $[(L\text{-}L)Pd(OH_2)_2]^{2+}$ 2 $[(OTs)]^-$ + CO/ethene + CH_3OD

The experiment was carried out as described above with $[(L\text{-}L)Pd(OH_2)_2]^{2+}$ 2 $[(OTs)]^-$ (1.36 x 10^{-4} moles) being used in place of [(L-L)Pd(dba)]. The reaction solution was analysed by ^{13}C NMR and the results are presented also in Table 5.11.

3. [(L-L)Pd(dba)] + Oct-1-ene + $MeSO_3H$ + CH_3OD

The catalyst Pd[L-L]dba (1.36 x 10^{-4} moles) was weighed into a 100ml round bottomed flask in a nitrogen filled glove box. The flask was then removed and connected to a standard vacuum/nitrogen line where degassed CH_3OD (30 ml) and oct-1-ene (10ml) were added. The acid, methanesulphonic acid (0.065g, 6.8 x 10^{-3} moles) was added and the catalyst solution immediately transferred to the nitrogen flushed autoclave. The reaction solution was then heated to 80°C and held at this temperature for 1 hour, before cooling and analysis by ^{13}C NMR. The solution removed from the autoclave showed no evidence for catalyst decomposition with no palladium metal evident.

Deuterated Methyl Propionate Isomer	[(L-L)Pd(dba)] + CO/ethene + 5$MeSO_3H$ + CH_3OD	$[(L\text{-}L)Pd(OH_2)_2]^{2+}$ 2 $[(OTs)]^-$ + CO/ethene + CH_3OD
$CH_3CH_2COOCH_3$ **(1)**	27%	32%
$CH_3CH\mathbf{D}COOCH_3$ **(2)**	16%	19%
$CH_3C\mathbf{D_2}COOCH_3$ **(3)**	0.5%	<0.5%
$CH_2\mathbf{D}CH_2COOCH_3$ **(4)**	23%	28%
$CH_2\mathbf{D}CH\mathbf{D}COOCH_3$ **(5)**	19%	13%
$CH_2\mathbf{D}C\mathbf{D_2}COOCH_3$ **(6)**	0.5%	<0.5%
$CH\mathbf{D_2}CH_2COOCH_3$ **(7)**	6%	4%
$CH\mathbf{D_2}CH\mathbf{D}COOCH_3$ **(8)**	10%	4%

Table 5.11 Distribution of Deuterium in Methyl Propionate Formed in CH_3OD

Product	[(L-L)Pd(dba)] + 5 $MeSO_3H$ + Oct-1-ene + CH_3OD
Oct-1-ene	<5%
Oct-2-ene *cis* and *trans*	40%
Oct-3-ene *cis* and *trans*	40%
Oct-4-ene	15%

Table 5.12 Results of Oct-1-ene Isomerisation using [(L-L)Pd(dba)] + 5 $MeSO_3H$ + Oct-1-ene + CH_3OD

5.8.6.2 Discussion

The results of the deuterium labeling experiments are represented in Table 5.11 and 5.12, they reveal several interesting features.

1. The major product is methyl propionate with no incorporated deuterium. This is very surprising given that in both the hydride and methoxycarbonyl mechanisms, the methanol proton is incorporated into the MeP via the termination process. Therefore, performing the reaction in 100% CH_3OD should give rise to at least one deuterium per MeP molecule. The presence of 30% non-deuterated MeP can be explained by the mechanism illustrated in Figure 5.4 below, where 1) coordination and dissociation of ethene, and 2) insertion of ethene into a palladium hydride, and the reverse β elimination process, are all very rapid reactions. The methoxycarbonyl mechanism can be ruled out due to the absence of unsaturated products, which would be expected if the alkene exchange and ethene insertion/ β elimination process were occurring via a methoxycarbonyl intermediate. An alternative to the above mechanism involves rapid H/D exchange between the palladium deuteride formed as a result of hydride mechanism termination and possibly a) water present in the acid or methanol or b) MeOH built up as a result of H/D exchange between CH_3OD and palladium hydride. This would result in the formation of a palladium hydride which would give non-deuterated MeP on following the hydride cycle. It is unlikely that the acid is the source of the protons which exchange with the palladium deuteride as the catalyst turnover in both examples is in excess of 2000 turnovers per palladium and we have only added 5 equivalents of HX per palladium If the insertion/β elimination process and the H/D exchange is very rapid then we can envisage building up significant MeOH levels. The CH_3OD is not felt to contain appreciable levels of water as no propionic acid is detected by GC analysis of the reaction solutions. This would be expected if water was present.

2. Widespread incorporation of the deuterium label has occurred on the ethyl fragment of the MeP molecule, including double and triple deuterium atoms per molecule. As for the synthesis of non-deuterated product this can only be explained on the basis of an extremely rapid ethene insertion/β elimination process. The formation of these products is illustrated in the Figure 5.4 below. Clearly, it is extremely complex to illustrate all of the

possible routes to each identified product. Some of the products have more than one route of formation and this will influence the amounts detected.

3. Initiating the catalysis from a palladium zero source with added acid, or starting from a palladium(II) source in the absence of added acid, leads to very little difference in the product spectrum. Whilst there are small differences in some cases, the same range of products is formed in both examples. This suggests that the same mechanism is in operation in both cases.

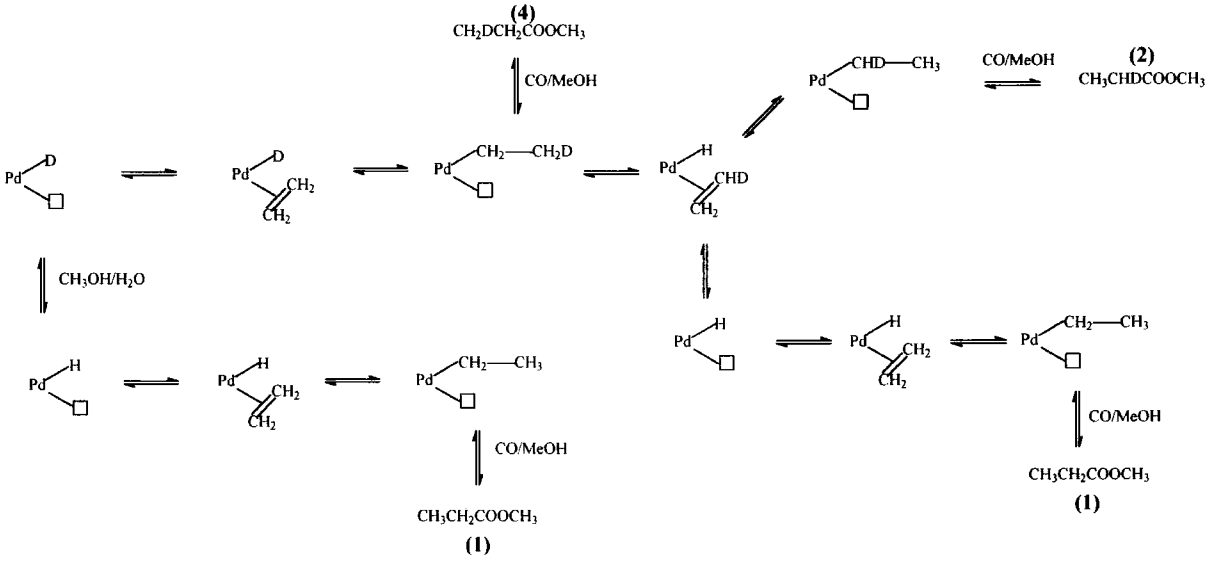

Figure 5.4 Suggested Mechanism for the Formation of the Major Products in Deuterium Labelling Studies

Considering Figure 5.4 above, the starting point on the left assumes that the hydride cycle is terminated by methanolysis with CH_3OD and a palladium deuteride is formed. This then has two reaction pathways, firstly it can undergo H/D exchange to form a palladium hydride which can then coordinate ethene and go once around the hydride cycle to liberate non-deuterated MeP **(1)** and a new palladium deuteride. Secondly the palladium deuteride can react itself in the hydride cycle, initially by coordination and insertion of ethene. The alkyl fragment resulting from insertion of ethene into the palladium deuterium bond also has

two reaction pathways open to it. Insertion of CO followed by methanolysis leads to the formation of **(4)** whilst β elimination now generates a palladium hydride. This new palladium hydride is a key intermediate in explaining the product spectrum in these reactions and is discussed further with reference to Figure 5.4. It can insert ethene in one of two ways to give either the original palladium alkyl or a new palladium alkyl in which the deuterium label is now on the carbon adjacent to the metal. Insertion of CO and methanolysis of this species leads to the formation of **(2)**. It is also possible that alkene exchange can occur and this would lead to the formation of non-deuterated MeP by an alternative route to that involving H/D exchange. It is plausible that this route contributes to the formation of **(1)** but given the number of steps in the reaction scheme it is unlikely to be the major route of formation.

The above diagram can then account for three of the major reaction products detected in the deuterium labeling study. If we count the minimum number of reaction steps to give each product, we find that the major species **(1)** is formed via 4 steps and the second most abundant species **(4)** is formed from only 3 steps. We can rationalize this by postulating that the H/D exchange reaction must be very fast and also that if MeOH is building up in the system as a result of H/D exchange then termination of the hydride cycle with MeOH will be competing with MeOD and thus a palladium hydride will result which then gives **(1)** via only 3 steps. The kinetic isotope effect then has an influence with the relative rates being influenced by the presence or absence of deuterium in the alkyl fragment. The shortest route to the third product **(2)** is from 5 steps or one β elimination/ reinsertion cycle more than the proposed scheme for **(4)** and the reduced yield of this species is consistent with this more involved pathway.

The reduced yield of **(5)** can also be rationalised in this way, with the shortest pathway involving six steps one of which is H/D exchange. If as seems reasonable we conclude that H/D exchange is extremely rapid then the route to **(5)** is similar to the route to **(2)** with both involving two β elimination/ re-insertion cycles.

The second diagram Scheme 5.5 can be used to explain the formation of the remainder of the products, which can all be rationalised as a result of a series of β

elimination/ re-insertion cycles and H/D exchange reactions. It is interesting to note the reduced yield of **(7)** relative to **(5)** which results from two β elimination/ reinsertion cycles and one H/D exchange similar to the formation of **(5)**. Furthermore the yield of **(8)** seems higher than the proposed route involving three β elimination/ reinsertion cycles and two H/D exchanges would suggest. There is literature precedent for the kinetic selection of palladium alkyls,[23] where carbonylation rates differ depending on the regio chemistry of the palladium alkyls. It is possible in this system that carbonylation rates of the different palladium alkyls differs sufficiently to have an effect on the product distribution. Clearly for the formation of **(8)**, the kinetic isotope effect would work against its formation in the observed higher yields, so we require an alternative explanation for the increased yields.

Work on the carbonylation of alkynes[24] has shown that H/D exchange between MeOD and alkynes in the presence of ($Pd(OAc)_2/PPh_2Py/CH_3SO_3H$) is a rapid reaction and has been invoked to account for the products formed.

We have not made any assumption about the reversibility of the CO insertion step as this would only serve to complicate the discussion. It is felt that the CO insertion is not readily reversible i.e. termination is rapid, consistent with the high selectivity to MeP observed and that the alkyl fragments are trapped on coordination and insertion of CO. If this were in fact the case we would expect the ratios of deuterated products and the reaction rates to be influenced by the pressure of CO in the reaction. It is known that the CO pressure does have an influence on the absolute reaction rate, but the labelling experiment has not been repeated at different CO pressures.

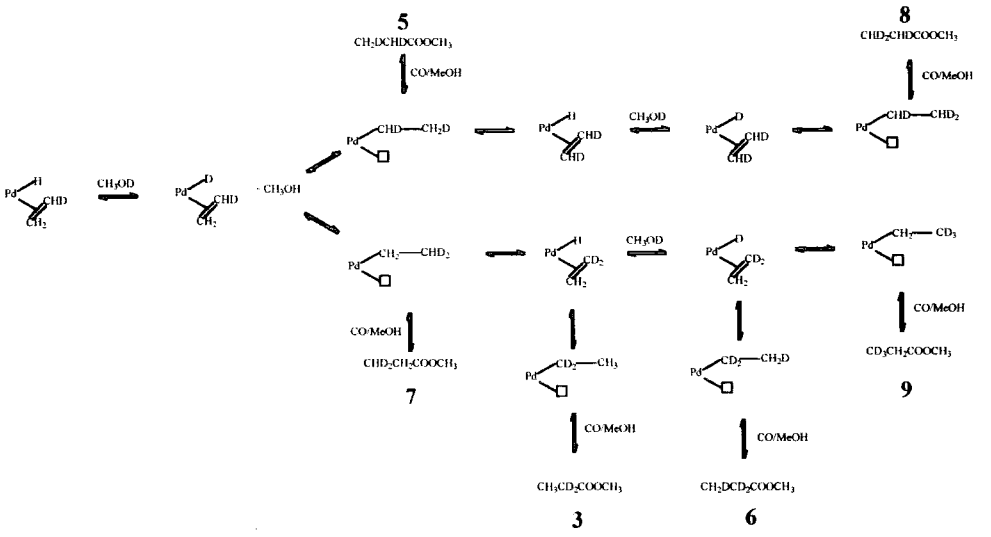

Scheme 5.5 Mechanism of Formation of Deuterium-Labelled MeP Isomers

The similarity of products formed using the acid free system is interesting as it indicates that the catalyst has a route to palladium hydrides which does not involve added acid. Reviews of the co-polymerisation catalysis postulate several routes to palladium hydride including water gas shift reactions and methanol oxidation.[25] Whilst we are unable to say anything about the route to the hydride, it is clear that they are present in the catalyst solution. The use of Pd(II) salts in the absence of acid has been established as a viable option for the initiation of co-polymerisation catalysis and it is widely speculated that these catalysts operate, at least in part via the methoxycarbonyl mechanism, where initiation is by initial attack of methanol at the Pd(II) centre. These results suggest that for this system, the formation of a palladium hydride is the preferred pathway. In the carbonylation of alkynes studied by Scrivanti the protonation of palladium(0) alkyne complexes is proposed as the hydride forming step. It is not unreasonable to assume the involvement/formation of Pd(0) species in the catalytic cycle, since it has been shown that $Pd(OAc)_2$ in the presence of an excess of tertiary phosphines and/or protic solvents(water or alcohols) gives Pd(0) species.

5.8.6.3 Isomerisation of Oct-1-ene

The Table 5.12. details the results of stirring oct-1-ene with a standard catalyst solution {[(L-L)Pd(dba)] + 5 CH_3SO_3H + MeOD}. It is evident that the catalyst is able to

isomerise oct-1-ene to a mixture of isomers. The formation of a mixture of internal isomers is not surprising with <5% oct-1-ene present after 1 hour at 80°C. In the presence of CO the carbonylation of oct-1-ene occurs to give mainly methylnonanoate, the result of carbonylation of the linear oct-1-ene.[26] A small amount of the iso product resulting from 2,1 insertion of the alkene into a palladium hydride is also formed, but no carbonylation products resulting from carbonylation of any of the internal alkenes are observed. These results are consistent with the series of reactions illustrated in Scheme 5.6. The rate of carbonylation of oct-1-ene is much greater than for the other octene isomers. Thus what is present reacts rapidly, thereby disturbing the equilibrium. This means that as the oct-1-ene reacts, more is produced, until all of the alkene is consumed.

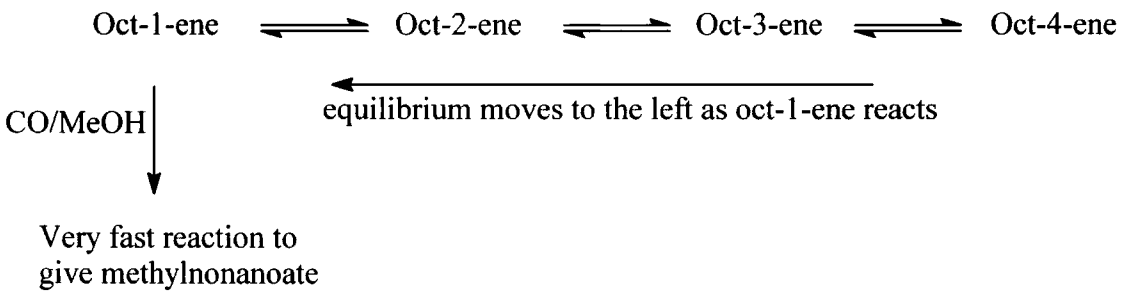

Scheme 5.6

One feature of this reaction which is interesting is the absence of deuterium label in any of the octene isomers. We have seen in the previous section that [(L-L)Pd(dba)] + $MeSO_3H$ + CO/ethene + CH_3OD results in the formation of several MeP isomers. The deuterium labelling in the MeP can only be rationalised by invoking the presence of palladium hydride, rapid alkene insertion/β-elimination reactions and rapid H/D exchange between metal hydride and CH_3OD. One possible explanation for this result is that the isomerisation of oct-1-ene is occurring via metal-allyl intermediates as shown in Scheme 5.7. This may have important implications for the catalysis as a whole because the alkene isomerisation via metal-allyl species involves formal oxidation/reduction of the metal centre and implies the presence of palladium(0) species.

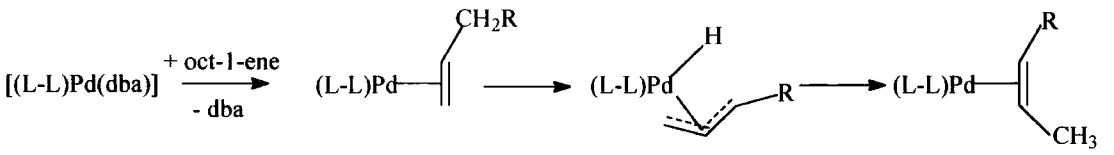

Figure 5.7

The last step in this mechanism is a reductive elimination to give a palladium(0) alkene complex and therefore we do not have metal hydride adjacent to η^2 alkene or a vacant site, which is a key intermediate in the proposed H/D exchange mechanism discussed above. However the results of this study (Chapter 4) and the work of Spencer have shown that palladium(0) complexes of the type [(L-L_Pd(η^2-alkene)] react with acid to give palladium(II) hydride/alkyl complexes, we might therefore anticipate octene isomerisation via a Pd(II) mechanism.

It should be remembered that the formation of allyl complexes is not possible in the CO/ethene system and also reaction to give MeP is occurring rapidly. The isomerisation of octene is studied here without the complication of ester formation occurring. It is known that the reduction of palladium hydride or many palladium(II) complexes can occur in methanol. It therefore seems reasonable that this could be occurring in this system in the absence of CO. The palladium(0) formed might then be intercepted by octene and the isomerisation process initiated. Thus alkene isomerisation via allyl intermediates is occurring in the absence of methoxycarbonylation activity and would likely be minimal in the presence of CO.

5.9 References

1. I. Toth, C. J. Elsevier, *J. Chem. Soc. Chem. Comm.* **1993**, 529.
   I. Toth, C. J. Elsevier, *Organometallics,* **1994**, 13, 2118.
   I. Toth, C. J. Elsevier, *J. Am. Chem. Soc.,* **1993**, 115, 10388.
   M. Portnoy, D. Milstein *Organometallics,* **1996**, 15, 5196.
   V. Grushin, *Chem. Rev.* **1996**, 96, 2011.
2. G. R. Eastham and R. P. Tooze ICI Internal report.
3. P. J. Stang, D. H. Cao, G. T. Poulter and A. M. Arif, *Organometallics*, **1995**, 1110.
   F. Benetollo, R. Bertoni, G. Bonbieri, L. Toniolo, *Inorganica Chemica Acta*, **1995**, 223, 5.
   J. Brown, *Angew. Chem. Int. Ed* **1996**, 35, 657.
4. I. Toth, C. J. Elsevier, *J. Chem. Soc. Chem. Commun.* **1993**, 529.
5. P. J. Stang, D. H. Cao, G. T. Poulter and A. M. Arif, *Organometallics,* **1995**, 1110.
6. R.H. Crabtree, *The Organometallic Chemistry of Transition Metals*, J. Wiley & Sons, New York
7. P. M. Maitlis, P. Espinet, M. J. H. Russell *Comprehensive Organometallic Chemistry 1, section 38.2, Complexes of Palladium(0)*
   E. C. Neiderhoffer, J. H. Timmons and A. E. Martell; *Chem Rev* **1984**, 84, 137 and references therein.
   J.P. Collman, L.S. Hegedus, R.G. Norton and R.G. Finke, *Principles and Applications of Organotransition Metal Chemistry*, University Science Books, Mill Valley (CA) USA,1987.
   J. S. Valentine, *Chem Rev*, **1973**, 73, 3, 235 and references therein.
8. C. Amatore, G. Broeker, A. Jutand and F. Khalil, *J. Am. Chem. Soc.*, **1997**, 119, 5176.
9. J.P. Collman, L.S. Hegedus, R.G. Norton and R.G. Finke, *Principles and Applications of Organotransition Metal Chemistry*, University Science Books, Mill Valley (CA) USA,1987.
10. T. Kashiwage, N. Yasuoaka, N. Kasai, M. Kakudo, S. Takahashi, N. Hagihara; *J. Chem. Soc. Chem. Comm.,* **1969**, 743.

11. J.P. Collman, L.S. Hegedus, R.G. Norton and R.G. Finke, *Principles and Applications of Organotransition Metal Chemistry*, University Science Books, Mill Valley (CA) USA,1987.

J. S. Valentine, *Chem. Rev.*, **1973**, 73, 3, 235 and references therein.

12. S Zacchini, PhD Thesis Interim Report

13. M. Kranenburg, J. G. P. Delis, P. C. J. Kamer, P. W. N. M. van Leeuwen, K. Vrieze, N. Veldman, A. L. Spek, K. Goubitz and J. Fraanje, *J. Chem. Soc. Dalton Trans.*, **1997**, 1839 and references therein.

14. B. Milani Poster and Presentation; *11th International Symposium On Homogeneous Catalysis.* **1998**.

B. Milani, *J. Chem. Soc. Dalton. Trans.*, **1994**, 1903.

B. Milani, J. Chem. Soc. Dalton. Trans., **1996**, 3139.

15. J. S. Valentine, *Chem. Rev.*, **1973**, 73, 3, 235.

16. R. W. Horn, E. Weissberger and J. P. Collman; *Inorg. Chem.* 9, 10, 2367.

17. K. Shobatake and K. Nakamoto; *J. Am. Chem. Soc.*, **1970**, 92, 3332.

18. G. R. Eastham and R. Robertson; Industrial placement report.

19. K. Nakamoto; *Infrared and Raman Spectra of Inorganic and Coordination Compounds* 4th Ed. Ch. 3, p232.

D. Stoilova, G. Nikolov and K. Balavar; *Izv. Nauk; SSSR; Ser Khim.* **1976**, 9, 371.

20. R. F. Heck *Org. React.*, **1982**, 27, 345.

21. P. K. Byers, A. J. Canty, B. W. Skelton and A. H. White, *J. Chem. Soc. Chem. Comm.* **1986**, 1722.

22. K. Francombe, K. Cavell, R. Knott and B. Yates; *J. Chem. Soc. Chem. Comm.* **1996**, 781.

23. K. H. Shaughnessy and R. M. Weymouth; *Organometallics*, **1997**, 1001.

24. A. Scrivanti, V. Beghetto, E. Campagna, M. Zanato and U. Matteoli; *Organometallics*, **1998**, 17, 4, 629.

25. E. Drent and P.H.M. Budzelaar, *Chem. Rev.*, **1996**, 96, 663-681.

26. P. Davies ICI Internal report.

CHAPTER 6.0

Mechanistic Conclusions

6.1 Introduction

The background to this study, as mentioned in the introduction, is the surprising difference in activity and selectivity of palladium catalysts based on certain alkyl substituted bidentate phosphine ligands patented by I.C.I. and Shell respectively when compared to the catalyst systems based on 1,3-bis(diphenylphosphino)propane. In the former case we observe very active catalysts with >99% selectivity for MeP in the methoxycarbonylation of ethene. In the latter, the patent literature describes active catalysts which are highly selective for the synthesis of high molecular weight ethene/CO co-polymers under the same conditions.

The purpose of this final chapter is to draw together a unifying mechanism which explains the exceptional activity and selectivity of catalysts based on 1,2-bis(di-*tert*-butylphosphinomethyl)benzene. Reference will be made to the relevant chapters but supporting arguments will not be repeated.

In order to explain the performance of the catalyst, nomenclature from the study of polymerization is thought to be useful, and the steps of the catalytic cycle are categorised as

1. Initiation
2. Propagation
3. Termination

These will be discussed in turn.

6.2 Initiation

The first point to note is the observation reported in Chapter 2 that the catalyst formed by treating the dba complex **(12)** with sulphonic acid results in the highest initial activities. The rationale for this is illustrated in Scheme 6.1 where the product of reaction between **(12)** and methanesulphonic acid is thought to have a facile route into the hydride cycle. In chapter 4 NMR evidence is presented to support the formation of an η^3-benzyl species from the reaction of the η^2-alkene complexes with acid . It is believed that this η^3-benzyl species offers a route into the preferred hydride cycle via the equilibrium with the η^1-complex. For less sterically demanding phosphines this equilibrium is shifted in favour of the η^3-complex. Others have reported on the inert nature of η^3-benzyl complexes of less hindered bidentate phosphine palladium complexes.[1]

The benzoquinone complex **(27)** on the other hand leads to lower initial rates and total turnover numbers. The reaction of this complex with methanesulphonic acid is clearly shown in chapter 4 to lead to the formation of the bis-sulphonate complex $[(L\text{-}L)Pd(OSO_2Me)_2]$ (or solvent adduct), which is a recognised point of entry into the methoxycarbonyl cycle. There is, however, no evidence for the formation of a stable methoxycarbonyl species or for the formation of MeP via a methoxycarbonyl mechanism. Deuterium labeling studies, discussed in chapter 5 indicate the same spectrum of deuterium containing products irrespective of whether the dba complex **(12)** activated with sulphonic acid or the Pd(II) complex $[(L\text{-}L)Pd(OH_2)_2]^{2+}$ $2[OTs]^-$, with no added acid, is used as the catalyst source. These products are all rationalised with reference to the hydride cycle. Furthermore, the absence of any unsaturated product (methyl acrylate) which would be anticipated if ethene insertion via a methoxycarbonyl cycle were occurring supports the theory that MeP is being produced exclusively via the hydride cycle with the 1,2-bis(di-*tert*-butylphosphinomethyl)benzene based catalyst.

This is clearly not the case for the catalysts which lead to the formation of high molecular weight co-polymers. Those catalysts which give rise selectively to co-polymer are most active when fed as the benzoquinone complex **(31)** with sulphonic acid. This leads to the formation of the bis sulphonate complex, which as stated previously, is the classic

methoxycarbonyl precursor (see mechanism in introduction). In these examples analysis of the product by MALDI-TOF mass spectrometry provides clear evidence for the methoxycarbonyl cycle (diester endgroups).

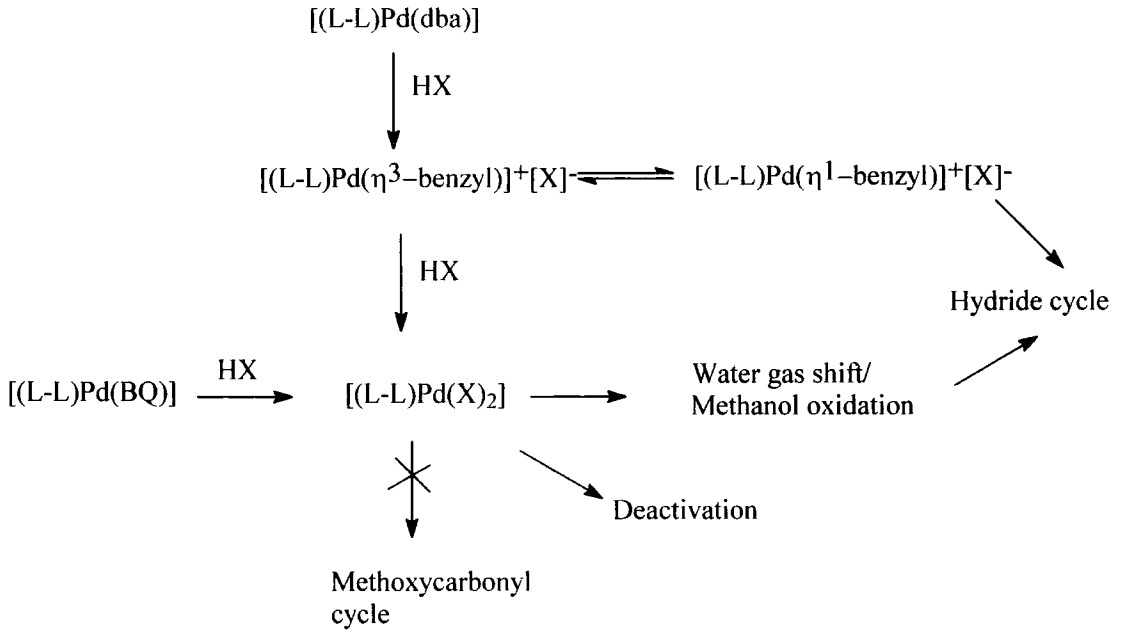

Scheme 6.1
Activation Of Precatalyst Complexes And Routes Into Catalytic Cycle

Several possibilities exist for the apparent insignificance of the methoxycarbonyl cycle, these include

1. The electrophillicity of the metal centre may favour an alternative reaction pathway, with methanol oxidation to give hydride and formaldehyde occuring in preference to methoxycarbonyl formation. Milstein[2] has shown evidence for the formation of a palladium hydride with methanol as the hydride source from palladium (II) complexes of 1,3-bis(di-*iso*-propylphosphino)propane. It seems reasonable to suggest that this reaction may be favoured for electron rich dialkyphosphines.

2. The catalyst methoxycarbonyl species formed are inactive or unstable. In the work of Brookhart et al using bidentate nitrogen ligands for the formation of ethene/CO co-polymers, the species $[(N\text{-}N)Pd(COOR)(CO)]^+ [X]^-$ is identified as the catalyst resting

state.[3] Complexes of this type are possible with 1,2-bis(di-*tert*-butylphosphinomethyl)benzene but may, due to the high *trans* effect of the CO and methoxycarbonyl ligands, lead to catalyst decomposition. Also possible is the stability of these complexes to product formation, perhaps because of the steric congestion imposed by the bulky phosphine ligand.

3. The initial palladium methoxide is not stable, leading to monodentate protonated phosphine and possibly catalyst decay. Consequently the required methoxycarbonyl intermediate is not formed (see scheme 6.2)

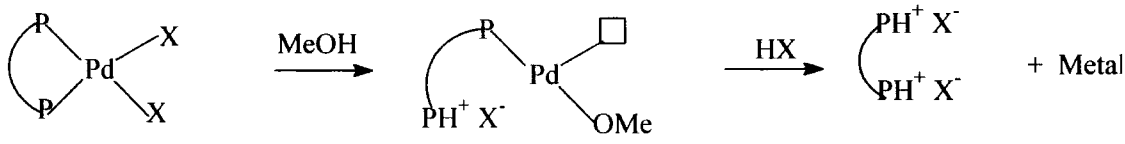

Scheme 6.2

6.3 Propagation

The first question which needs to be addressed is the high activity of catalysts based on the ligand 1,2-bis(di-*tert*-butylphosphinomethyl)benzene. We observe initial rates in excess of 50,000 moles MeP/mole Pd/hr for the styrene complex **(26)**. This compares to rates of < 1000 moles CO/ethene consumed/mole Pd/hr for the co-polymerisation catalysts reported in this thesis. Two possibilites are considered likely.

1. The ^{31}P NMR study of the reaction of **(12)** with sulphonic acid indicates quantitative conversion of the alkene complex to the benzyl. It is envisaged then that all of the catalyst is rapidly converted to a reactive intermediate and in the absence of mass transfer limitations produces MeP. The concentration of catalytically active palladium in the co-polymerisation catalysis is not clear but it is not thought to be as efficiently activated.

2. The work of Hoffman describes theoretical modelling studies where the optimum phosphine ligand bite angle is determined for insertion reactions at square planar platinum and palladium complexes. This angle is in the range 105-115^0. From this work and the

experimental studies of other workers there is clear evidence that the rate of insertion reactions is influenced by the bite angle of the phosphine ligand. At its most simplistic level the reason for this is that increasing the P-Pd-P bite angle forces together the reacting groups on the other face of the metal centre. This argument can be used to explain the very high activities of catalysts based on 1,2-bis(di-*tert*-butylphosphinomethyl)benzene and also the difference in activity observed for the 1,3-bis(di-*tert*-butylphosphino)propane based catalyst. In this latter catalyst the bite angle determined from analysis of single crystal X-ray data is some 3-4^0 less and this may well account for the lower rates observed.

The activity of triphenylphosphine based catalysts is also discussed in chapter 3 with reference to the large bite angle (115^0) observed in the complex **(22)**. It is suggested that the catalytic activity of TPP based catalysts results from a low concentration of a very highly active species. The high activity of this species results from the rapid insertion reactions thought to be made possible by the large bite angle in these *cis* phosphine complexes. The implication of this is that it may be possible to develop catalysts based on more stable aryl phosphines which have large bite angles.

The second question to address when considering propagation is why are catalysts based on the ligand 1,2-bis(di-*tert*-butylphosphinomethyl)benzene so selective.

1. Analysis of single crystal X-ray data for a number of the palladium(0) pre-catalysts in chapter 3 of this thesis reveals a relationship between the in plane pocket angle and catalyst selectivity. In summary those catalysts selective for MeP have the smallest in plane pocket angles. This may be directly related to the accessibility of the dz^2 orbital, in that the pocket angle, below which we observe MeP selectivity is simply a measure of the cut off point at which the dz^2 orbital becomes inaccessible to incoming substrate.

2. The single crystal X-ray data studied in chapter 3 perhaps support an explanation involving restricted access to the dz^2 molecular orbital on the metal centre. Molecular modelling studies have indicated a role for five coordinate palladium complexes in the co-polymerisation reaction, in which the incoming substrate (CO/ethene) is coordinated to the fifth position before insertion occurs. Visual inspection of the crystallographic data for these complexes confirm the steric congestion above and below the metal centre where, the dz^2

orbital would be expected to be located. Those catalysts which give rise to co-polymer are not similarly congested in this region.

6.4 Termination

If the hydride cycle is operating, then the termination reaction is methanolysis of an acyl complex. Two choices are possible; these are metal-mediated and non metal-mediated and possible mechanisms are illustrated in scheme 6.3. The above two termination steps cannot be distinguished on the basis of reaction products.

The evidence of this study indicates that phosphine labilisation may be important. This is implicated by three pieces of evidence.

1. Firstly the MeP selective catalysts analysed as palladium(0) complexes have the largest dihedral angles, a possible indication of steric congestion.

2. Further evidence for the idea of phosphine labilisation as a part of the catalytic cycle comes from an analysis of the palladium acyl chloride complex which has been isolated and discussed in chapter 4 of this thesis. The Pd-P bond *trans* to the acyl ligand is 2.48Å in length, a very long Pd-P bond, and its relevance is discussed in more detail in chapter 5.

3. Detailed inspection of the palladium phosphorus bond lengths reveals a trend with the most sterically demanding and most basic phosphines 1,2-bis(di-*tert*-butylphosphinomethyl)benzene and 1,4-bis(di-*tert*-butylphosphino)butane, leading to complexes having the longest palladium phosphorus bond lengths. Within the ortho-xylene derived phosphines, as we decrease steric bulk and decrease electron donation, we see a shortening of the palladium phosphine bond. Thus we observe a difference of 0.07 Å between the *tert*-butyl complex **(12)** and the phenyl complex **(18)**. It is noteworthy that the catalytic selectivity of catalysts based on these two complexes is very different, with the longest Pd-P bonds present in the MeP selective catalyst. Also noteworthy is the selectivity of catalysts based on the complexes **13** and **14**, where both MeP and co-polymer are produced and the Pd-P bond lengths are intermediary between those of active MeP catalysts and active co-polymerisation catalysts.

The implication is that phosphine labilisation is required for MeP selectivity and that, in the absence of this labilisation, the catalysts are either inactive or make only co-polymer. Put another way, rigid chelates are required for co-polymer formation and the breakdown of the chelate ring allows chain termination to occur readily. The mechanism of this catalysis is a subtle, but significant, modification of that already proposed by Drent et al[5] to explain the difference in selectivity between catalysts based on monodentate and bidentate phosphine ligands (see introduction). Here it is suggested that labilisation of the phosphine does not drive an isomerisation of the complex, and thus favour termination over propagation, but is an intimate part of the termination process.

Taking all of the above into consideration, a mechanism involving phosphine labilisation as the selectivity-determining step in the catalysts is proposed. This is illustrated in Figure 6.3 for the hydride mechanism. The nature of the phosphine backbone is an important consideration in designing new palladium phosphine catalysts for MeP synthesis. We require one arm of the chelate to dissociate without complete dissociation of the ligand. One factor which is important is the flexibility in the ligand backbone which ideally limits the distance which the labilised arm moves away from the metal, thus allowing a facile recoordination. It is suggested that this may contribute to the explanation of the difference in activity between the xylene based I.C.I. catalysts and the propane bridged Shell catalysts. On dissociation of the phosphine, the rigidity of the xylene backbone and the steric bulk of the *tert*-butyl groups limit the ability of the phosphorus lone pair to rotate away from the metal; consequently they can more easily re-coordinate to the metal. In support of this is the lack of activity observed for the catalysts based on 1,4-bis(di-*tert*-butylphosphino)butane and 1,8-bis(di-*tert*-butylphosphinomethyl)naphthalene (chapter 2), which have low in-plane pocket angles and long palladium phosphorus bonds indicative of active catalyt precursors. It is suggested that labilisation in these cases leads either to complete dissociation of phosphine or no recoordination to the metal. The butane bridged family of bidentate phosphines are known to prefer *trans* geometry in palladium(II) complexes, infact this is offered as an explanation by Drent and Budzelaar[6] to explain the lower activity of dppb versus dppp in the co-polymerisation reaction.

For co-polymerisation, phosphine labilisation is not required to occur after one insertion of ethene and CO, but only after hundreds or thousands of such events. Intuitively,

the situation where the palladium is ligated by only one phosphorus centre looks inherently unstable, and this appears consistent with the results presented in chapter 2 that co-polymerisation catalysts are more stable than MeP catalysts.

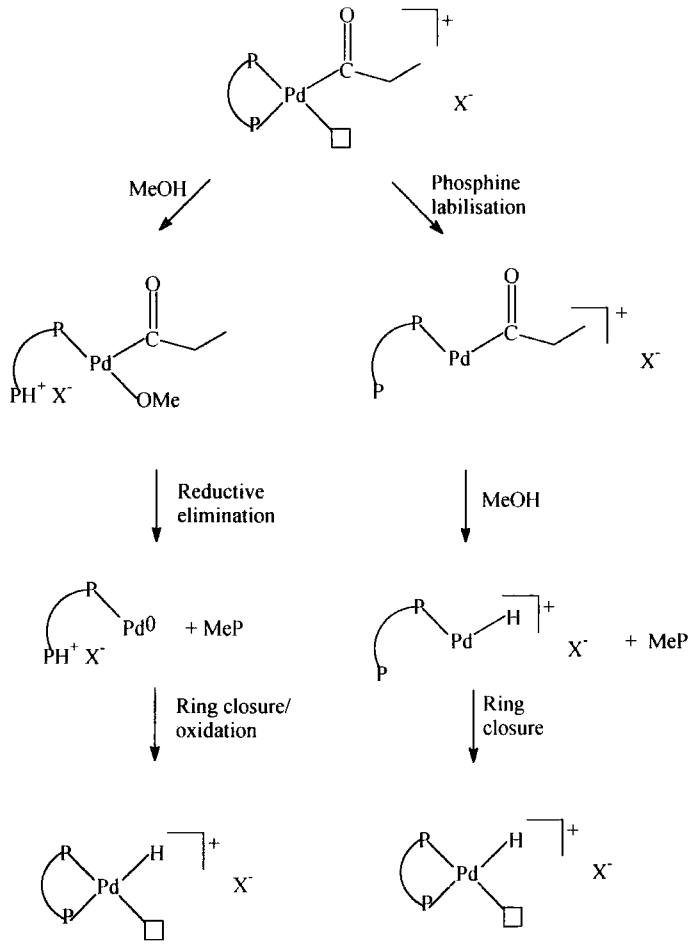

Scheme 6.3
Chain Termination Mechanisms in the Hydride Cycle Involving Phosphine Labilisation

The two mechanisms proposed are only suggestive of what may be occurring and clearly more work is required before either can be accepted. Several features of the mechanism are unknown. 1). Does the labilisation process take place independently of methanol attack? 2). Is the termination reaction involving methanol metal mediated? It can be envisaged as a non metal mediated attack at the δ +ve acyl carbon, leading to MeP and H^+. Equally it can be drawn as a metal mediated process involving transfer of the proton to either the metal centre or the labile phosphorus. 3). Does the recoordination step involve a Pd(0) or

Pd(II) metal centre? Re-coordination to a Pd(0) metal centre would clearly be a more favoured reaction given the coordination chemistry studied in Chapter 3 and 5, where the coordination to Pd(0) followed by oxidation is the favoured route to the generation of Pd(II) complexes of **(1)** .

In chapter 4, phosphine labilisation is found to occur in palladium(II) complexes of both 1,3-bis(di-*tert*-butylphosphino)propane and **(1)** independent of the presence of methanol. It is felt that the combination of steric bulk introduced by the presence of the tertiary butyl groups and the large bite angles found in complexes of these ligands, which are not ideal for Pd(II), lead to the labilisation. In the examples studied here with ancillary acetate ligands a facile route exists to thermodynamically more stable compounds in which *cis* geometry of the phosphines is no longer enforced. When the less sterically demanding ligand **(3)** is employed the complex, which has *cis* phosphines, is stable in solution for a period of days, indicating that phosphine labilisation with this ligand is a less facile process.

6.5 Stability

The stability to CO with respect to palladium metal formation, of co-polymerisation catalysts, reported in chapter 5, is easy to envisage in a catalytic cycle which maintains the chelate ring intact. Infact, the formation of stable complexes such as $[(L\text{-}L)Pd(CO)_2]$ is well known for dppp and other phosphine ligands known to catalyze the formation of co-polymer[7]. The instability of the catalysts derived from the dba complex **(12)** is not well understood . Here the phosphine ligand is recovered as the doubly protonated salt from both exposure to CO in the presence of acid and catalytic testing.

Three possible explanations are proposed, illustrated in Scheme 6.4.

1. The formation of complexes $[(L\text{-}L)Pd(CO)_2]$ which are unstable and rapidly decompose to palladium metal. The reduction of Pd(II) in this manner to give zerovalent carbonyl complexes is well documented. Infact complexes of the ligands **(2), (3), (8)** and dpephos used in this study, all give what have been identified as palladium(0) phosphine complexes on reaction with CO (chapter 5). With the aforementioned sterically undemanding phosphine ligands, these zerovalent complexes appear quite stable. It seems reasonable to

assume that the reaction pathway of Pd(II) complexes of **(1)** will be similar, and therefore that similar species are being formed, but are too short lived and rapidly decompose to palladium metal.

2. The formation of bimetallic complexes such as hydrido-carbonyl dimers which are themselves unstable. The formation of these compounds is well documented for phenyl and *iso*-propyl substituted bidentate phosphines (chapter 5). However there is literature precedent in the work of Spencer for the instability of bimetallic platinum complexes of **(1)** (Chapter 1).

3. Competition between phosphine ligand re-coordination and CO coordination at the available site in the coordination sphere of the metal. This may be part of the catalytic cycle or independent of catalysis possibly induced by CO.

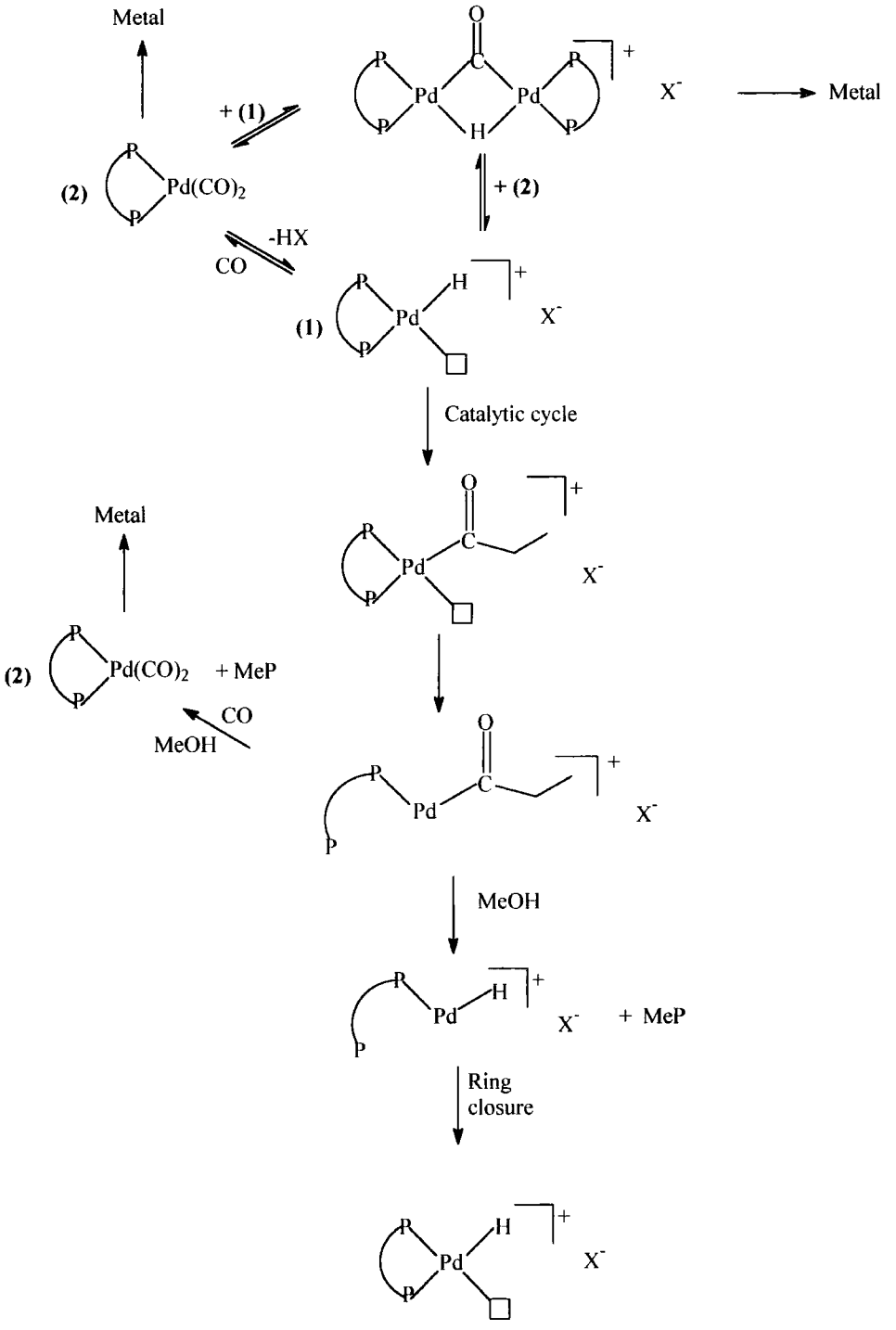

Scheme 6.4 Suggested Mechanisms for Catalyst Deactivation

6.6 References

1. E. Drent and P. H. M. Budzelaar, *Chem. Rev.*, **1996**, 96, 663.
2. M. Portnoy, F. Frolov and M. Milstein, *Organometallics,* **1991**, 10, 3960.
3. F. C. Rix and M. Brookhart; *J. Am. Chem. Soc.*, **1995**, 117, 1137.
4. D. L. Thorn and R. Hoffmann, *J. Am. Chem. Soc.*, **1978**, 2079.
5. E. Drent and P. H. M. Budzelaar, *Chem. Rev.*, **1996**, 96, 663.
6. E. Drent, J.A.M. van Broekhowen and M. J. Doyle, *J. Organomet. Chem.*, **1991**, 417, 235.
7. Chapter 4 and references therein.

APPENDIX 1

PICTORIAL REPRESENTATIONS OF SELECTED CRYSTALLOGRAPHIC DATA

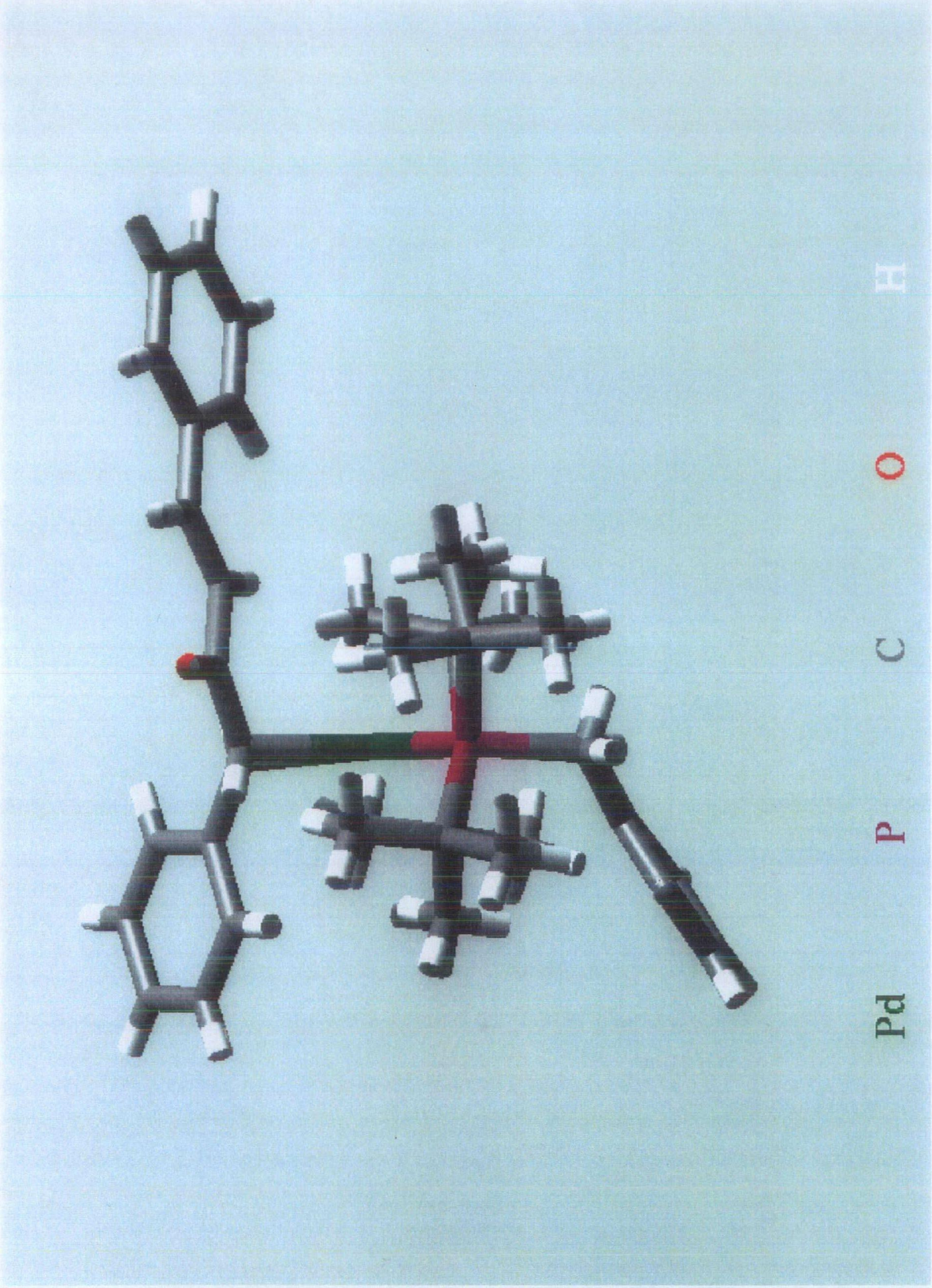

[*o*–$C_6H_4(CH_2PBu^t_2)_2Pd(dba)$] (12)

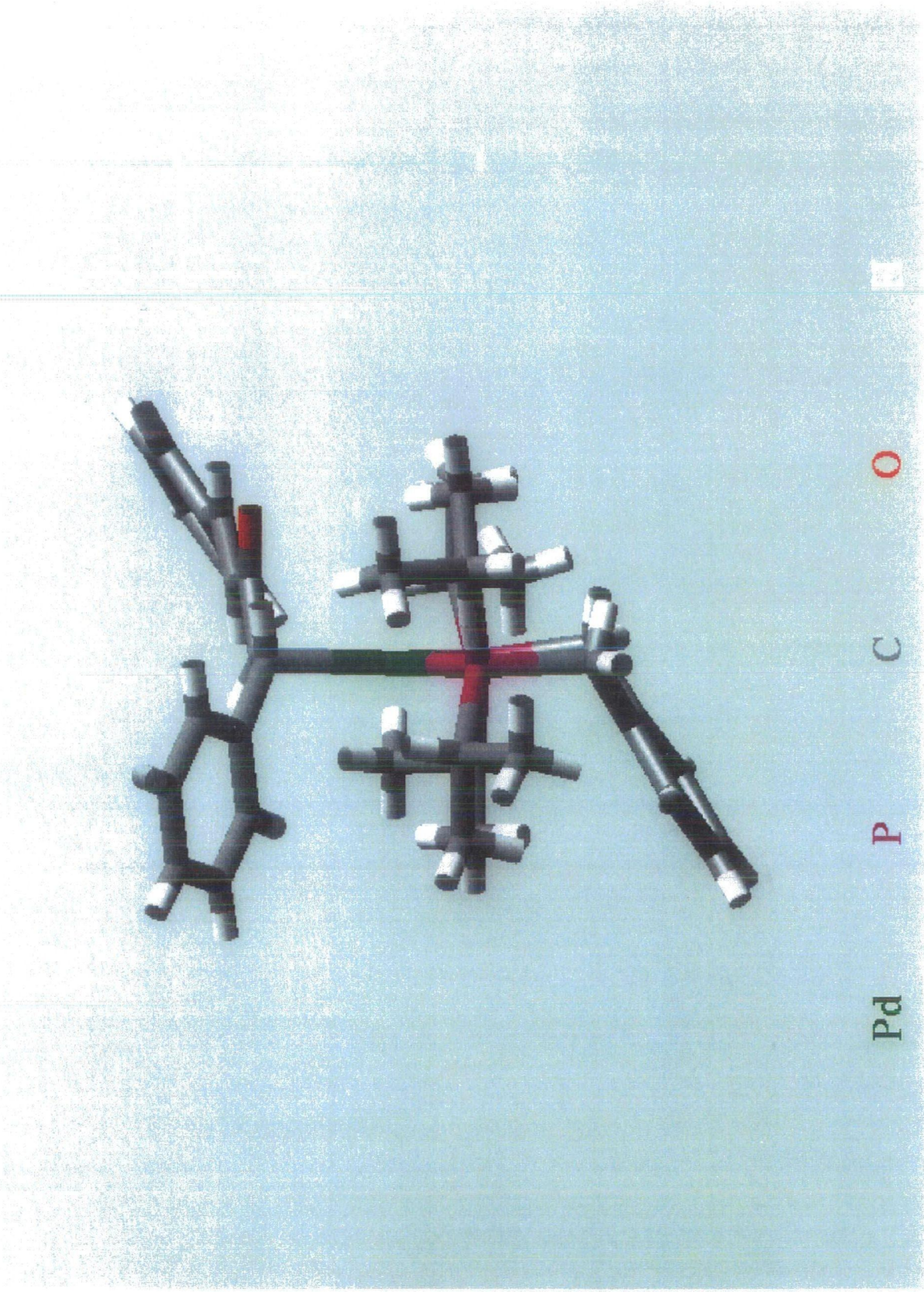

[*o*–$C_6H_4(CH_2PPr^i{}_2)_2Pd(dba)$] (13)

[*o*–$C_6H_4(CH_2PCy_2)_2Pd(dba)$] (14)

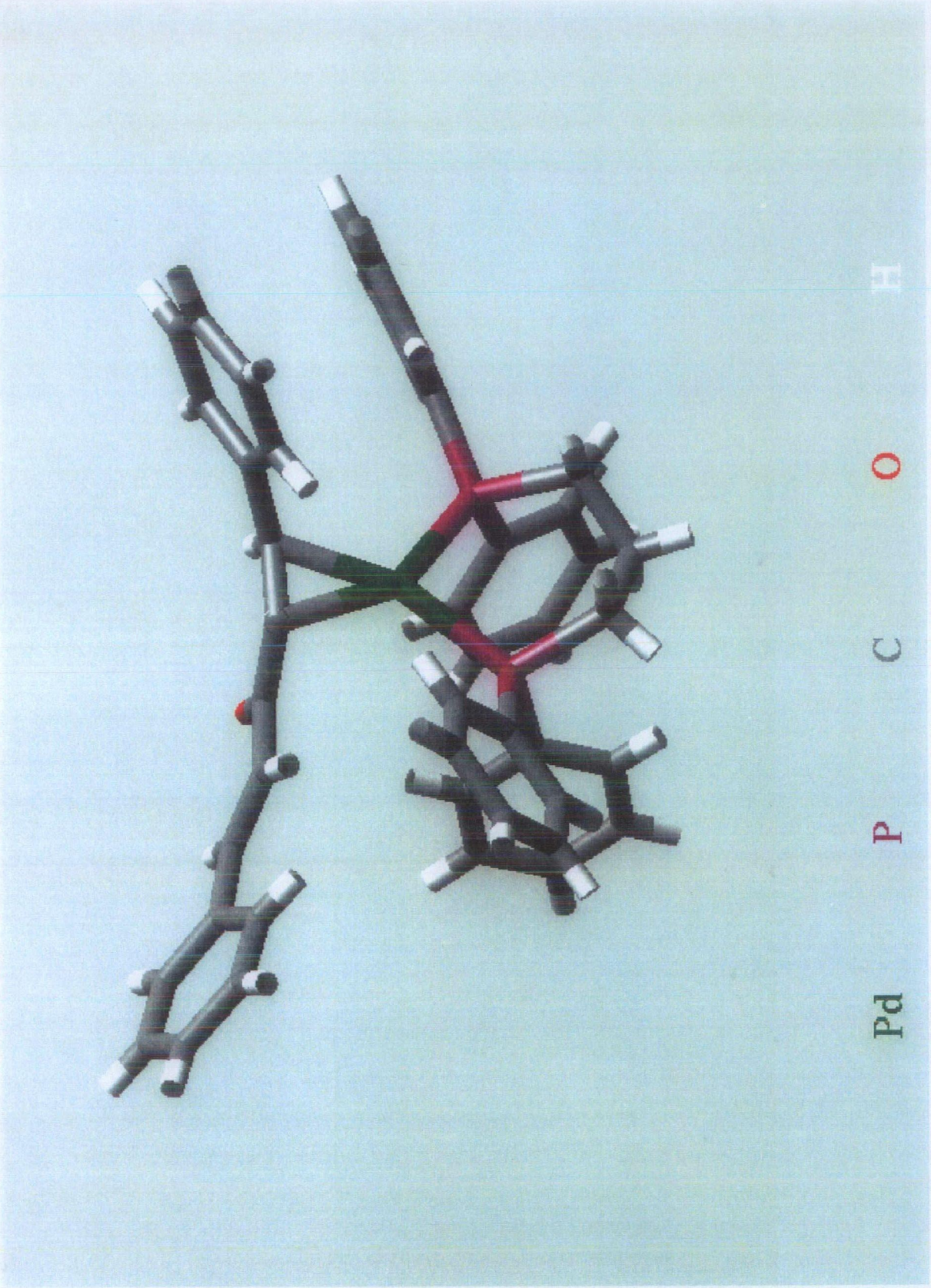

[1,3–$C_3H_6(PPh_2)_2Pd(dba)$] (21)

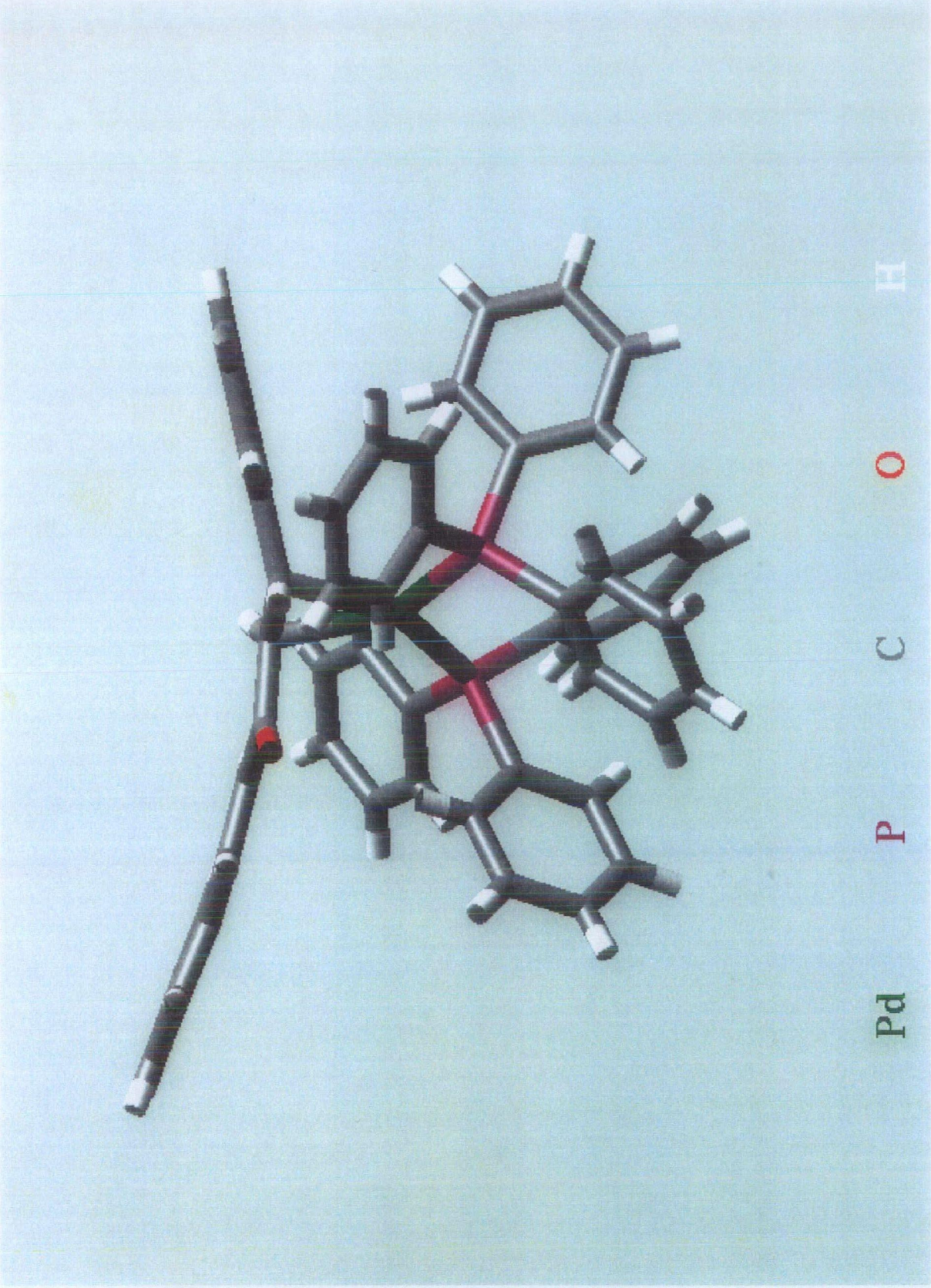

[(PPh$_3$)$_2$Pd(dba)] (22)

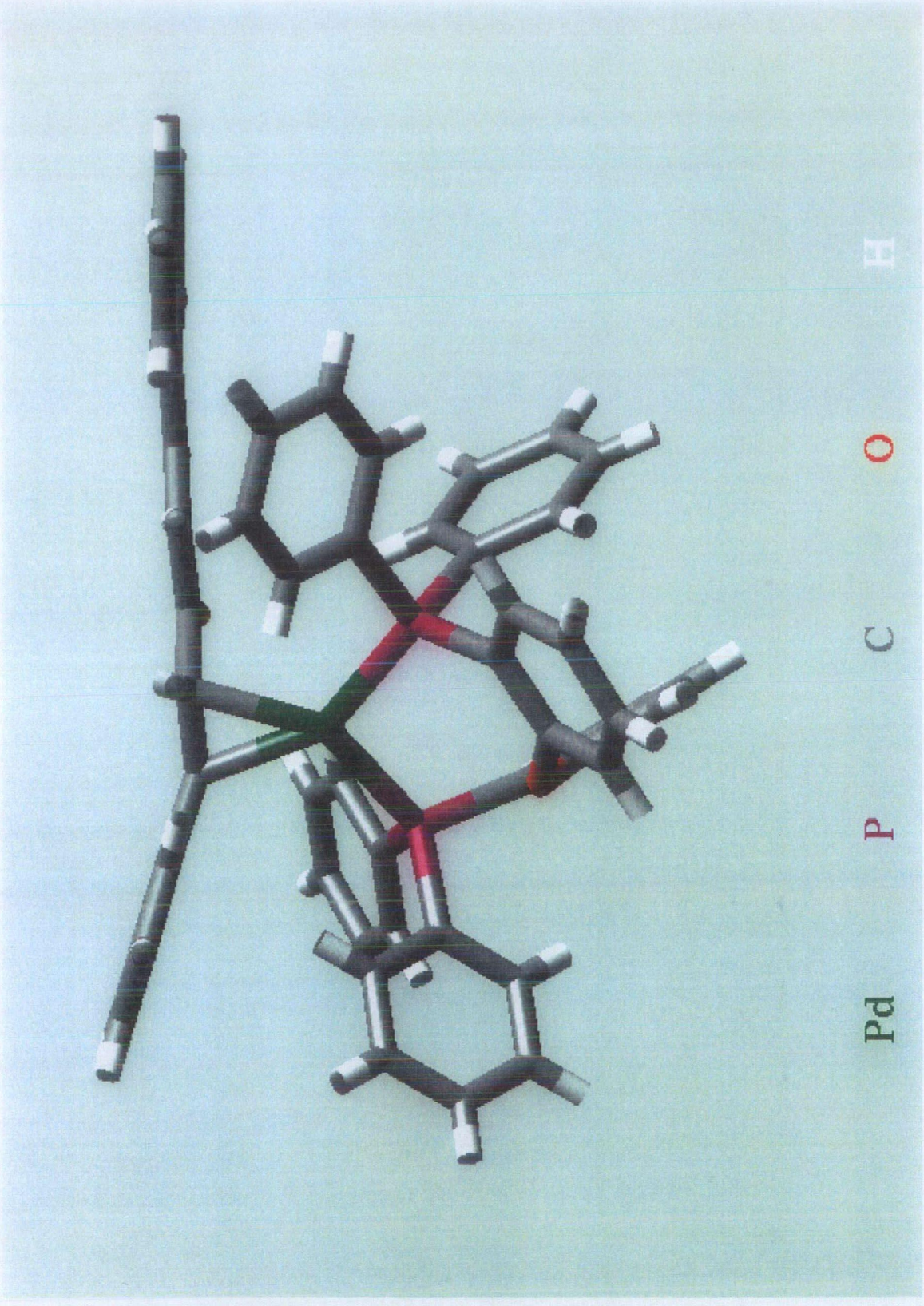

[{DPEphos}Pd(dba)] (24)

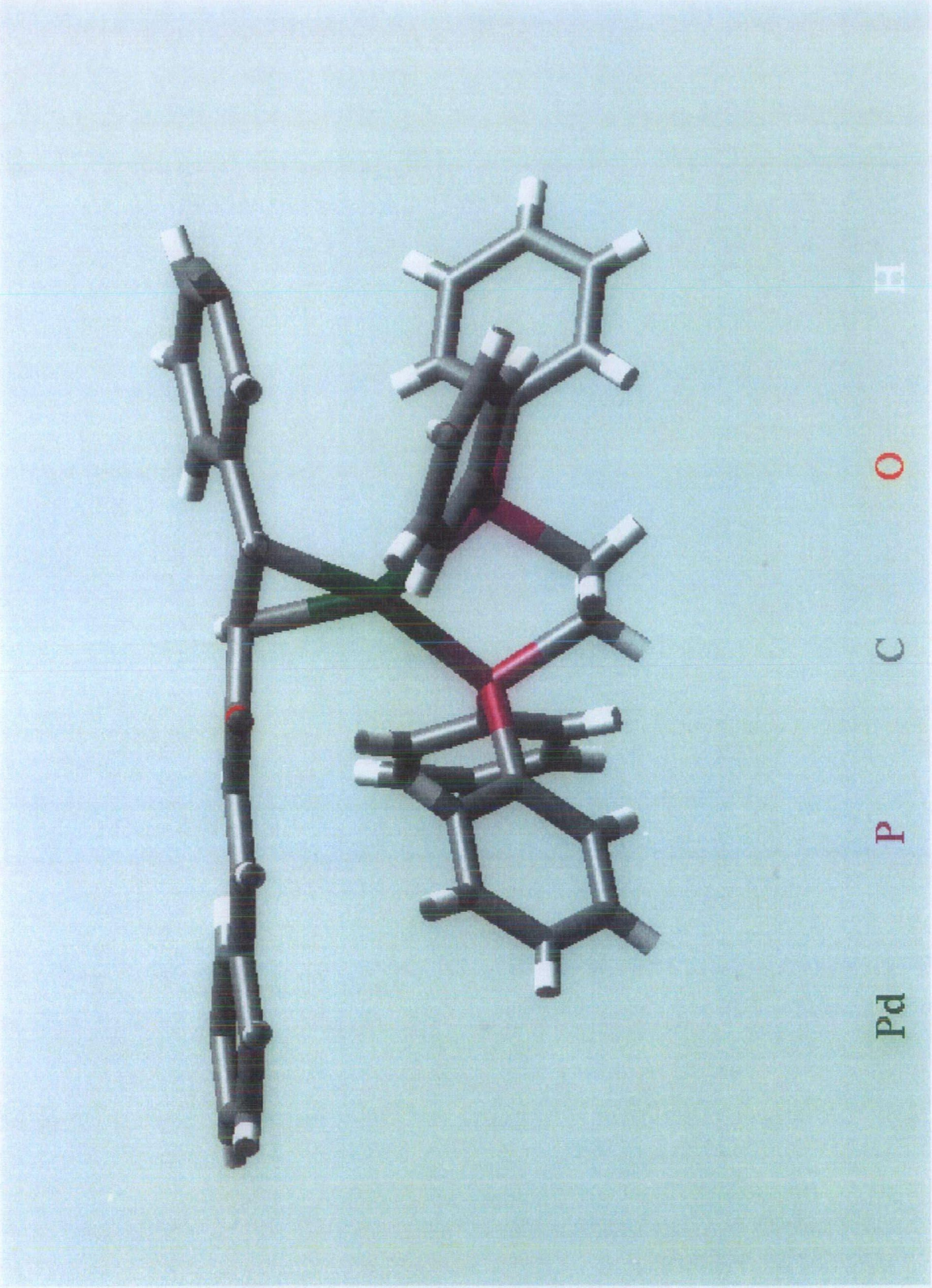

[1,2–$C_2H_4(PPh_2)_2Pd(dba)$]

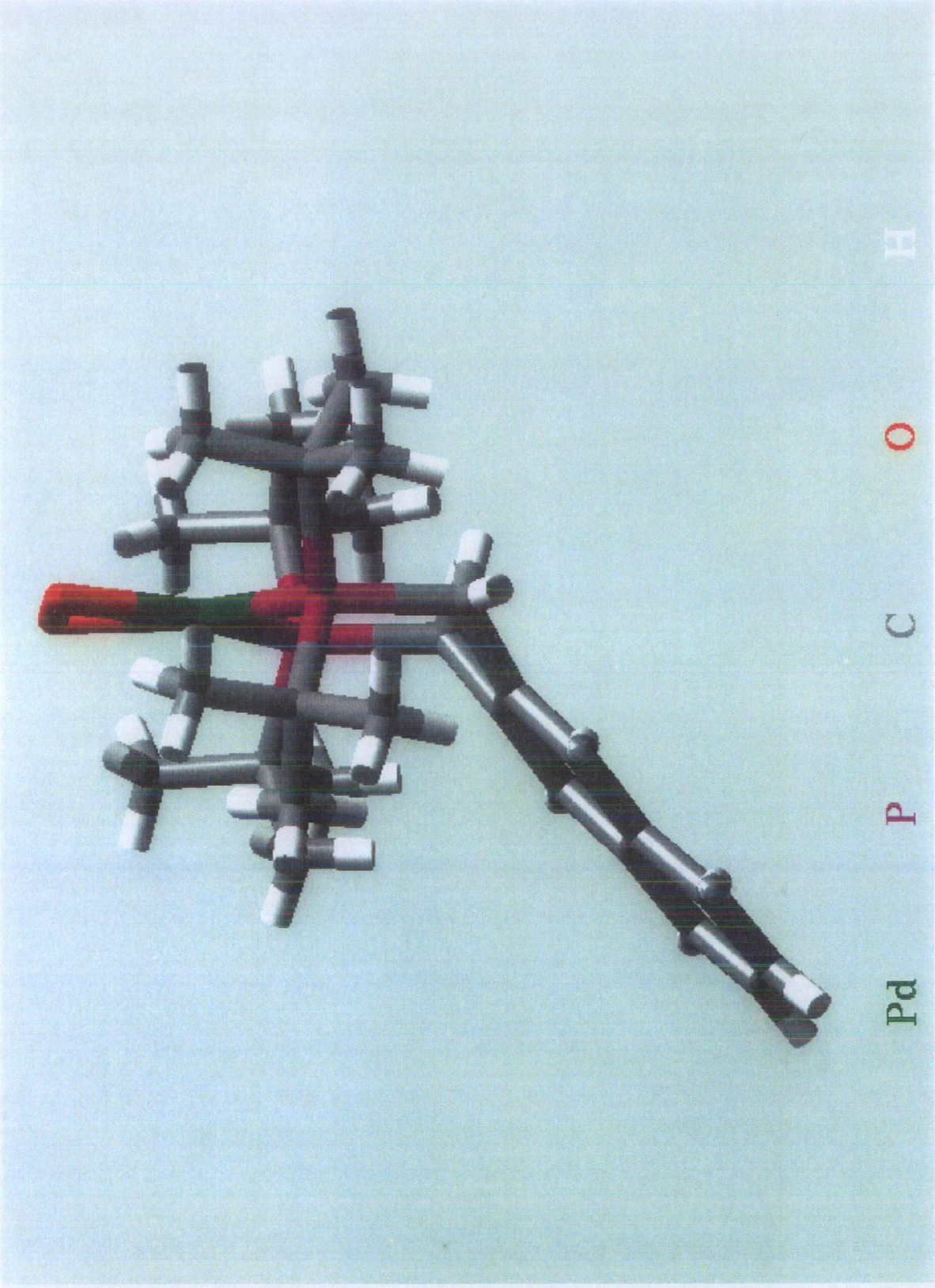

$[C_{10}H_6(2,3\text{–}CH_2PBu^t{}_2)_2Pd(O_2)]$ (47)

APPENDIX 2

PICTORIAL REPRESENTATIONS OF THE CALCULATION OF CONE ANGLES FROM SELECTED CRYSTALLOGRAPHIC DATA

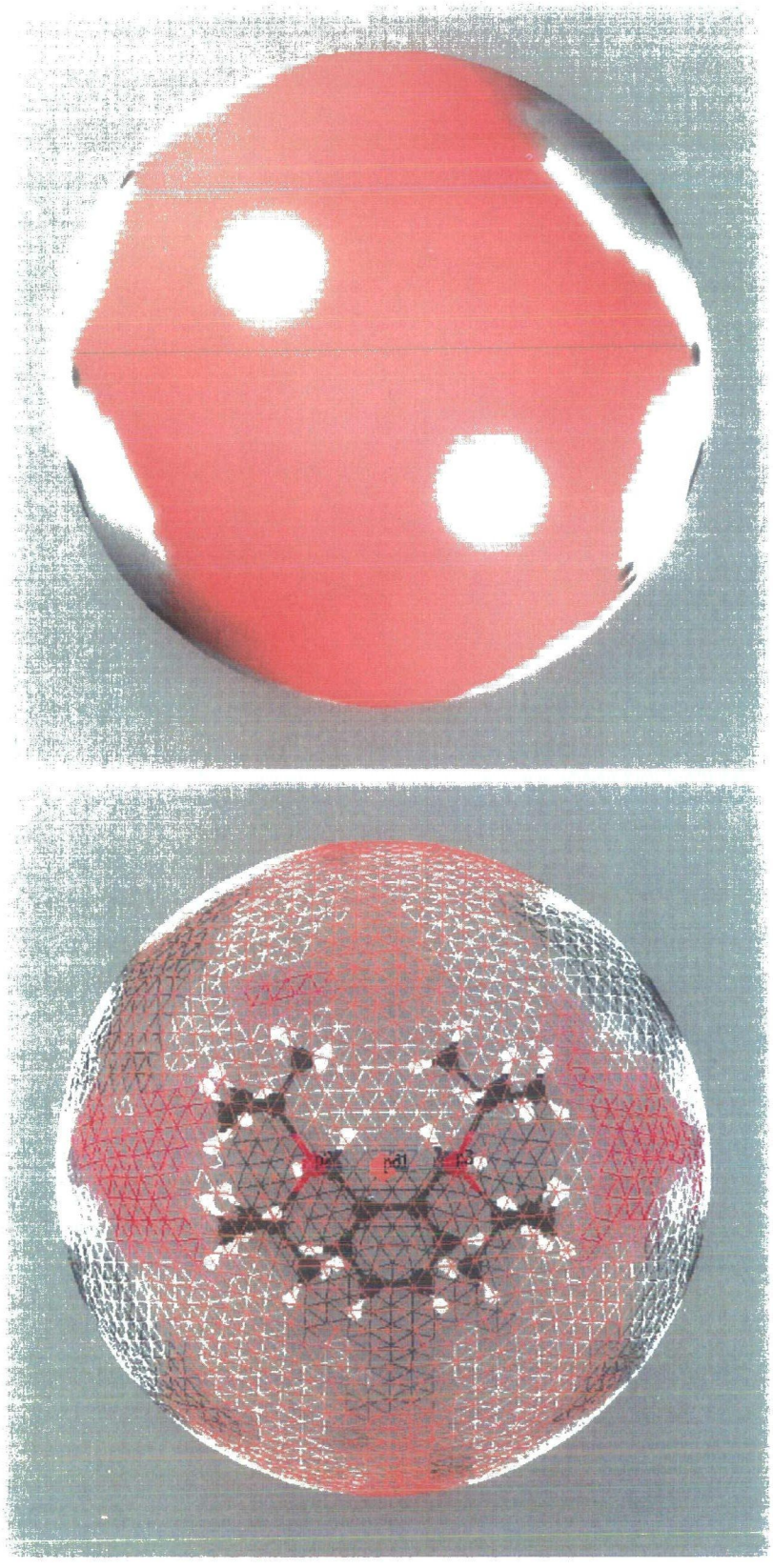

[*o*−$C_6H_4(CH_2PBu^t_2)_2Pd$]

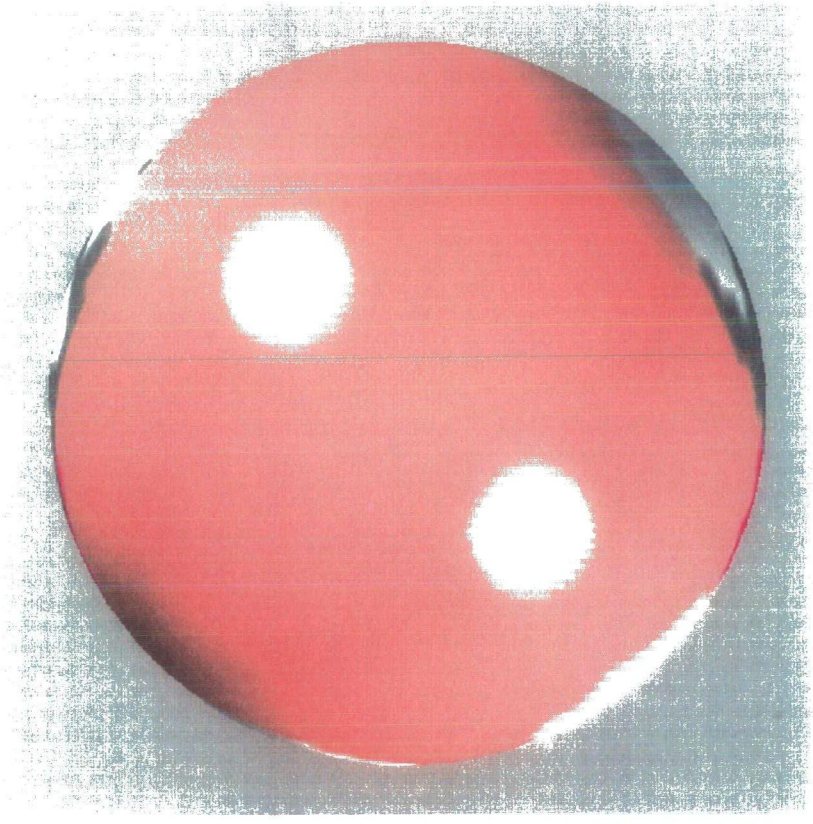

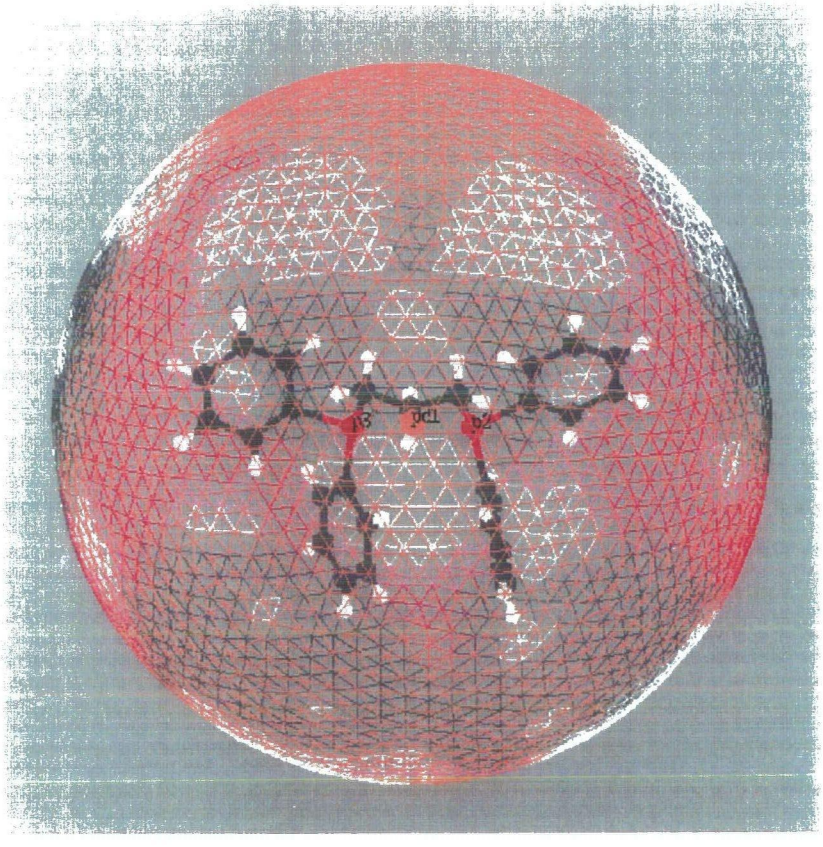

[1,3–$C_3H_6(PPh_2)_2Pd$]

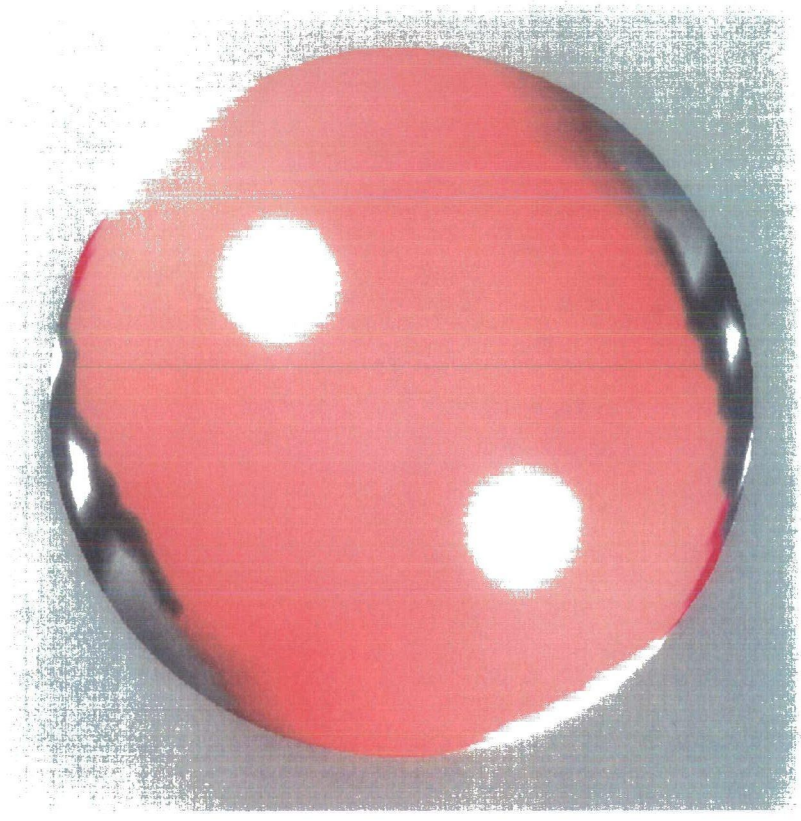

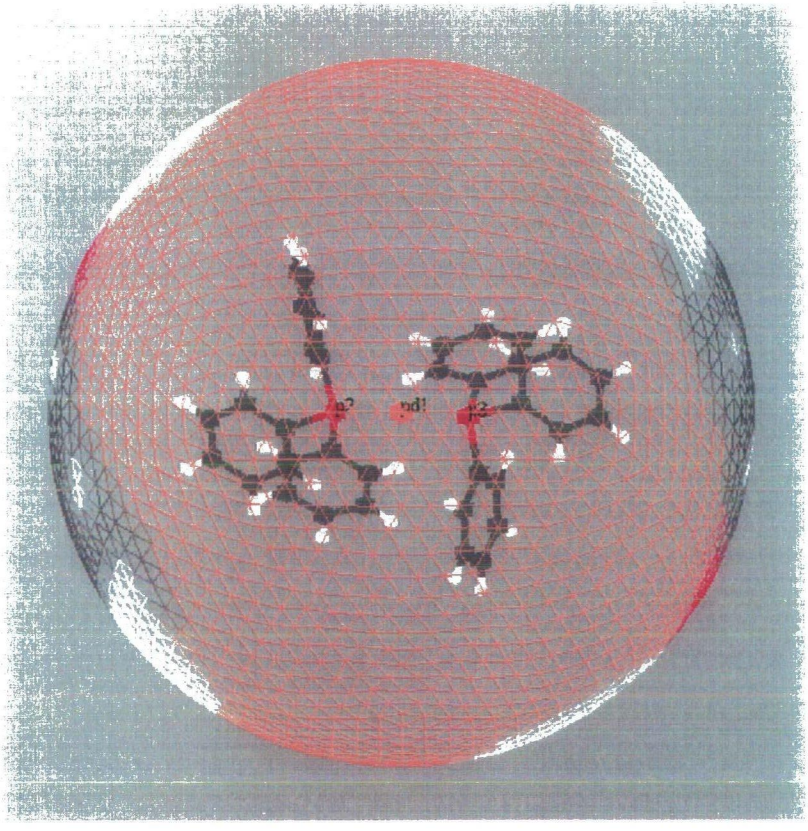

[(PPh3)2Pd]

APPENDIX 3

PICTORIAL REPRESENTATIONS SHOWING VAN-DERWAALS RADII OF SELECTED CRYSTALLOGRAPHIC DATA

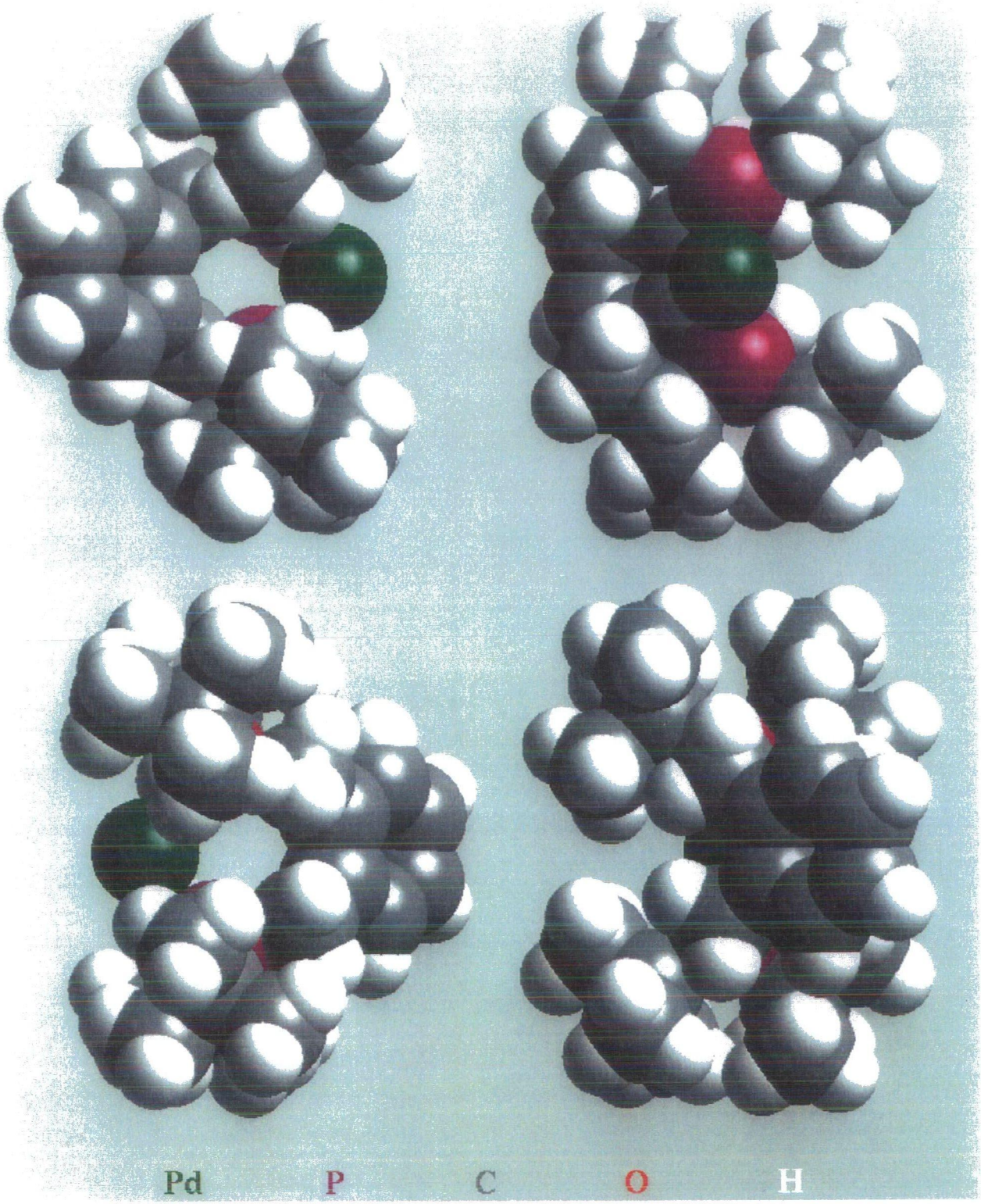

[*o*–$C_6H_4(CH_2PBu^t_2)_2Pd$] (12)

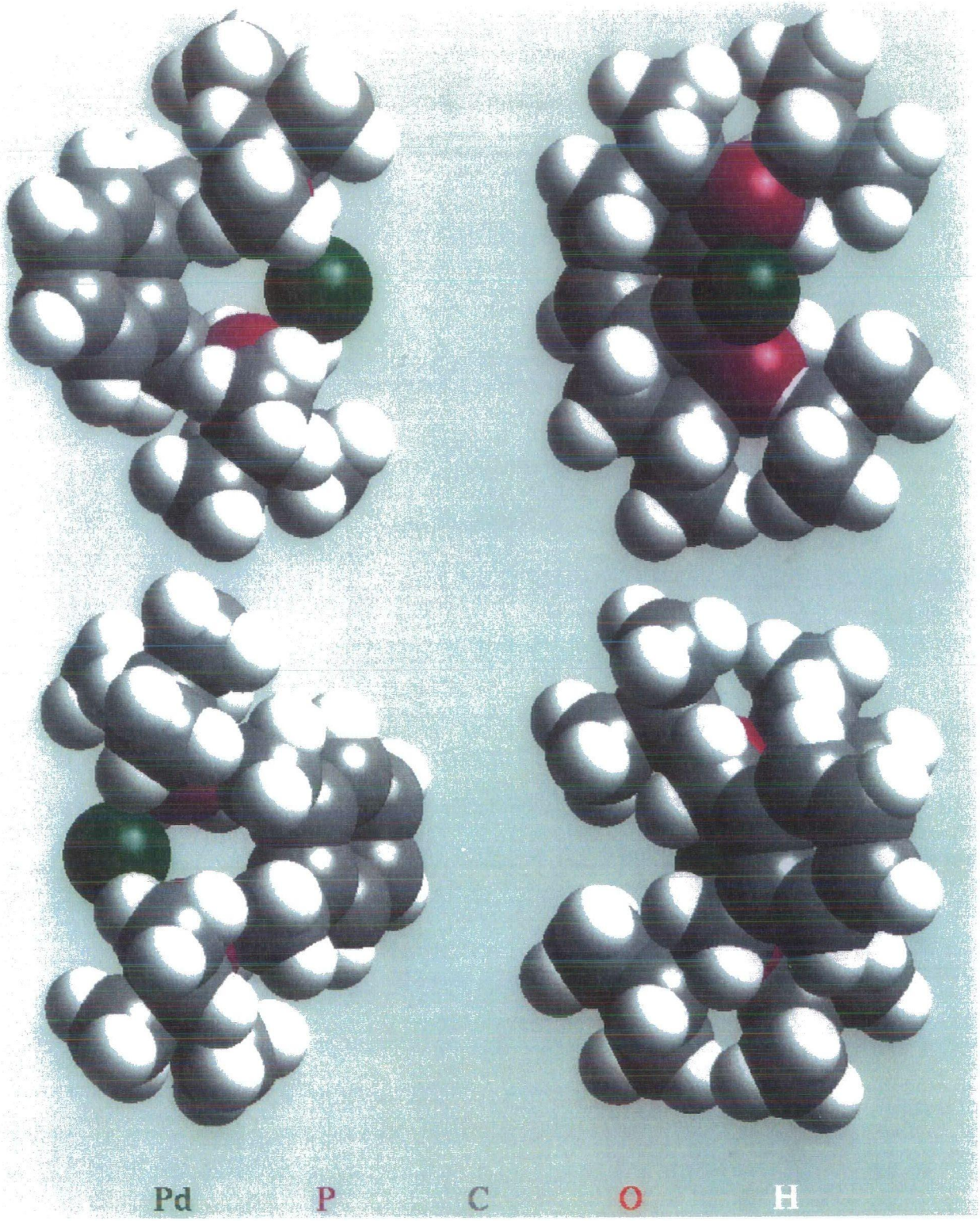

[*o*–$C_6H_4(CH_2PPr^i{}_2)_2Pd$] (13)

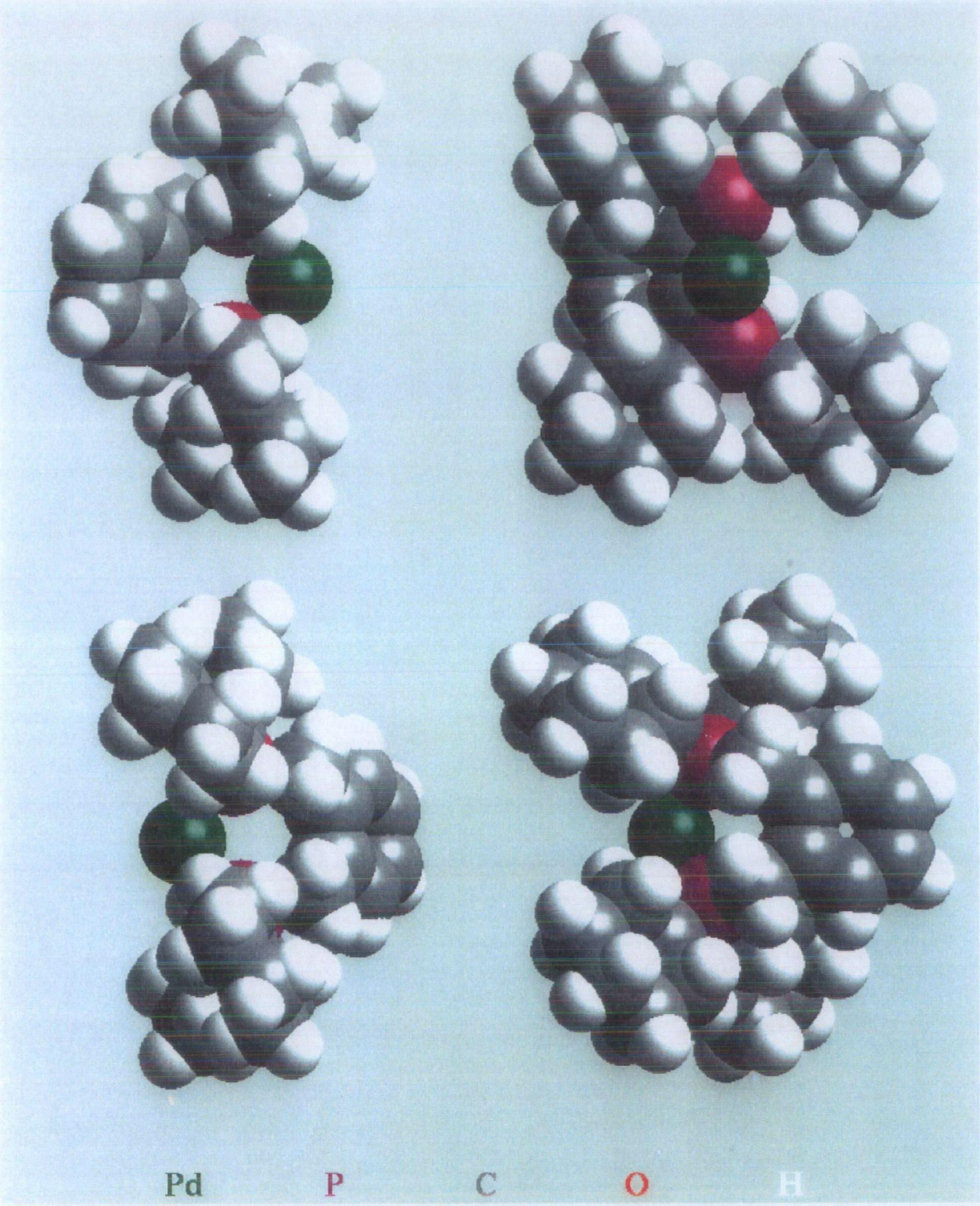

[*o*–$C_6H_4(CH_2PCy_2)_2Pd$] (14)

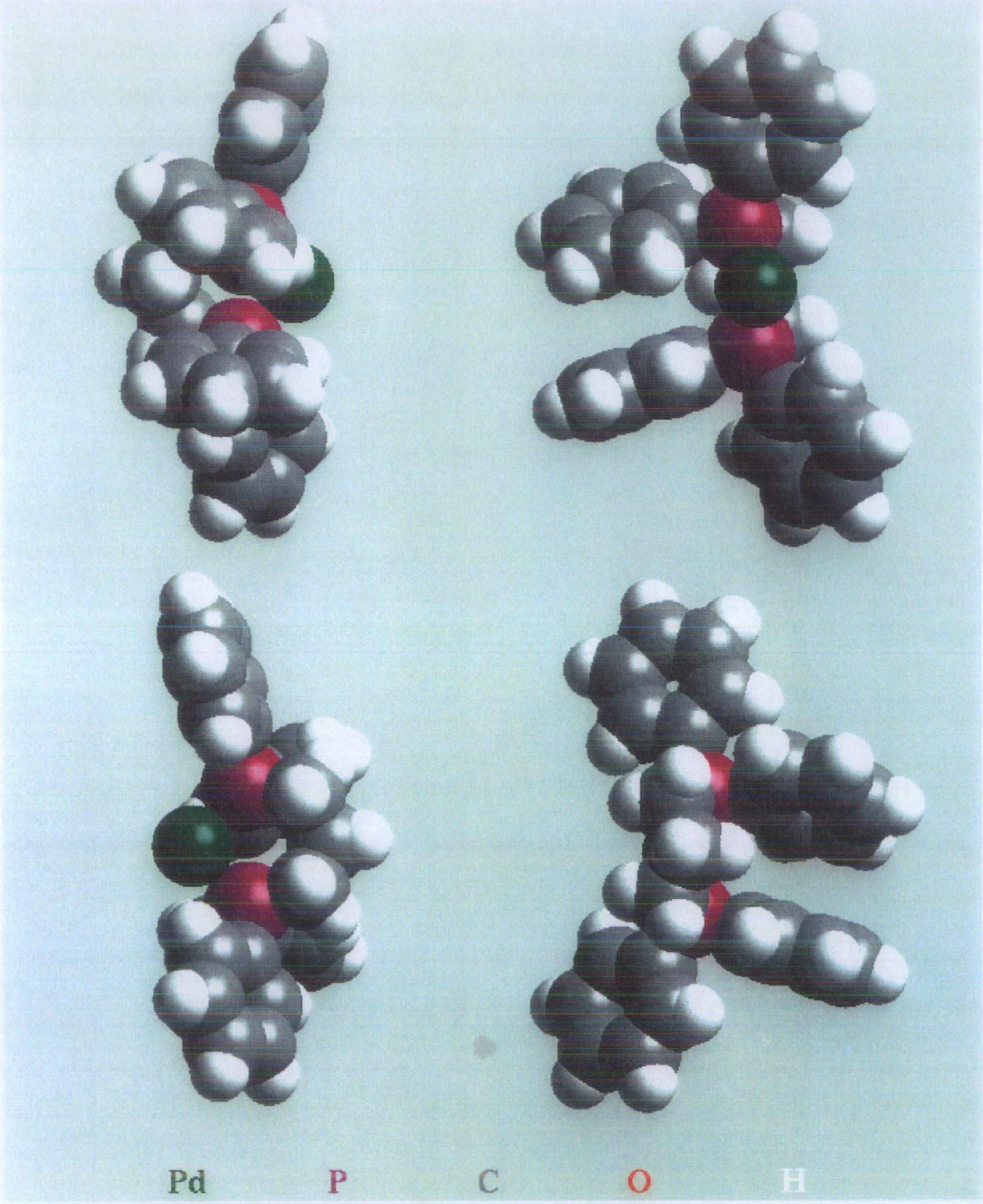

[1,3–$C_3H_6(PPh_2)_2Pd$] (21)

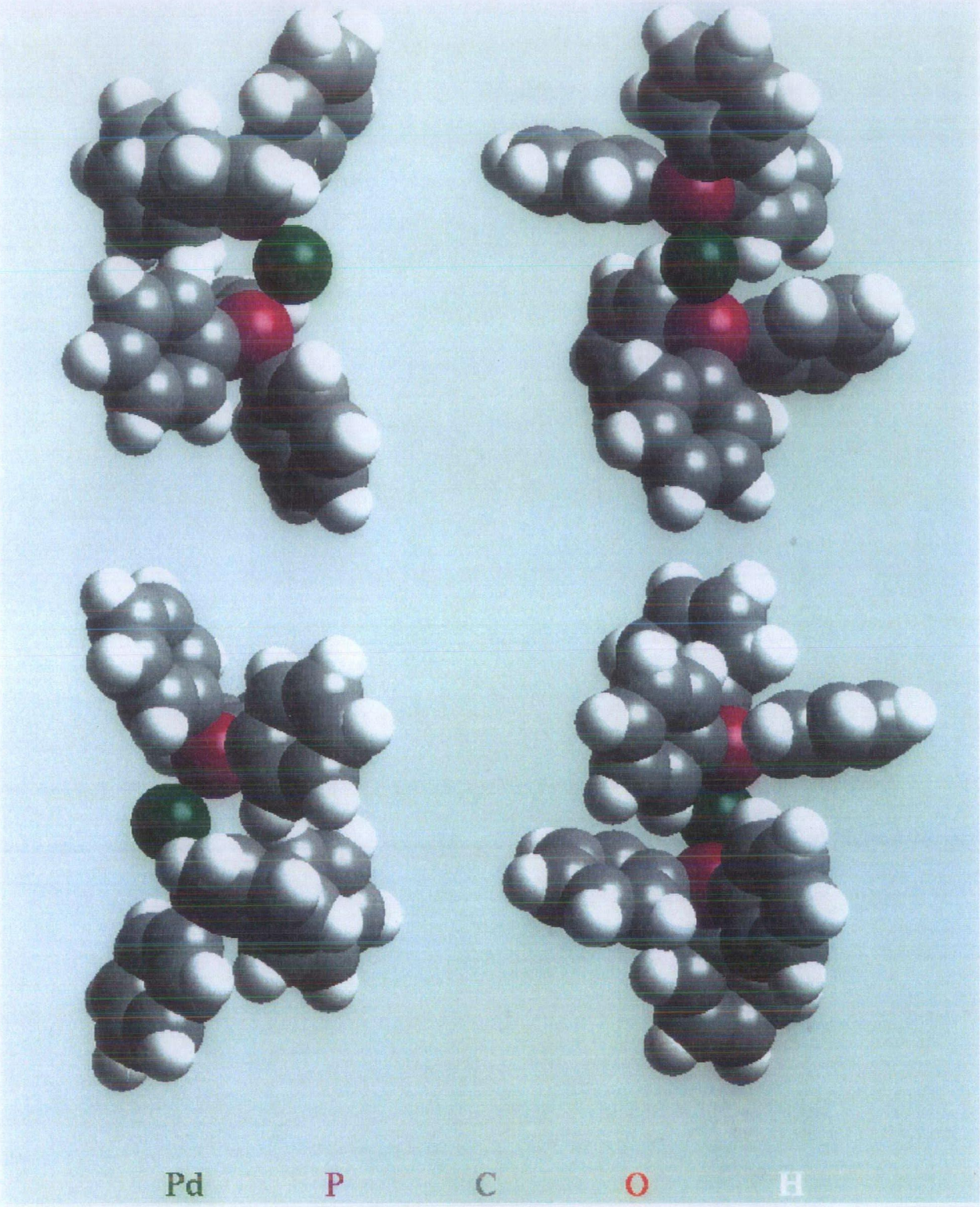

[$(PPh_3)_2Pd$] (22)

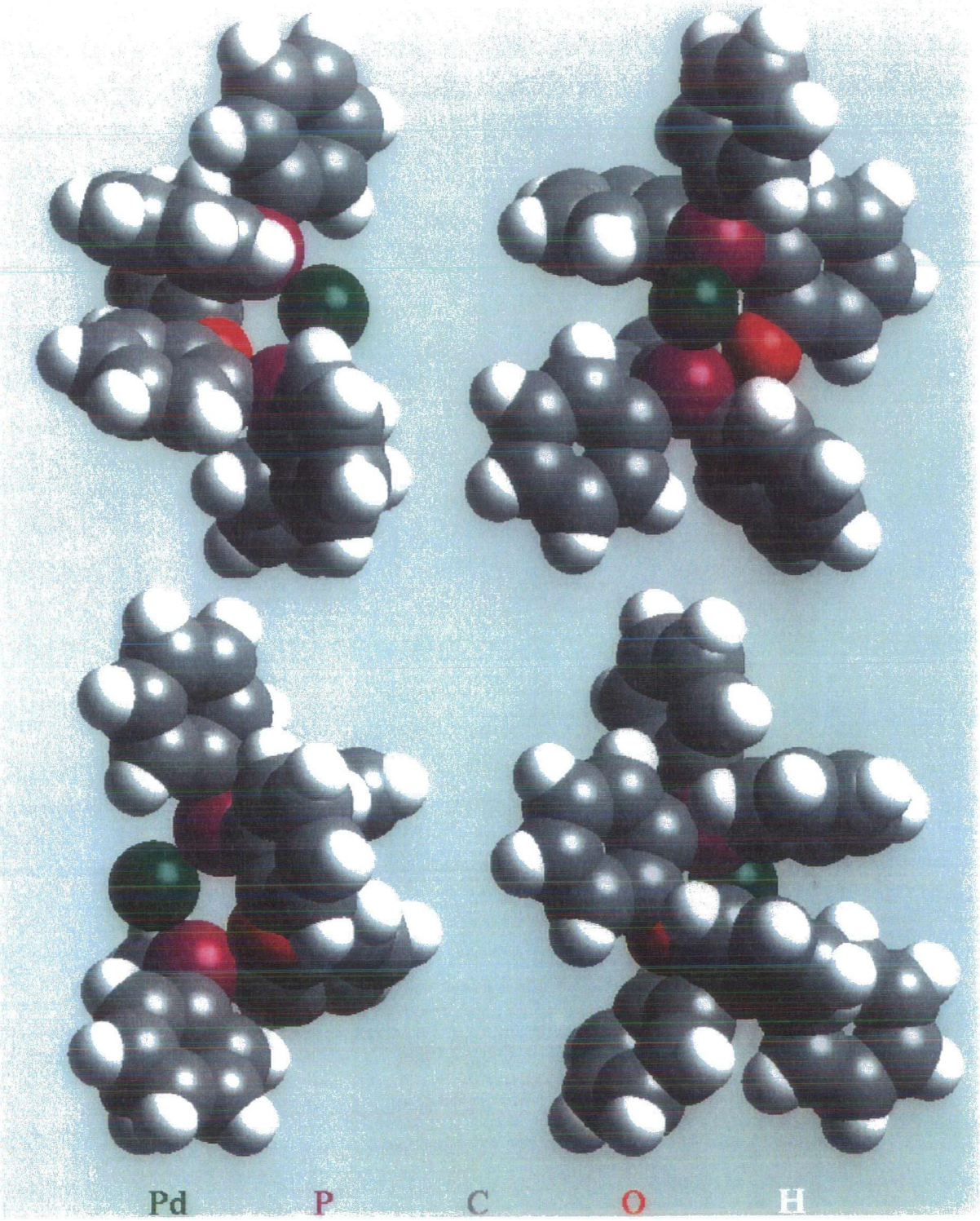

[{DPEphos}Pd] (24)

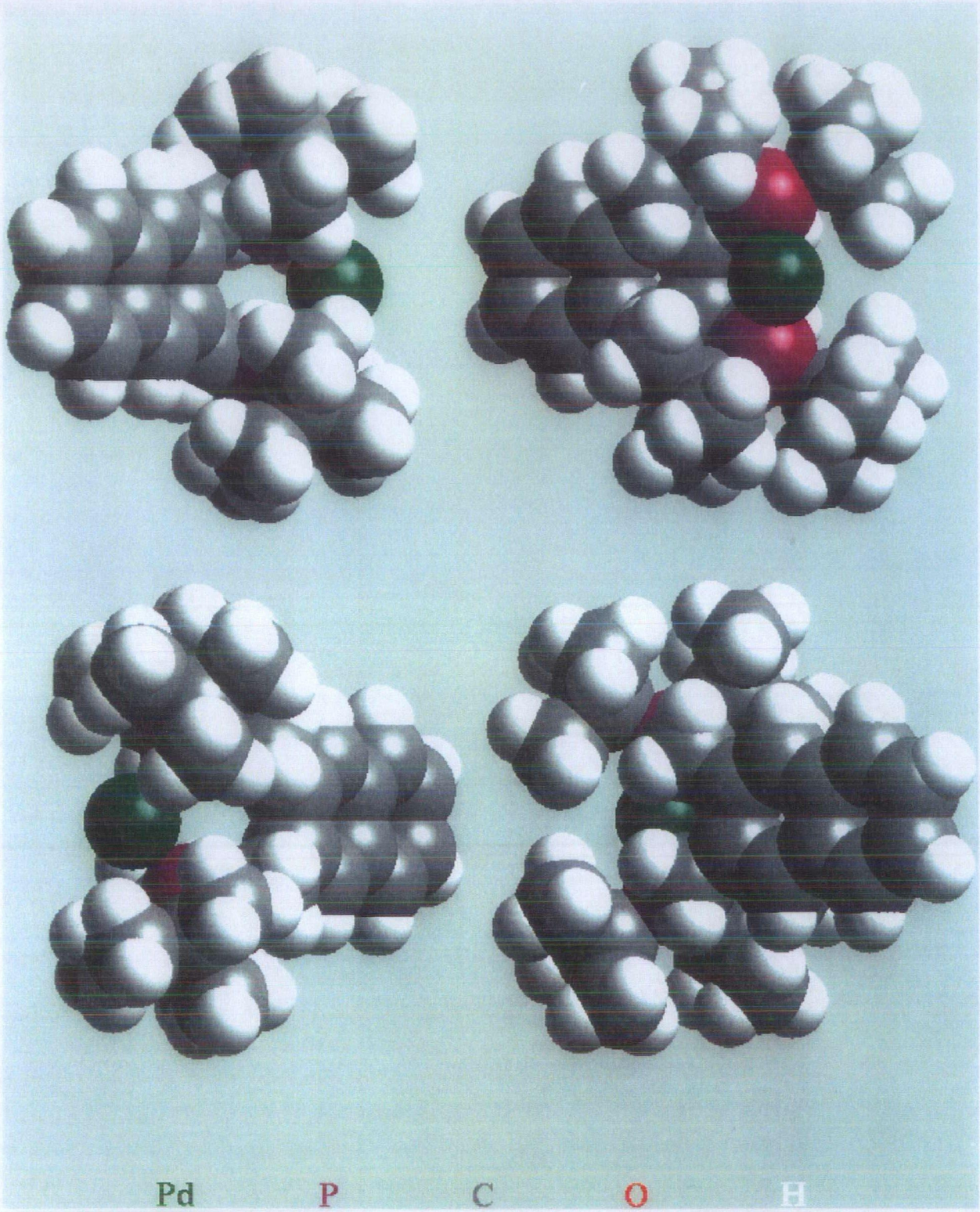

$[C_{10}H_6(2,3\text{–}CH_2PBu^t{}_2)_2Pd]$ (47)

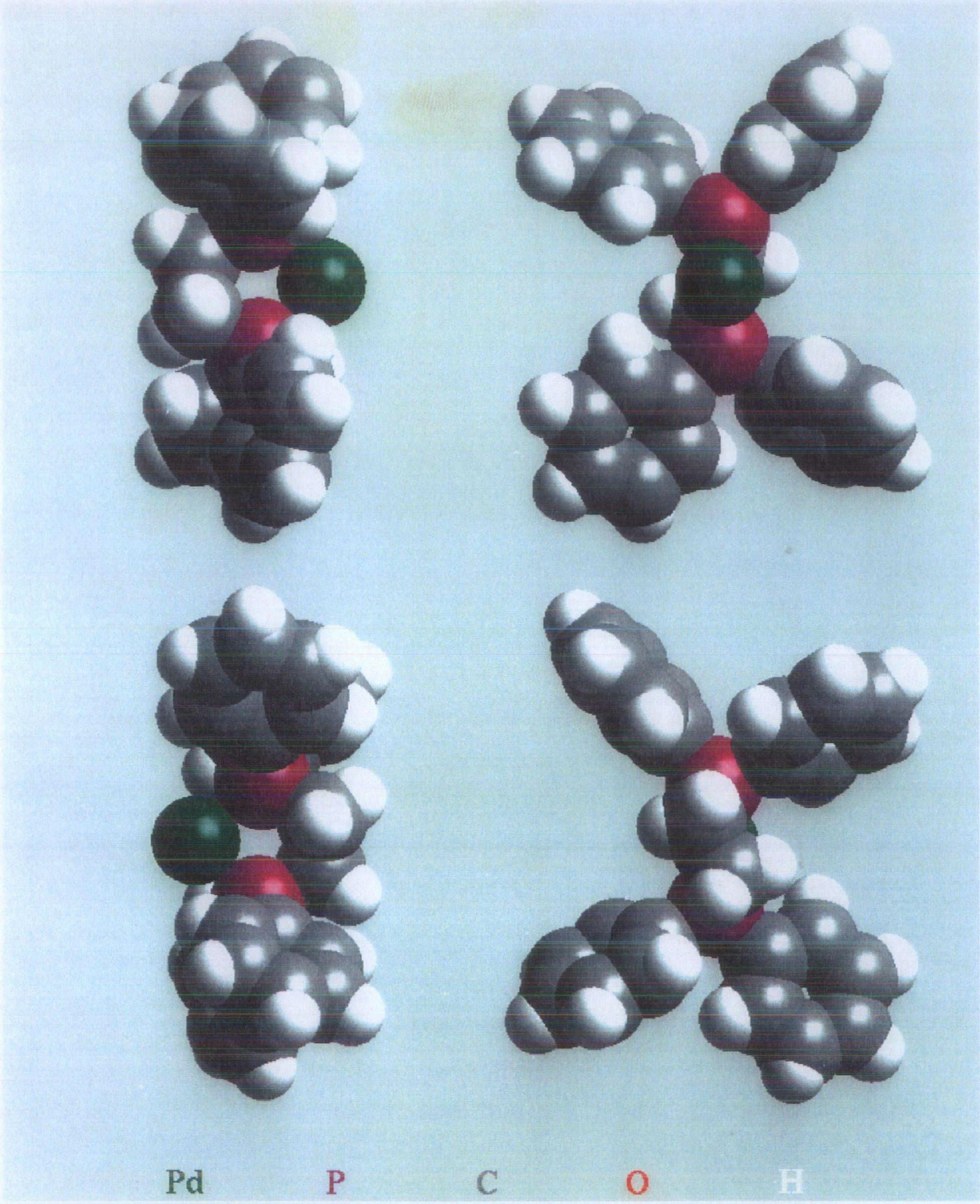

[1,2–$C_2H_4(PPh_2)_2Pd$]